Maximum Lyapunov Exponent Calculation

Vasiliy D. Pechuk[1], Tatyana S. Krasnopolskaya[2], and Evgeniy D. Pechuk[3]

[1] Kyiv National University of Construction and Architecture, Kyiv, Ukraine
(E-mail: pechuk.vd@knuba.edu.ua)
[2] Institute of Hydromechanics NASU, Kyiv, Ukraine
(E-mail: t.krasnopolskaya@tue.nl)
[3] Institute of Hydromechanics NASU, Kyiv, Ukraine
(E-mail: evgdmp@gmail.com)

Abstract. The maximum Lyapunov exponent characterizes the degree of exponential divergence of close trajectories. The presence of a positive Lyapunov exponent in the system indicates a rapid divergence over time of any two close trajectories and sensitivity to the values of the initial conditions. Therefore, the determination of the Lyapunov exponent makes it possible to identify a dynamical system as a system with chaotic dynamics in it. When studying the output signals of dynamic systems, it is often necessary to quantify the degree of randomness of the output signal when equations of the system are unknown. In this paper, the possibilities of accuracy improvement of the numerical algorithms of Benettin and Wolf for estimating the maximum Lyapunov exponents of an attractor of a dissipative dynamical system are shown. Under these procedures a system itself can be specified both analytically (by a system of differential equations) and only by output signal.
Keywords: Maximum Lyapunov exponent, Algorithms of Benettin, Algorithms of Wolf, Initial conditions, Chaotic modeling.

1 Introduction

As is known, one of the necessary conditions for the randomness of the dynamic behavior of the system is sensitivity to the values of the initial conditions (G. Benettin, L. Galgani and J.M. Strelcyn [1], G. Benettin *et al.* [2], A. Wolf *et al.* [3], S. P. Kuznetsov [4], J. Laskar, K. Froschle and A. Celletti [5], V. A. Golovko [6] F. Moon [7]). As a quantitative criterion for this concept, the senior Lyapunov exponent (Lyapunov exponent) is usually used. Let a dynamical system be given analytically by a system of differential equations in the Cauchy form:

$$\frac{dx(t)}{dt} = f(x(t), t), \tag{1}$$

where $x \in \mathbb{R}^n$, $\mathbb{R}^n$ – is the phase space of the system, the initial conditions $x(t_0) = x_0$, $f: \mathbb{R}^{n+1} \to \mathbb{R}^n$– are a continuous vector - function satisfying the Lipschitz conditions for all arguments, except for time t. Then a solution to system (1) exists and is unique. Let us denote by x_i a point in the phase space $\mathbb{R}^n$ of the dynamical system corresponding to the radius vector of the state $\mathrm{x}(t_i)$. If in the course of time the solution of system (1) approaches a certain manifold A when time goes to infinity, then we call A the attractor of system (1). There can be one or several attractors in the phase space, hidden, large, etc.,

depending on the properties of the system itself (1). In this case, the most important characteristics of the system are (S. P. Kuznetsov [4], V. A. Golovko [6], P. Berger, I. Pomo and K. Vidal. [8], D. P. Crutchfield [9]):

• chaos or regularity (presence or absence of chaotic dynamics);
• dissipation or conservatism (presence or absence of energy dissipation);
• topological invariants of the attractor (for example, fractal dimension).

Depending on these characteristics, the behavior of the solution of the system in the phase space changes significantly. Let the solution of the system be obtained for some initial conditions and, after the transient process, a certain attractor is found. To find out whether the attractor has a sensitivity to the values of the initial conditions, which is characteristic of a strange (chaotic) attractor, let us calculate the maximum Lyapunov exponent (MLE).

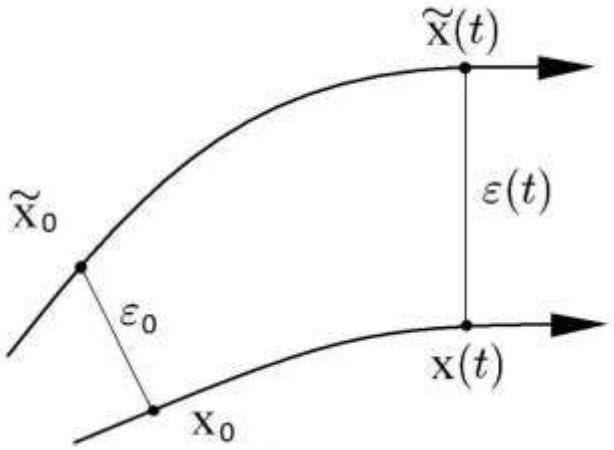

Fig. 1. Evolution of two close points on the attractor
dynamic system

Consider a point x_0 on the attractor of a dynamical system (Fig. 1.) at the initial moment of time t_0. Having given some small value ε_0, we choose one more point $\tilde{x}_0$ on the attractor that satisfies the condition

$$|\widetilde{x_0} - x_0| = \varepsilon_0.$$

It should be noted here that for correct operation it is a point on the attractor that is needed, and not close to the attractor (S. P. Kuznetsov [4], V. A. Golovko [6], P. Berger, I. Pomo and K. Vidal. [8], D. P. Crutchfield [9]). Otherwise, the obtained result will characterize not the behavior of the trajectory on the attractor, but near it, which is the main source of errors in calculating the MLE for non-conservative systems.

Through a period of time Δt, the points x_0 and $\tilde{x}_0$ evolve into points $x(t)$ and $\tilde{x}(t)$. The Distance between them is denoted by $\varepsilon(t)$, here $t = t_0 + \Delta t$. The value $\varepsilon(t)$ depends on the initial position of the points x_0 and $\tilde{x}_0$, as well as the time interval Δt and the dynamic system as a whole. However, approximately, we can assume that

$$\varepsilon(t) \approx \varepsilon_0 e^{\lambda \Delta t},$$

where λ is the MLE. Thus, the parameter characterizing the dynamics of the representing point on the attractor is (G. Benettin, L. Galgani and J.M. Strelcyn [1], G. Benettin *et al.* [2], A. Wolf *et al.* [3], S. P. Kuznetsov [4])

$$\lambda \approx \frac{1}{\Delta t} \ln \frac{\varepsilon(t)}{\varepsilon_0}. \quad (2)$$

Here it is necessary to take into account the fact that the boundedness of the attractor implies boundedness $\varepsilon(t)$ and, therefore, Δt should increase until $\varepsilon(t)$ is significantly less than the size of the attractor, otherwise λ will be equal to zero at $\Delta t \to \infty$. The value λ obtained in accordance with (2) should be considered as averaged over all the initial points x_0 of the attractor. Therefore,

$$\lambda = \overline{\lim_{\Delta t \to \infty} \frac{1}{\Delta t} \ln \frac{\varepsilon(t)}{\varepsilon_0}},$$

where $\varepsilon(t)$ is much smaller as the size of the attractor. This approach is based on the Oseledts ergodic theorem, see V. I. Oseledets [10], according to which the exponential divergence of two randomly selected points on the attractor characterizes the maximum Lyapunov exponent with probability equals 1.

In practice, the Benettin algorithm is used to find the values of the maximum Lyapunov exponent. Proposed by a team of authors in 1976 for the conservative Hénon-Heiles system (G. Benettin, L. Galgani and J.M. Strelcyn [1]), this calculation method works well and is suitable, first of all, for conservative systems. In their 1980 work G. Benettin *et al.* [2], the same authors used their results for smooth Hamiltonian dynamical systems. Due to the lack of alternatives, it is often used for dissipative systems, but in this case errors inevitably arise due to the fact that the dimension of the attractor of such a system is lower than the dimension of the phase space.

And the application of the classical Benettin's algorithm in the case of the existence of several attractors in the system and, moreover, hidden attractors, is generally incorrect. In this paper, we propose methods to improve the accuracy of this algorithm for the case of a dissipative dynamical system.

2 Procedure for improving the accuracy of Benettin's algorithm.

Let us denote by x_0 a point $x(t_0)$ on the attractor of the dynamical system (1) at the initial moment t_0, after the transient process. We choose a positive value ε - much less than the linear dimensions of the attractor and a point $\widetilde{x_0}$ satisfying the equality

$$|\widetilde{x_0} - x_0| = \varepsilon. \quad (3)$$

Let's track the evolution of points x_0 and $\widetilde{x_0}$ after a short period of time T. The resulting values will be denoted by x_1 and $\widetilde{x_1}$ (Fig. 2).

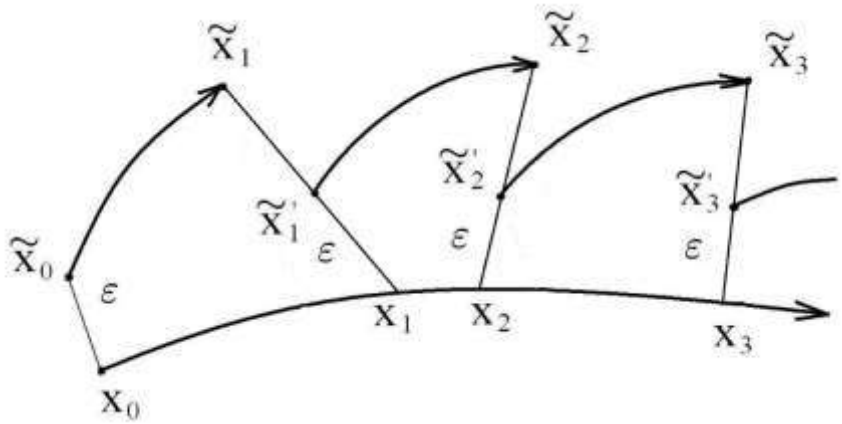

Fig. 2. Benettin's algorithm for computation
the maximum Lyapunov exponent

The vector $\Delta x_1 = \widetilde{x_1} - x_1$ is called the vector of disturbance, and its absolute value $|\Delta x_1|$ is called the amplitude of the disturbance. The MLE value for this stage is estimated by the formula:

$$\lambda_1 = \frac{1}{T}\ln\frac{|\widetilde{x_1} - x_1|}{\varepsilon} = \frac{1}{T}\ln\frac{|\Delta x_1|}{\varepsilon}.$$

Then the following renormalization is performed:

$$\Delta x_1' = \frac{\Delta x_1}{|\Delta x_1|}\,\varepsilon,$$

and the described procedure is repeated for points $\widetilde{x_1'} = x_1 + \Delta x_1'$ and x_1, instead of $\widetilde{x_0}$ and x_0 (Fig. 2). After M repetitions, we find the MLE as the arithmetic mean of the values obtained at each stage

$$\lambda \approx \frac{1}{M}\sum_{k=0}^{M}\lambda_k = \frac{1}{M}\sum_{k=0}^{M}\frac{1}{T}\ln\frac{|\Delta x_k|}{\varepsilon} = \frac{1}{MT}\sum_{k=0}^{M}\ln\frac{|\Delta x_k|}{\varepsilon}.$$

It is clear that the algorithm works well in conservative models, where the volume of the phase space does not change over time. For example, in problems of mixing liquids in a tank, where the result obtained in this way directly characterizes the degree of mixing of the points of the medium (T. S. Krasnopolskaya *et al.* [11], V. V. Meleshko *et al.* [12]), where, however, it is shown that the maximum value of the maximum Lyapunov exponent does not guarantee the best mixing quality.

The main problem of this method in the case of a dissipative system is the fact that the points $\widetilde{x_1'}$, $\widetilde{x_2'}$, …, generally speaking, do not lie on the attractor. The dimension of the attractor is lower than the dimension of the phase space; therefore, the probability of a randomly taken point hitting it is zero. So, for example, if the only attractor of the system is the limit cycle, then as a result of the application of Benettin's algorithm, the MLE will be negative, but should be zero. The following hitting options for a point are possible x_k':

• on the investigated attractor (probability zero);
• on another, possibly hidden attractor (probability zero);
• into the basin of attraction of the investigated attractor (the probability is positive);
• into the basin of attraction of another attractor (the probability is positive).

In the last two most probable cases, the value λ_k will characterize not the MLE value of the attractor, but the behavior of the trajectory close to it and introduce an error into the calculation result. To avoid this and increase the calculation accuracy, you need to select points $\widetilde{x_0}, \widetilde{x_1'}, \widetilde{x_2'}$,... on the investigated attractor. With the known right-hand sides of system (1), the solution can be obtained numerically, and the algorithm can look as follows. After the transient process, we select points x_0 and $\widetilde{x_0}$ on the solution of the system of equations (1) so that condition (3) is satisfied for some small one ε. Solving the system further, after T we get points x_1 and $\widetilde{x_1}$, respectively. Find the first value

$$\lambda_1 = \frac{1}{T}\ln\frac{|\widetilde{x_1} - x_1|}{\varepsilon}.$$

Next, we fix one of the obtained points, for example x_1, and we find $\widetilde{x_1'}$ by solving the system further from the point $\widetilde{x_1}$ until the condition $0 < |\widetilde{x_1'} - x_1| \leq$

ε. is fulfilled. Repeating this procedure M once, we find the MLE as the arithmetic mean of the values obtained at each stage:

$$\lambda \approx \frac{1}{M}\sum_{k=0}^{M}\lambda_k.$$

The obtained value, according to the ergodic theorem of Oseledts (see V. I. Oseledets [10]), characterizes the maximum Lyapunov exponent of the attractor under study with a probability of 1.

3 The method of applying the Wolf's algorithm.

When studying the output signals of dynamic systems, it is often necessary to quantify the degree of randomness of the output signal, with unknown equations of the system. In this case, the method proposed by A. Wolf *et al.* [3] in 1985 for calculating the Lyapunov exponent from the chaotic time realization of the system under study is usually used. It is based on the classical Benettin's algorithm and Takens theorem, see F. Takens [13]. According to this theorem, having an one-dimensional time realization $a(t)$ of a dynamical system belonging to a smooth manifold - an attractor of dimension d,, the delay method can be used to reconstruct the original attractor as a n- dimensional set of state vectors $x(t) \in \mathbb{R}^n$, for $n \geq 2d + 1$

$$x(t) = \big(a(t), a(t+\tau), \dots, a(t+(n-1)\tau)\big).$$

The method for calculating the maximum Lyapunov exponent is as follows. Let the time realization $a(t)$ be given over a finite time interval at the moments

$$t_i = i\Delta t,\ i = 0, \dots, N.$$

Let us denote by a x_i point in space $\mathbb{R}^n$ corresponding to the radius – vector of the state $x(t_i)$. Then, as a result of reconstruction, we obtain the attractor of the system as a sequence of points in space $\mathbb{R}^n$:

$$x_i = \big(a(i\Delta t), a(i\Delta t+\tau), \dots, a(i\Delta t+(n-1)\tau)\big), \qquad (4)$$

here $\tau = m\Delta t,\ i = 0, \dots, N-(n-1)m.$

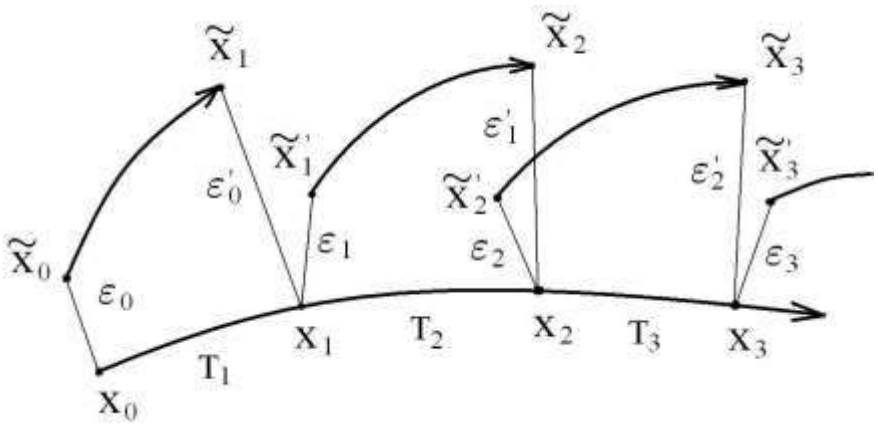

Fig. 3. Wolf's algorithm for computing
the maximum Lyapunov exponent from the output signals set

Take an arbitrary point from the sequence (4) and denote it an x_0. Further, passing through the sequence (4), we find on it a point $\widetilde{x_0}$, satisfying the inequality

$$|\widetilde{x_0} - x_0| = \varepsilon_0 \leq \varepsilon,$$

where ε is some constant significantly less than the linear dimensions of the reconstructed attractor. In this case, the points x_0 and $\widetilde{x_0}$ must be separated in time. After that, we track their evolution in time on the attractor until the distance between them exceeds a given value ε_{max}.. Let's designate this time interval as T_1. Then, again going through the sequence (4), we find a point $\widetilde{x_1'}$ close to x_1, that the inequality

$$|\widetilde{x_1'} - x_1| = \varepsilon_1 \leq \varepsilon,$$

realized and vectors $\widetilde{x_1} - x_1$ and $\widetilde{x_1'} - x_1$ have the closest direction. The procedure is repeated again, only instead of points x_0 and $\widetilde{x_0}$ are taken already x_1 and $\widetilde{x_1'}$. After M repetitions, the maximum Lyapunov exponent is estimated as follows:

$$\lambda \approx \frac{1}{M} \sum_{k=0}^{M-1} \frac{\ln(\varepsilon_k'/\varepsilon_k)}{T_{k+1}}.$$

The considered Wolf algorithm is applicable only for a chaotic output signals set implementation (with a positive Lyapunov exponent), which somewhat reduces the universality of its practical application. In this paper, a modification of this algorithm is considered, which makes it possible to obtain both positive and negative values of MLE. The difference is as follows. The evolution of the selected starting points x_0 and $\widetilde{x_0}$ is tracked over an interval T, of a fixed length,

and the distance ε_0' between the points x_1 and $\widetilde{x_1}$ obtained in this case is used to evaluate the MLE. The same is repeated for points x_1 and $\widetilde{x_1'}$. After M such length T steps, the value of the Lyapunov exponent can be estimated:

$$\lambda \approx \frac{1}{MT}\sum_{k=0}^{M-1} \ln(\varepsilon_k'/\varepsilon_k).$$

In the study the interaction in the human cardiorespiratory system (T. P. Konovalyuk *et al.* [14]), chaotic modes generated by the interaction of the respiratory and cardio subsystems were found. The classical Benettin's algorithm did not allow identifying the differences between quasiperiodic and chaotic dynamics. The use of the above upgrades made it possible to increase the accuracy of calculation the maximum Lyapunov exponent by an order of magnitude. For example, in the system of discrete maps describing the cardiorespiratory system, quasiperiodic and chaotic modes were found (Fig. 4 and Fig. 5). After the application of the classical Benettin's algorithm for the quasiperiodic regime $\lambda_1 \approx 0.008$, and for the chaotic regime were obtained $\lambda_2 \approx 0.01$. As a result of the application of the modified algorithm, the values were obtained as following $\lambda_1 \approx 0.001$ and $\lambda_2 \approx 0.01$, that made it possible to more accurately characterize the dynamics of the model.

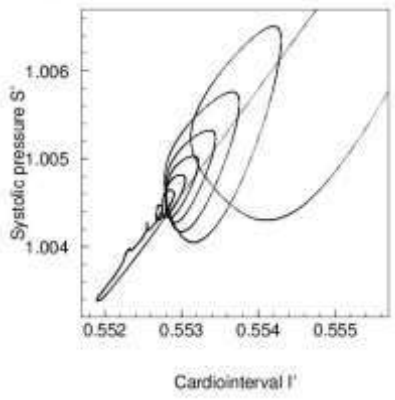

Fig. 4. Quasiperiodic mode in the system of discrete maps of the cardiorespiratory system model

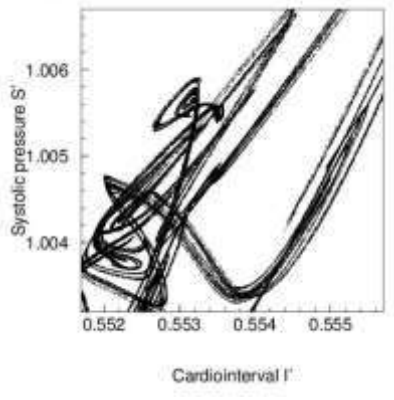

Fig. 5. Chaotic mode in the system of discrete maps of the cardiorespiratory system model

	quasiperiodic regime	chaotic regime
Benettin's algorithm	0.008365	0.009623
modified algorithm	0.001224	0.010334

Conclusions

Numerical calculation of the maximum Lyapunov exponent based on the classical Benettin's algorithm does not always give a good result if there is energy dissipation in the dynamic system. The article discusses modifications that improve the accuracy of calculations and expand the scope of the well-known algorithms of Benettin and Wolf. The use of the proposed modifications for the model of the human cardiorespiratory system made it possible to more accurately identify the differences between quasiperiodic and chaotic dynamics generated by the interaction of the respiratory and cardio subsystems.

References

1. G. Benettin, L. Galgani and J.M. Strelcyn. Kolmogorov entropy and numerical experiments. Phys. Rev. A4, 2338 – 2342, 1976.
2. G. Benettin L. Galgani, A. Giorgilli and J.M. Strelcyn. Lyapunov Characteristic Exponents for smooth dynamical systems and for Hamiltonian systems; A method for computing all of them. Meccanica, 9 – 30, 1980.
3. A. Wolf, J.B. Swift, H.L. Swinney and J.A. Vastano. Determining Lyapunov exponents from a time series. Physica 16 D, 285 – 317, 1985.
4. S. P. Kuznetsov. Dynamic chaos, Fizmatlit, Moscow, 2001.
5. J. Laskar, K. Froscchle and A. Celletti. Measuring chaos using the numerical analysis of fundamental frequencies, Appendix to the standard map. Translation from English - A.G. Arzamastseva, 1992.
6. V. A. Golovko. Neural network methods for processing chaotic processes. Scientific session of MEPhI , Moscow: MEPhI, 43 – 91, 2005.
7. F. Moon. Chaotic oscillations, Translation from English. Yu. A. Danilova and A.M.Shukurova, Mir, Moscow, 1990.
8. P. Berger, I. Pomo and K. Vidal. Order in chaos. On the deterministic approach to turbulence, Translated from French. Yu.A. Danilova, Mir, Moscow, 1991.
9. D. P. Crutchfield. Chaos. In the world of science, 2, 18 – 28, 1987.
10. V. I. Oseledets, Multiplicative ergodic theorem. Lyapunov characteristic exponents of dynamical systems. Proceedings of the Moscow Mathematical Society, 19, 179 – 210, 1968.
11. T. S. Krasnopolskaya, V.V. Meleshko, G.W. M. Peters and H. E. H. Meijer. Mixing in Stokes flow in an annular wedge cavity. Eur. J. Mech., B_Fluids, 18, 793 – 822, 1999.
12. V. V. Meleshko, T. S. Krasnopolskaya, G.W. M. Peters and H. E. H. Meijer. Coherent structures and scales of Lagrangian turbulence. Advances in Turbulence_VI, Dordrecht, Kluwer, 601 – 604, 1996.
13. F. Takens. Detecting strange attractors in turbulence. Lecture Notes in Mathematics, Springer-Verlag, Berlin, 898, 366 – 381, 1980. and in Dynamical System in Turbulence, Warlock, Eds. D. Rand and L. S. Young, 1980.
14. T. P. Konovalyuk, E. D. Pechuk, T. V. Sobol and T. S. Krasnopolskaya. Influence of the Heart Rate on Dynamics of Cardiorespiratory System. Springer Proceedings in Complexity, 211 – 216, 2020.

New fractal features for textural morphologic analysis

Alexander A. Potapov[1,2], Viktor A. Kuznetsov[3], and Anton N. Pototskiy[3]

[1] V. A. Kotelnikov Institute of Radio Engineering and Electronics, Russian Academy of Sciences, Moscow, Russia
(E-mail: potapov@cplire.ru)

[2] JNU-IREE RAS Joint Lab. of Information Technology and Fractal Processing of Signals, JiNan University, Guangzhou, 510632, China
(E-mail: potapov@cplire.ru)

[3] Air Force Academy, Voronezh, Russia
(E-mail: kuzzviktor@mail.ru, AntonPototskiy@mail.ru)

Abstract. Significantly increased resolution of image formation systems (down to a few centimetres) causes a possibility of more effective using of objects textural features and signs in case of thematic processing of radar and optical images. The existing methods of image fractal features measurement allows to evaluate numerically the following topological characteristics of image texture: fractal dimension FD; directional FD in the analysis directions (DFD); multifractal dimension MFD (a widespread case – the spectrum of Renyi dimensions (SRD)); morphological multifractal exponent (MME); fractal signature FS and directional FS (DFS); morphological MFS (MMFS) and lacunarity. However today there are no complex methods allowing to measure at the same time parameters of the scaling, multifractal and anisotropic properties of a texture possessing reciprocal relationships. In this work the specificities of new Directional Multifractal Blanket method (morphological) ($DMBM_M$) for fractal features measurement of an image textures synthesized on the basis of two best ABRG and MBM_M methods in the groups, are considered. Simultaneous accounting of multifractal, singular and anisotropic properties of the image texture with limited scaling character allowed to increase measuring accuracy both FD, and FS at each analysis scale. This feature is the most representative on comparing with all features considered in this work as the functional correlation of the derived features. The increased informativeness of the developed feature in case of image processing is caused by additional determination, along with multifractal and singular properties, anisotropic properties and their joint account and implied the possibility of its using for the properties description of different images textures and also in images clustering and segmentation tasks.

Keywords: Fractal dimension, Multifractal signature, Directional features, Anisotropic textures.

Headings content

Abbreviations

ABRG – augmented iterative covering blanket method with rotating grid.
AFS – anisotropic fractal surface.
DFD – directional fractal dimension.
DFS – directional fractal signature.
$DMBM_M$ – directional multifractal blanket method (morphological).
DMFS – directional multifractal signature.
DMMFS – directional morphological multifractal signature.
FD – fractal dimension.
FS – fractal signature.
L – lacunarity.
LFD – local fractal dimension.
LMME – local morphological multifractal exponent.
MBM_M – morphological multifractal iterative covering blanket method.
MFD – multifractal dimension.
MFS – multifractal signature.
MME – morphological multifractal exponent.
MMFS – morphological multifractal signature.
SRD – spectrum of Renyi dimensions.

1 Introduction

The modern air- and space-based monitoring systems of Earth pro-vides formation of high resolution optical and radar images for the wide range solutions of remote sensing, reconnaissance and special tasks. Significantly increased resolution of image formation systems (down to a few centimeters) causes a possibility of more effective using of objects textural features and signs in case of thematic processing of radar and optical images [1, 2]. Textural approach [3] is based on the fact, that in most cases spatial configurations of high resolution images brightness units within boundaries of heterogeneous classes of objects have essential differences. Specific numerical values of textural features decide on the help of different mathematical apparatuses among which it is possible to select the wavelet-analysis, Fourier analysis, variance analysis and also a number of the modern methods, based on the fractal theory [1, 2].

In fundamental research in the fractal theory field [1, 4], and also related practical applications of digital image processing [5–10], formulated and proved statements about presence of fractal properties and the characteristic features corresponding to them at images of natural objects. The most distinctive properties of fractal sets are the scale invariance (scaling), the continuity and nondifferentiability described within the mathematical theory of the fractional integro-differential equations [1, 4].

Fractal processing implies receiving numerical evaluations of scale invariance indices of the image texture, by means of a research of local and global topological features of spatial structure of its intensity field, and the subsequent image differentiation on homogeneous areas on the basis of the measured values [1, 10]. Now the methods of the automatic analysis and thematic processing of images based on separate using of the estimated values of different fractal features are developed. Such widely used features include the fractal and the multifractal dimensions (FD and MFD), the fractal and the multifractal signatures (FS and MFS), allowing to find areas of textural homogeneity on images with different efficiency.

Both in foreign, and in domestic scientific publications there was a many results describing researches of new methods of measurement of scaling, spatial, statistical and other parameters of fractal sets taking into account textural images formation features (see, for example, [1, 2, 10–14]). At the same time such properties of images as multifractality, singularity (in a broad sense – the local non-uniformity), limited scaling feature and anisotropic are taken into account. However today there are no complex methods allowing to measure at the same time parameters of the scaling, multifractal and anisotropic properties of a texture possessing reciprocal relationships.

The purpose of this work is to synthesize of a new directional morphological multifractal signature computation method for image texture, a research of its functional capabilities, assessment of measuring accuracy of some fractal features by the developed method when processing of the test synthesized and real images both fitting, and not meeting a self-similarity condition and also determination of new textural-fractal features informativeness in tasks of the images textural analysis.

2 Description of images texture fractal features

The existing methods of the image fractal features measurement al-lows to evaluate numerically the following topological characteristics of image texture: the FD; the directional FD in the analysis directions (DFD); the MFD (in the wide sense – the spectrum of Renyi dimensions (SRD)); the morphological multifractal exponent (MME); the FS and the directional FS (DFS); the morphological MFS (MMFS) and lacunarity (L) [1, 2, 15]. These fractal features are systematized in Table 1. The main properties of these features are characterized as follows.

Table 1 – Fractal features of an images texture

Sign	Symbol	Mathematical formulations
FD	D	$D = \lim\limits_{\varepsilon \to 0} \dfrac{\log N(\varepsilon)}{\log(1/\varepsilon)}$
MFD	$\left[D_q \right]$	$D_q = (1-q)^{-1} \lim\limits_{\varepsilon \to 0} \dfrac{\log(I(\varepsilon))}{\log(1/\varepsilon)}$
DFD	$\left[D(\varphi_n) \right]$	$D(\varphi_n) = \lim\limits_{\varepsilon \to 0} \dfrac{\log N(\varepsilon, \varphi_n)}{\log(1/\varepsilon)}$
FS	$\mathbf{S} = \left[D(\varepsilon) \right]$	$D(\varepsilon) = \left(\log \dfrac{\varepsilon}{\varepsilon+1} \right)^{-1} \log \dfrac{A(\varepsilon+1)}{A(\varepsilon)}$
DFS	$\mathbf{S}_n = \left[D(\varepsilon, \varphi_n) \right]$	$D(\varepsilon, \varphi_n) = \left(\log \dfrac{\varepsilon}{\varepsilon+1} \right)^{-1} \log \dfrac{A(\varepsilon+1, \varphi_n)}{A(\varepsilon, \varphi_n)}$
MME	$\left[L_q \right]$	$L_q = \dfrac{1}{\lvert q \rvert} \lim\limits_{\varepsilon \to 0} \dfrac{\log(Z(q, \varepsilon))}{\log(1/\varepsilon)}$
MFS	$\mathbf{S}_q = \left[L_q(\varepsilon) \right]$	$L_q(\varepsilon) = \left(\log \dfrac{\varepsilon}{\varepsilon+1} \right)^{-1} \log \dfrac{Z(q, \varepsilon+1)}{Z(q, \varepsilon)}$
L	$\left[\Lambda(\varepsilon) \right]$	$\Lambda(\varepsilon) = \left(M^2(\varepsilon) - (M(\varepsilon))^2 \right) \Big/ (M(\varepsilon))^2$
	$\left[C(\varepsilon) \right]$	$C(\varepsilon) = (M(\varepsilon) - N(\varepsilon)) \big/ (M(\varepsilon) + N(\varepsilon))$
DMFS	$\mathbf{S}_{q,n} = \left[L_q(\varepsilon, \varphi_n) \right]$	$L_q(\varepsilon, \varphi_n) = \left(\log \dfrac{\varepsilon}{\varepsilon+1} \right)^{-1} \log \dfrac{Z(q, \varepsilon+1, \varphi_n)}{Z(q, \varepsilon)}$
	$\mathbf{S}_{q,n}^{\text{opt}} = \left[L_q\left(\varepsilon\left(\varphi_{n_{opt}} \right) \right) \right]$	$\exists L_q\left(\varepsilon\left(\varphi_{n_{opt}} \right) \right) \in \left[L_q(\varepsilon, \varphi_n) \right]$, $n_{\text{opt}} = \left\lfloor \Delta\varphi^{-1}(\pi/2 + \psi(q, \varepsilon)) \right\rfloor$

In geometry terms, the FD D characterizes a level of the isotropic surface texture «roughness» (in case of $D = 2$ the surface formed by a combination of the image brightness units is absolutely smooth, and in case of $D = 2$ – infinitely «wrinkled»).

The Renyi dimensions D_q are sensitive to the inhomogeneities of the analyzable surface which is characterized by combining of areas with different the FD's and allow to describe the global and local topological features of the texture. The DFD components collection $D(\varphi_n)$ allows to define correctly a level of the anisotropic fractal surface (AFS) «roughness» which is characterized by the different values of the FD along the analysis different angular directions $n_{\max}$.

In [2, 16, 17] it is marked that in case the FD computation D of the images texture loss of information on its singularities can happen by the known methods. This negative aspect is caused by the fact that the image **I** self-similarity remains only within some limited range of degree dependence of the evaluated image measure on the analysis scale ε constructed in double logarithmic scale and approximated by linear dependence. At the same time the great value is acquired by the «personal» topological features of the image texture, but not average implementations having often absolutely other character [1, 2, 9, 14, 18].

For successful permission of this mismatch in the above-mentioned articles the signature approach consisting in finding of the local fractal dimensions (LFD) $D(\varepsilon)$ calculated for the adjacent analysis scales ε and $\varepsilon + 1$ is offered and reasonable and with their subsequent combining in an ordered set – the FS $S = \{D(\varepsilon)\}$, where $\varepsilon = \overline{1, \varepsilon_{\max} - 1}$, and $\varepsilon_{\max}$ is the maximum number of analyzable scales.

The FS distinctive feature of the images having strictly scale and invariant properties is the persistence of the LFD values in all range of the analyzable scales. Computation of the FS allows to reveal the images texture singularities even in that case when they have no the fractal properties. Thus, the FS **S** characterizes the scaling ratio of a measure variation of the researched surface and existence of the scale singularities of its texture.

It is necessary to mark a number of articles [19–26] devoted to the description of the anisotropic properties of a texture in the case of measurement of the DFS Sn in the tasks of automated processing of X-ray images of a human bone tissue and microsamples of the constructional materials. This sign is closely related to the parameterization of the texture directional properties taking into account scale singularities.

The sign $\left[L_q\right]$ is the SRD $\left[D_q\right]$ alternative in the case of the MME spectrum calculation with using the image morphological processing.

The applying of the MMFS $\mathbf{S}_q$ is intended for assessment of the local MME variation measure (LMME) $L_q(\varepsilon)$ and allows to consider at the same time both the singular and multifractal texture properties.

The lacunarities $\left[\Lambda(\varepsilon)\right]$ and $\left[C(\varepsilon)\right]$ respectively allow to obtain the average information on (filling) of the fractal surface «mass» distribution at the big and small analysis scales.

Arguments of the features shown in Table 1 are provided by the following parameters: $N(\varepsilon)$ is the number of cubes with the side (scale) ε in the case of cellular partition completely covering the researched image surface; $\mathbf{I}(q,\varepsilon)$ is the generalized statistical amount (a probability multifractal measure of the image surface area distribution) with number of the scaling moments orders q; $Z(q,\varepsilon)$ is the generalized statistical amount evaluated in the case of morphological computation $\mathbf{I}(q,\varepsilon)$ with use of the structural elements set which value w corresponds to the analyzable scale, where $w = 2\varepsilon + 1$; $A(\varepsilon)$ is the image surface area evaluated at the scale ε; $M^2(\varepsilon)$ is the fractal set mass; $(M(\varepsilon))^2$ is the fractal set expected mass; n is the analysis angular direction number; $\Delta\varphi$ is the elementary angular direction; $\mathbb{Z}$ is the set of integer numbers; $[\cdot]$ is the array of values; $\exists$ is the existential quantifier at least the one element from the definition range.

The high resolution optical and radar images with the significantly heterogeneous texture are characterized by the both scale singularities, and the anisotropic and multifractal properties therefore the productive applying of the known fractal features in the case of image processing of the similar character encounters a restrictions number. This is because, on the one hand, the fractal features describes preferentially separated aspects of the texture properties, without its complex, integrative character, and on the other hand, in the case of their sharing, the correlations existence accounting between the texture elements components is not carried out, i.e. the signs components connected, in essence, in fact are calculated «separately» (independent) from each other. Finally, the characteristics measured in this way lose the image texture specified properties description integrity.

The peculiarities discussed in terms of the high resolution images fractal theory and the also limited information pithiness of the listed fractal features point to need for the complex morphological method development allowing to derive at the same time scaling, multifractal and anisotropic properties of the image texture with measurement of the most relevant of them that is taking into account their reciprocal relationships.

3 Synthesis of the directional morphological multifractal signature measurement method

Basis of the new method allowing to reveal not only multifractal and singular, but also anisotropic properties of processed images, the morphological implementation of the augmented iterative covering blanket method with rotating grid (ABRG) [24] with the modified choice procedures of the rotating grid size and formation of the horizontally oriented structural elements set makes. The choice in favor of morphological processing is because the morphological

extension (dilatation) and the morphological corrupting (erosion) of the processed image surface by the structural element allows to consider all surface irregularities which extent we will commensurate with the size of the structural element, and, thus, to make the image analysis at the given scale ε. Besides, the FD and the FS measurement methods by means of the morphological implementation have the high accuracy. For accounting of the multifractal properties of an image texture in this work the morphological multifractal iterative covering blanket method (MBM_M) is used [17].

The entity of the developed method consists in computation of the upper and lower coverings set by means of the ABRG method [24] rotating grid modified by authors, the LMME $L_q(\varepsilon,\varphi_n)$ used in the computation case (see a line 9 of Table 1) for the required number of the analysis angular directions of the processed image by the MBM_M method and formation of the directional morphological multifractal signature (DMMFS) in the «direction-scale» coordinates for each order q of the scaling moment.

The procedure of the image $\mathbf{I}$ texture DMMFS $\boldsymbol{S}_{q,n}$ computation can be presented in a general view by the linear and non-linear operators set

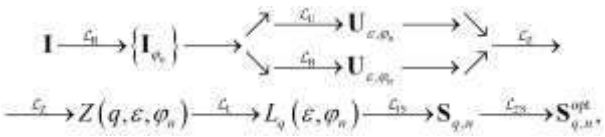

where L_R is the set $\left\{\mathbf{I}_{\varphi_n}\right\}$ formation function of turned on the required number angular provisions of source image I copies; L_U and L_B is the calculation functions according to the dilatation and the erosion $\left\{\mathbf{I}_{\varphi_n}\right\}$ with use of the horizontally oriented structural elements set Yε; L_Z is the calculation function of the generalized statistical amount $Z(q,\varepsilon,\varphi_n)$; L_L is the LMME $\left[L_q(\varepsilon,\varphi_n)\right]$ array calculation function; L_{1S} is the $\mathbf{S}_{q,n}$ formation operator; L_{2S} is the realizing the LMME $L_q\left(\varepsilon\left(\varphi_{n_{opt}}\right)\right)$ choice operator which is corresponding to the prevailing direction of a texture elements orientation for each scale of the analysis from a set $\left[L_q(\varepsilon,\varphi_n)\right]$ and the $\mathbf{S}_{q,n}^{opt}$ formation, where nopt is the image turn number (the analysis direction) corresponding to the prevailing direction of a texture elements orientation.

As the input, intermediate and output variables serve: $\mathbf{I}=\left[I(i,j)\right]$, $I_{i,j}\in\overline{0,2^{v-1}}$, $i=\overline{1,M}$, $j=\overline{1,N}$ is the digital grayscale image containing M lines and N columns, presented in the matrix form with the quantized brightness levels in the appropriate image pixel; v is the brightness quantization level; $\left\{\mathbf{I}_{\varphi_n}\right\}$ is the

array (set) of the source image **I** turned copies, where $n = \overline{1, n_{\max}}$, $n_{\max} = \pi/\Delta\varphi$ is the number of turns (the image analysis directions); $\mathbf{U}_{\varepsilon,\varphi_n}$ and $\mathbf{B}_{\varepsilon,\varphi_n}$ is the «upper» and «lower» surfaces set created as a result of morphological processing $\left\{\mathbf{I}_{\varphi_n}\right\}$, where $\mathbf{U}_\varepsilon = \left[U_\varepsilon(i,j)\right]$ and $\mathbf{B}_\varepsilon = \left[B_\varepsilon(i,j)\right]$; $\mathbf{Y}_\varepsilon = \left[Y_1, Y_2, ..., Y_{\varepsilon_{\max}}\right]$ is the «plane» structural elements set in the horizontally oriented lines form of pixels which length w corresponds to the analyzable scale $w = 2\varepsilon + 1$; $Z(q,\varepsilon,\varphi_n)$ is the generalized statistical amount with number of the scaling moments orders $-\infty < q < \infty$, $q \neq 0$; $L(\varepsilon,\varphi_n)$ is the LMME created for n analysis directions; $\mathbf{S}_{q,n}$ is the directional morphological multifractal signature; $\mathbf{S}_{q,n}^{\text{opt}}$ is the directional morphological multifractal signature with the reduced dimensionality which formation method explicitly was considered in the work [26], considering only the prevailing directions of a texture elements orientation at the different spatial scales.

Computation according to the source image **I** with size by $M \times N$ pixels of the upper and lower coverings is made for the nmax copies $\mathbf{I}_{\varphi_n}$ of the image turned on the angle $\Delta\varphi = \overline{\frac{\pi}{180}, \frac{\pi}{2}}$ of the size $M' \times M'$ using of the dilatation and the erosion operations by the modified set of the structural elements Yε, where $M' = \left\lceil \sqrt{(M+1)^2 + (N+1)^2} \right\rceil + 1$; $\lceil \square \rceil$ is the rounding operator to the nearest whole to the big side. At the same time the upper $\mathbf{U}_{\varepsilon,\varphi_n}$ and lower $\mathbf{B}_{\varepsilon,\varphi_n}$ coverings values for scale $\varepsilon = 0$ are equal to the source images on an output of the turn operator $\mathrm{L_R}$

$$\mathbf{U}_{0,\varphi_n} = \mathbf{B}_{0,\varphi_n} = \mathbf{I}_{\varphi_n}, \tag{1}$$

and for the scales $\varepsilon > 1$ are defined by the expressions

$$U_{\varepsilon,\varphi_n}(i,j) = \max \mathbf{I}'_{\varphi_n}; B_{\varepsilon,\varphi_n}(i,j) = \min \mathbf{I}'_{\varphi_n}, \ \mathbf{I}'_{\varphi_n} \in \mathbf{X}_\varepsilon, \tag{2}$$

where $\mathbf{X}_\varepsilon = \left\{I_{\varphi_n}(i,j')\right\}, |j' - j| \le \lceil (w-1)/2 \rceil$ is the definition range of a structural element at the scale ε.

The surface area of the turned image $\mathbf{I}_{\varphi_n}$ sequentially is calculated for each scale on the basis of calculated the upper $\mathbf{U}_{\varepsilon,\varphi_n}$ and lower $\mathbf{B}_{\varepsilon,\varphi_n}$ coverings $S(\varepsilon,\varphi_n) = V(\varepsilon,\varphi_n)/2\varepsilon$, where $V(\varepsilon,\varphi_n) = \sum_{i=1}^{W}\sum_{j=1}^{W}\left(U_{\varepsilon,\varphi_n}(i,j) - B_{\varepsilon,\varphi_n}(i,j)\right)$ is the

image surface «volume» in the $W\times W$ window concluded between the lower and upper coverings.

The generalized statistical amount $Z(q,\varepsilon,\varphi_n)$ as a distribution function of a multifractal q-order set measure of at each analyzable scale ε for each turned image $\mathbf{I}_{\varphi_n}$ is determined by the equation

$$Z\left(q,\varepsilon,\varphi_n\right)=S\left(\varepsilon,\varphi_n\right)\sum_{i=1}^{W}\sum_{j=1}^{W}\left|U_{\varepsilon,\varphi_n}\left(i,j\right)-B_{\varepsilon,\varphi_n}\left(i,j\right)\right|^{q}V^{-1}\left(\varepsilon,\varphi_n\right), \tag{3}$$

where the scaling moment order q lies in value range $q\in\square$, $q\neq 0$, $\square$ is the integral numbers set. Here the $\mathbf{S}(\varepsilon,\varphi_n)$ provides computation of the morphological FD, entered in [27] (the similarity dimensionality analog $D_q\big|_{q=0}$ determined by the multifractal cellular method by means of the Renyi dimension spectrum finding), in the case of $Z_q\left(\varepsilon,\varphi_n\right)\big|_{q=1}$.

The MFS formation is carried out by the generalized statistical amount $Z(q,\varepsilon,\varphi_n)$ behavior determination between the adjacent analysis scales. The LMME calculation $Lq(\varepsilon,\varphi_n)$ according to expression is for this purpose made:

$$L\left(q,\varepsilon,\varphi_n\right)=\left(\log\frac{\varepsilon}{\varepsilon+1}\right)^{-1}\log\frac{Z\left(q,\varepsilon+1,\varphi_n\right)}{Z\left(q,\varepsilon\right)}. \tag{4}$$

The DMMFS array $\mathbf{S}_{q,n}$ values registers in the look

$$\mathbf{S}_{q,n}=\begin{bmatrix}\mathbf{L}_{-\infty}\left(\varepsilon_1\right) & \mathbf{L}_{-\infty}\left(\varepsilon_2\right) & \cdots & \mathbf{L}_{-\infty}\left(\varepsilon_{\max}-1\right)\\ \vdots & \vdots & \cdots & \vdots\\ \mathbf{L}_{-1}\left(\varepsilon_1\right) & \mathbf{L}_{-1}\left(\varepsilon_2\right) & \cdots & \mathbf{L}_{-1}\left(\varepsilon_{\max}-1\right)\\ \mathbf{L}_{1}\left(\varepsilon_1\right) & \mathbf{L}_{1}\left(\varepsilon_2\right) & \cdots & \mathbf{L}_{1}\left(\varepsilon_{\max}-1\right)\\ \vdots & \vdots & \ddots & \vdots\\ \mathbf{L}_{\infty}\left(\varepsilon_1\right) & \mathbf{L}_{\infty}\left(\varepsilon_2\right) & \cdots & \mathbf{L}_{\infty}\left(\varepsilon_{\max}-1\right)\end{bmatrix}, \tag{5}$$

where $\mathbf{L}_q\left(\varepsilon\right)=\left[L_q\left(\varepsilon,\varphi_1\right)\quad L_q\left(\varepsilon,\varphi_2\right)\quad\cdots\quad L_q\left(\varepsilon,\varphi_{n_{\max}}\right)\right]^{\mathrm{T}}$ is the column vector LMME of dimensionality nmax of an order q of the given analysis scale ε, $\left[\square\right]^{\mathrm{T}}$ is the transposing operator.

In the work [26] for lowering of the DMMFS dimensionality and accounting only of the significant anisotropic properties of the analyzable image the procedure of the texture elements prevailing orientation directions determination based on approximations by the LMME values set ellipses

$\left[L_q\left(\varepsilon,\varphi_n\right)\right]$ in the case of the given indices q and ε in a polar coordinate system and determination of the ellipticity coefficient $kec(q,\varepsilon)$ and the ellipse slope angle $\psi(q,\varepsilon)$ with the subsequent formation of the DMMFS with the reduced dimensionality $\mathbf{S}_{q,n}^{\text{opt}}$ is offered. The accounting of the prevailing orientation direction of a texture elements in the DMMFS $\mathbf{S}_{q,n}$ is carried out by a choice from the LMME array $\left[L_q\left(\varepsilon,\varphi_n\right)\right]$ for each q and ε the measure value $L_q\left(\varepsilon\left(\varphi_{n_{opt}}\right)\right)$ in the turn number case $n_{\text{opt}}=\left\lfloor\Delta\varphi^{-1}\left(\pi/2+\psi\left(q,\varepsilon\right)\right)\right\rfloor$ provided that there $kec(q,\varepsilon)$ is the less threshold value ktr, where $\lfloor\cdot\rfloor$ is the rounding operator to the nearest whole to the smaller side.

As a result of the LMME $L_q(\varepsilon,\varphi_n)$ choice by the criterion of the texture elements prevailing (optimum) orientation direction, the DMMFS takes the form

$$\mathbf{S}_{q,n}^{\text{opt}}=\begin{bmatrix} L_{q\min}\left(\varepsilon_1\left(\varphi_{n_{opt}}\right)\right) & \cdots & L_{q\min}\left(\varepsilon_{\max-1}\left(\varphi_{n_{opt}}\right)\right)\\ \vdots & \cdots & \vdots \\ L_{-1}\left(\varepsilon_1\left(\varphi_{n_{opt}}\right)\right) & \cdots & L_{-1}\left(\varepsilon_{\max-1}\left(\varphi_{n_{opt}}\right)\right)\\ L_{1}\left(\varepsilon_1\left(\varphi_{n_{opt}}\right)\right) & \cdots & L_{1}\left(\varepsilon_{\max-1}\left(\varphi_{n_{opt}}\right)\right)\\ \vdots & \ddots & \vdots \\ L_{q\max}\left(\varepsilon_1\left(\varphi_{n_{opt}}\right)\right) & \cdots & L_{q\max}\left(\varepsilon_{\max-1}\left(\varphi_{n_{opt}}\right)\right) \end{bmatrix}. \quad (6)$$

Thus, the DMMFS and the DMMFS with reduced dimensionality receiving numerical evaluations peculiar properties by using the directional morphological multifractal blanket method ($DMBM_M$) by the fractal signatures computation means for the given scaling moments orders q taking into account the prevailing orientation directions of the image texture elements are considered.

Conclusions

In this work the specificities of the new $DMBM_M$ method for fractal features measurement of an image textures synthesized on the basis of two best the ABRG and the MBM_M methods in their groups, are considered. Simultaneous accounting of the multifractal, singular and anisotropic properties of the image texture with limited scaling character allowed to increase measuring accuracy both the FD, and he LFD at each analysis scale.

References

1. A. A. Potapov Fractals in Radiophysics and Radiolocation: Sample Topology, Universitetskaya kniga, Moscow, 2005, [in Russian].
2. A. A. Potapov Postulate “The Topology Maximum at the Energy Minimum” for Textural and Fractal-and-Scaling Processing of Multidimensional Super Weak Signals against a Back-ground of Noises, In: L. A. Uvarova, A. B. Nadykto, A.V. Latyshev Nonlinearity: Problems, Solutions and Applications, 2nd edition, Nova Science Publ., New York, 2017.
3. R. M. Haralick, K. Shanmugan, I. Dinstein Textural Features for Image Classification, IEEE Trans SMC-3(6), 610{621, 1973.
4. B. B. Mandelbrot The Fractal Geometry of Nature. Freeman, New York, 1982.
5. A. P. Pentland Fractal-based description of natural scenes, IEEE Trans Pattern Annal Mach Intell, 6(6), 661{674, 1984.
6. H.-O. Peitgen, B. Saupe The Science of Fractal Images, Springer, New York, 1988.
7. K. J. Falconer The Geometry of fractal sets, Cambridge tracts in mathematics, Vol. 85, University Press, Cambridge, 1985.
8. L. M. Novak Thinking in Patterns: Fractals and Related Phenomena in nature, World Scientific, Singapore, 2004.
9. R. F. Voss Random fractals: Characterization and measurement, Physica Scripta, 13, 27{32, 1986.
10. A. A. Potapov, Yu. V. Guliaev, S. A. Nikitov, A. A. Pakhomov, V. A. German Latest Techniques of Image Processing, Fizmatlit, Moscow, 2008, [in Russian].
11. G. A. Andreev, A. A. Potapov, A. V. Gorbunov Sravnitel'nyy analiz statisticheskikh priznakov opticheskikh i radioizobrazheniy pochvenno-rastitel'nykh ob'yektov, Issledovanie Zemli iz kosmosa, 1, 112{121, 1990, [in Russian].
12. A. A. Potapov, T. V. Galkina, T. I. Orlova, Ya.L. Khlyavich Dispersion detection method of de-termined object at texture optical and radar images of earth surface, Radiotekhnika i Electronica, 35(11), 2295{2301, 1990, [in Russian] .
13. A. A. Potapov, T. V. Galkina, A. I. Kolesnikov O klassifikatsii izobrazheniy po ikh teksturnym priznakam, Issledovanie Zemli iz kosmosa, 2, 91{96, 1990, [in Russian].
14. A. A. Potapov, V. A. German Methods of measuring the fractal dimension and fractal signatures of a multidimensional stochastic signal, Journal of Communications Technology and Electronics, 49(12), 1370{1391, 2004, [in Russian].
15. V. A. Kuznetsov, A. N. Pototsky Method of measuring directional morphological multifractal signatures of the texture images, Achievements of Modern Radioelectronics, 3, 39{52, 2017, [in Russian].
16. S. Peleg, J. Naor, R. Hartley Multiple resolution texture analysis and classification, IEEE Trans Pattern Annal Mach Intell, 6(4), 518{523, 1984.
17. Y. Xia, D. Feng, R. Zhao, Y. Zhang Multifractal signature estimation for textured image segmentation, Pattern Recognit Lett, 31, 163{169, 2010.
18. A. A. Potapov Topology of Sample, Journal Nonlinear World, 2(1), 4{13, 2004, [in Russian].
19. G. Jacquet, W. Ohley, C. Fortin Bone texture characterization by oriented fractal analysis, In Proceedings of the 18th IEEE on Bioengineering, 18, 22{23, 1988.

20. W. J. Yi, M. S. Heo, S. Lee Direct measurement of trabecular bone anisotropy using directional fractal dimension and principal axes of inertia, Oral Surg Oral Med Oral Pathol Oral Radiol Endod, 104, 110{116, 2007.
21. J. A. Lynch, D. J. Hawkess, J. C. Bukland-Wright Analysis of texture in macroradiographs of osteoarthritic knees, using the fractal signature, Phys Med Biol, 36(6), 709{722, 1991.
22. P. Podsiadlo, G. W. Stachowiak The development of the modified Hurst Orientation Transform for the characterization of surface topography of wear particles, Tribology Lett, 3, 215{229, 1998.
23. M. Wolski, P. Podsiadlo, G. W. Stachowiak Directional fractal signature analysis of trabecu-lar bone: evaluation of different methods to detect early osteoarthritis in knee radiographs, Proc Inst Mech Eng, 223(2), 211{236, 2009.
24. M. Wolski, P. Podsiadlo, G. W. Stachowiak Directional Fractal Signature Analysis of Self-Structured Surface Textures, Tribology Lett, 47, 323{340, 2012.
25. A. A. Potapov, V. V. Bulavkin, V. A. German, O. F. Vyacheslavova Fractal signature methods for profiling of processed surfaces, Technical Physics, 75(5), 560{575, 2005, [in Russian].
26. A. N. Pototskiy, V. A. Kuznetsov, S. F. Galiev Sposob izmereniya morfologicheskoy mul'tifraktal'noy signatury, Patent RU2647675, 16.03.2018, [in Russian].
27. J. Samarabandu, R. Acharya, E. Hausmann Analysis of Bone X-Rays Using Morphological fractals, IEEE Trans Med Imaging, 12(3), 466{470, 1993.

The role of the angular momentum in shaping collective effects

E. Prozorova[i]
Mathematical-Mechanical Department St. Petersburg State
University Av. 28, Peterhof, 198504, Russia
(E-mail: e.prozorova@spbu.ru)

Abstract. The main goal of the work is to clarify the consequences arising from the disregard of the law of the angular momentum as an independent law. As a result, some of the collective effects in mechanics are not taken into account but they are essential. The main laws in physics and mechanics are the laws of conservation of mass, momentum, energy, angular momentum, charge, and some others. In the article it is shown that the sum of the forces is insufficient for a complete description of the interacting particles. Any redistribution of particles is accompanied by the emergence of collective effects, which is associated with the action of the angular momentum and, consequently, with the action of an additional force. The effect always manifests itself, regardless of the branch of science: the formation of fluctuations, structures, quantum mechanics and some others. When constructing a theory, it is impossible to restrict oneself to potential forces that depend only on the distance between particles, since when the particles move, the center of inertia shifts, forming a moment. In continuum mechanics, for example, the stress tensor loses its symmetry for this reason.
Keywords: Conference, CHAOS, Chaotic Modeling, CMSIM Style

1. Introduction.

Classical mechanics deals with material points and, as a rule, with closed systems. The definition of material points in mathematics and physics is different. The main equation in theoretical mechanics is the Liouville equation, which describes the motion of a system of material points of a closed system. Collective interactions occur through an external force, but the main interaction is the binary interaction of particles. The initial and boundary conditions are not considered, although the impossibility of considering them is stipulated due to the huge number of particles. However, Hamilton's formalism is legitimate to use in the case of a no dissipative system, when there is no dependence on the velocity, which is not observed in the presence of disturbing surfaces or under conditions of large gradients of velocities, temperatures, densities, or other characteristics. Using the formalism of N.N. Bogolyubov [1], for certain conditions the Boltzmann equation is derived. When deriving the Boltzmann equation and other kinetic equations, the assumption is made that the process is “Markov”, that is, there is no dependence on the “past”. In reality, however, it is partially manifested through flows at the border. The effect of the boundary is essentially visible in the calculations by the molecular dynamics method and in the numerical solution of the Boltzmann equation [2].
The solutions coincide if a large number of particles are taken and there are no flows across the border. Thus, the Boltzmann equation takes into account the change in state only within the elementary volume. Therefore, it is only suitable for small gradients. In addition, the Boltzmann equation does not fulfill the law of conservation of angular momentum. In the same work, the validity of Hilbert's hypothesis is proved about the dependence of the distribution function on time only through the dependence on macroparameters. The Navier-Stokes (Barnett, etc.) equations are derived from the Boltzmann equation by the Chapman - Enskiy method or by some other method, and the continuity equation is determined, which coincides in form with the Liouville equation. Thus, the consistency of the whole theory is proved. The concepts of “closed” and “open” systems are introduced on the example of systems of “particles”, the motion of which is described by the reversible Hamilton equations. These include, for example, the "Boltzmann" gas - a system of "structureless atoms" [3]. However, the "mathematical" and "physical" points are very different. While we are considering a “mathematical point" we are not very interested in whether it rotates or not. For a physical "point", both its rotation and the structure of the "point" under consideration are important. It is known that the moment of force (angular momentum) is responsible for rotation. The role of the angular momentum is manifested in all processes associated with the uneven distribution of particles or their physical parameters. The magnitude of the additional force is determined by the value of the gradient of physical quantities (density, speed, momentum, temperature). The action of the angular momentum, i.e. moment of forces essentially depends on the position of the axis of inertia (center of inertia). The angular momentum is a vector quantity. Additive schemes for calculating intermolecular interactions, in which non-additivity is included in the parameters of atom-atomic potentials, does not take into account the entire variety of conditions.

Analysis of the parameters included in the description of the rarefied gas flow showed that for the equilibrium distribution function the ratio of the gas mean free path l to the characteristic macro length d [4]:
for 37% of trajectories l / d> 1.0,
for 90% of trajectories l / d> 0.1,
for 99% of trajectories l / d> 0.01, etc.
The commonly used criterion l / d> 1.0, indicated above, takes the form Kn> 1; Kn = 1.0 means that l / d> 1.0 for only 37% of the trajectories, which does not satisfy the condition l / d> 1.0, while Kn = 10 satisfies the condition l / d> 1.0 for 90% of the trajectories, and Kn = 100 - for 99%.
The theory originally proposed for the solution of relaxation problems is extrapolated to the solution of problems associated with gas dynamics, including for solving problems of gas flow near the surface. Limitations of the scheme N.N. Bogolyubov stipulated by the author himself and is associated with the fulfillment of the conditions for the weakening of correlations, the existence of four characteristic time scales (respectively, spatial scales), a particular

class of solutions for the s-particle distribution function as a function that depends on time through a single-particle distribution function $f_s(t) = f_s(f)$, binary central interactions providing the law preserving the angular momentum in collision integral, the potential U rapidly falling with distance, the dominance of volume effects and neglect borders. Potential of interaction of molecules $\Phi = \Phi|\boldsymbol{r} - \boldsymbol{r}_0|$. An additional implicit assumption is the weak deviation of the distribution function from the equilibrium state. For relaxation problems and elastic collisions, all assumptions are satisfied. The case is excluded when the characteristic relaxation times of the single-particle F_1 and the two-particle $F_2$are commensurable. It should be noted that for molecules with a more complex interaction potential depending on the angle, averaging over the angle is performed before calculating the collision cross section (potential averaging). There are no studies concerning the influence of the permutation of the operations of averaging the collision cross section and the potential. Here f is the distribution function in the phase γ-space. When deriving the modified equation, the designations will remain generally accepted, that is, r is the radius vector; x - point coordinate; ξ is the velocity of the point, m is the molecular weight, and, according to the definition of the distribution function f_N, the probability of finding the system at the points $(x_i,\ \xi_i)$ in the intervals $dx_i d\xi_i$ is $f_N\ (t, x_1, \dots, x_N, \xi_1, \dots, \xi_N) dx_1, \dots, d\xi_1, \dots, d\ \xi_N)$. When calculating macroparameters through the distribution function and projecting values on the coordinate axis, the symmetry of some quantities may be violated. This can happen when calculating the pressure and the pressure tensor: $P_{ij} = m \int \mathbf{c_i}\, c_j f(\mathrm{t},\mathbf{x},\boldsymbol{\xi})\ \mathrm{d}\boldsymbol{\xi}$. The symmetry of the stress tensor is postulated on the basis of this form.
In aeromechanics, the projections of the calculated values are used, and not the indices of the velocities included in the formula. Therefore, there is no way to speak unambiguously about symmetry. Symmetry will be observed provided that the rotation of the elementary volume is canceled. The Navier-Stokes equations are obtained under the indicated condition.

An important difference between the interaction of gas and plasma molecules is the long-range nature of the interaction of plasma molecules. A distinctive feature of plasma is a combination of properties characteristic of both a continuous medium (long-range nature of the Coulomb interaction) and systems of individual particles. Therefore, the kinetic theory of plasma differs from the kinetic theory for gas. As we have already noted, there are significant differences in the definitions of mathematical and physical points. Hence, it became necessary to develop a generalized kinetic theory. The need for general definitions of physically infinitesimal scales has matured and is currently given, for example, in [3]. Fluctuations of particles in a liquid play a separate and important role. Their behavior is also determined by collective interactions. The nature of the interaction differs from the interaction of molecules in a gas and from the interaction in a plasma. It should be noted that the generally accepted kinetic equations, by virtue of considering only the translational motion of the medium, without taking into account rotation and fluxes through the boundary, do not take into account the action of the moment of force and diffusion fluxes through the boundaries. The need to take into account certain effects depends on the specific task. For example, when considering waves in a "cold" isotropic plasma, it is not necessary to take into account the angular momentum and diffusion. In any case, the absence of motion of heavy particles also does not require taking into account the moment and diffusion. The movement of electrons alone does not create a change in the position of the center of inertia (due to the difference in masses) if there is no movement of the ions. When considering the Landau collision integral (the kinetic equation for a weakly interacting gas, including a Coulomb plasma), it is necessary to take into account the influence of the moment. The question of Landau damping, which consists in the damping of a perturbation in a plasma as it propagates from the point of origin, despite the collisionless (without binary collisions) nature of the interaction of molecules, requires additional research. This work is devoted to the study of the influence of the angular momentum in collective interactions.

2. Kinetic equations

The classical derivation of the Boltzmann equation is to write the particle balance in terms of the relation for the one-particle distribution function

$f(t + dt, \boldsymbol{r} + \boldsymbol{\xi_i}\, dt, \boldsymbol{\xi_i} + \boldsymbol{F_i}\, dt\ )\, d\boldsymbol{r}\, d\boldsymbol{\xi_i} = f(\ t, \boldsymbol{r}, \boldsymbol{\xi_i}) d\boldsymbol{r}\, d\boldsymbol{\xi_i} + (\frac{\partial f}{\partial t})_{coll}\, dt$

The latter is often written in the form

$$\boldsymbol{f(t + dt, r + \ \xi_i\, dt, \xi_i + F_i\, dt)\ =\ f(t, r, \xi_i) + \widetilde{(\frac{\partial f}{\partial t})_{coll}}\, dt}\ .$$

where $(\frac{\partial f}{\partial t})_{coll}, (\frac{\partial \tilde{f}}{\partial t})_{coll}$ - are the collision integrals written in different phase spaces. Outwardly, these equalities are identical, however, the second relation is fulfilled at the times of interaction of molecules and all interactions are correlated. For gas-dynamic problems, the characteristic length of the elementary volume, for which equality (2) is written, equal to cm is small and the requirement for a large number of particles in the elementary volume is not fulfilled for altitudes of 120-300 km in the earth's atmosphere. Indeed, the required minimum size is 10^{-3}cm. Since, $N = \pi R^2 \cdot \boldsymbol{\xi} \cdot \boldsymbol{\tau} \cdot \boldsymbol{n}$, here R is the radius of the cylinder of the elementary volume; τ is the mean time of free path, then for statistical independence the number of particles N must be at least 100. Then, i.e. see. In addition, the possibility of reducing the characteristic size is limited not only by the limited computer memory, but also by the limits of applicability of the model [5,6], as well as by the growth of computational errors. In this equation, it is assumed that the elementary volume does not rotate and there are no incoming particles through the side surfaces.
When working with a physical elementary volume, it is necessary to take into account the action of the angular momentum responsible for rotation, and due to the finite value of the radius, it is necessary to take into account the arrival of molecules with a selected speed due to diffusion. We consider the hydrodynamic approximation, assuming the definition of a point in terms of the mean free path.

The usual transition to the Boltzmann equation involves expanding the function in a series and obtaining the following equation

$$\left(\frac{\partial}{\partial t} + \boldsymbol{\xi_i}\nabla_r + \boldsymbol{F_i}\nabla_i\right) \boldsymbol{f}(\boldsymbol{t},\boldsymbol{r},\boldsymbol{\xi_i}) = \left(\frac{\partial f}{\partial t}\right)_{coll} \boldsymbol{dt} = \mathrm{I}$$

Taking into account rotation and diffusion, the equation () has the form

$$f(t+dt,\boldsymbol{r} + \boldsymbol{\xi_i}\,dt + r\times\,\omega,\,\boldsymbol{\xi_i} + \boldsymbol{F_i}\,dt + \frac{\partial \mathrm{M}}{\partial \mathrm{r}}dt)\,d\boldsymbol{r}\,d\boldsymbol{\xi_i} + G_2\,(t+dt,\boldsymbol{r} + \boldsymbol{\xi_i}\,dt + r\times\,\omega,\,\boldsymbol{\xi_i} + \boldsymbol{F_i}\,dt + \frac{\partial \mathrm{M}}{\partial \mathrm{r}}dt) =$$

$$f(\,t,\boldsymbol{r},\boldsymbol{\xi_i})\boldsymbol{dr}\,\boldsymbol{d\xi_i} + G_1(t,\boldsymbol{r},\boldsymbol{\xi_i}) + \left(\frac{\partial f}{\partial t}\right)_{coll} dt.$$

M is the moment associated with the collective action of all particles on each other as a result of the displacement of the center of inertia, which is the result of the movement of particles with different speeds. G_1 and G_2 - flows through the boundaries of the considered elementary volume. Let's calculate these values.

$$G_1 = m\boldsymbol{\xi_i}\frac{\partial f}{\partial \mathbf{r}}.$$

Accounting for flows across the borderG_1, G_2) leads to the equations of S.V. Vallander [7,8]

Here E is the internal energy, $E = \mathrm{c}_v T$, where c_v is the heat capacity coefficient

$$Q_x = D_1\frac{\partial\rho}{\partial x} + D_2\frac{dT}{dx}, \quad Q_y = D_1\frac{d\rho}{dy} + D_2\frac{dT}{dy}, \quad Q_z = D_1\frac{d\rho}{dz} + D_2\frac{dT}{dz},$$

$$t_x = k_1\frac{d\rho}{dx} + k_2\frac{dT}{dx},\ t_y = k_1\frac{d\rho}{dy} + k_2\frac{dT}{dy},\ t_z = k_1\frac{d\rho}{dz} + k_2\frac{dT}{dz}$$

$$D_1 = \frac{\mu}{\rho}\alpha_1,\ D_2 = \frac{\mu}{T}\alpha_2,\quad k_1 = \frac{\mu c_v T}{\rho},\ k_2 = \mu c_v\,\beta_2,\quad \lambda = \alpha\mu,$$

Where $\alpha_1,\ \alpha_2,\ k_1,\ k_2$ are numerical constants depending on the type of gas.

Q_x, Q_y, Q_z are the mass fluxes across the face perpendicular to the coordinate axes of the moving gas with the velocity V, ρ-density, D_1, D_2 are the coefficients of self-diffusion and thermal diffusion,k_1, k_2 are the thermal conductivity coefficients, and R is the gas constant.

Here I consider it necessary to add to these equations a term related to the velocity gradient (bulk viscosity D_3, so that $Q_x = D_1\frac{\partial\rho}{\partial x} + D_2\frac{dT}{dx} + D_3\frac{\partial u}{\partial x}$. The rest of the values change in the same way. Let us recall the difference between the values obtained through the distribution function and by the molecular dynamics method [9-12].

The general formula for the distribution function (dependence on r).

$$f = f\,(t,\boldsymbol{r}(t),\boldsymbol{\xi}(t))$$

$$\frac{\partial f}{\partial t}\Big|_{r=const} = \frac{\partial}{\partial t}\frac{\sum_{i=1}^{n}\delta(\boldsymbol{r_i}-\boldsymbol{r})}{\sum_{i=1}^{N}\delta(\boldsymbol{r_i}-\boldsymbol{r})}.$$

By construction $\delta(\boldsymbol{r_i}-\boldsymbol{r})$ – depends on t only through the $\boldsymbol{r_i}\,(\boldsymbol{t}) - \boldsymbol{r}(\boldsymbol{t})$. Here n is number molecules in elementary volume, N – in full volume.

A more complex option when there are time-dependent flows across the border

1.Without flow across the border

$$\frac{F_1}{F_3} - \frac{F_2}{F_4} = \frac{\sum_{i=1}^{n}\delta(\boldsymbol{r_i}-\boldsymbol{r}) + \sum_i^n \Delta t\frac{\partial\delta(\boldsymbol{r_i}-\boldsymbol{r})}{\partial t} + \cdots}{\sum_{i=1}^{N}\delta(\boldsymbol{r}_i-\boldsymbol{r}) + \sum_i^N \Delta t\frac{\partial\delta(\boldsymbol{r}_i-\boldsymbol{r})}{\partial t} + \cdots} - \frac{\sum_{i=1}^{n}\delta(\boldsymbol{r_i}-\boldsymbol{r})}{\sum_{i=1}^{N}\delta(\boldsymbol{r_i}-\boldsymbol{r})} \approx$$

$$\approx \frac{\sum_{i=1}^{n}\delta(\boldsymbol{r_i}-\boldsymbol{r}) + \sum_i^n \Delta t\frac{\partial\delta(\boldsymbol{r_i}-\boldsymbol{r})}{\partial t} + \cdots}{\sum_{i=1}^{N}\delta(r_i-r)}\left(1 - \frac{\sum_i^N \Delta t\frac{\partial\delta(\boldsymbol{r_i}-\boldsymbol{r})}{\partial t} + \cdots}{\sum_{i=1}^{N}\delta(\boldsymbol{r_i}-\boldsymbol{r})}\right) - \frac{\sum_{i=1}^{n}\delta(\boldsymbol{r_i}-\boldsymbol{r})}{\sum_{i=1}^{N}\delta(r_i-r)}$$

$$\approx \frac{\sum_i^n \Delta t\frac{\partial\delta(\boldsymbol{r_i}-\boldsymbol{r})}{\partial t} + O\,((\Delta t)^2}{\sum_{i=1}^{N}\delta(\boldsymbol{r_i}-\boldsymbol{r})}.$$

$\frac{\partial\delta(\boldsymbol{r_i}-\boldsymbol{r})}{\partial t}$ – thus, when solving the Boltzmann equation, the time derivative of distribution function will indeed be determined by the dependence through the macro parameters. This approximation, which is made in the theory of rarefied gas in the construction of the Enskog-Chapman solution

2. If there is a flow across the border, depending only on time. The force is not.

$$\frac{F_1}{F_3} - \frac{F_2}{F_4} = \frac{\sum_{i=1}^{n}\delta(\boldsymbol{r_i}-\boldsymbol{r}) + \sum_i^n \Delta t\frac{\partial\delta(\boldsymbol{r_i}-\boldsymbol{r})}{\partial t} + \sum_j\frac{p_j\Delta t}{m}\delta\,(r_j-r) + \sum_j\frac{p_j}{m}\Delta t^2\frac{\partial\delta\,(r_j-r)}{\partial t} + \cdots}{\sum_{i=1}^{N}\delta(\boldsymbol{r_i}-\boldsymbol{r}) + \sum_i^N \Delta t\frac{\partial\delta(\boldsymbol{r_i}-\boldsymbol{r})}{\partial t} + \sum_j\frac{p_j}{m}\delta\,(r_j-r) + \sum_j\frac{p_j}{m}\Delta t\frac{\partial\delta\,(r_j-r)}{\partial t} + \cdots} - \frac{\sum_{i=1}^{n}\delta(\boldsymbol{r_i}-\boldsymbol{r})}{\sum_{i=1}^{N}\delta(r_i-r)}.$$

$\sum_j\frac{p_j}{m}\delta\,(r_j-r) = J_2 - J_1$ – is a flow of fast molecules from neighboring cells. The first two terms correspond to the number of molecules in the volume and their motion.Thus, for large gradients the role of flows across the border is increasing. The distribution function can no give a correct contribution to the distribution of molecules. We need

in large number particles in elementary volume. There remains the method of molecular dynamics with a very small time step.

Most often, the kinetic Boltzmann equation is taken as the initial one, and one of the variants of the perturbation theory in a small parameter is used to pass to the aeromechanical equations. As we can see, the Boltzmann equation, depending on the problem, requires modifications, since it does not fulfill one of the laws of theoretical mechanics, the conservation law of angular momentum. For the obtained equations, for example, for Navier-Stokes, additional assumptions are made: discarding the rotational velocity component and using Pascal's law obtained for the equilibrium case to nonequilibrium flows. As a result, the pressure becomes a scalar. Using the Boltzmann equation, we obtain an equation for the internal stress tensor. Here, the gas-dynamic functions ρ, u, T are the moments of the velocity v or the deviation of the velocity from its mean value: $\delta v = v - u$.

$$P_{ij}(r,t) = mn \int \delta v_i \, \delta v_j f(r,p,t) dp,$$

$$\left(\frac{\partial p}{\partial t} + u_k \frac{\partial p}{\partial r_k} + \frac{5}{3}\frac{\partial u_k}{\partial r_k}\right)\delta_{ij} + p\left(\frac{\partial u_i}{\partial r_j} + \frac{\partial u_j}{\partial r_i} - \frac{2}{3}\delta_{ij}\frac{\partial u_k}{\partial r_k}\right) = mn \int \delta v_i \, \delta v_j I_B(r,p,t) dp,$$

$$P_{ij}(r,t) = \delta_{ij} p(r,t) + \pi_{ij}$$

Pascal's formula does not follow from the formula and pressure is not defined as 1/3 of the sum of the pressures on the coordinate pads. An interesting feature of the all research is the emphasis on the openness of the considered elementary volumes and, despite the "openness", the use of conservation laws for closed volumes. For example, the law of conservation of energy. We have already shown that the distribution function gives an idea of a probabilistic state in an elementary volume without the influence of boundaries and, therefore, information about flows across the boundary is lost. In addition, information about the "rearrangement" of the arrangement of molecules due to the influence of the motion of the center of inertia is lost. These collective effects should be taken into account when writing kinetic equations and for equations of a continuous medium. "A unified description of kinetic and hydrodynamic processes" [3] requires the same correction. In this case, there is no contradiction between the kinetic equations, the equations for fluctuations, the Fokker-Planck equation, and the Landau damping in plasma. It is essential that these terms are not included in the collision integral. Formally, the equation is without dissipation and is reversible, but in fact the diffusion flows have dissipative properties. It should be recalled that to satisfy Hilbert's hypothesis, one should take the macroparameters of the modified Navier-Stokes equation in the solution for the locally equilibrium function, but not Euler to match the orders of approximation in the Chapman-Enskiy solution. In addition, the definition of pressure must be changed and a torque gradient must be entered. Then the nonequilibrium Chapman-Enskiy solution implies the existence of a vector distribution function, which is observed in numerical calculations when solving the Boltzmann equation [10], the proof of this is the different temperature values along the coordinate axes

Recall that the stress tensor is not symmetric and the symmetry condition for the stress tensor is one of the conditions for closing the problem; to fulfill the condition, it is required to discard the rotation of the elementary volume. For numerical calculation, the latter simplifies programming only slightly. The classic Chapman-Ensky solution is given below.

$$nf(r,p,t) = \frac{\rho/m}{(2\pi m k_b T)^{3/2}} \, exp\left[-\frac{(p-mu)^2}{2\pi m k_b T}\right] \times \left[1 + \frac{\pi_{ij}}{2p}\,\frac{m\delta v_i \delta v_j}{3k_b T} + \frac{m(\delta v_i q)}{p k_b T}\left(\frac{m(\delta v)^2}{3k_b T} - 1\right)\right].$$

Changes in the values will be in the macroparameters of the local equilibrium distribution function, the collision integral will not change. In kinetic theory, when considering the role of delay for rarefied gas, one must understand the question of what is measured in the experiment: instantaneous values or averages. If the experiment deals with average values, then it is important to choose the time and scale of averaging. At the agreed times, in this case, it is not necessary to take into account the delay, except for the cases of commensurability of the relaxation and retardation times.

3. Damping of longitudinal oscillations of an electron plasma (Landau damping), kinetic equations of Langevin and Fokker-Planck

Let us consider oscillations in a plasma without collisions, that is, let us proceed to the study of waves propagating in a plasma, the frequency of which is high in comparison with the frequency of pair collisions of electrons and ions. In this case, there are several options to consider. Landau collisional damping for large Knudsen numbers; for small Knudsen numbers in unbounded plasma; for small Knudsen numbers in a confined plasma. They differ from each other. When studying oscillations, we will consider small deviations from equilibrium [3,13-18].

Since we are interested in wave attenuation, we need to consider the plasma dielectric constant ε, which is determined by the attenuation coefficient γ. First, let's trace the waves in the "cold" isotropic plasma. The variant corresponds to the "collisionless" wave approximation. In this case, the Maxwell distribution functions

$$f_e^{(0)} = \frac{1}{(2\pi m_e k_b T)^{3/2}} exp\left(-\frac{p^2}{2m_e k_b T}\right), \quad f_i(p) = \delta(p). \; \frac{r_D}{l} \ll \frac{\lambda}{l} \ll 1,$$

the damping is determined by diffusion, but not by the Landau damping. The influence of the thermal motion of plasma particles on such oscillations is always small [3].

Here $f_e^{(0)}$ is the equilibrium distribution function, l is the mean free path r_D is the Debye radius, λ is the wavelength, the rest of the notation is generally accepted. Consider an unbounded plasma for small Knudsen numbers $l \ll \lambda$. Diffusion works here as well. Let us consider the dispersion and damping of longitudinal oscillations of an electron plasma under the influence of the thermal motion of plasma particles. Let us investigate a variant of a limited plasma, a free-molecular flow with a region of wavelengths (values of wave numbers) for which the contribution corresponding to Landau damping is the main one.
$l \to L\ (l \gg L),\ \ r_D \ll \gamma \ll \sqrt{r_D L}\ \ (r_D \ll L \ll l)$

We must use the Vlasov kinetic equations [18] with a self-consistent field. Since we are interested in high-frequency oscillations, for which $\omega\tau \gg 1$, where τ is the average time between pair collisions of particles, we can ignore the integrals of particle collisions in the kinetic equations. Longitudinal oscillations of an electron plasma in the classical case are described by the following two equations (collisionless case, Vlasov equation)

$$\frac{\partial \delta f}{\partial t} + v\frac{\partial \delta f}{\partial r} + e\delta E\frac{\partial f_0}{\partial p} = 0,$$
$$div\ \delta E = 4\pi \int dp\delta f\ .$$

$$\varepsilon_l(\omega,k)e\int dp\delta f(p,k,\omega) = i\int dre^{-ikr}e\int dp\frac{\delta f(p,r,t_0)}{\omega - kv}.$$

Suggested variant is

$$\frac{\partial \delta f}{\partial t} + v\frac{\partial \delta f}{\partial r} + e\delta E\frac{\partial f_0}{\partial p} + \frac{\partial \delta M}{\partial r}\frac{\partial f_0}{\partial p} + \frac{\partial}{\partial r}D\frac{\partial \delta f}{\partial r} = 0,$$
$$div\ \delta E = 4\pi \int dp\delta f\ .$$

$$\varepsilon_l(\omega,k)e\int dp\delta f(p,k,\omega) = i\int dre^{-ikr}e\int dp\frac{\delta f(p,r,t_0)}{\omega - kv} + i\int dre^{-ikr}\int dp\frac{\delta M(p,r,t)}{\omega - kv}\frac{\partial f_0}{\partial p}.$$

Qualitatively, we can say that for this case, diffusion plays a small role and, since part of the energy is converted into rotational motions (the action of the moment), the reversible operator will act as a dissipative one. Note that at the initial moment, the distributed moment of force also exists and concentrates a certain amount of energy. For monochromatic waves of large amplitude, the action can lead to the formation of a vertical velocity component, forming complex plane flows. Despite the collisionless nature of the movement binary collisions exist, as follows from the table of mean free paths presented in the introduction. They create additional dissipation. It should be noted that the generalized equation for a unified description of kinetic and gas-dynamic processes is suitable for "weak" interactions. As before, the contribution of the angular momentums in the motion of molecules is not taken into account. Most likely, the difference between the most probable and average values is due precisely to the lack of taking into account the rotational movements for which the moment is responsible. Similar effects will be essential for Brownian motion. The theory of Brownian motion is one of the main branches of the statistical theory of open systems. Fluctuation (from Latin fluctuatio - fluctuation) - any random deviation of any value. In mechanics, a deviation from the mean value of a random variable characterizing a system of a large number of chaotically interacting particles. In the theory of Brownian motion elementary objects are small particles, while in kinetic theory, the main objects are molecules. Both models are macromodels, but the level of description of the structure of the environment is different. Fluctuations exist both in nonequilibrium states and in unsteady processes; in their absence, relaxation would be a "smooth" process and they could be described by single-valued functions of time. The presence of thermal fluctuations causes random deviations of real processes from such a "smooth" flow. The kinetic equation corresponds to a more detailed description. We believe that the environment is in equilibrium. We will consider two approaches to solving problems: the equation for a single particle and for an ensemble of particles (the Fokker-Planck equation) To take into account the atomic structure of a liquid, Langevin introduced an additional force into the equations of motion

$$F_L = My(t),\ \ F = -M\gamma v,\ \ \gamma = \frac{6\pi a}{M}\,\eta, \qquad \eta = \rho\nu.$$

Equations

$\frac{dr}{dt} = v,\ \frac{dp}{dt} + \gamma p = F_0 + My(t),\ \ F_0 = -gradU.\ F_0 -$ external force.

$< y_i(t) >, < y_i(t), y_i(t') > = 2D\delta_{ij}(t - t'),$ the coefficient D was determined by Einstein.

First, about a single particle. Let us repeat the reasoning performed in [3,19], but replace y (t) with the moment of force M_i calculated for a given period of time. It can be calculated using the operation algorithm. As before, we assume that the characteristic correlation time of the values of the Langevin force is $\tau_{cor}^L \ll \tau_{rel} = \frac{1}{\gamma}$. As a result, we arrive at an expression for two time moments:

$$< M_i(t) > = 0, < M_i(t)M_j(t') > = 2D\delta_{ij}(t - t').$$

$D = \gamma \frac{k_b T}{m}$ – - Einstein's coefficient, parenthesis means a function from a function (functional)

When using the kinetic description of Brownian motion, it is necessary to introduce an ensemble of noninteracting Brownian particles — the corresponding Gibbs ensemble. In this case, we represent the ensemble of Brownian particles as a continuous medium. However, the difference lies in the use of the "Hamiltonian" formalism for moving particles; for a continuous medium, in this case, the Langevin equation is used. The kinetic classical Fokker-Planck equation has the form [18,19]

$$\frac{\partial f}{\partial t} + v\frac{\partial f}{\partial r} - \frac{1}{M}\frac{\partial U}{\partial r}\frac{\partial f}{\partial v} = D\frac{\partial^2 y}{\partial v^2} + \frac{\partial}{\partial v}(\gamma v f).$$

The equation of A. Vlasova

$$\left\{\frac{\partial f}{\partial t} + v\frac{\partial f}{\partial r} + e\left(E + \frac{1}{c}[vB]\right)\frac{\partial}{\partial p}\right\}F(r,p,t) = 0.$$

Here E, B are the total electric and magnetic fields, which are composed of external and self-consistent fields generated by plasma particles. They satisfy Maxwell's equations.

In the classical case, equilibrium is possible between Brownian particles and the medium; the particles can be distributed evenly [20]. However, such an assumption can be considered unlikely due to the distribution of particles over velocities and the formation of new moments for individual particles due to the motion of the center of inertia. The fact is that in this case the action of the moment creates a force that distributes the particles not only in terms of velocities, but also in coordinates. The proposed modified Fokker-Planck equation has the form:

$$\frac{\partial f}{\partial t} + v\frac{\partial f}{\partial r} - \frac{1}{M}\frac{\partial U}{\partial r}\frac{\partial f}{\partial v} + \frac{1}{M}\frac{\partial M}{\partial r}\frac{\partial f}{\partial v} = D\frac{\partial^2 y}{\partial v^2} + \frac{\partial}{\partial v}(\gamma v f).$$

Thus, in the kinetic theory for a gas, for the Landau damping and the motion of Brownian particles, the nonuniform distribution of particles in velocities and coordinates is supported by the angular momentum and creates fluctuations in physical quantities that must be taken into account. Consider the consequences associated with taking into account the moment in the mechanics of a continuous medium.

4.The influence of the angular momentum in the equations of continuum mechanics.

Conservation laws were obtained experimentally and therefore were originally written in integral form. Differential laws are obtained in two ways: using the finite volume method for an elementary volume and using the Ostrogradsky Gauss theorem by replacing the surface integral to the volume integral, that is, taking the integral by parts with further use of the theorems on the conditions Integral turning in zero. Usually the derivation of conservation laws is analyzed using the Ostrogradsky-Gauss theorem for a fixed volume without moving. The theorem is a consequence of the application of the integration in parts at the spatial case. In reality, in mechanics and physics gas and liquid move and not only progressively, but also rotate. Let us consider the consequences that arise from the generally accepted conservation laws in the mechanics of a continuous medium and which do not correspond to classical theoretical mechanics and mathematics. The speeds of various processes at the time of writing the equations were relatively small compared to modern ones. In further studies, the scope of the theory developed for potential flows to flows with significant gradients of physical parameters was expanded. It was based on the laws of balance of forces, the law of conservation of moment was considered as a consequence of the fulfillment of the law of balance of forces. Allocating the rotational velocity component and ignoring it leads to a symmetric stress tensor. The symmetric tensor is obtained only if the rotational velocity component is neglected. However, this variant of closing the problem is one of the possible variants of solving the system of three equations in the plane case for four unknowns [9-11]. A similar conclusion can be made for the three-dimensional case. For modern computer technology, it is possible to solve the complete equations of fluid mechanics, rather than truncated ones (like Navier-Stokes). From the definition of pressure, both from the classical Boltzmann equation and the modified one, it does not follow that the hydrostatic pressure is one third of the sum of the pressures on the coordinate areas. Using Pascal's law for equilibrium, the pressure is chosen equal to one third of the pressure on the coordinate pads. However, the theory remains the same when determining the different pressure on each of the sites, i.e. p_x, p_y, p_z. The use of one pressure is possible under equilibrium conditions (Pascal's law), but for nonequilibrium conditions the fact is not obvious. Neglecting outside the integral term when taking integrals by parts (the Ostrogradsky-Gauss theorem) is possible only for slow laminar flows. Writing out separately the law of equilibrium for forces and separately for moments of forces without taking into account the mutual influence, although the moment creates an additional force, we come to the conclusion about the symmetry of the stress tensor. If we consider different pressures in different directions, we lose a moment of force, but the pressure gradient is a force. The proposed modified equations of continuum mechanics include the action of the moment and are given in [9-11] and new equations:

$$\rho\left(\frac{\partial u}{\partial t}+u\frac{\partial u}{\partial x}+\ v\ \frac{\partial u}{\partial y}+w\frac{\partial u}{\partial z}\right)=\rho f_1+\frac{\partial \sigma_{xx}}{\partial x}+\frac{\partial \sigma_{yx}}{\partial y}+\frac{\partial \sigma_{zx}}{\partial z}+\rho\ f_{M_x},$$

$$\rho\left(\frac{\partial v}{\partial t}+u\frac{\partial v}{\partial x}+\ v\ \frac{\partial v}{\partial y}+w\frac{\partial v}{\partial z}\right)=\rho f_2+\frac{\partial \sigma_{xy}}{\partial x}+\frac{\partial \sigma_{yy}}{\partial y}+\frac{\partial \sigma_{zy}}{\partial z}\ +\rho\ f_{M_y},$$

$$\rho\left(\frac{\partial w}{\partial t}+u\frac{\partial w}{\partial x}+\ v\ \frac{\partial w}{\partial y}+w\frac{\partial w}{\partial z}\right)=\ \rho f_3+\ \frac{\partial \sigma}{\partial x}+\frac{\partial P\sigma_{yz}}{\partial y}+\frac{\partial \sigma_{zz}}{\partial z}+\rho\ f_{M_z},$$

$$y\left(\frac{\partial \sigma_{xz}}{\partial x}\ +\frac{\partial \sigma_{yz}}{\partial y}+\frac{\partial \sigma_{zz}}{\partial z}+\rho f_3\right)-\ z\left(\frac{\partial \sigma_{xy}}{\partial x}+\frac{\partial \sigma_{yy}}{\partial y}+\frac{\partial \sigma_{zy}}{\partial z}+\ \rho f_2\right)+\ \sigma_{zy}-\ \sigma_{zy}+\ +M_x=0,$$

$$x\left(\frac{\partial \sigma_{xy}}{\partial x}+\frac{\partial \sigma_{yy}}{\partial y}+\frac{\partial \sigma_{zy}}{\partial z}\ +\rho f_2\right)-\ y\left(\frac{\partial \sigma_{xx}}{\partial x}\ +\frac{\partial \sigma_{yx}}{\partial y}+\frac{\partial \sigma_{zx}}{\partial z}+\rho f_1\right)+\ \sigma_{yx}-\sigma_{xy}+\ +M_y=0,$$

$$x\left(\frac{\partial \sigma_{xz}}{\partial x}+\frac{\partial \sigma_{yz}}{\partial y}+\frac{\partial \sigma_{zz}}{\partial z}+\rho f_1\right)-z\left(\frac{\partial \sigma_{xx}}{\partial x}\ +\frac{\partial \sigma_{yx}}{\partial y}+\frac{\partial \sigma_{zx}}{\partial z}+\ \rho f_2\right)+\ \sigma_{zx}-\sigma_{xz}+\ +\ M_z=0.$$

Here all designations are standard, $f_{M_x}, f_{M_y}, f_{M_z}$ forces created by the moment, M_x, M_y, M_z are external moments.

5. Conclusion

The paper proposes to take into account the influence of the angular momentum (force) in kinetic equations and in stochastic processes. The definitions of a material point in mathematics and physics are different. As a result, some of the collective effects in mechanics are not taken into account. The main laws in physics and mechanics are the laws of conservation of mass, momentum, energy, angular momentum, charge, and some others. In the article it is shown that not all of the forces are enter for a complete description of the interacting particles. Any redistribution of particles is accompanied by the emergence of collective effects, which is associated with the action of the angular momentum and, consequently, with the action of an additional force. The effect always manifests itself, regardless of the branch of science: the formation of fluctuations, structures, quantum mechanics and some others. When constructing a theory, it is impossible to restrict oneself to potential forces that depend only on the distance between particles, since when the particles move, the center of inertia shifts, forming an angular momentum. In continuum mechanics, for example, the stress tensor loses its symmetry for this reason. Some modification of the theory is suggested.

Reference

1. N.N. Bogolyubov. Problems of dynamic theory in statistical physics. M: Gostekhizdat. 1946, 146 p.
2. K.P. Gurov. Foundations of the kinetic theory. M .: Nauka, 1966.350 p.
3.YL Klimontovich. Statistical theory of open systems. T. 1.2. Moscow: Lenand, 2019
4. F. Goodman, G. Vachmann. Dynamics of gas scattering by a surface. M .: Mir, 1980. 423p.
5 E.V. Prozorova Mathematical modeling of the processes of mechanics with large gradients. St.Petersburg. St. Petersburg University. 2005. 339c.
6.E.V. Prozorova The influence of dispersion in models of continuum mechanics. St.Petersburg. St. Petersburg University. 2013, 94 p.
7. S.V. Vallander. Equations of motion of a viscous gas. Reports of the Academy of Sciences of the USSR, 1951, vol. 78 (1), p. 25-27.
8. S.V. Vallander, M.P. Elovskih. The theoretical dependence of the heat conductivity of gases on temperature. Reports of the ANAS, 1951, v. 79 (1), p. 37-40.
9. E. V. Prozorova. Features of the rarefied gas description in terms of a distribution function. APhM2018.IOP Conf. Series: Journal of Physics: Conf. Series 1250 (2019) 012023.IOP Publishing. doi:10.1088/1742-6596/1250/1/012023 2.
10.Evelina Prozorova. Influence the form of writing conservation laws in computation. JP Journal of Heat and Mass Transfer, October 28, 2019; Accepted: November 23, 2019
10. Evelina Prozorova. The Effect of Angular Momentum and Ostrogradsky-Gauss Theorem in the Equations of Mechanics WSEAS TRANSACTIONS on FLUID MECHANICS DOI: 11.37394/232013.2020.15.2
11.Evelina Prozorova The influence of the no symmetric stress tensor on the flow separation WSEAS TRANSACTIONS on APPLIED and THEORETICAL MECHANICS DOI: 10.37394/232011.2020.15.9
12.Evelina Prozorova Consequences of the Ostrogradsky-Gauss theorem for numerical simulation in aeromechanics. Elsever Granthaalayah, Volume 8 Issue 6 June 2020 DOI: https://doi.org/10.29121/granthaalayah.v8.i6.2020.549
13. R. Balescu. Equilibrium and nonequilibrium statistic mechanics. A Wiley-Intersciences Publication John Willey and Sons. New-yourk-London…1975.
14. N.G. Van Kampen. Stochastic processes in physics and chemistry. North-Holland. 1984.

15. A.I. Akhiezer, I.A. Akhiezer, R.V. Polovin, A.G. Sitenko, K.N. Stepanov. Plasma electrodynamics. M.: Science, 1974
16..P. Silin. Introduction to the kinetic theory of gases. M .: Science. 1971.
17.S. Ishimaru. Basic principles of plasma physics. M .: Atomizdat. 1975.
18. A.A. Vlasov. Nonlocal statistical mechanics. M.: Science 1978.
19.Peter M¨orters and Yuval Peres Brownian .Notes on Brownian motion and related phenomena Deb Shankar Ray∗ Department of Physical Chemistry, Indian Association for the Cultivation of Science, Jadavpur, Calcutta 700032,. (February 2, 2008)
20. E. Prozorova. Mechanism of Formation for Fluctuation Phenomena. Nature Springer. Chaotic Modeling and Simulation International Conference, 978-3-030-70794-1, 497208_1_En, (Chapter 47)

Non-autonomous Two Channel Chaotic Generator: Computer Modelling, Analysis and Practical Realization

Volodymyr Rusyn[1], Christos H. Skiadas[2], Aceng Sambas[3]

[1] Department of Radio Engineering and Information Security, Yuriy Fedkovych Chernivtsi National University, Chernivtsi, Ukraine
(E-mail: rusyn_v@ukr.net)
[2] Technical University of Crete, University Campus, 73100 Chania, Crete, Greece
(E-mail: skiadas@cmsim.net)
[3] Department of Mechanical Engineering, Universitas Muhammadiyah Tasikmalaya, Tasikmalaya, Indonesia
(E-mail: acenx.bts@gmail.com)

Abstract. Circuit of the non-autonomous two channel chaotic generator that contains two operational amplifiers, four capacitors, two resistors and two sinusoidal voltage sources is presented. Regimes of chaotic behavior was modeled by using NI's software MultiSim. Analysis of chaotic attractor, time series and spectra are shown. The layout and 3D model of realization of the non-autonomous two channel chaotic generator was designed by using software Proteus 8.
Keywords: Non-autonomous, Chaotic Generator, Two-Channel, MultiSim, Proteus.

1 Introduction

Chaos has great potential and useful in many different engineering areas, such as computer and information sciences, biomedical systems, optics, power systems, robotics, memristors, telecommunications, and cyber security [1-16].
Nonlinear theory is the most interdisciplinary areas; it includes nonlinear phenomena and complex analysis that have been intensively studied and regard in many different areas ranging from mathematics and engineering to natural sciences (biology, ecology, economy) [17-22].
Some nonlinear systems were realized using Arduino and FPGA boards [23-26].
There are many different scheme-technical realizations of chaotic generators [27-32]. Great interest are non-autonomous generators that demonstrate chaotic behavior.
In this paper, we present a new non-autonomous chaotic generator that was built as two channel generator. Chaotic behavior was detected due to the frequency ratio of the two sinusoidal generators.
The paper is organized as follows. In Sect. 2, computer modelling of the circuit, main information properties such as chaotic attractor, time series and spectrum using software MultiSim are presented. In the following section, the practical realization, i.e. layout and 3D model using Proteus 8 are presented. The conclusionsare summarized in the last section.

2 Computer Modelling of the Non-Autonomous Chaotic Generator

Figure 1 shows proposed electrical scheme that realize non-autonomous two channel chaotic generator. This circuit was realized around two operational amplifiers, namely TL082. The elements used and their values were: capacitors C1 = C2 = 1 uF, C3 = C4 = 100 nF, resistors R1 = R2 = 100 Ω. The circuit was powered by a symmetrical power source of ± 9 V. Also, for realize chaotic behavior was used two sinusoidal generators with next parameters: GB1 (amplitude U_1 = 5 V, frequency f = 500 Hz) and GB2 (amplitude U_2 = 5 V, frequency f = 1000 Hz).
Simulations of the circuit behavior were carried out by using NI's MultiSim platform.

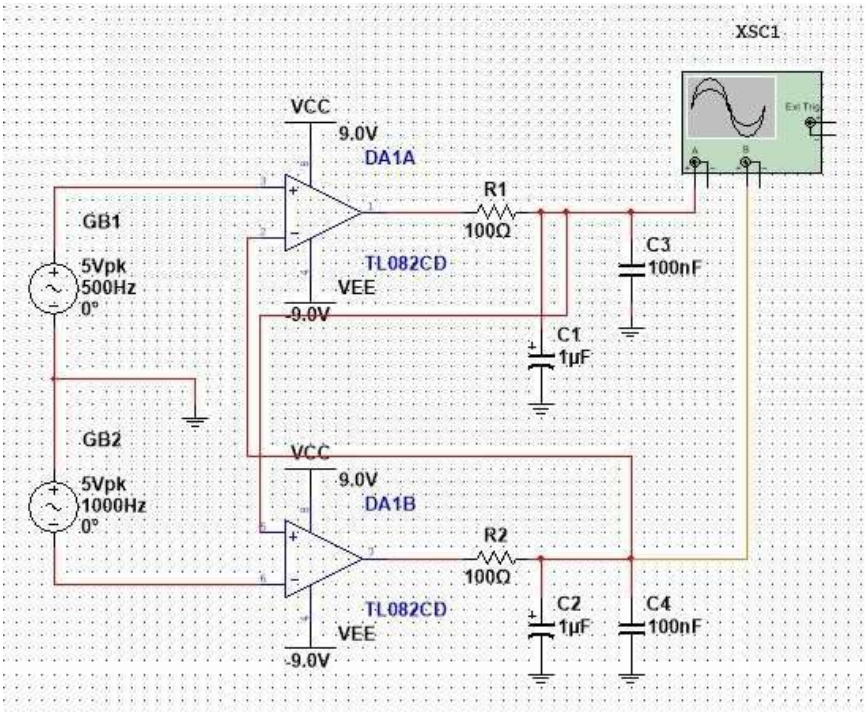

Fig. 1. Non-autonomous two channel chaotic generator

In Figure 2 the generated phase portrait namely "heart scroll" based on the circuit's chaotic signals is presented on the platform's virtual oscilloscope. The *x*-axis corresponds to the voltage of capacitor C3 (U_{C3}), which will be called the *x-signal*; while the *y*-axis corresponds to the voltage of capacitor C4 (U_{C4}), which will be called the *y-signal*. It is noted that the channels' settings were for channel A, 5 V/div and channel B, U_2 = 5 V/div. The chaotic nature of the produced attractor, as this comes out of the its complex structure, is evident.

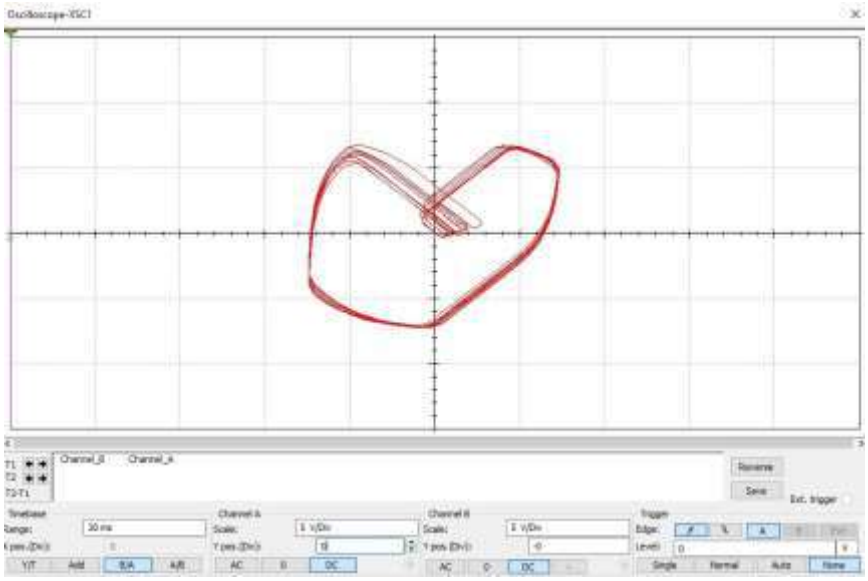

Fig. 2. The simulated chaotic attractor of the new non-autonomous chaotic oscillator

In Figure 3 the timeseries of both *x*- and *y-signals* appear. Their non-periodic nature is evident. Fig. 3 shows time dependences of the coordinates X (top) and Y (bottom) respectively (the channels' settings were for channel A, 10 V/div and for channel B, 10 V/div. Timescale 2 ms/div.

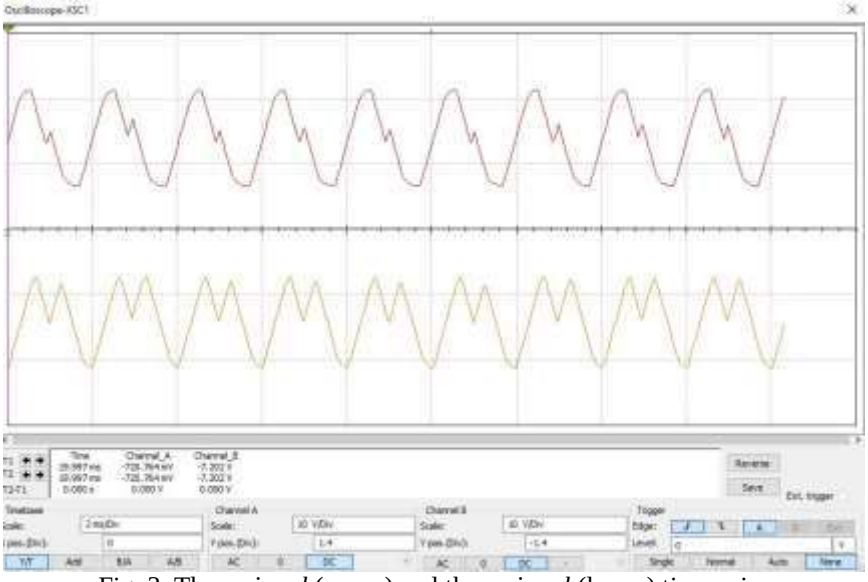

Fig. 3. The *x-signal* (upper) and the *y-signal* (lower) timeseries

Finally, in Figure 4 and Figure 5 the power spectrum for each of the two signals appears. Apparently, the power spectra of the produced signals are broadband, typical of chaotic signals. They span to a frequency range that goes beyond 5 kHz. The peak of the frequency spectrum was measured to be at 0.6 kHz, and it corresponds to a prevailing frequency of the implementing oscillating loop.

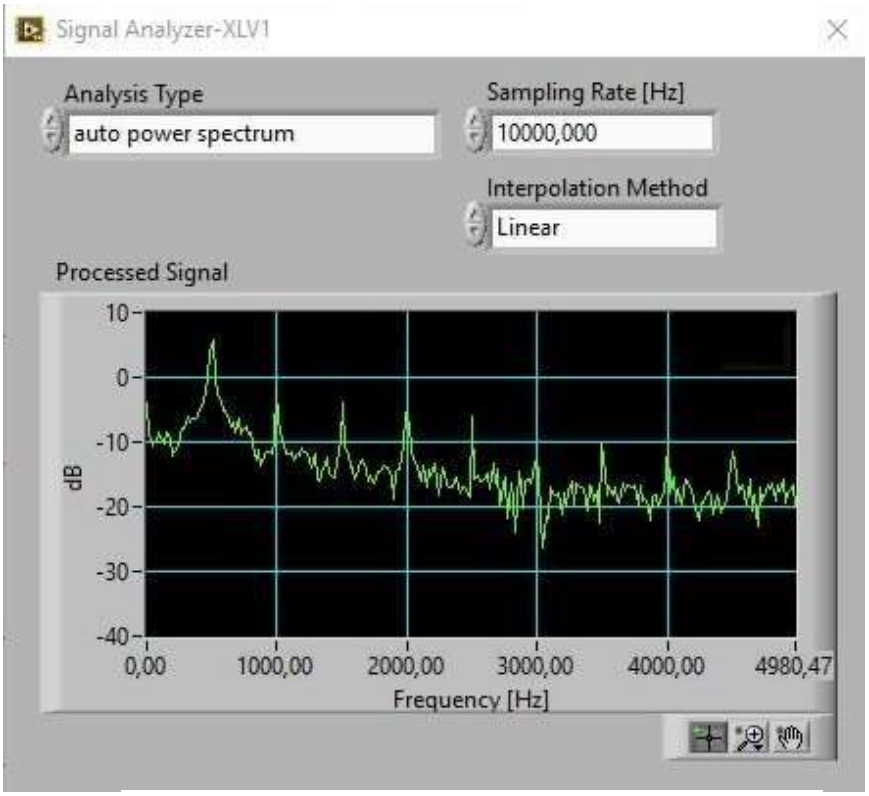

Fig. 4. The spectral distribution of the *x-signal*, typical of chaotic signals

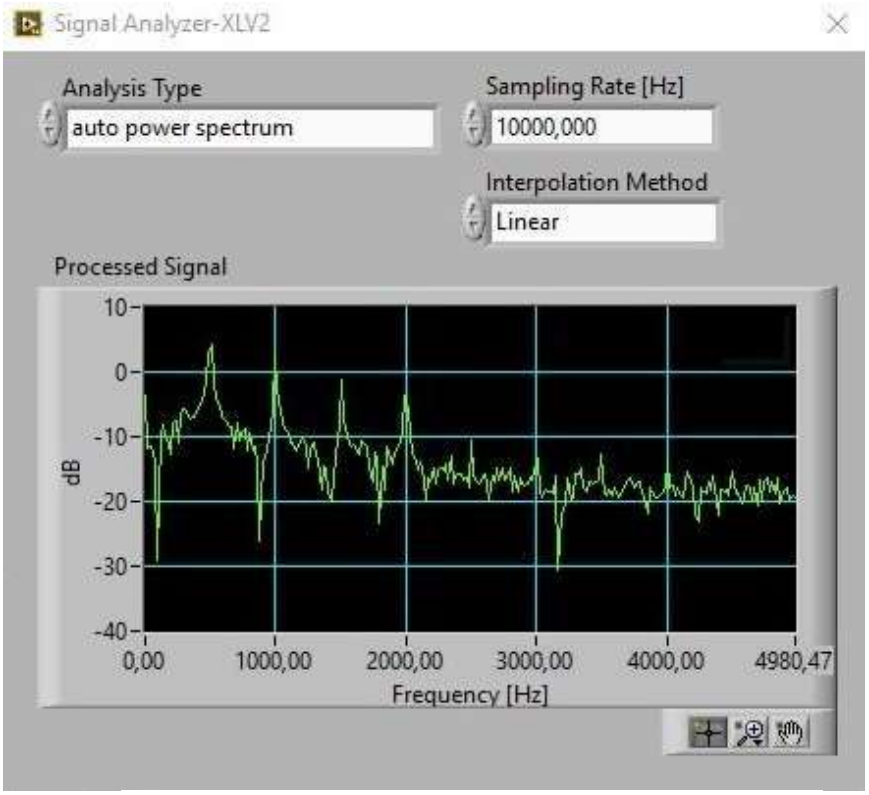

Fig. 5. The spectral distribution of the *y-signal*, typical of chaotic signals

3 Practical Realization of the New Non-autonomous Chaotic Generator

For engineers is important a practical realization. In this Section we present designed layout (Figure 6) and 3D model (Figure 7) using Proteus 8. Layout sizes are 45*30 mm.

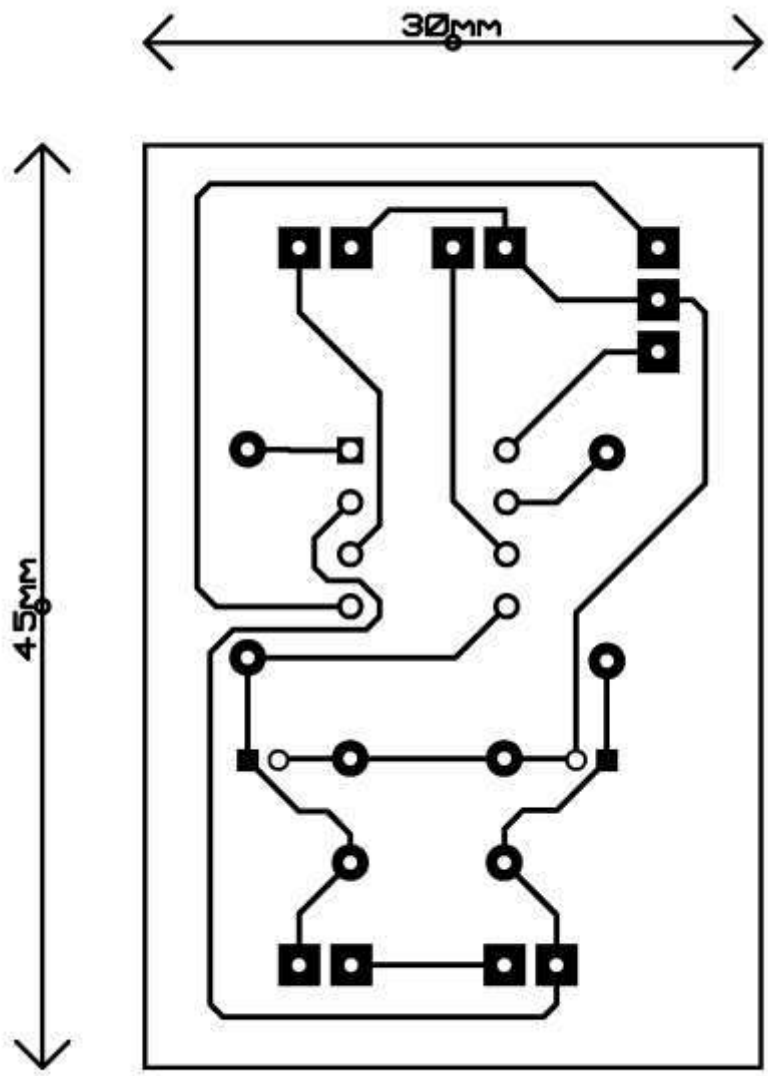

Fig. 6. The designed layout of the new non-autonomous chaotic generator

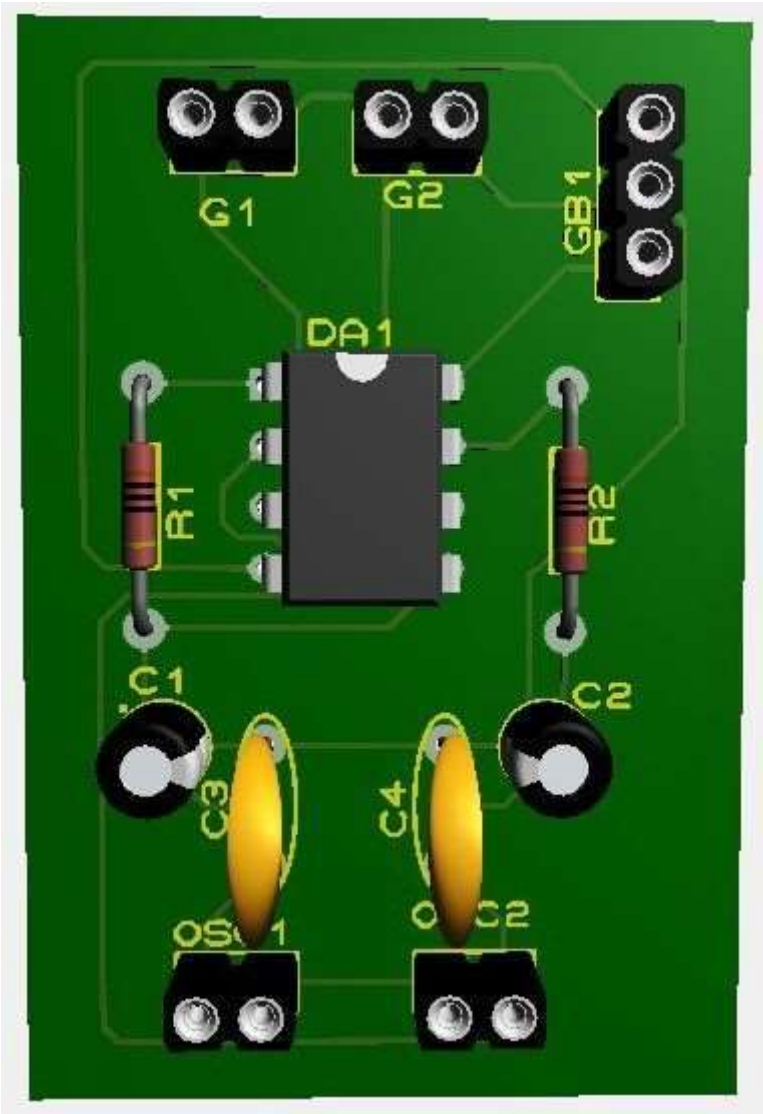

Fig. 7. 3D model of the new non-autonomous chaotic generator

Conclusions

Designed new two channel non-autonomous chaotic generator is presented. Computer modelling results of the circuit realization and main information properties are shown. For demonstrate of these properties was using MultiSim software. Also, layout and 3D model of the new two channel non-autonomous chaotic generator using software Proteus are presented. This non-autonomous generator can be used as

a one of the main portable part of the modern communication system for masking and decrypt of the information.

References

1. Rusyn V. (2017) *Modeling and Research Information Properties of Rucklidge chaotic system using LabView.* CHAOS 2017 – Proceedings: 10th Chaotic Modeling and Simulation International Conference, 739-744.
2. Rusyn, V., Samila, A., Skiadas, Ch. (2020) *Computer modeling and practical realization of chaotic circuit with a light-emitting diode*. In: Fourteenth International Conference on Correlation Optics, Chernivtsi, 16-19 September 2019, pp. 113690D.
3. Sambas A., Sanjaya WS. M., Mamat M., Putra Prastio R., Azar A.T. (2016) *Mathematical modelling of chaotic jerk circuit and its application in secure communication system*. Studies in Fuzziness and Soft Computing, Vol. 337, 133-153.
4. Rusyn V., Mujiarto, Mamat M., Azharul F., Mada Sanjaya W.S., Sambas A., Dwipriyoko E., Sutoni A. *Computer Modelling of the Information Properties of Hyper Chaotic Lorenz System and Its Application in Secure Communication System*. Journal of Physics: Conference Series, 1764, 012205.
5. Chua, L. (1971) *Memristor – the missing circuit element*. IEEE Trans. Circuit Theory, Vol. 18, No. 5, 507-519.
6. Rusyn, V., Khrapko, S. (2019) *Memristor: Modeling and research of information properties.* Springer Proceedings in Complexity, 229-238.
7. Petras I., Chen Y., Coopmans C. (2009) *Fractional-order memristive systems*. ETFA 2009 - 2009 IEEE Conference on Emerging Technologies and Factory Automation, art. no. 5347142.
8. Coopmans C., Petras I., Chen Y. (2010) *Analogue fractional-order generalized memristive devices*. Proceedings of the ASME International Design Engineering Technical Conferences and Computers and Information in Engineering Conference 2009, DETC2009, Vol. 4, PART B, 1127 – 1136.
9. Itoh, M., Chua, L. (2017) *Dynamics of Hamiltonian systems and memristor circuits*. International Journal of Bifurcation and Chaos, 27(2): 1730005.
10. Yu, D., Zheng, C., Iu, H. H. C., Fernando, T., Chua, L. O. (2017) *A new circuit for emulating memristors using inductive coupling*. IEEE Access 5, 1284-1295.
11. Petras I., Chen Y. (2012) *Fractional-order circuit elements with memory*. Proceedings of the 2012 13th International Carpathian Control Conference, ICCC 2012, 552-558, art. no. 6228706.
12. Petras I. (2011) *An effective numerical method and its utilization to solution of fractional models used in bioengineering applications*. Advances in Difference Equations, 2011, art. no. 652789
13. Milicka, P., Cížek, P., Faigl, J. (2016) *On Chaotic Oscillator-based Central Pattern Generator for Motion Control of Hexapod Walking Robot*. CEUR Workshop Proceedings, 1649, 131-137.
14. Sambas, A., Sanjaya, M. WS, Mamat, M., Diyah, H. (2013) *Design and analysis bidirectional chaotic synchronization of rossler circuit and its application for secure communication*. Applied Mathematical Sciences, Vol 7(1), 11-21.
15. Sambas A., Sanjaya WS. M., Mamat M., Putra Prastio R., Azar A.T. (2016) *Mathematical modelling of chaotic jerk circuit and its application in secure communication system*. Studies in Fuzziness and Soft Computing, Vol. 337, 133-153.
16. Rusyn, V., Skiadas, Ch.H., Sambas, A., Mamat, M., Vaidyanathan, S. (2020) *Process of pulse transformation of the analog nonlinear signals*. Telecommunications and Radio Engineering, Vol. 79(13), 1141–1147.

17. Rhif, A., Vaidyanathan, S., Sambas, A., Mujiarto, and Subiyanto. (2019) *A Fish Biology Chaotic System and its Circuit Design*. IOP Conference Series: Journal of Physics, Vol. 1179, art. no. 012011.
18. Vaidyanathan, S., Feki, M., Sambas, A., Lien C. H. (2018) *A new biological snap oscillator: its modelling, analysis, simulations and circuit design*. International Journal of Simulation and Process Modelling, Vol. 13(5), 419-432.
19. Rusyn V., Savko O. (2015) *Modeling of Chaotic Behavior in the Economic Model*. CHAOS 2015 – 8th Chaotic Modeling and Simulation International Conference, Proceedings 2015, 705-712.
20. Vaidyanathan S., Sambas A., Kacar S., Cavusoglu U. (2019) *A new finance chaotic system, its electronic circuit realization, passivity based synchronization and an application to voice encryption*. Nonlinear Engineering, Vol. 8, Issue 1, 193-205.
21. Skiadas, C.H., Skiadas, C. (2008) Chaotic Modelling and Simulation: Analysis of Chaotic Models, Attractors and Forms. In: Taylor & Francis Group, pp. 1–345, LLC.
22. Skiadas, C.H. (2010) *Exact solutions of stochastic differential equations: Gompertz, generalized logistic and revised exponential*. Methodology and Computing in Applied Probability, Vol 12(2), 261-270.
23. Rusyn, V., Subbotin, S. and Sambas, A. (2020) *Analysis and experimental realization of the logistic map using Arduino Pro Mini*. CEUR Workshop Proceedings, 2608, 300-310.
24. Sambas A., Vaidyanathan S., Bonny T., Zhang S., Sukono, Hidayat Y., Gundara G., Mamat M. (2021) *Mathematical Model and FPGA Realization of a Multi-Stable Chaotic Dynamical System with a Closed Butterfly-Like Curve of Equilibrium Points*. Applied Sciences, 11(2), 788.
25. En-Zeng Dong, Rong-Hao Li, Sheng-Zhi Du (2020) *A Multi-directional Controllable Multi-scroll Conservative Chaos Generator: Modelling, Analysis and FPGA Implementation*. Chinese Physics B, 30(2), art. no. 020505.
26. Xuenan Peng, Yicheng Zeng, Mengjiao Wang, Zhijun Li (2021) Generating Multi-layer Nested Chaotic Attractor and Its FPGA Implementation. Chinese Physics B, 30(6), art. no. 060509.
27. Lien C.-H., Vaidyanathan S., Sambas A., Sukono, Mamat M., Sanjaya W.S.M., Subiyanto (2018) *A new two-scroll chaotic attractor with three quadratic nonlinearities, its adaptive control and circuit design*. IOP Conference Series: Materials Science and Engineering, Vol. 332, Issue 1, art. no. 012010.
28. Sambas A., Vaidyanathan S., Mamat M., Mada Sanjaya W.S. (2018) *A six-term novel chaotic system with hidden attractor and its circuit design*. Studies in Systems, Decision and Control, Vol. 133, 365-373.
29. Rusyn, V., Skiadas, Ch. (2020) *Threshold Method for Control of Chaotic Oscillations*. Springer Proceedings in Complexity. Springer, pp. 217-229.
30. Rusyn, V., Mohamad, M.A., Purwandari, D., Mamat, M., Titaley, J., Pinontoan, B. (2020) *Chaotic and Controlling Regimes of a New Modified Chua's Generator*. Journal of Advanced Research in Dynamical & Control Systems, Vol. 12, Issue 02, 556-561.
31. Rusyn, V., Mohamad, M., Titaley, J., Nainggolan, N., Mamat, M. (2020) *Design, computer modelling, analysis and control of the new chaotic generator*. Journal of Advanced Research in Dynamical & Control Systems, Vol. 12, Issue 02, 2306-2311.
32. Rusyn, V., Sadli, M., Mamat, M., Mujiarto, Mada Sanjaya, W.S. (2020) *Computer modelling of a new simple chaotic generator*. Journal of Physics: Conference Series, 1477, 022010.

External synchronization of solitary states and chimeras in unidirectionally coupled neural networks

E. Rybalova[1], A. Zakharova[2], and G. Strelkova[1]

[1] Institute of Physics, Saratov State University, 83 Astrakhanskaya Street, Saratov, 410012, Russia
[2] Institut für Theoretische Physik, Technische Universität Berlin, Hardenbergstr. 36, 10623 Berlin, Germany
(E-mail: rybalovaev@gmail.com)

Abstract. We perform numerical simulation of the dynamics of a multiplex network consisting of two unidirectionally coupled rings of FitzHugh-Nagumo neurons with nonlocal interaction. When uncoupled, one ring demonstrates solitary state regimes and the other one exhibits chimera states. We explore in detail how the synchronization degree between the layers depends on the type of unidirectional interlayer coupling (via fast or slow variables) and on the structures in the driver layer. It is shown that the structure in the response layer can be suppressed and is replaced by the driver layer structure. However, the degree of external synchronization is higher in the case when the driver layer demonstrates solitary states and when the unidirectional coupling is executed via the fast variables. In the case of coupling via the slow variables, external synchronization of neither solitary states nor chimeras cannot be achieved in the considered network.
Keywords: synchronization, FitzHugh-Nagumo neuron, multiplex network, chimera state, solitary state.

1 Introduction

Exploring various properties of cooperative dynamics of multicomponent systems, as well as the effects observing in such systems and synchronization between their elements is one of the main part of nonlinear dynamics [1–6]. This is inextricably linked to the fact that most systems in the world are complex networks with various individual elements and types of coupling between them. There is a plenty of works devoted to synchronization phenomena in systems of completely different nature, such as physics [7–10], chemistry [11,12], neuroscience [13–18], sociology [19–21], etc., as well as in real-world systems, for instance, communication systems [22], power grids [23,24], transportation networks [25].

Dynamics of ensembles of nonlocally coupled elements, when each node is coupled with a finite number of its nearest neighbors, has recently attracted much interest due to the discovery of a new spatiotemporal structure, later called "chimera state" [26,27]. This structure is a striking example of cluster synchronization when a network dynamics spontaneously splits into coherent (synchronous behavior) and incoherent (desynchronized dynamics) clusters with well-defined boundaries in the network space. Although these structures

have been found in networks with different individual elements [26–32], with different types of coupling between them [28,33–37], as well as in real experiments [7–11,38,39], greater interest in these structures was caused by their connection with natural and man-made dynamics [14,17,22–25].

Solitary states are another example of partial synchronization [40]. With this type of synchronization, solitary nodes appear on the coherent profile of the system and are evenly distributed over the entire ensemble. Oscillators in the solitary state regime fundamentally differ in their dynamics from the other oscillators of the network. This kind of pattern has been observed in networks of the Kuramoto models [40–42], the discrete-time systems [43], the FitzHugh-Nagumo systems [44–46], and others. They have also been detected in experiments with mechanical pendulums [39]. Later, solitary state chimeras were revealed when an incoherent cluster includes several solitary states and coexists with coherent clusters [46,47].

Studying interaction between different spatiotemporal structures is an imporant task in the numerical simulation of collective dynamics of complex systems. It was shown in [30] that chimera states can be observed in a ring of nonlocally coupled FitzHugh-Nagumo oscillators. Later, these studies were expanded in [46] and it was found out that this network can also demonstrate solitary states. The interaction between chimeras and solitary states was explored for the first time in [48] where two rings of nonlocally coupled FitzHugh-Nagumo oscillators were bidirectionally coupled either via fast or slow variables. The objective of the present paper is to study the peculiarities of external synchronization of chimeras and solitary states in a two-layer network of unidirectionally coupled rings of FitzHugh-Nagumo oscillators depending on the type of interlayer coupling (via activators or inhibitors) and of the spatiotemporal structures in a driver and a response layer. The identity of synchronous structures in the considered network is quantified using a global interlayer synchronization error.

2 Model under study

The model under study represents a multiplex network consisting of two unidirectionally coupled layers. Each layer is given by a ring of nonlocally coupled FitzHugh-Nagumo oscillators [49,50]. The network is governed by the following

system of equations:

$$\varepsilon \frac{du_{1i}}{dt} = u_{1i} - \frac{u_{1i}^3}{3} - v_{1i} + \frac{\sigma}{2P}\sum_{j=i-P}^{i+P}[b_{uu}(u_{1j}-u_{1i}) + b_{uv}(v_{1j}-v_{1i})] + c^u(u_{2i}-u_{1i}),$$
$$\frac{dv_{1i}}{dt} = u_{1i} + a + \frac{\sigma}{2P}\sum_{j=i-P}^{i+P}[b_{vu}(u_{1j}-u_{1i}) + b_{vv}(v_{1j}-v_{1i})] + c^v(v_{2i}-v_{1i}),$$
$$\varepsilon \frac{du_{2i}}{dt} = u_{2i} - \frac{u_{2i}^3}{3} - v_{2i} + \frac{\sigma}{2P}\sum_{j=i-P}^{i+P}[b_{uu}(u_{2j}-u_{2i}) + b_{uv}(v_{2j}-v_{2i})] + s^u(u_{1i}-u_{2i}),$$
$$\frac{dv_{2i}}{dt} = u_{2i} + a + \frac{\sigma}{2P}\sum_{j=i-P}^{i+P}[b_{vu}(u_{2j}-u_{2i}) + b_{vv}(v_{2j}-v_{2i})] + s^v(v_{1i}-v_{2i}). \quad (1)$$

Dynamical variables u_{li} correspond to the activators or the fast variables, and v_{li} are the inhibitors or the slow variables in each ring, where $l = 1, 2$ is the layer number, and $i = 1, 2, \ldots, N = 300$ is the node number in each ring (all indices are modulo N). Individual FitzHugh-Nagumo oscillators can demonstrate either excitable ($|a| > 1$) or oscillatory ($|a| < 1$) regimes, which depend on the excitability threshold parameter a. In the present study, all the FitzHugh-Nagumo oscillators in the network (1) operate in the oscillatory regime at $a = 0.5$ and the time-scale separation parameter is also fixed $\varepsilon = 0.05$ for all the network nodes.

The nonlocal intralayer coupling in each layer is given by the coupling strength σ and the coupling range P which denotes the number of nearest neighbors of the ith node from both sides in each layer. In our numerical simulation we choose $\sigma = 0.3$ and $P = 105$ in both rings. The intralayer interaction of the FitzHugh-Nagumo neurons in the system (1) has not only direct couplings between activator (u) and inhibitor (v) variables but also cross ones which are executed according to a rotational coupling matrix:

$$B = \begin{pmatrix} b_{uu} & b_{uv} \\ b_{vu} & b_{vv} \end{pmatrix} = \begin{pmatrix} \cos\phi & \sin\phi \\ -\sin\phi & \cos\phi \end{pmatrix}, \quad (2)$$

where $\phi \in [-\pi; \pi)$. In the work [30] this type of coupling was used for the first time and it has been shown that chimera states can be observed in the ring of nonlocally coupled FitzHugh-Nagumo neurons at $\phi = \pi/2 - 0.1$. This research was expanded in the paper [46] where the effect of parameter ϕ on the regimes observed in the FitzHugh-Nagumo ring was explored in detail. It was particularly shown that this ensemble can demonstrate not only chimera states but also solitary states. In the present research the parameter ϕ_l ($l = 1, 2$) values are set in such a way to observe a solitary state regime in the first ring and chimera states in the second one.

The interlayer coupling in the network (1) is organized to be unidirectional with coefficients c^u, c^v, s^u, and s^v. Therefore, when the first layer affects the second one (solitary states affect chimeras) we have $c^u = 0$, $c^v = 0$, $s^u \neq 0$, $s^v \neq 0$, where the superscripts correspond to the coupling via the fast (u)

or the slow (v) variables. Vice versa, when the first layer is subjected to the second one (chimeras affect solitary states), the interlayer coupling is defined by $c^u \neq 0$, $c^v \neq 0$, $s^u = 0$, $s^v = 0$. In our simulations, initial conditions are chosen to be randomly distributed on circle $u^2 + v^2 \leqslant 2^2$. The layers are coupled from the initial time $t = 0$, and the equations (1) are integrated using the Runge–Kutta–Fehlberg method with step $h = 0.02$.

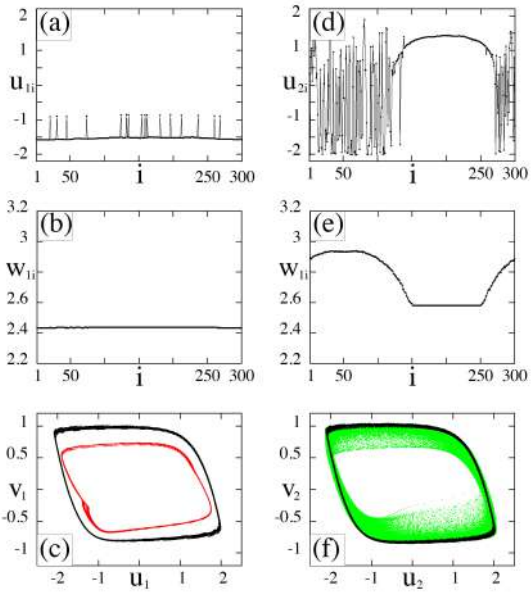

Fig. 1. Dynamics of uncoupled rings ($c^u = 0$, $c^v = 0$, $s^u = 0$, $s^v = 0$): the solitary states in the first ring (a)-(c) and the chimera state in the second ring (d)-(f). Snapshots of variables u_{1i} and u_{2i} (upper row), mean phase velocity profiles (middle row, ω_{1i}, ω_{2i}) and phase portraits for all elements of the rings (lower row, (u_1, v_1) and (u_2, v_2)). Black lines on the phase portraits correspond to elements in the coherent mode, red curves to the solitary nodes, and green ones to the incoherent cluster of the chimera state. Parameters: $\sigma = 0.3$, $P = 105$, $\phi_1 = \pi/2 - 0.2$, $\phi_2 = \pi/2 - 0.04$, $\varepsilon = 0.05$, $a = 0.5$, and $N = 300$. (For interpretation of the references to colour in this figure legend, the reader is referred to the web version of this article.)

Figure 1 shows typical spatiotemporal structures which can be observed in uncoupled FitzHugh-Nagumo rings for the chosen intralayer coupling parameter values. The first layer demonstrates the solitary states (Fig. 1,a-c), and the second layer exhibits the chimera state (Fig. 1,d-f). As can be seen from Fig. 1,a, the solitary nodes are evenly distributed along the coherent profile, while the mean phase velocity profile is rather flat (Fig. 1,b) (this parameter is calculated with the formula $\omega_{li} = \frac{2\pi M_i}{\Delta T}$, where M_i is the number of complete rotations around the origin performed by the ith oscillator during the time interval ΔT [30], $l = 1, 2$ is the layer number). Differences in the dynamics of the solitary nodes and the oscillators from the coherent part can be observed in

the (u_1, v_1) phase plane (Fig. 1,c), where the attracting set with a large radius (black dots) corresponds to the oscillators from the coherent region, and the small cycle (red dots) to the solitary nodes. In the case of chimera states, the snapshot of the second ring dynamics splits into two clusters (Fig. 1,d): one includes elements $150 \leqslant i \leqslant 250$ with coherent dynamics, and the other one consists of nodes $1 \leqslant i \leqslant 149$ and $251 \leqslant i \leqslant 300$ which behave incoherently. In the mean phase velocity profile (Fig. 1,e), the coherent domain is characterized by a smooth distribution, while an arc-like dependence is characteristic for the nodes from the incoherent cluster. There are also two intersecting sets in the (u_2, v_2) phase plane (Fig.1,f): the green attractor reflects the dynamics of the elements from the incoherent cluster of the chimera state and the black set refers to the nodes from the coherent domain. As can be seen from the phase portraits, the green attracting set is essentially thick if compared with a limit cycle for a single FitzHugh-Nagumo system [49,50], and unlike the solitary states, these sets are overlapping.

To analyze the degree of synchronous behavior (or identity of synchronous structures) of the coupled layers we apply a global interlayer synchronization error:

$$\delta = \frac{1}{N} \sum_{i=1}^{N} \left(\frac{1}{t_2 - t_1} \int_{t_1}^{t_2} (u_{1i} - u_{2i}) dt \right), \tag{3}$$

where $N = 300$. Since the coupled FitzHugh-Nagumo rings (1) are not identical, the external interlayer synchronization can be considered in its effective sense. In our numerical studies, imposing certain quantitative conditions for the global interlayer synchronization error we can distinguish effective external synchronization if $0.001 < \delta < 0.01$ and full (complete) external synchronization when $\delta < 0.001$.

3 Unidirectional interlayer coupling via fast variables

We study numerically the case when the FitzHugh-Nagumo rings (1) are unidirectionally coupled via the fast variables, i.e., $c^u \neq 0,\ s^u \neq 0$ and $c^v = 0,\ s^v = 0$. It was shown in [48] that in the presence of this type of the interlayer coupling in a system of two symmetrically coupled rings, first chimera states are formed in both rings, then with an increase in the coupling strength, the rings are completely synchronized and their dynamics correspond to coherent spatial profiles. However, at certain values of the interlayer coupling strength, the regime of solitary states can also be observed in both rings.

3.1 Impact of solitary states on chimera

Let us first consider the possibility of suppressing the chimera structure in the second ring and the establishment of solitary states under the unidirectional influence of the first ring which demonstrates the solitary states. In this case the first FitzHugh-Nagumo ring is a driver ($c^u = 0,\ c^v = 0$), while the second one is a response ($s^u \neq 0,\ s^v = 0$). Figure 2 illustrates the dependence of

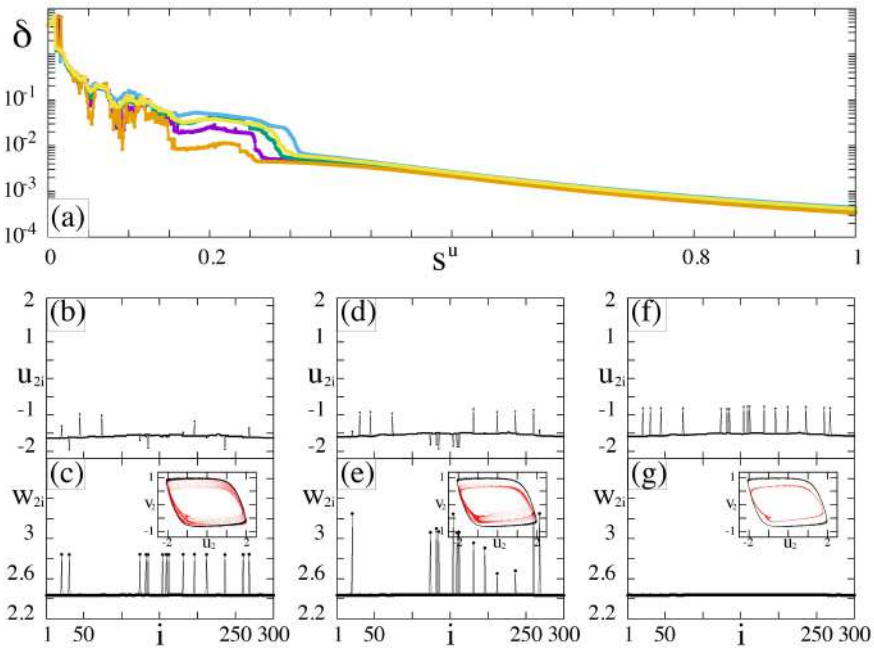

Fig. 2. Unidirectional impact of the first ring (solitary states) on the second one (chimera) via the fast variables: $s^u \neq 0$, $s^v = 0$, $c^u = 0$, $c^v = 0$ in the network (1). (a) Dependence of δ (3) on the interlayer coupling strength s^u plotted for 5 different sets of random initial conditions in each ring (marked by different colors). (b-g) Dynamics of the second ring for increasing s^u: 0.035 (b,c), 0.13 (d,e), 0.35 (f,g). (b,d,f) Snapshots of variables u_{2i}, (c,e,g) mean phase velocity profiles w_{2i} and phase portraits for all ring elements (insets (u_2, v_2)): black lines indicate the coherent dynamics, red curves correspond to the solitary nodes. Other parameters: $\sigma = 0.3$, $P = 105$, $\phi_1 = \pi/2 - 0.2$, $\phi_2 = \pi/2 - 0.04$, $\varepsilon = 0.05$, $a = 0.5$, and $N = 300$. (For interpretation of the references to colour in this figure legend, the reader is referred to the web version of this article.)

the global interlayer synchronization error and the evolution of the second ring dynamics when the interlayer coupling strength s^u grows. As can see from Fig. 2,b, already for a sufficiently weak coupling, the chimera state in the second ring completely disappears and is replaced by the regime of solitary states. However, the observed structure is not synchronous with that one in the driver (see Fig. 1,a and Fig. 2,b): the frequency of the solitary nodes is not equal to that of the elements from the coherent part of the ring (Fig.2,c), and the corresponding attracting set (red points) in the phase plane (inset in Fig.2,c) is wider than that shown in Fig. 1,c. As follows from Fig. 2,a, when the interlayer coupling is sufficiently weak ($s^u < 0.15$), the synchronization error δ does not satisfy the effective synchronization condition.

Even when s^u slightly increases, the observed solitary state regime in the second ring is still not synchronous to the mode in the first ring (Fig. 2,d,e).

However, as can be seen from the phase portrait in Fig. 2,e, the set corresponding to the solitary nodes (red points) is separated from the oscillators from the coherent profile (black line). Starting from the region where the dependence $\delta(s^u)$ becomes smooth ($s^u > 0.33$ in Fig. 2,a), the solitary nodes in the second ring begin to correspond to the solitary nodes in the first ring (Fig. 1,c). In this case we have a smooth frequency profile and two phase portraits clearly separated in the phase space (Fig. 2,f,g). On the other hand, already starting from $s^u > [0.15; 0.28]$ (the exact value depends on the initial conditions) the global interlayer synchronization error becomes less than 0.01 and we can talk about effective synchronization. Only when $s^u > 0.67$ (Fig. 2,a), complete external synchronization ($\delta < 0.001$) occurs in the network (1).

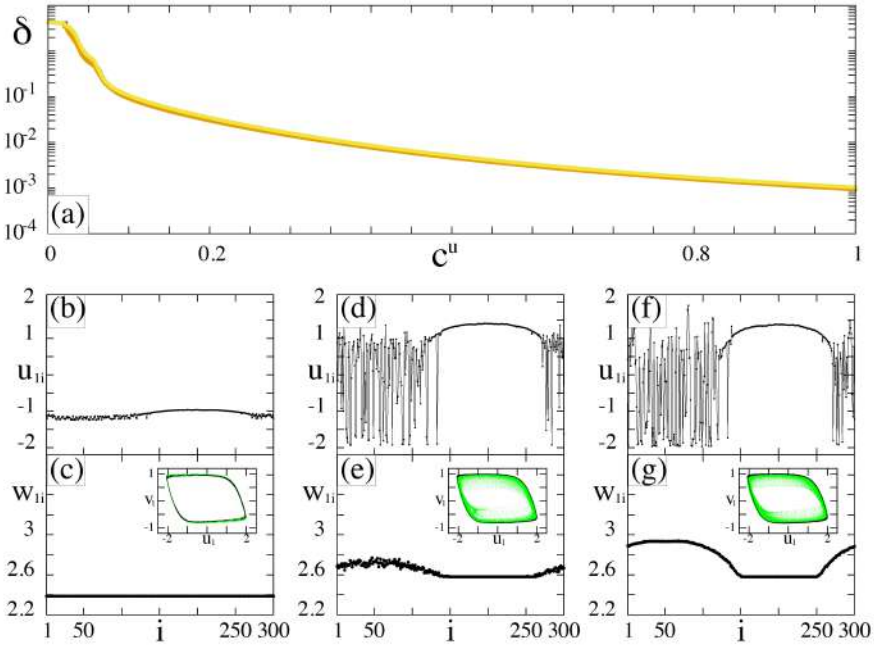

Fig. 3. Unidirectional impact of the second ring (chimera) on the first ring (solitary states) via the fast variables: $c^u \neq 0$, $s^u = 0$, $s^v = 0$, $c^v = 0$ in the network (1). (a) Dependence of δ (3) on the interlayer coupling strength c^u plotted for 5 different sets of random initial conditions in each ring (marked by different colors). (b-g) Dynamics of the first ring in (1) for increasing c^u: 0.014 (b,c), 0.06 (d,c), 0.235 (f,g). (b,d,f) Snapshots of variables u_{1i}, (c,e,g) mean phase velocity profiles w_{1i} and phase portraits for all ring elements (insets (u_1, v_1)): black lines indicate the coherent dynamics, red curves correspond to the solitary nodes. Other parameters are as in Fig. 2. (For interpretation of the references to colour in this figure legend, the reader is referred to the web version of this article.)

3.2 Impact of chimera on solitary states

When the second ring exhibiting the chimera state is the driver, the global synchronization error δ demonstrates a smooth dependence on the interlayer coupling strength c^u over the entire interval of its variation (Fig. 3,a). This can be explained by the fact that there is no need to synchronize individual elements (solitary nodes) which introduce deviations into dependence $\delta(c^u)$. In this case, the solitary states in the first ring also quickly disappear, and the snapshot splits into coherent and incoherent clusters (Fig. 3,c). However, the arc-like dependence does not immediately appear on the frequency profile (Fig. 3,c). Increasing c^u leads to the appearance of the arc in the frequency profile, which at first looks a bit noisy (Fig. 3,e). Only when c^u grows ($c^u > 0.1$), the frequency profile becomes smooth (Fig. 3,g). As follows from the snapshots (Fig. 3,d and f) and the phase portraits (insets in Fig .3,e and g), already at a very weak interlayer coupling c^u, the first ring (response) starts behaving similarly to the second ring (driver) (see Fig. 1,d,f and Fig. 3,d,e).

In contrast to the previously considered case, in this situation the global interlayer synchronization error does not fall below the 0.001 level even for a rather strong unidirectional interlayer coupling (Fig.3,a). This means that only effective external synchronization of the chimera state takes place.

4 Unidirectional interlayer coupling via slow variables

We now turn to the case when the two rings (1) are unidirectionally coupled via the slow variables, i.e., $c^v \neq 0$, $s^v \neq 0$, while there is no coupling via the fast variables, $c^u = 0$, $s^u = 0$. Our previous studies [48] showed that with this type of coupling in a system of two bidirectionally coupled rings, firstly the chimera states in the second ring disappear and are replaced by uniformly distributed solitary nodes, but they are not synchronous with the solitary nodes in the first ring. At the same time, the solitary nodes in the first ring gradually disappear. A further increase of the coupling strength between the layers leads to a coherent regime in the first ring and the solitary state chimera in the second ring. By increasing the coupling strength, we can observe the classical chimera states in both rings, which behave quite synchronously. With a further increase in the coupling strength the dynamics of the two-layer network is similar to the dynamics of the rings which are coupled through the fast variables. The rings are completely synchronized and their behavior corresponds to coherent spatial profiles. Moreover, at certain values of the interlayer coupling strength (more than 1.0), the solitary state mode can be observed in both rings.

4.1 Impact of solitary states on chimera

Consider the case when the second ring in the chimera state is driven via the slow variables by the first ring in the solitary state regime. In this case the chimera state also quickly disappears and is replaced by the solitary nodes (Fig. 4,b-e). However, the solitary nodes are distributed throughout the whole ring and their location does not coincide with that in the driver layer (see

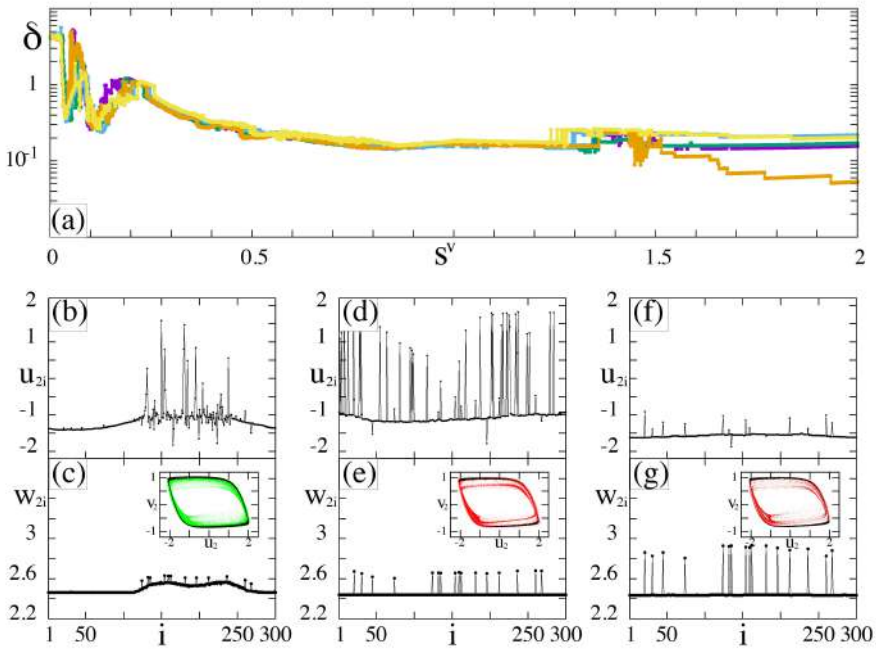

Fig. 4. Numerical results for the case when the first ring (solitary states) is unidirectionally coupled with the second one (chimera state) via the slow variables: $s^v \neq 0$, $s^u = 0$, $c^u = 0$, $c^v = 0$. (a) Dependence of δ (3) on the interlayer coupling strength s^v plotted for 5 different sets of random initial conditions in each ring (marked by different colors). (b-g) Dynamics of the second ring for increasing s^v: 0.025 (b,c), 0.062 (d,c), 0.5 (f,g). (b,d,f) Snapshots of variables u_{2i}, (c,e,g) mean phase velocity profiles w_{2i} and phase portraits for all ring elements (insets (u_2, v_2)): black lines indicate the coherent dynamics, red curves correspond to the solitary nodes. Other parameters: $\sigma = 0.3$, $P = 105$, $\phi_1 = \pi/2 - 0.2$, $\phi_2 = \pi/2 - 0.04$, $\varepsilon = 0.05$, $a = 0.5$, and $N = 300$. (For interpretation of the references to colour in this figure legend, the reader is referred to the web version of this article.)

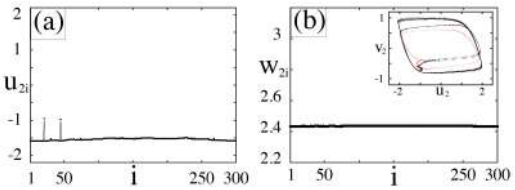

Fig. 5. Dynamics of the second ring under the unidirectional impact from the first ring at $s^v = 1.446$ ($s^u = 0$, $c^u = 0$, $c^v = 0$). (a) Snapshots of variables u_{2i}, (b) mean phase velocity profiles w_{2i} and phase portraits for all ring elements (insets (u_2, v_2)): black lines indicate the coherent dynamics, red curves correspond to the solitary nodes. Other parameters are as in Fig. 4. (For interpretation of the references to colour in this figure legend, the reader is referred to the web version of this article.)

Fig. 1,a and Fig. 4,d). It is also evident that the frequencies of several solitary nodes are not equal to the frequency of the other oscillators, as it should be (Fig. 4,e). Moreover, in the phase portrait, the trajectories of some solitary nodes do not lie separately from the phase portrait of the oscillators from the coherent domain, i.e., there is an intersection of the red and black sets (inset in Fig. 4,e). When the interlayer coupling increases, the most part of the solitary nodes disappears but the remaining nodes are not synchronized with those in the first ring (Fig. 4,f,g). A further increase in s^v does not lead to the observation of a more synchronous mode of oscillations of the second ring with the first one, but, on the contrary, leads to the fact that the phase portraits of the elements change greatly and the rings are never synchronized (for example, Fig. 5).

Let us pay attention to the change in the global interlayer synchronization error δ as s^v increases (Fig. 4,a). Within the interval $s^v \in [0; 0.2]$, the dependence has several minima and maxima and does not smoothly decrease when s^v grows. This is due to the fact that initially, under the influence of the first ring, the chimera state in the second ring is gradually destroyed (the first minimum is at $s^v \approx 0.04$). Then a lot of solitary nodes appear in the second ring, which do not correspond to the solitary nodes in the first ring and are not synchronized with them (maximum is at $s^v \approx 0.055$) (see Fig.1,a and Fig.4,d). Afterwards, the solitary nodes gradually disappear with increasing coupling strength (minimum is at $s^v \approx 0.11$). Finally, the solitary nodes in the second ring correspond to the same oscillators as in the first ring (maximum is at $s^v \approx 0.2$) (see Fig. 1,a and Fig. 4,f), and the rings are partially synchronized with a further increase of the coupling strength s^v. However, even for a rather strong coupling strength s^v, even effective external synchronization is not observed in the network (1) since $\delta > 0.01$.

4.2 Impact of chimera on solitary states

Finally, we explore the network (1) dynamics when the driver layer (the second ring) exhibits the chimera state. In this case, the network dynamics is similar to that which is observed when the unidirectional coupling is executed via the fast variables. The solitary nodes in the first ring gradually disappear as the coupling strength c^v increases (Fig. 6,b,c), and the snapshots of the first ring dynamics (Fig.6,d,e) consist of incoherent and coherent parts, that is related to the chimera state. However, even with a strong coupling, in the presence of a well-developed chimera state in the first layer, the frequency profile demonstrates only a barely noticeable arc-like structure (Fig. 6,f,g). Synchronization between the rings is not achieved even for a very strong interlayer coupling: the global interlayer synchronization error never goes below 0.1 (see Fig. 6,a). However, for certain sets of random initial conditions in each ring, the values of δ can be lower than for the other sets (see the blue line in Fig. 6,a).

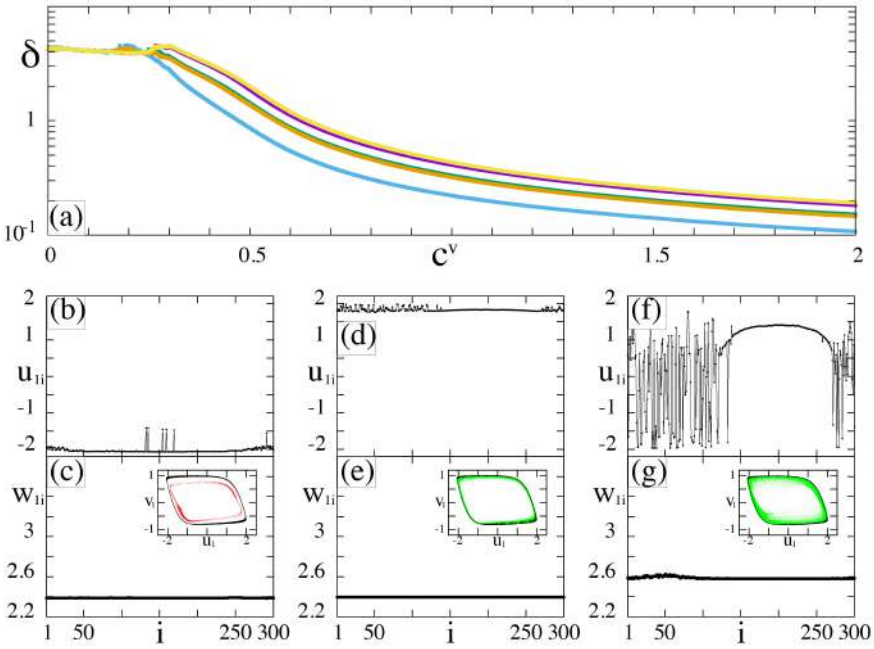

Fig. 6. Numerical results for the case when the first ring (solitary states) in the network (1) is driven by the second ring (chimera) via the slow variables: $c^v \neq 0$, $s^v = 0$, $s^u = 0$, $c^u = 0$. (a) Dependence of δ (3) on the interlayer coupling strength c^u plotted for 5 different sets of random initial conditions in each ring (marked by different colors). (b-g) Dynamics of the first ring in (1) for increasing c^v: 0.025 (b,c), 0.223 (d,c), 1.6 (f,g). (b,d,f) Snapshots of variables u_{1i}, (c,e,g) mean phase velocity profiles w_{1i} and phase portraits for all ring elements (insets (u_1, v_1)): black lines indicate the coherent dynamics, red curves correspond to the solitary nodes. Other parameters are as in Fig. 4. (For interpretation of the references to colour in this figure legend, the reader is referred to the web version of this article.)

5 Conclusion

In this paper we have presented results of numerical simulation of a two-layer multiplex network of unidirectionally coupled rings of FitzHugh-Nagumo oscillators. Our studies have shown that in the case of unidirectional coupling via the fast variables (activators), it is possible to suppress both chimera states and solitary states and establish a different spatiotemporal regime. However, with external synchronization of solitary states, the global interlayer synchronization error shows a stronger similarity between the rings than in the case of synchronization of chimera states. This fact is easily explained by the structure of these states. Since the oscillators in the coherent cluster are synchronized more easily, it is natural to assume that the solitary states will demonstrate a higher degree of synchronization.

In the case of unidirectional coupling between the FitzHugh-Nagumo rings via the slow variables (inhibitors), although the initial structure of the ring is

rapidly destroyed under external influence, the structure of the driver layer can be only partially reproduced in the response layer. This fact is confirmed by the global interlayer synchronization error which does not fall below 0.01.

Thus, our studies have shown that both solitary states and chimera states can be suppressed when the two layers are unidirectionally coupled via both the fast and the slow variables. The response layer reproduces the structure of the driver layer instead of its own. However, the effect of external synchronization (both effective and complete) is observed only when the layers are coupled via the activators. These studies can be useful in practical applications when it is needed to suppress one of the structures and establish another one. Thus, one can control the dynamics of multilayer networks.

Acknowledgments

This work was supported by the Deutsche Forschungsgemeinschaft (DFG, German Research Foundation)—Projektnummer 163436311—SFB 910 and by the RFBR and the DFG according to the Research Project No. 20-52-12004.

References

1. V.S. Afraimovich, V.I. Nekorkin, G.V. Osipov, V.D. Shalfeev. *Stability, structures and chaos in nonlinear synchronization networks*, World Scientific, 1995.
2. V.N. Belykh, I.V. Belykh, E. Mosekilde. Cluster synchronization modes in an ensemble of coupled chaotic oscillators, *Physical Review E*, 63, 3, 036216, 2001.
3. V. Nekorkin, M.G. Velarde. *Synergetic phenomena in active lattices: patterns, waves, solitons, chaos*, Springer Science & Business Media, 2002.
4. G.V. Osipov, J. Kurths, Ch. Zhou. *Synchronization in oscillatory networks*, Springer Science & Business Media, 2007.
5. V.I. Nekorkin, A.S. Dmitrichev, D.V. Kasatkin, V.S. Afraimovich. Relating the sequential dynamics of excitatory neural networks to synaptic cellular automata, *Chaos: An Interdisciplinary Journal of Nonlinear Science*, 21, 4, 043124, 2011.
6. S. Boccaletti, A.N. Pisarchik, C.I. Del Genio, A. Amann. *Synchronization: from coupled systems to complex networks*, Cambridge University Press, 2018.
7. A.M. Hagerstrom, T.E. Murphy, R. Roy, P. Hövel, I. Omelchenko, E. Schöll. Experimental observation of chimeras in coupled-map lattices, *Nature Physics*, 8, 9, 658–661, 2012.
8. F. Rogister, R. Roy. Localized excitations in arrays of synchronized laser oscillators, *Physical review letters*, 98, 10, 104101, 2007.
9. M. Wickramasinghe, I.Z. Kiss. Spatially organized partial synchronization through the chimera mechanism in a network of electrochemical reactions, *Physical Chemistry Chemical Physics*, 16, 34, 18360–18369, 2014.
10. D.P. Rosin, D. Rontani, N.D. Haynes, E. Schöll, D.J. Gauthier. Transient scaling and resurgence of chimera states in networks of Boolean phase oscillators, *Physical Review E*, 90, 3, 030902, 2014.
11. M.R. Tinsley, S. Nkomo, K. Showalter. Chimera and phase-cluster states in populations of coupled chemical oscillators, *Nature Physics*, 8, 9, 662–665, 2012.
12. J.F. Totz, J. Rode, M.R. Tinsley, K. Showalter, H. Engel. Spiral wave chimera states in large populations of coupled chemical oscillators, *Nature Physics*, 14, 3, 282–285, 2018.

13. A.E. Pereda. Electrical synapses and their functional interactions with chemical synapses, *Nature Reviews Neuroscience*, 15, 4, 250–263, 2014.
14. T. Chouzouris, I. Omelchenko, A. Zakharova, J. Hlinka, P. Jiruska, E. Schöll. Chimera states in brain networks: Empirical neural vs. modular fractal connectivity, *Chaos: An Interdisciplinary Journal of Nonlinear Science*, 28, 4, 045112, 2018.
15. P.J. Uhlhaas, W. Singer. Neural synchrony in brain disorders: relevance for cognitive dysfunctions and pathophysiology, *Neuron*, 52, 1, 155–168, 2006.
16. P. Jiruska, M. De Curtis, J.G. Jefferys, C.A. Schevon, S.J. Schiff, K. Schindler. Synchronization and desynchronization in epilepsy: controversies and hypotheses, *The Journal of physiology*, 591, 4, 787–797, 2013.
17. R.G. Andrzejak, C. Rummel, F. Mormann, K. Schindler. All together now: Analogies between chimera state collapses and epileptic seizures, *Scientific reports*, 6, 1, 1–10, 2016.
18. C. Hammond, H. Bergman, P. Brown. Pathological synchronization in Parkinson's disease: networks, models and treatments, *Trends in neurosciences*, 30, 7, 357–364, 2007.
19. M. Girvan, M.E. Newman. Community structure in social and biological networks, *Proceedings of the national academy of sciences*, 99, 12, 7821–7826, 2002.
20. R. Amato, A. Díaz-Guilera, K.K. Kleineberg. Interplay between social influence and competitive strategical games in multiplex networks, *Scientific reports*, 7, 1, 1–8, 2017.
21. R. Amato, N.E. Kouvaris, M. San Miguel, A. Díaz-Guilera. Opinion competition dynamics on multiplex networks, *New Journal of Physics*, 19, 12, 123019, 2017.
22. S. Hong, Y. Chun. Efficiency and stability in a model of wireless communication networks. Social Choice and Welfare. 34, 3, 441–454, 2010.
23. P.J. Menck, J. Heitzig, J. Kurths, H.J. Schellnhuber. How dead ends undermine power grid stability, *Nature communications*, 5, 1, 1–8, 2014.
24. B. Wang, H. Suzuki, K. Aihara. Enhancing synchronization stability in a multi-area power grid, *Scientific reports*, 6, 1, 1–11, 2016.
25. A. Cardillo, M. Zanin, J. Gómez-Gardenes, M. Romance, A.J. del Amo, S. Boccaletti. Modeling the multi-layer nature of the European Air Transport Network: Resilience and passengers re-scheduling under random failures, *The European Physical Journal Special Topics*, 215, 1, 23–33, 2013.
26. Y. Kuramoto, D. Battogtokh. Coexistence of Coherence and Incoherence in Nonlocally Coupled Phase Oscillators. *Nonlinear Phenomena in Complex Systems*, 5, 4, 380–385, 2002.
27. D.M. Abrams, S.H. Strogatz. Chimera states for coupled oscillators, *Physical review letters*, 93, 17, 174102, 2004.
28. I. Omelchenk, Y. Maistrenko, P. Hövel, E. Schöll. Loss of coherence in dynamical networks: spatial chaos and chimera states, *Physical review letters*, 106, 23, 234102, 2011.
29. M.J. Panaggio, D.M. Abrams. Chimera states: coexistence of coherence and incoherence in networks of coupled oscillators, *Nonlinearity*, 28, 3, R67, 2015.
30. I. Omelchenko, E. Omelchenko, P. Hövel, E. Schöll. When nonlocal coupling between oscillators becomes stronger: patched synchrony or multichimera states. *Physical review letters*, 110, 22, 224101, 2013.
31. A. Zakharova, M. Kapeller, E. Schöll. Chimera death: Symmetry breaking in dynamical networks, *Physical review letters*, 112, 15, 154101, 2014.
32. S.A. Bogomolov, A.V. Slepnev, G.I. Strelkova, E. Schöll, V.S. Anishchenko. Mechanisms of appearance of amplitude and phase chimera states in ensembles of

nonlocally coupled chaotic systems, *Communications in Nonlinear Science and Numerical Simulation*, 43, 25–36, 2017.
33. S. Ulonska, I. Omelchenko, A. Zakharova, E. Schöll. Chimera states in networks of Van der Pol oscillators with hierarchical connectivities, *Chaos: An Interdisciplinary Journal of Nonlinear Science*, 26, 9, 094825, 2016.
34. E. Schöll. Synchronization patterns and chimera states in complex networks: Interplay of topology and dynamics, *The European Physical Journal Special Topics*, 225, 6, 891–919, 2016.
35. J. Sawicki, I. Omelchenko, A. Zakharova, E. Schöll. Chimera states in complex networks: interplay of fractal topology and delay, *The European Physical Journal Special Topics*, 226, 9, 1883–1892, 2017.
36. S.I. Shima, Y. Kuramoto. Rotating spiral waves with phase-randomized core in nonlocally coupled oscillators, *Physical Review E*, 69, 3, 036213, 2004.
37. M.J. Panaggio, D.M. Abrams. Chimera states on a flat torus, *Physical review letters*, 110, 9, 094102, 2013.
38. E.A. Martens, S. Thutupalli, A. Fourriere, O. Hallatschek. Chimera states in mechanical oscillator networks, *Proceedings of the National Academy of Sciences*, 110, 26, 10563–10567, 2013.
39. T. Kapitaniak, P. Kuzma, J. Wojewoda, K. Czolczynski, Y. Maistrenko. Imperfect chimera states for coupled pendula, *Scientific reports*, 4, 6379, 2014.
40. Y. Maistrenko, B. Penkovsky, M. Rosenblum. Solitary state at the edge of synchrony in ensembles with attractive and repulsive interactions, *Physical Review E*, 89, 6, 060901, 2014.
41. H. Wu, M. Dhamala. Dynamics of Kuramoto oscillators with time-delayed positive and negative couplings, *Physical Review E*, 98, 3, 032221, 2018.
42. P. Jaros, S. Brezetsky, R. Levchenko, D. Dudkowski, T. Kapitaniak, Y. Maistrenko. Solitary states for coupled oscillators with inertia, *Chaos: An Interdisciplinary Journal of Nonlinear Science*, 28, 1, 011103, 2018.
43. E. Rybalova, N. Semenova, G. Strelkova, V. Anishchenko. Transition from complete synchronization to spatio-temporal chaos in coupled chaotic systems with nonhyperbolic and hyperbolic attractors, *The European Physical Journal Special Topics*, 226, 9, 1857–1866, 2017.
44. L. Schülen, D.A. Janzen, E.S. Medeiros, A. Zakharova. Solitary states in multiplex neural networks: Onset and vulnerability, *Chaos, Solitons & Fractals*, 145, 110670, 2021.
45. L. Schülen, S. Ghosh, A.D. Kachhvah, A. Zakharova, S. Jalan. Delay engineered solitary states in complex networks, *Chaos, Solitons & Fractals*, 128, 290–296, 2019.
46. E. Rybalova, V.S. Anishchenko, G.I. Strelkova, A. Zakharova. Solitary states and solitary state chimera in neural networks. *Chaos: An Interdisciplinary Journal of Nonlinear Science*, 29, 7, 071106, 2019.
47. A. Bukh, E. Rybalova, N. Semenova, G. Strelkova, V. Anishchenko. New type of chimera and mutual synchronization of spatiotemporal structures in two coupled ensembles of nonlocally interacting chaotic maps, *Chaos: An Interdisciplinary Journal of Nonlinear Science*, 27, 11, 111102, 2017.
48. E.V. Rybalova, A. Zakharova, G.I. Strelkova. Interplay between solitary states and chimeras in multiplex neural networks. *Chaos, Solitons & Fractals*, 148, 111011, 2021.
49. R. FitzHugh. Impulses and physiological states in theoretical models of nerve membrane. *Biophysical journal*, 1, 6, 2061–2070, 1961.
50. J. Nagumo, S. Arimoto, S. Yoshizawa. An Active Pulse Transmission Line Simulating Nerve Axon. *Proceedings of the IRE*, 50, 10, 2061–2070, 1962.

On a Cournot Duopoly Game with Relative Profit Maximization

Sarafopoulos Georges[1], Papadopoulos Kosmas[2]

[1] Department of Economics, Democritus University of Thrace, Komotini, Greece
(E-mail: gsarafop@econ.duth.gr)
[2] Department of Economics, Democritus University of Thrace, Komotini, Greece
(E-mail: kpapa@econ.duth.gr)

Abstract. In this article, the authors investigate the dynamics of an oligopoly game in which, they consider a nonlinear Cournot-type duopoly game with homogeneous goods and heterogeneous expectations. The authors investigate the case, where managers have a variety of attitudes toward relative performance that are indexed by their type. In this game they suppose a linear demand and quadratic cost functions. The game is modeled with a system of two difference equations. Existence and stability of equilibriua of the system are studied. The authors show that the models gives more complex, chaotic and unpredictable trajectories, as a consequence of change in the parameter k of speed of the player's adjustment, the parameter d of the horizontal product differentiation and the relative profit parameter μ. The chaotic features are justified numerically via computing Lyapunov numbers and sensitive dependence on initial conditions.
Keywords: Cournot duopoly game; Relative profit maximization; Discrete dynamical system; Nash equilibrium; Stability; Bifurcation diagrams; Lyapunov numbers; Strange attractors; Chaotic Behavior.

1. Introduction

Oligopoly is a market structure between monopoly and perfect competition in which there are only a few number of firms producing homogeneous products. The dynamic of an oligopoly game is more complex because the players (sellers) must consider not only the consumers' behavior but also, the competitors' reactions, i.e., their expectations concerned in how their rivals will act. In 1838 Antoine Augustin Cournot was the first that introduced a formal theory of oligopoly. Joseph Louis Francois Bertrand, the French mathematician in 1883 modified Cournot's game suggesting that the players (sellers) actually choose prices rather the quantities. Cournot and Bertrand models originally were based on the premise that all players take decisions by naïve way, so that in every step, each player assumes the last values were taken by the competitors without an estimation of their future reactions. However, under the conditions of real market, such an assumption is very unlikely since not all players share naïve beliefs. Different approaches to firm behavior were proposed. Some of the authors considered duopolies under homogeneous expectations and found a variety of complex dynamics in their games, such as appearance of strange attractors (Agiza 1999; Agiza et al. 2002; Agliari et al. 2005, 2006; Bischi and

Kopel 2001; Kopel 1996; Puu 1998, 2005; Sarafopoulos 2015a,b; Zhang et al. 2009). Also, models with heterogeneous agents were studied (Agiza and Elsadany 2003, 2004; Agiza et al. 2002; Den Haan 2001; Hommes 2006; Fanti and Gori 2012; Gao 2009; Sarafopoulos and Papadopoulos 2017, 2019, 2020; Tramontana 2010; Zhang et al. 2007; Wu et al. 2010).
In real market, producers do not know the entire demand function, though it is possible that they have a perfect knowledge of technology, represented by the cost function. Here it is more likely that firms employ some local estimate of the demand. This issue has been previously analyzed (Baumol and Quandt 1964; Singh Vives 1984; Puu 1991, 1995; Westerhoff 2006; Naimzada and Ricchiuti 2008; Askar 2013, 2014). Bounded rational players (sellers) update their strategies based on discrete time periods and by using a local estimate of the marginal profit. With such local adjustment mechanism, the players are not requested to have a complete knowledge of the demand and the cost functions (Agiza and Elsadany 2004; Elsadany 2017; Naimzada and Sbragia 2006; Zhang et al. 2007; Askar 2014).
In this paper the concept of generalized relative profit in a Cournot – type duopoly game with homogeneous goods, linear demand and quadratic cost functions is introduced. The paper is organized as follows: In Section 2, the dynamics of the Cournot duopoly game with homogeneous goods and generalized relative profit maximization for two players are analyzed. Heterogeneous expectations, linear demand and quadratic cost functions are supposed. The existence and local stability of the equilibrium points are also analyzed. In Section 3 numerical simulations are used to show complex dynamics via computing Lyapunov numbers, bifurcations diagrams, strange attractors and sensitive dependence on initial conditions. Finally, the paper is concluded in Section 4.

2. The game

2.1 The construction of the game

Two firms offer their products at discrete-time periods (t = 0, 1, 2…) on a common market. A simple Cournot-type duopoly market where firms (players) produce homogeneous goods and their production decisions are taken at discrete-time periods is considered. This study contains heterogeneous players and more specifically, the first firm chooses its production quantity in a rational way following an adjustment mechanism (bounded rational player) and the second firm decides by naïve way choosing this production quantity that maximizes its utility function (naïve player). At each period t, every firm must form an expectation of the rival's output in the next time period in order to determine the corresponding profit-maximizing quantities for period t+1. The variables q_1, q_2 are the production quantities of each firm, and the inverse

demand function (as a function of quantities) for each i firm is given by the following equation:

$$p_i = \alpha - Q \text{ , with } \quad i = 1, 2 \tag{1}$$

where p_i is the product price of firm i, $Q = q_1 + q_2$ and α is a positive parameter which expresses the market size.
Specifically, for each firm the inverse demand functions are given by the following equations:

$$p_1 = \alpha - q_1 - q_2 \qquad \text{and} \qquad p_2 = \alpha - q_2 - q_1 \tag{2}$$

In this duopoly game quadratic cost functions are supposed:

$$C(q_i) = c \cdot q_i^2, \qquad \text{with} \quad i = 1, 2 \tag{3}$$

where c > 0, is the same cost parameter for two firms.
With these assumptions the profits of the firms are given by:

$$\Pi_1(q_1, q_2) = p_1 q_1 - C(q_1) = p_1 q_1 - c q_1^2 = \left[\alpha - (q_1 + q_2)\right] q_1 - c q_1^2 \tag{4}$$

and

$$\Pi_2(q_1, q_2) = p_2 q_2 - C(q_2) = p_2 q_2 - c q_2^2 = \left[\alpha - (q_1 + q_2)\right] q_2 - c q_1^2 \tag{5}$$

Potential managers take on a continuum of attitudes toward relative performance which is captured by their type μi. The utility function of a manager of type μi puts weight of (1- μi) on own profits and a weight μi on the difference between own profits and the profits of the firm's rival. This is equivalent to putting unit weight on own profits and weight - μi on the rival's profit. Hence we can write the objective function of a type μi manager working for firm i as:

$$\begin{aligned} U_i &= (1 - \mu_i) \cdot \Pi_i + \mu_i \cdot (\Pi_i - \Pi_j) \\ &= \Pi_i - \mu_i \cdot \Pi_j \quad , \qquad i, j = 1, 2 \quad , \qquad i \neq j \end{aligned} \tag{6}$$

The parameter $\mu_i \in [0,1]$ is formed by the profile of each player i and the higher (lower) value of μi, the more (less) the player i takes into account the profit of player j. To make our calculations easier it supposed that μ = μi, which means that the two player have the same profile in their utility function.

Then the marginal utilities are given by:

$$\frac{\partial U_1}{\partial q_1} = \alpha - 2(1 + c) q_1 - (1 - \mu) q_2 \tag{7}$$

and

$$\frac{\partial U_2}{\partial q_2} = \alpha - 2(1 + c) q_2 - (1 - \mu) q_1 \tag{8}$$

It is supposed that the first firm decides to increase its level of adaptation if it has a positive marginal utility, or decreases its level if the marginal utility is

negative (bounded rational player). If k > 0 the dynamical equation of player i is:

$$\frac{q_1(t+1)-q_1(t)}{q_1(t)} = k \cdot \frac{\partial U_1}{\partial q_1} \tag{9}$$

k > 0 the speed of adjustment of player 1, it is a positive parameter which gives the extent of production variation of the firm following a given profit signal. Moreover it captures the fact that relative effort variations are proportional to the marginal utility.

On the other hand the second firm decides by naïve way choosing a production that maximizes its profits (naïve player):

$$q_2(t+1) = \arg\max_y U_2(q_1(t), q_2(t)) \tag{10}$$

The dynamical system of the players is described by:

$$\begin{cases} q_1(t+1) = q_1(t) + k \cdot q_1(t) \dfrac{\partial U_1}{\partial q_1} \\ q_2(t+1) = \dfrac{\alpha + (\mu - 1) \cdot q_1(t)}{2(1+c)} \end{cases} \tag{11}$$

The dynamics of this system focus on the parameter k (first player's speed of adjustment) and the parameter μ (relative profit parameter).

2.2 Dynamical analysis

2.2.1 The equilibriums of the game

The equilibriums of the dynamical system (11) are obtained as nonnegative solutions of the algebraic system:

$$\begin{cases} q_1^* \cdot \dfrac{\partial U_1}{\partial q_1} = 0 \\ q_2^* = \dfrac{\alpha + (\mu - 1) \cdot q_1^*}{2(1+c)} \end{cases} \tag{12}$$

which obtained by the following settings: $q_1(t+1) = q_1(t) = q_1^*$ and $q_2(t+1) = q_2(t) = q_2^*$.

- If $q_1^* = 0$, and $\frac{\partial U_2}{\partial q_2} = 0$, then it gives $q_2^* = \frac{\alpha}{2(1+c)}$ and the equilibrium position is:

$$E_0 = \left(0, \frac{\alpha}{2(1+c)}\right) \tag{13}$$

- If $\frac{\partial U_1}{\partial q_1} = \frac{\partial U_2}{\partial q_2} = 0$, then it gives $q_1^* = q_2^* = \frac{\alpha}{2(1+c)+(1-\mu)}$ and the Nash equilibrium is:

$$E_* = \left(q_1^*, q_2^*\right) = \left(\frac{\alpha}{2(1+c)+(1-\mu)}, \frac{\alpha}{2(1+c)+(1-\mu)}\right) \tag{14}$$

The effect of the parameter k (speed of adjustment) and the parameter μ (relative profit parameter) on the dynamics of this system is investigated.

2.2.2 Stability of equilibriums

To study the stability of game's equilibriums, the Jacobian matrix is used. The Jacobian matrix $J(q_1, q_2)$ along the variable strategy (q_1, q_2) is:

$$J(q_1, q_2) = \begin{bmatrix} f_{q_1} & f_{q_2} \\ g_{q_1} & g_{q_2} \end{bmatrix} \tag{15}$$

where:

$$f(q_1, q_2) = q_1 + k \cdot q_1 \cdot \frac{\partial U_1}{\partial q_1} \tag{16}$$

and

$$g(q_1, q_2) = \frac{\alpha + (\mu - 1) \cdot q_1}{2(1+c)} \tag{17}$$

The Jacobian matrix becomes as:

$$J\left(q_1^*, q_2^*\right) = \begin{bmatrix} 1 + k \cdot \left(\frac{\partial U_1}{\partial q_1} + q_1^* \cdot \frac{\partial^2 U_1}{\partial q_1^2}\right) & k \cdot (\mu - 1) \cdot q_1^* \\ \frac{\mu - 1}{2(1+c)} & 0 \end{bmatrix} \tag{18}$$

For the E_0 the Jacobian matrix becomes as:

$$J(E_0)=\begin{bmatrix} 1+k\cdot\dfrac{\alpha(2c+1+\mu)}{2(1+c)} & 0 \\ \dfrac{\mu-1}{2(1+c)} & 0 \end{bmatrix} \tag{19}$$

with $Tr=1+k\cdot\dfrac{\alpha(2c+1+\mu)}{2(1+c)}$ and $Det=0$.

The characteristic equation of $J(E_0)$, gives the nonnegative eigenvalue:

$$r_1=Tr=1+k\cdot\frac{\alpha(2c+1+\mu)}{2(1+c)}$$

it's clearly seems that $|r_1|>1$ and the E_0 equilibrium is unstable.

For the E_* the Jacobian matrix becomes as:

$$J(E_*)=\begin{bmatrix} 1-2k\cdot(1+c)\cdot q_1^* & -k\cdot(1-\mu)\cdot q_1^* \\ \dfrac{\mu-1}{2(1+c)} & 0 \end{bmatrix} \tag{20}$$

with

$$Tr=1-2k\cdot(1+c)\cdot q_1^* \qquad \text{and} \qquad Det=-k\cdot\frac{(1-\mu)^2}{2(1+c)}\cdot q_1^* \tag{21}$$

To study the stability of Nash equilibrium the method of three conditions is used and the equilibrium position is locally asymptotically stable when they are satisfied simultaneously:

$$\begin{aligned} &\text{(i)} && 1-Det>0 \\ &\text{(ii)} && 1-Tr+Det>0 \\ &\text{(iii)} && 1+Tr+Det>0 \end{aligned} \tag{22}$$

The first condition (i) gives:

$$1-Det>0 \;\Leftrightarrow\; 1+k\cdot\frac{(1-\mu)^2}{2(1+c)}q_1^*>0 \tag{23}$$

which is always satisfied.
The second condition (ii) gives:

$$1-Tr+Det>0 \;\Leftrightarrow\; k\cdot\left[4(1+c)^2-(1-\mu)^2\right]\cdot q_1^*>0 \tag{24}$$

and it's always satisfied because $4(1+c)^2-(\mu-1)^2>0$, for $c > 0$ and $\mu_i\in[0,1]$.

Finally, the condition (iii) becomes as:

$$1+\mathrm{Tr}+\mathrm{Det}>0 \quad \Leftrightarrow \quad 2-k\frac{\alpha\cdot\left[4(1+c)^2+(1-\mu)^2\right]}{2(1+c)\cdot\left[2(1+c)+(1-\mu)\right]}>0 \qquad (25)$$

and it gives the stability condition of Nash Equilibrium E_*.

Proposition:
The Nash equilibrium of the discrete dynamical system Eq.(11) is locally asymptotically stable if:

$$2-k\frac{\alpha\cdot\left[4(1+c)^2+(1-\mu)^2\right]}{2(1+c)\cdot\left[2(1+c)+(1-\mu)\right]}>0$$

3. Numerical simulations

3.1 Stability space

At first the stability space (Fig.1) is made including the main two parameters that the dynamical analysis focuses on, the parameters k (speed of adjustment) and μ (relative profit parameter). This two-dimensional space is obtained by the stability condition that is described above in Proposition, setting specific values for the other parameters α = 5 and c = 0.20.

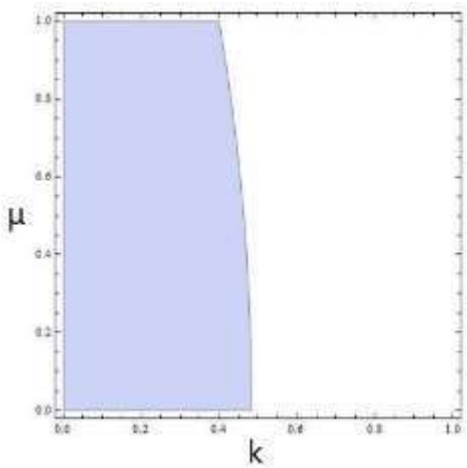

Figure 1: Region of stability between k (horizontal axis) and μ (vertical axis) for α = 5 and c = 0.20.

3.2 Focusing on the parameter k (speed of adjustment)

In this section various numerical results focusing on the parameter k, including bifurcation diagrams, strange attractors, Lyapunov numbers and sensitive dependence on initial conditions (Kulenovic, M. and Merino, O.) are presented. Focusing on the parameter k the stability condition becomes as:

$$0 < k < \frac{4(1+c)\cdot\left[2(1+c)+(1-\mu)\right]}{\alpha\cdot\left[4(1+c)^2+(1-\mu)^2\right]} \tag{26}$$

Choosing the specific values of the parameters: $\alpha = 5$, $c = 0.20$ and $\mu = 0.50$ the coordinates of Equilibrium position can be calculated as: $q_1^* = q_2^* \approx 1.72$ and the stability space for the parameter is described as:

$$0 < k < 0.48$$

It is verified by the bifurcation diagrams of the parameter k against the variables q_1^* (left) and q_2^* (right) that are shown in Fig.2 and Fig.3. These two figures show that the equilibrium undergoes a flip bifurcation at $k = 0.48$. Then a further increase in speed of adjustment implies that a stable two-period cycle emerges for $0.48 < k < 0.58$. As long as the parameter k reduces a four-period cycle, cycles of highly periodicity and a cascade of flip bifurcations that ultimately lead to unpredictable (chaotic) motions are observed when k is larger than 0.62.

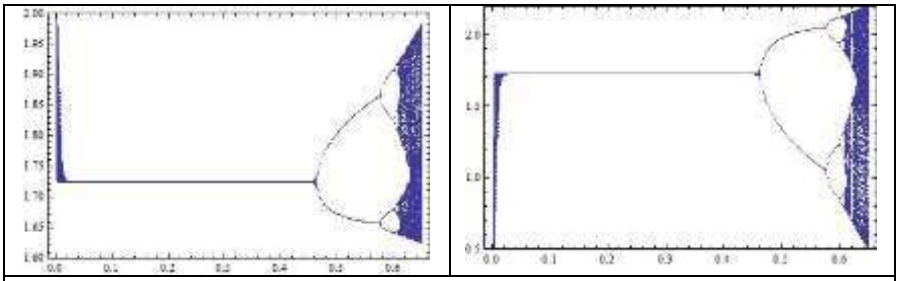

Fig.2: Bifurcation diagrams with respect to the parameter k against the variables q_1 (left) and q_2 (right) with 400 iterations of the map Eq.(11) for $\alpha = 5$, $c = 0.20$ and $\mu = 0.50$.

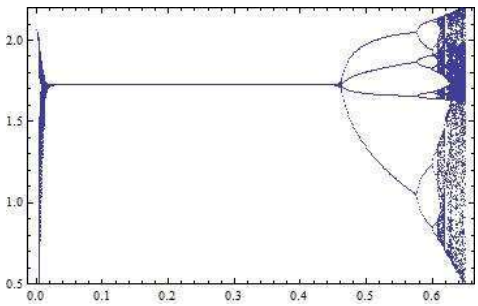

Figure 3: Two bifurcation diagrams of Fig.2 are plotted in one.

This unpredictable (chaotic) behavior of the system Eq.(11) is visualized in Fig. 4 (left) with the strange attractor for $k = 0.65$. This is the graph of the orbit of (0.1,0.1) with 8000 iterations of the map Eq.(11) for $\alpha = 5$, $c = 0.20$, $\mu = 0.50$ and $k = 0.65$. Also, we use the useful tool of Lyapunov numbers (Fig.4 (right)) (i.e. the natural logarithm of Lyapunov exponents) as a function of the parameter of interest. Figure 4 (right) shows the Lyapunov numbers of the same orbit. It is known that if the Lyapunov number is greater than 1, one has evidence for chaos.

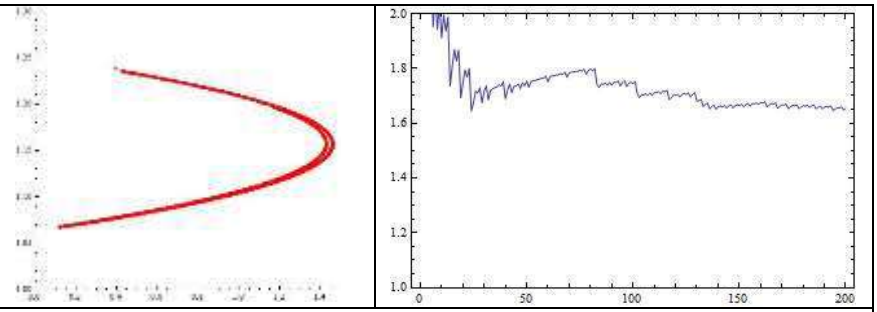

Fig. 4: Phase portrait (strange attractor) (left) and Lyapunov numbers (right) of the orbit of (0.1,0.1) with 8000 iterations of the map Eq.(11) for $\alpha = 5$, $c = 0.20$, $\mu = 0.50$ and $k = 0.65$.

Another characteristic of deterministic chaos is the sensitivity dependence on initial conditions. In order to show the sensitivity dependence on initial conditions of the system Eq.(11), we have computed two orbits with initial points (0.1,0.1) and (0.101,0.1) respectively. Figure 5 shows the sensitivity dependence on initial conditions for q_1 – coordinate of the two orbits, for the system Eq.(11), plotted against the time with the parameter values $\alpha = 5$, $c = 0.20$, $\mu = 0.50$ and $k = 0.65$. At the beginning the time series are indistinguishable; but after a number of iterations, the difference between them builds up rapidly. From these numerical results when all parameters are fixed

and only k is varied the structure of the game becomes complicated through period doubling bifurcations, more complex bounded attractors are created which are aperiodic cycles of higher order or chaotic attractors.

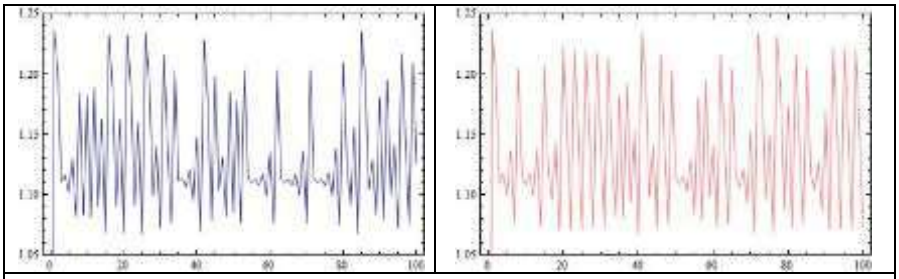

Fig. 5: Sensitive dependence on initial conditions for q_1-coordinate plotted against the time: the orbit of (0.1,0.1) (left) and the orbit of (0.101,0.1) (right) of the system Eq.(11) for $\alpha = 5$, $c = 0.20$, $\mu = 0.50$ and $k = 0.65$.

3.3 Focusing on the parameter μ (relative profit maximization)

As it seems the Nash Equilibrium Eq.(14) is independent of the parameter k (the speed of adjustment) but it depends on the values of the other parameters. As a result when the values of the parameters α , c and k remain constant and only the parameter μ varies, this makes the Nash Equilibrium not to be constant, but it changes for each different value of the parameter μ. Focusing on the parameter μ the stability condition becomes as:

$$k\alpha\mu^2 + \left[4(1+c) - 2k\alpha\right]\mu + k\alpha - 4(1+c) + 4(1+c)^2(k\alpha - 2) < 0 \qquad (27)$$

with

$$\Delta_1 = 16(1+c)^2 \cdot \left(1 + 2k\alpha - k^2\alpha^2\right) \qquad (28)$$

The inequality (27) can be satisfied if:

$$\Delta_1 > 0 \Rightarrow -k^2\alpha^2 + 2k\alpha + 1 > 0 \qquad (29)$$

and

$$\mu \in (\mu_1, \mu_2) \ , \quad \text{where } \mu_{1,2} = \frac{-2(1+c) \pm 2(1+c)\sqrt{1 + 2k\alpha - k^2\alpha^2}}{k\alpha} + 1 \qquad (30)$$

The Eq.(29) becomes true if:

$$\left.\begin{array}{l} k \in (-\infty, k_1) \cup (k_2 + \infty) \\ k > 0 \\ k_{1,2} = \dfrac{1 \pm \sqrt{2}}{\alpha} \end{array}\right\} \Rightarrow 0 < k < \frac{1+\sqrt{2}}{\alpha}$$

Finally, the stability condition Eq.(27) is satisfied if:

$$\left.\begin{array}{l}\mu \in (\mu_1, \mu_2) \\ \mu > 0 \\ 0 < k < \dfrac{1+\sqrt{2}}{\alpha}\end{array}\right\} \Rightarrow \left.\begin{array}{l}\mu \in (0, \mu_2) \\ 0 < k < \dfrac{1+\sqrt{2}}{\alpha}\end{array}\right\} \Rightarrow \left.\begin{array}{l}0 < \mu < \dfrac{2(1+c)\sqrt{1+2k\alpha - k^2\alpha^2} - 1}{k\alpha} + 1 \\ 0 < k < \dfrac{1+\sqrt{2}}{\alpha}\end{array}\right\}$$

Setting the specific values of the parameters: $\alpha = 5$, $c = 0.20$ and $k = 0.475$ it gives that the stability space focusing on the parameter μ becomes as:

$$0 < \mu < 0.32$$

Using the stability space (Fig.1) when $\alpha = 5$, $c = 0.20$ and $k = 0.475$, it can be verified that there is a stable equilibrium for $\mu \in (0, 0.32)$ and it is also verified by the bifurcation diagrams of μ against q_1 (left) and q_2 (right) (Fig.6). Also, the chaotic behavior for the system Eq.(11) appears only for values of the parameter μ (relative profit parameter) larger than 1 so if $k = 0.475$ in this market the parameter μ cannot make the system unpredictable. Finally, the stability space between the main parameters k and μ (Fig.1) gives the useful result that for small values of the parameter k, the Nash Equilibrium remain stable for every value of the parameter μ and in this area the parameter μ cannot destabilize the economy.

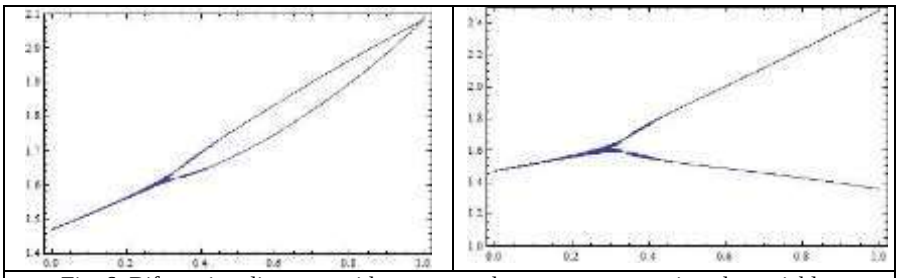

Fig. 6: Bifurcation diagrams with respect to the parameter μ against the variables q_1 (left) and q_2 (right) with 400 iterations of the map Eq.(11) for $\alpha = 5$, $c = 0.20$ and $k = 0.475$.

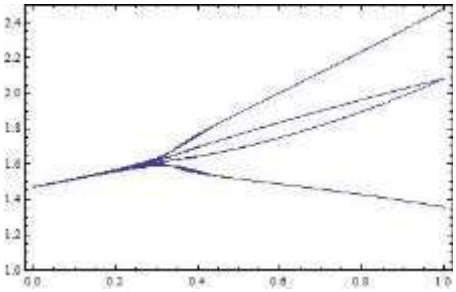

Figure 10: Two bifurcation diagrams of Fig.9 are plotted in one.

Now, if the other parameter take the values: $\alpha = 5$, $c = 0.20$ and $k = 0.60$, it seems that first a fixed period 2 trajectory is created and then it enters a period doubling and as the parameter μ takes higher values the system enters a chaotic orbit and becomes unpredictable. (Fig.11-12). The larger the values of the parameter μ more Strange attractors and Lyapunov numbers larger than 1 (Fig.13) are appeared for the same values of the paramaters α, c and k. Also, the system becomes sensitive on initial condition (Fig.14) for these large values of the parameter μ (outside the stability space of μ).

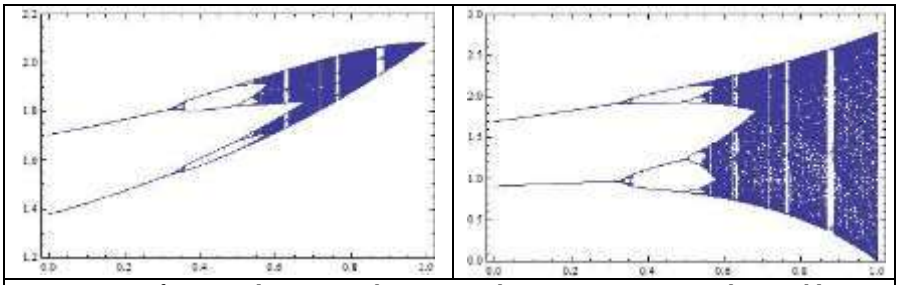

Fig. 11: Bifurcation diagrams with respect to the parameter μ against the variables q_1 (left) and q_2 (right) with 400 iterations of the map Eq.(11) for $\alpha = 5$, $c = 0.20$ and $k = 0.60$.

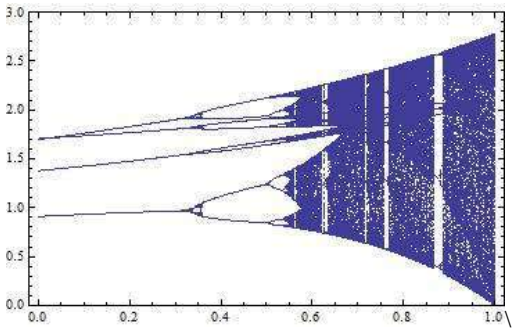

Figure 12: Two bifurcation diagrams of Fig.11 are plotted in one.

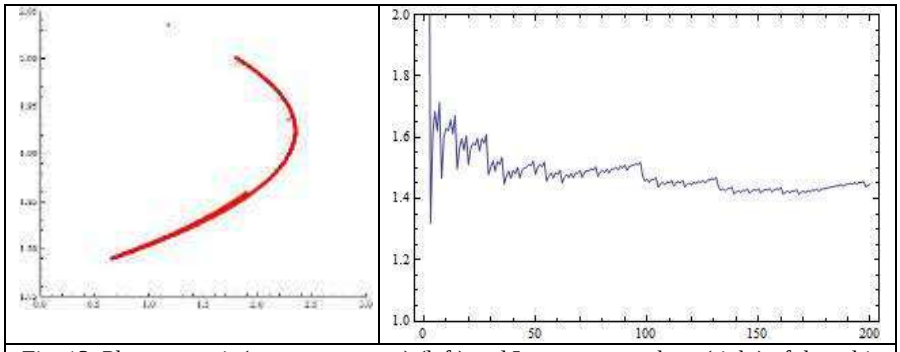

Fig. 13: Phase portrait (strange attractor) (left) and Lyapunov numbers (right) of the orbit of (0.1,0.1) with 8000 iterations of the map Eq.(11) for $\alpha = 5$, $c = 0.20$, $k = 0.60$ and $\mu = 0.80$.

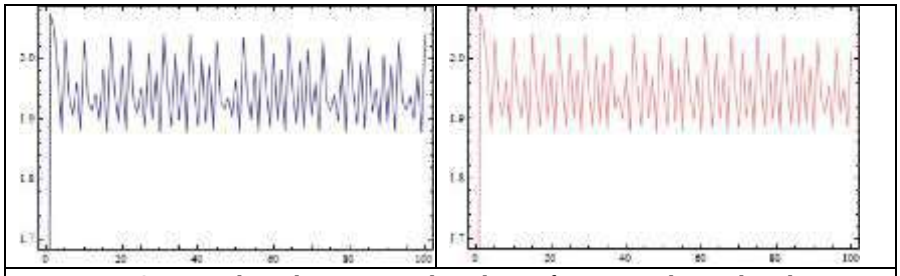

Figure 14: Sensitive dependence on initial conditions for q_1 -coordinate plotted against the time: the orbit of (0.1,0.1) (left) and the orbit of (0.101,0.1) (right) of the system Eq.(11) for $\alpha = 5$, $c = 0.20$, $k = 0.60$ and $\mu = 0.80$.

4. Conclusions

In this paper the dynamics of a differentiated Cournot duopoly with heterogeneous expectations, linear demand and quadratic cost functions are analyzed. By assuming that at each time period each firm maximizes its expected relative profit function U under bounded rationality expectation, a discrete dynamic system was obtained. Existence and stability of equilibrium of this system are studied. It is numerically shown that the model gives chaotic and unpredictable trajectories. The main result is that higher values of the speed of adjustment and relative profit parameter may destabilize the Cournot–Nash equilibrium. Finally, it is proved that for lower values of the speed of adjustment the equilibrium is stable for every value of the relative profit parameter.

References

1. Agiza HN., On the stability, bifurcations, chaos and chaos control of Kopel map. Chaos Solitons Fract. 11: 1909-16, 2004.
2. Agiza HN, Elsadany AA, Chaotic dynamics in nonlinear duopoly game with heterogeneous players. Appl. Math. Comput. 149: 843–860, 2004.
3. Agiza HN, Elsadany AA., Nonlinear dynamics in the Cournot duopoly game with heterogeneous players. Physica A 320: 512–24, 2003.
4. Agiza HN, Hegazi AS, Elsadany AA.m., Complex dynamics and synchronization of duopoly game with bounded rationality. Math. Comput. Simulat. 58: 133–46, 2002.
5. Agliari, A., Gardini, L., & Puu, T., Some global bifurcations related to the appearance of closed invariant curves. Mathematics and Computers in Simulation, 68, 201–219, 2005.
6. Agliari, A., Gardini, L., & Puu, T., Global bifurcations in duopoly when the Cournot point is destabilized via a subcritical Neimark bifurcation. International Game Theory Review, 8, 1–20, 2006.
7. Askar, S.S., On complex dynamics of monopoly market, Economic Modelling, 31: 586-589, 2013.
8. Askar, S. S., Complex dynamic properties of Cournot duopoly games with convex and log-concave demand function, Operations Research Letters 42, 85–90, 2014.
9. Baumol, W.J., Quandt, R.E., Rules of thumb and optimally imperfect decisions, American Economic Review 54 (2): 23–46, 1964.
10. Bischi GI, Kopel M., Equilibrium selection in a nonlinear duopoly game with adaptive expectations. J. Econom Behav. Org. 46: 73–100, 2001.
11. Den Haan WJ., The importance of the number of different agents in a heterogeneous asset-pricing model. J. Econom. Dynam. Control, 25:721–46, 2001.
12. Elsadany A.A., Dynamics of a Cournot duopoly game with bounded rationality based on relative profit maximization. Applied Mathematics and Computation 294, 253–263, 2017.
13. Elaydi, S., An Introduction to Difference Equations, third ed., Springer-Verlag, New York, 2005.
14. Fanti, L., & Gori, L., The dynamics of a differentiated duopoly with quantity competition. Economic Modelling, 29, 421–427, 2012.
15. Hommes, C.H., Heterogeneous agent models in economics and finance, in: L. Tesfatsion, K.L. Judd (Eds.), Handbook of Computational Economics, Agent-Based Computational Economics, vol. 2, Elsevier Science B.V: 1109–1186, 2006.
16. Gandolfo G., Economic dynamics. Berlin: Springer, 1997.
17. Gao Y., Complex dynamics in a two dimensional noninvertible map. Chaos Solitons Fract. 39: 1798–810, 2009.
18. Kopel M., Simple and complex adjustment dynamics in Cournot duopoly models. Chaos Solitons Fract. 12: 2031–48, 1996.
19. Kulenonic, M., Merino, O., Discrete Dynamical Systems and Difference Equations with Mathematica, Chapman & Hall/Crc., 2002.
20. Naimzada, A.K., Ricchiuti G., Complex dynamics in a monopoly with a rule of thumb, Applied Mathematics and Computation 203: 921–925, 2008.
21. Naimzada, A., Sbragia, L., Oligopoly games with nonlinear demand and cost functions: two boundedly rational adjustment processes, Chaos Solitons Fractals 29 (3), 707–722, 2006.
22. Puu, T., The chaotic monopolist, Chaos, Solitons & Fractals 5 (1): 35–44, 1995.
23. Puu T., The chaotic duopolists revisited. J Econom. Behav. Org. 37: 385–94, 1998.
24. Puu T., Chaos in duopoly pricing. Chaos Solitons Fract.1:573–81, 1991.

25. Puu T., Complex oligopoly dynamics. In: Lines M, editor. Nonlinear dynamical systems in economics. Springer Wien NewYork: CISM; p. 165–86, 2005.
26. Sarafopoulos G., On the dynamics of a duopoly game with differentiated goods, Procedia Economics and Finance, 19, 146 – 153, 2015.
27. Sarafopoulos G., Complexity in a duopoly game with homogeneous players, convex, log linear demand and quadratic cost functions, Procedia Economics and Finance, 33, 358 – 366, 2015.
28. Sarafopoulos G., Papadopoulos K., On a Cournot duopoly game with differentiated goods, heterogeneous expectations and a cost function including emission costs, Scientific Bulletin - Economic Sciences , vol. 16 (1), 11-22, 2017.
29. Sarafopoulos G., Papadopoulos K., Complexity in a Bertrand duopoly game with heterogeneous players and differentiated goods, Springer Proceedings in Business and Economic, Article: 2, pages: 15 – 26, Springer Nature Switzerland AG, (ISBN: 978-3-030-12169-3), 2019.
30. Sarafopoulos G., Papadopoulos K., On a Bertrand dynamic game with differentiated goods, heterogeneous expectations and asymmetric cost functions, Springer Proceedings in Business and Economic Article: 14, pages: 223 – 241, Springer Nature Switzerland AG, (ISBN: 978-3-030-39927-6), 2020.
31. Singh, N., Vives, X., Price and quantity competition in a differentiated duopoly. The RAND Journal of Economics 15, 546–554, 1984.
32. Tramontana, F., Heterogeneous duopoly with isoelastic demand function. Economic Modelling 27, 350–357, 2010.
33. Westerhoff, F., Nonlinear expectation formation, endogenous business cycles and stylized facts, Studies in Nonlinear Dynamics and Econometrics 10 (4) (Article 4), 2006.
34. Wu, W., Chen, Z., Ip, W.H., Complex nonlinear dynamics and controlling chaos in a Cournot duopoly economic model. Nonlinear Analysis: Real World Applications 11, 4363–4377, 2010.
35. Zhang, J., Da, Q.,Wang, Y., Analysis of nonlinear duopoly game with heterogeneous players. Economic Modelling 24, 138–148, 2007.
36. Zhang J., Da Q., Wang Y., The dynamics of Bertrand model with bounded rationality, Chaos, Solitons and Fractals 39, 2048-2055, 2009.

Chaotic Behavior in a Duopoly Market and application of the d-Backtest Method

Georges Sarafopoulos[1], Evaggelos Drimpetas[2], Kosmas Papadopoulos[3] , Dimitrios Vezeris[4]

[1] Department of Economics, Democritus University of Thrace, Komotini, Greece
(E-mail: gsarafop@econ.duth.gr)
[2] Department of Economics, Democritus University of Thrace, Komotini, Greece
(E-mail: edrimpet@econ.duth.gr)
[3] Department of Economics, Democritus University of Thrace, Komotini, Greece
(E-mail: kpapa@econ.duth.gr)
[4] Department of Electrical & Computer Engineering, Democritus University of Thrace, Xanthi, Greece
(E-mail: d.vezeris@ioniki.net)

Abstract: This paper investigates the dynamics of a nonlinear duopoly game with bounded rational players and differentiated goods. We suppose linear demand and the cost functions are derived from the study of a duopoly in the Greek market (two oil companies Hellenic Petroleum and Motor Oil). The game is modeled with a system of two difference equations. Existence and stability of equilibrium of this system are studied. We examine the effect of the parameters in the dynamic of the model and we show that the model gives more complex chaotic and unpredictable trajectories as a consequence of change in the parameter of speed of adjustment and in the parameter of the product differentiation. The chaotic features are justified numerically via computing Lyapunov numbers, sensitive dependence on initial conditions, bifurcations diagrams and strange attractors. Finally, we apply the d-Backtest method for dynamic parameter selection and examine the stability of the system[1].

Keywords: Dupoly game; Discrete dynamical system; Nash equilibrium; Stability; Bifurcation; Chaotic Behavior; d-Backtest Method.

---

[1] This research is carried out / funded in the context of the project "Nonlinear dynamics in oligopoly market: Chaotic behavior, complexity control using machine learning and application in an oligopoly of the Greek market" (MIS 5049905) under the call for proposals "Researchers' support with an emphasis on young researchers – 2nd Cycle". The project is co-financed by Greece and the European Union (European Social Fund – ESF) by the Operational Programme "Human Resources Development, Education and Lifelong Learning 2014-2020".

1 Introduction

An Oligopoly is a market structure between monopoly and perfect competition, where there are only a few number of firms in the market producing homogeneous products. The dynamic of an oligopoly game is more complex because firms must consider not only the behaviors of the consumers, but also the reactions of the competitors i.e. they form expectations concerning how their rivals will act. Cournot, in 1838 has introduced the first formal theory of oligopoly. In 1883 another French mathematician Joseph Louis Francois Bertrand modified Cournot game suggesting that firms actually choose prices rather than quantities. Originally Cournot and Bertrand models were based on the premise that all players follow naive expectations, so that in every step, each player (firm) assumes the last values that were taken by the competitors without estimation of their future reactions. However, in real market conditions such an assumption is very unlikely since not all players share naive beliefs. Therefore, different approaches to firm behavior were proposed. Some authors considered duopolies with homogeneous expectations and found a variety of complex dynamics in their games, such as appearance of strange attractors (Agiza, 1999, Agiza et al., 2002, Agliari et al., 2005, 2006, Bischi, Kopel, 2001, Kopel, 1996, Puu, 1998, Sarafopoulos, 2015, Zhang , 2009). Also models with heterogeneous agents were studied (Agiza, Elsadany , 2003, 2004, Agiza et al., 2002, Den Haan , 20013, Fanti, Gori, 2012, Tramontana, 2010, Zhang , 2007).

In the real market producers do not know the entire demand function, though it is possible that they have a perfect knowledge of technology, represented by the cost function. Hence, it is more likely that firms employ some local estimate of the demand. This issue has been previously analyzed by Baumol and Quandt, 1964, Puu 1995, Naimzada and Ricchiuti, 2008, Askar, 2013, Askar, 2014. Bounded rational players (firms) update their strategies based on discrete time periods and by using a local estimate of the marginal profit. With such local adjustment mechanism, the players are not requested to have a complete knowledge of the demand and the cost functions (Agiza, Elsadany, 2004, Naimzada, Sbragia, 2006, Zhang *et al*, 2007, Askar, 2014).

In this paper we study the dynamics of a Bertrand- type duopoly with differentiated goods where each firm behaves with homogeneous expectations. We show that the model gives more complex chaotic and unpredictable trajectories as a consequence of change of the speed of players' adjustment (parameter k). The paper is organized as follows: In Section 2, the dynamics of the duopoly game with homogeneous expectations, linear demand and asymmetric cost functions for two players are analyzed. We set both players as bounded rational. The existence and local stability of the equilibrium points are also analyzed. In Section 3 numerical simulations are used to verify the algebraic results of Section 2 plotting the bifurcation diagrams of the game's system and to show the complex dynamics via computing Lyapunov numbers, and sensitive dependence on initial conditions. Finally, in section 4 the application of d-Backtest in this duopoly game is presented as an attempt to control the chaotic of the discrete dynamical system that appears.

2 The game

2.1 The construction of the game

In this study we consider homogeneous players and more specifically, we consider that both firms choose their products' prices in a rational way, following an adjustment mechanism (bounded rational players). We consider a simple Bertrand-type duopoly market where firms (players) produce differentiated goods and offer them at discrete-time periods on a common market. Price decisions are taken at discrete time periods t = 0, 1, 2,… At each period t, every firm must form an expectation of the rival's strategy in the next time period in order to determine the corresponding profit-maximizing prices for period t+1. We suppose that q_1, q_2 are the production quantities of each firm. Also, we consider that the preferences of consumers represented by the equation:

$$U(q_1, q_2) = \alpha(q_1 + q_2) - \frac{1}{2}\left(q_1^2 + q_2^2 + 2dq_1q_2\right) \quad (1)$$

where α is a positive parameter (α > 0), which expresses the market size and $d \in (-1,1)$ is the parameter that reveals the differentiation degree of products. For example, if $d = 0$ then both products are independently and each firm participates in a monopoly. But, if $d = 1$ then one product is a substitute for the other, since the products are homogeneous. It is understood that for positive values of the parameter d the larger the value, the less diversification we have in both products. On the other hand negative values of the parameter d are described that the two products are complementary and when $d = -1$ then we have the phenomenon of full competition between the two companies. The inverse demand functions (as functions of quantities) coming from the maximizing of (1) are given by the following equations:

$$p_1(q_1, q_2) = \alpha - q_1 - dq_2 \quad \text{and} \quad p_2(q_1, q_2) = \alpha - q_2 - dq_1 \quad (2)$$

The direct demand functions (as functions of prices):

$$q_1(p_1, p_2) = \frac{\alpha(1-d) - p_1 + dp_2}{1-d^2} \quad \text{and} \quad q_2(p_1, p_2) = \frac{\alpha(1-d) - p_2 + dp_1}{1-d^2} \quad (3)$$

In this work, data were collected from the financial reports of two companies. The data related to sales quantities in thousands of metric tons (k MT) and total revenue in millions of euro (m €) for each quarter of the years from 2011 to 2020. With this data and using regression analysis we tried to approach the form of the cost function of each company. According to this analysis we can assume that the cost function of the first player is quadratic and of the second player is linear[2].

[2] The coefficients of determination of the regressions are relatively small 0.51 and 0.39 respectively. This is due to the fact that the cost functions of the companies depend on many unpublished factors.

We suppose that the cost function of the first player (Motor Oil Group) is:

$$C_1(q_1) = c_1 \cdot q_1^2 + c_2 \cdot q_1 + c_3 \tag{4}$$

with $c_1 > 0,\ c_2 \geq 0,\ c_3 \geq 0$ and $c_2^2 \leq 4 \cdot c_1 \cdot c_3$ (quadratic cost's conditions).

and the cost function of the second player (Hellenic Petroleum Group) is linear:

$$C_2(q_2) = c_4 \cdot q_2 + c_5 \tag{5}$$

where $c_4 > 0$ and $c_5 \geq 0$ (linear cost function's conditions).

With these assumptions the profits of the firms are given by:

$$\Pi_1(p_1, p_2) = p_1 q_1 - C_1(q_1) = (p_1 - c_2) \cdot \frac{\alpha(1-d) - p_1 + dp_2}{1-d^2} - c_1 \cdot \left[\frac{\alpha(1-d) - p_1 + dp_2}{1-d^2}\right]^2 - c_3 \tag{6}$$

and

$$\Pi_2(p_1, p_2) = p_2 q_2 - C_2(q_2) = (p_2 - c_4) \cdot \frac{\alpha(1-d) - p_2 + dp_1}{1-d^2} - c_5 \tag{7}$$

Then the marginal profits at the point of the strategy space are given by:

$$\frac{\partial \Pi_1}{\partial p_1} = \frac{1}{\left(1-d^2\right)^2}\left[\alpha(1-d)\left(1-d^2+2c_1\right) + c_2\left(1-d^2\right) - 2\left(1-d^2+c_1\right)\cdot p_1 + d\left(1-d^2+2c_1\right)\cdot p_2\right] \tag{8}$$

and

$$\frac{\partial \Pi_2}{\partial p_2} = \frac{\alpha(1-d) + c_4 - 2p_2 + dp_1}{1-d^2} \tag{9}$$

Both players are characterized as bounded rational players. According to the existing literature it means that they decide their prices following a mechanism that is described by the equation:

$$\frac{p_i(t+1) - p_i(t)}{p_i(t)} = k \cdot \frac{\partial \Pi_i}{\partial p_i}\ ,\ k > 0 \tag{10}$$

Through this mechanism the player i, increases his level of adaptation when his marginal profit is positive or decreases his level when his marginal profit is negative, where k is the speed of adjustment of player, it is a positive parameter (k > 0), which gives the extend variation of price of the Hellenic Petroleum and Motor Oil Groups, following a given utility signal.

The dynamical system of the players is described by:

$$\begin{cases} p_1(t+1) = p_1(t) + k \cdot p_1(t) \cdot \dfrac{\partial \Pi_1}{\partial p_1} \\ p_2(t+1) = p_2(t) + k \cdot p_2(t) \cdot \dfrac{\partial \Pi_2}{\partial p_2} \end{cases} \tag{11}$$

We will focus on the dynamics of this system to the parameter k.

2.2 Dynamical analysis

The dynamical analysis of the discrete dynamical system involves finding equilibrium positions and studying them for stability. The ultimate goal of this algebraic study is to formulate a proposition that will be the stability condition

of the Nash Equilibrium position. Finally, these algebraic results are verified and visualized doing some numerical simulations using the program of Mathematica.

2.2.1 The equilibrium positions

The equilibriums of the dynamical system (11) are obtained as the nonnegative solutions of the algebraic system:

$$\begin{cases} p_1^* \cdot \dfrac{\partial \Pi_1}{\partial p_1} = 0 \\ p_2^* \cdot \dfrac{\partial \Pi_2}{\partial p_2} = 0 \end{cases} \tag{12}$$

which is obtained by setting : $p_1(t+1) = p_1(t) = p_1^*$ and $p_2(t+1) = p_2(t) = p_2^*$.

- If $p_1^* = p_2^* = 0$ then the equilibrium position is the point:

$$E_0 = (0,0) \tag{13}$$

- If $p_1^* = 0$ and $\dfrac{\partial \Pi_2}{\partial p_2} = 0$ then: $p_2^* = \dfrac{\alpha(1-d)+c_4}{2}$ and the equilibrium position is the point:

$$E_1 = \left(0, \frac{\alpha(1-d)+c_4}{2}\right) \tag{14}$$

- If $p_2^* = 0$ and $\dfrac{\partial \Pi_1}{\partial p_1} = 0$ then: $p_1^* = \dfrac{\alpha(1-d)\left(1-d^2+2c_1\right)+c_2\left(1-d^2\right)}{2\left(1-d^2+c_1\right)}$

and the equilibrium position is the point:

$$E_2 = \left(\frac{\alpha(1-d)\left(1-d^2+2c_1\right)+c_2\left(1-d^2\right)}{2\left(1-d^2+c_1\right)}, 0\right) \tag{15}$$

- If $\dfrac{\partial \Pi_1}{\partial p_1} = \dfrac{\partial \Pi_2}{\partial p_2} = 0$ then the following system is obtained:

$$\begin{cases} \alpha(1-d)\left(1-d^2+2c_1\right)+c_2\left(1-d^2\right)-2\left(1-d^2+c_1\right)\cdot p_1^* + d\left(1-d^2+2c_1\right)\cdot p_2^* = 0 \\ \alpha(1-d)+c_4-2p_2^*+dp_1^* = 0 \end{cases} \tag{16}$$

and the nonnegative solution of this algebraic system gives the Nash Equilibrium position $E_* = \left(p_1^*, p_2^*\right)$ where:

$$p_1^* = \frac{\left(1-d^2+2c_1\right)\cdot\left[\alpha(1-d)(2+d)+dc_4\right]+2c_2\left(1-d^2\right)}{4\left(1-d^2+c_1\right)-d^2\left(1-d^2+2c_1\right)} \tag{17}$$

and

$$p_2^* = \frac{2\left(1-d^2+c_1\right)\cdot\left[\alpha(1-d)+c_4\right]+d(1-d)\cdot\left[\alpha\left(1-d^2+2c_1\right)+c_2(1+d)\right]}{4\left(1-d^2+c_1\right)-d^2\left(1-d^2+2c_1\right)} \quad (18)$$

From the three equilibrium positions E_1, E_2 and E_* the following conditions arise:

$$\alpha(1-d)+c_4>0 \quad (19)$$

$$\alpha(1-d)\left(1-d^2+2c_1\right)+c_2\left(1-d^2\right)>0 \quad (20)$$

$$2\left(1-d^2+c_1\right)>0 \quad (21)$$

$$2\left(1-d^2+c_1\right)\cdot\left[\alpha(1-d)+c_4\right]+d(1-d)\cdot\left[\alpha\left(1-d^2+2c_1\right)+c_2(1+d)\right]>0 \quad (22)$$

$$4\left(1-d^2+c_1\right)-d^2\left(1-d^2+2c_1\right)>0 \quad (23)$$

2.2.2 Stability of equilibrium points

To study the stability of the equilibrium positions we need the Jacobian matrix of the dynamical system Eq.(11) which is the matrix:

$$J\left(p_1^*,p_2^*\right)=\begin{bmatrix} f_{p_1} & f_{p_2} \\ g_{p_1} & g_{p_2}\end{bmatrix} \quad (24)$$

where:

$$\begin{aligned} f(p_1,p_2) &= p_1+k\cdot p_1\cdot\frac{\partial\Pi_1}{\partial p_1} \\ g(p_1,p_2) &= p_2+k\cdot p_2\cdot\frac{\partial\Pi_2}{\partial p_2}\end{aligned} \quad (25)$$

and as a result the Jacobian matrix of game's discrete dynamical system Eq.(11) is the following matrix:

$$J\left(p_1^*,p_2^*\right)=\begin{bmatrix} 1+k\cdot\left(\frac{\partial\Pi_1}{\partial p_1}+p_1^*\cdot\frac{\partial^2\Pi_1}{\partial p_1^2}\right) & k\cdot p_1^*\cdot\frac{\partial^2\Pi_1}{\partial p_1\partial p_2} \\ k\cdot p_2^*\cdot\frac{\partial^2\Pi_2}{\partial p_2\partial p_1} & 1+k\cdot\left(\frac{\partial\Pi_2}{\partial p_2}+p_2^*\cdot\frac{\partial^2\Pi_2}{\partial p_2^2}\right)\end{bmatrix} \quad (26)$$

For the E_0 the Jacobian matrix becomes as:

$$J(E_0)=\begin{bmatrix} 1+k\cdot\frac{\partial\Pi_1}{\partial p_1}(E_0) & 0 \\ 0 & 1+k\cdot\frac{\partial\Pi_2}{\partial p_2}(E_0)\end{bmatrix} \begin{matrix} A=1+k\cdot\frac{\partial\Pi_1}{\partial p_1}(E_0) \\ = \\ B=1+k\cdot\frac{\partial\Pi_2}{\partial p_2}(E_0)\end{matrix} \begin{bmatrix} A & 0 \\ 0 & B\end{bmatrix} \quad (27)$$

with

$$\mathrm{Tr} = \mathrm{A} + \mathrm{B} \text{ and } \mathrm{Det} = \mathrm{A} \cdot \mathrm{B}.$$

The characteristic equation of $\mathrm{J}(\mathrm{E}_0)$ is the following:

$$r^2 - \mathrm{TrJ}(\mathrm{E}_0) \cdot r + \mathrm{DetJ}(\mathrm{E}_0) = 0 \Leftrightarrow$$

$$\Leftrightarrow r^2 - (\mathrm{A} + \mathrm{B}) \cdot r + \mathrm{A} \cdot \mathrm{B} = 0 \Leftrightarrow (r - \mathrm{A})(r - \mathrm{B}) = 0$$

The eigenvalues of $\mathrm{J}(\mathrm{E}_0)$ are:

$$r_1 = \mathrm{A} = 1 + k\frac{\alpha(1-d)\left(1-d^2+2c_1\right)}{\left(1-d^2\right)^2} \quad \text{and} \quad r_2 = \mathrm{B} = 1 + k\frac{\alpha(1-d)+c_4}{1-d^2}$$

As it is clearly seems $|r_1|, |r_2| > 1$, because of Eq. (19) and Eq. (20). It means that the equilibrium position E_0 can be characterized as unstable.

For the position E_1 the Jacobian matrix becomes as:

$$\mathrm{J}(\mathrm{E}_1) = \begin{bmatrix} 1 + k \cdot \frac{\partial \Pi_1}{\partial p_1}(\mathrm{E}_1) & 0 \\ k \cdot p_2^* \cdot \frac{\partial^2 \Pi_2}{\partial p_2 \partial p_1}(\mathrm{E}_1) & 1 + k \cdot p_2^* \cdot \frac{\partial^2 \Pi_2}{\partial p_2^2}(\mathrm{E}_1) \end{bmatrix} \begin{matrix} C = 1 + k \cdot \frac{\partial \Pi_1}{\partial p_1}(\mathrm{E}_1) \\ = \\ D = 1 + k \cdot p_2^* \cdot \frac{\partial^2 \Pi_2}{\partial p_2^2} \end{matrix} \begin{bmatrix} C & 0 \\ E & D \end{bmatrix} \tag{28}$$

with $\mathrm{Tr} = C + D$ and $\mathrm{Det} = C \cdot D$.

From the characteristic equation of $\mathrm{J}(\mathrm{E}_1)$, the nonnegative eigenvalue are found as:

$$r_1 = C = 1 + k \cdot \frac{1}{\left(1-d^2\right)^2}\left[\alpha(1-d)\left(1-d^2+2c_1\right) + c_2\left(1-d^2\right) + d\left(1-d^2+2c_1\right) \cdot p_2^*\right]$$

and

$$r_2 = \mathrm{B} = 1 - k\frac{\alpha(1-d)+c_4}{1-d^2}$$

Since, Eq. (20) it's clearly seems that $|r_1| > 1$ and the E_1 equilibrium is unstable.

For the position E_2 the Jacobian matrix becomes as:

$$\mathrm{J}(\mathrm{E}_2) = \begin{bmatrix} 1 + k \cdot p_1^* \cdot \frac{\partial^2 \Pi_1}{\partial p_1^2}(\mathrm{E}_2) & k \cdot p_1^* \cdot \frac{\partial^2 \Pi_1}{\partial p_1 \partial p_2}(\mathrm{E}_2) \\ 0 & 1 + k \cdot \frac{\partial \Pi_2}{\partial p_2}(\mathrm{E}_2) \end{bmatrix} \begin{matrix} F = 1 + k \cdot p_1^* \cdot \frac{\partial^2 \Pi_1}{\partial p_1^2}(\mathrm{E}_2) \\ = \\ G = 1 + k \cdot \frac{\partial \Pi_2}{\partial p_2}(\mathrm{E}_2) \end{matrix} \begin{bmatrix} F & H \\ 0 & G \end{bmatrix} \tag{29}$$

with $\mathrm{Tr} = F + G$ and $\mathrm{Det} = F \cdot G$.

From the characteristic equation of $\mathrm{J}(\mathrm{E}_2)$, the nonnegative eigenvalue are found as:

$$r_1 = C = 1 - k \cdot \frac{1}{\left(1-d^2\right)^2}\left[\alpha(1-d)\left(1-d^2+2c_1\right) + c_2\left(1-d^2\right) - 2\left(1-d^2+c_1\right) \cdot p_1^*\right]$$

and

$$r_2 = B = 1 + k\frac{\alpha(1-d) + c_4 + dp_1^*}{1-d^2}$$

Since, Eq. (19) it's clearly seems that $|r_2| > 1$ and the E_2 equilibrium is unstable.

For the E_* the Jacobian matrix becomes as:

$$J(E_*) = \begin{bmatrix} 1 + k \cdot p_1^* \cdot \dfrac{\partial^2 \Pi_1}{\partial p_1^2} & k \cdot p_1^* \cdot \dfrac{\partial^2 \Pi_1}{\partial p_1 \partial p_2} \\ k \cdot p_2^* \cdot \dfrac{\partial^2 \Pi_2}{\partial p_2 \partial p_1} & 1 + k \cdot p_2^* \cdot \dfrac{\partial^2 \Pi_2}{\partial p_2^2} \end{bmatrix} \tag{30}$$

with

$$Tr = 2 + k \cdot p_1^* \cdot \frac{\partial^2 \Pi_1}{\partial p_1^2} + k \cdot p_2^* \cdot \frac{\partial^2 \Pi_2}{\partial p_2^2} \tag{31}$$

and

$$Det = \left(1 + k \cdot p_1^* \cdot \frac{\partial^2 \Pi_1}{\partial p_1^2}\right)\left(1 + k \cdot p_2^* \cdot \frac{\partial^2 \Pi_2}{\partial p_2^2}\right) - k^2 \cdot p_1^* \cdot p_2^* \cdot \frac{\partial^2 \Pi_1}{\partial p_1 \partial p_2} \cdot \frac{\partial^2 \Pi_2}{\partial p_2 \partial p_1} \tag{32}$$

To study the stability of Nash equilibrium we use three conditions that the equilibrium position is locally asymptotically stable when they are satisfied simultaneously:

$$\begin{aligned} &\text{(i)} && 1 - Det > 0 \\ &\text{(ii)} && 1 - Tr + Det > 0 \\ &\text{(iii)} && 1 + Tr + Det > 0 \end{aligned} \tag{33}$$

It's easy to find that the first condition (i) becomes as:

$$1 - Det > 0 \quad \Leftrightarrow$$

$$\Leftrightarrow \left[4\left(1-d^2+c_1\right) - d^2 \cdot \left(1-d^2+2c_1\right)\right] \cdot k - 2\left(1-d^2\right)\left[\frac{\left(1-d^2+c_1\right)}{p_2^*} + \frac{\left(1-d^2\right)}{p_1^*}\right] < 0 \tag{34}$$

Also, the condition (ii) gives:

$$1 - Tr + Det > 0 \quad \Leftrightarrow$$

$$\Leftrightarrow k \cdot p_1^* \cdot p_1^* \cdot \frac{4\left(1-d^2+c_1\right) - d^2 \cdot \left(1-d^2+2c_1\right)}{\left(1-d^2\right)^3} > 0 \tag{35}$$

and it's always satisfied because of Eq. (23).

Finally, the condition (iii) becomes as:

$$1+\mathrm{Tr}+\mathrm{Det}>0 \quad \Leftrightarrow$$

$$k^2\cdot p_1^*\cdot p_2^*\cdot\frac{\left[4\left(1-d^2+c_1\right)-d^2\cdot\left(1-d^2+2c_1\right)\right]}{\left(1-d^2\right)^3}-4\cdot k\cdot\frac{\left[p_1^*\cdot\left(1-d^2+c_1\right)+p_2^*\cdot\left(1-d^2\right)\right]}{\left(1-d^2\right)^2}+4>0 \quad (36)$$

Proposition:
The Nash equilibrium of the discrete dynamical system Eq.(11) is locally asymptotically stable if:

$$\left[4\left(1-d^2+c_1\right)-d^2\cdot\left(1-d^2+2c_1\right)\right]\cdot k-2\left(1-d^2\right)\left[\frac{\left(1-d^2+c_1\right)}{p_2^*}+\frac{\left(1-d^2\right)}{p_1^*}\right]<0$$

and

$$k^2\cdot p_1^*\cdot p_2^*\cdot\frac{\left[4\left(1-d^2+c_1\right)-d^2\cdot\left(1-d^2+2c_1\right)\right]}{\left(1-d^2\right)^3}-4\cdot k\cdot\frac{\left[p_1^*\cdot\left(1-d^2+c_1\right)+p_2^*\cdot\left(1-d^2\right)\right]}{\left(1-d^2\right)^2}+4>0$$

where

$$p_1^*=\frac{\left(1-d^2+2c_1\right)\cdot\left[\alpha(1-d)(2+d)+dc_4\right]+2c_2\left(1-d^2\right)}{4\left(1-d^2+c_1\right)-d^2\left(1-d^2+2c_1\right)}$$

and

$$p_2^*=\frac{2\left(1-d^2+c_1\right)\cdot\left[\alpha(1-d)+c_4\right]+d(1-d)\cdot\left[\alpha\left(1-d^2+2c_1\right)+c_2(1+d)\right]}{4\left(1-d^2+c_1\right)-d^2\left(1-d^2+2c_1\right)}$$

3 Numerical simulations

3.1 Focusing on the parameter k

In this section some numerical simulation including bifurcation diagrams, strange attractors, Lyapunov numbers graph and Sensitive dependence on initial conditions are presented focusing on the parameter k when the other parameters are fixed taking the values: $\alpha = 5$, $c_1 = 1$, $c_2 = 0.5$, $c_3 = 0.4$, $c_4 = 1$, $c_5 = 0.3$ and $d = 0.50$. At first, the Nash Equilibrium for the values of these parameters becomes as:

$$p_1^*\approx 3.06 \quad \text{and} \quad p_2^*\approx 2.51 \Rightarrow E_*\left(p_1^*,p_2^*\right)\equiv E_*(3.06,2.51) \quad (37)$$

and for the stability conditions (proposition 1) it means that the parameter k must take values into the interval:

$$k\in(0,0.10) \quad (38)$$

This algebraic result is verified by the bifurcation diagrams of p_1^* (Fig.1) and p_2^* (Fig.2) with respect to the parameter k. As it seems there is a locally asymptotically stable orbit until the value of 0.10 for the parameter k and after this value doubling period bifurcations are appeared and finally, for higher values of the parameter k the system's behavior becomes chaotic and unpredictable.

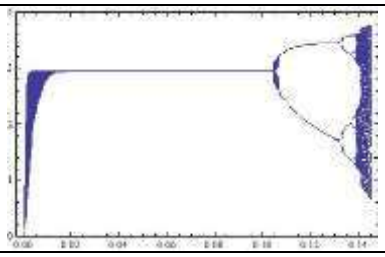

Fig. 1. Bifurcation diagram with respect to the parameter k against the variable p_1^* with 400 iterations of the map Eq.(11) for $\alpha = 5$, $c_1 = 1$, $c_2 = 0.5$, $c_3 = 0.4$, $c_4 = 1$, $c_5 = 0.3$ and $d = 0.50$.

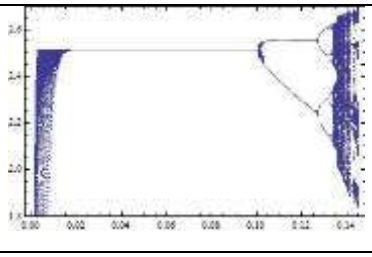

Fig. 2. Bifurcation diagram with respect to the parameter k against the variable p_2^* with 400 iterations of the map Eq.(11) for $\alpha = 5$, $c_1 = 1$, $c_2 = 0.5$, $c_3 = 0.4$, $c_4 = 1$, $c_5 = 0.3$ and $d = 0.50$.

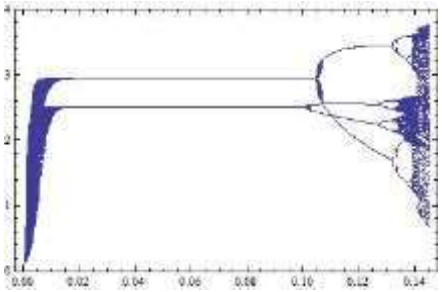

Fig.3. The two previous bifurcation diagrams of Fig.1 and Fig.2 in one.

This chaotic trajectory can create strange attractors (Fig.4) for a higher value of the parameter k like 0.147, outside the stability space. Also, computing the Lyapunov numbers (Fig.5) for this value of the parameter k and setting the same fixed values for the other parameters α, c_1, c_2, c_3, c_4, c_5 and d, it seems that they are getting over the value of 1 as an evidence for the chaotic trajectory.

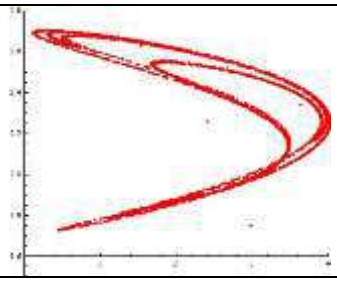

Fig. 4. Phase portrait (strange attractor) of the orbit of (0.1,0.1) with 8000 iterations of the map Eq.(11) for $\alpha = 5$, $c_1 = 1$, $c_2 = 0.5$, $c_3 = 0.4$, $c_4 = 1$, $c_5 = 0.3$, $d = 0.50$ and $k = 0.147$.

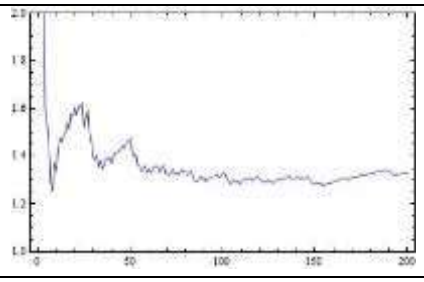

Fig. 5. Lyapunov numbers of the orbit of (0.1,0.1) with 8000 iterations of the map Eq.(11) for $\alpha = 5$, $c_1 = 1$, $c_2 = 0.5$, $c_3 = 0.4$, $c_4 = 1$, $c_5 = 0.3$, $d = 0.50$ and $k = 0.147$.

This chaotic trajectory makes the system sensitive on initial conditions, which means that only a small change on a coordinate may change completely the system's behavior. For example, choosing two different initial conditions (0.1,0.1) (Fig.6) and (0.101,0.1) (Fig.7) with a small change at the p_1^*-coordinate and plotting the time series of system it seems that at the beginning the time series are indistinguishable, but after a number of iterations, the difference between them builds up rapidly.

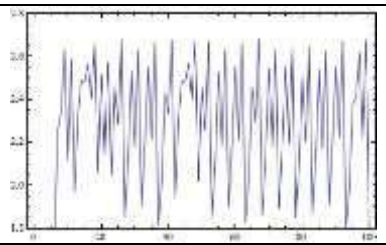

Fig. 6. Sensitive dependence on initial conditions for p_1^*-coordinate plotted against the time: the orbit of (0.1,0.1) of the system Eq.(11) for $\alpha = 5$, $c_1 = 1$, $c_2 = 0.5$, $c_3 = 0.4$, $c_4 = 1$, $c_5 = 0.3$, $d = 0.50$ and $k = 0.147$.

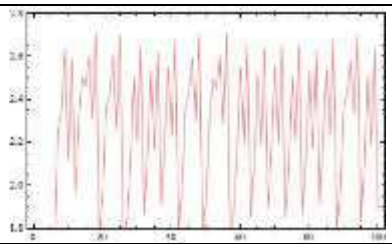

Fig. 7. Sensitive dependence on initial conditions for p_1^*-coordinate plotted against the time: the orbit of (0.101,0.1) of the system Eq.(11) for $\alpha = 5$, $c_1 = 1$, $c_2 = 0.5$, $c_3 = 0.4$, $c_4 = 1$, $c_5 = 0.3$, $d = 0.50$ and $k = 0.147$.

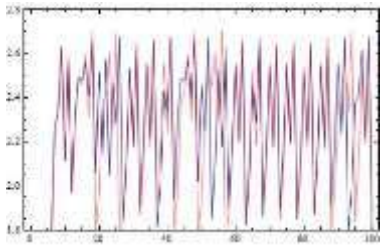

Fig.8. The two previous bifurcation diagrams of Fig.6 and Fig.7 in one.

4 Chaos control applying the d-Backtest method

4.1 The application of the d-Backtest method

The d-Backtest parameters' optimization method is a method developed for financial predictions, Vezeris et al. (2018). It works by determining the optimal backtesting period that should be consulted when selecting parameters for a trading system that will trade over a next period. The method uses verification periods of various lengths in order to evaluate backtesting periods using various methods that look into average profits, minimum profit factors and other metrics. It also uses validation periods of fixed length in order to evaluate the methods used for the verification periods. After selecting the most promising method it uses it in order to suggest a backtesting period. The system can then be examined over that backtesting period in order to determine the optimal parameters that can then be used over the next period. The method has undergone many iterations and improvements through the last years from using weeks instead of months as the measure of periods to introducing additional methods and measures for the evaluation of verification periods, Vezeris et al. (2019), Vezeris et al. (2020). In our research, the method was used in order to determine dynamic values for k, for each player.

The d-Backtest method was combined with the duopoly game by using it to determine dynamic k values for each player. More specifically each player, instead of using a constant value for k to determine their next price with system's difference equations, used the d-Backtest method to determine a new value for k for each step, feeding all the data from the past steps to the d-Backtest method. Each player used the d-Backtest method separately from the other with the goal of the method being to determine k values that would result in less fluctuations in prices and a more stable system. Because of the dynamic nature of k the price values determined by the difference equations had to have a lower bound of 0.001 so that no negative numbers would appear as price values.

In order to use the d-Backtest method in the context of the duopoly game, it had to undergo a few changes. The first change was the calculation of periods in steps instead of weeks or months. The next change was the selection of an appropriate measurement that would give a value for the variability of prices over a period, since the d-Backtest method is used with a goal of minimizing the fluctuations of the prices. We used a simple root mean square deviation calculated over the whole period:

$$\mathrm{RMSD} = \sqrt{\frac{\sum_{i=1}^{n}\left(x_i - \bar{x}\right)^2}{n-1}} \tag{39}$$

In close connection to the above are the changes in the methods used to sort the verification periods. Since variability is the only measure we extract from the backtesting periods, we used two groups of methods, a simple average variability method group and an exponential variability method group. Each method group has the same variations as the original d-Backtest methods apart

from the simple averages, namely the restrictions that the verification periods have to be bigger than 1 and 2 steps, the use of the most backtesting occurrences in the verification periods and the combinations of the two aforementioned.
Another very important change is the calculations on the backtesting periods. The number of the backtesting periods examined in each step was 30, as was the case with the financial data. In the financial applications of the d-Backtest method, the backtesting calculations could safely assume that the actions of the trader could not meaningfully change the prices on the market and the outcome of the test depended solely on the trader, so it is easy to determine what could have happened in the past for the different values of the system's parameters. In the case of the duopoly, the prices of each player in each step are a combination of both players' prices in the previous steps recursively. In order to calculate the prices that could have been in a past period for different values of k, each player takes the other's historic prices as a given and calculates only their own prices for a k value and then computes the variability measure for that k with these prices.
Each player has to separately do the calculations for the backtests and apply the d-Backtest method in each step, in order to determine a backtesting period that can then be used to determine the best k value to use in the calculation of their price in the next step. The d-Backtest method needs an amount of past data in order to have enough data points to calculate the metrics for the verification methods. For this reason, each player starts with an initial price of 0.1 and a constant value for k for the first 10 steps and after that the d-Backtesting method takes over.

4.2 The d-Backtest method's results

Experiments with various initial values for k were run. The plots below show the price values, the k values and the backtesting periods for three different experiments with k values of 0.147, 0.3 and 0.7.

Fig.9. Price values of each player for initial k=0.147

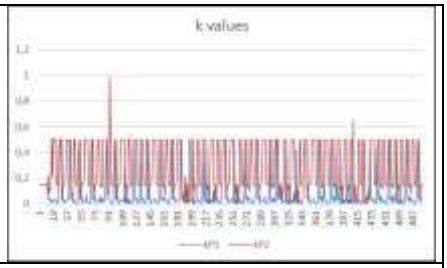

Fig.10. k values selected by the d-Backtest method for each player for initial k=0.147

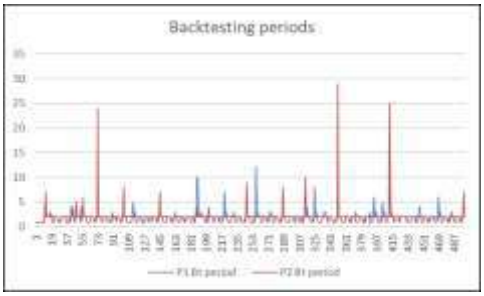

Fig.11. Backtesting periods chosen by the d-Backtest method for each player for initial k=0.147

Fig.12. Price values of each player for initial k=0.30

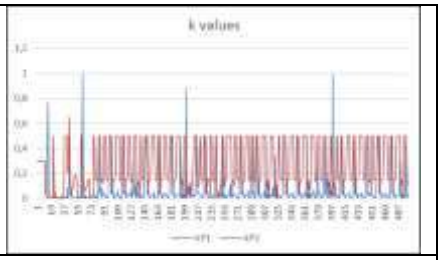

Fig.13. k values selected by the d-Backtest method for each player for initial k=0.30

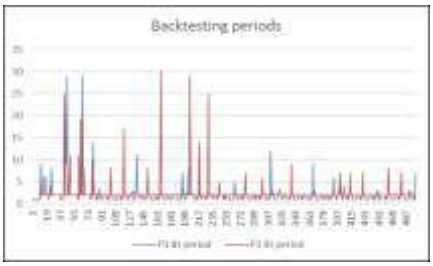

Fig.14. Backtesting periods chosen by the d-Backtest method for each player for initial k=0.30

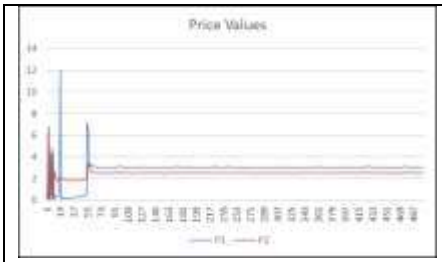

Fig.15. Price values of each player for initial k=0.70

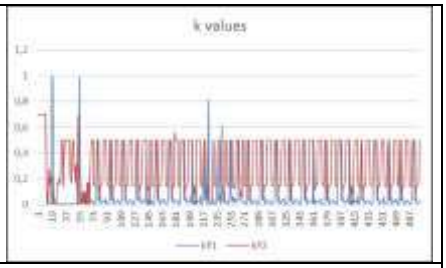

Fig.16. k values selected by the d-Backtest method for each player for initial k=0.70

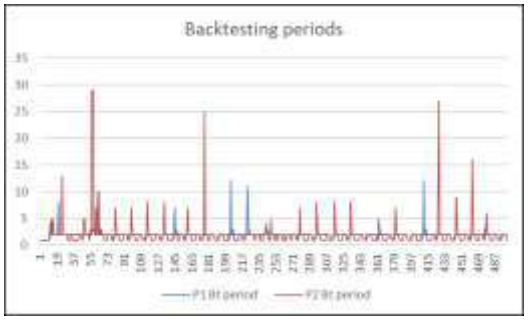

Fig.17. Backtesting periods chosen by the d-Backtest method for each player for initial k=0.70

It can be seen that, in all three experiments, the price values end up around the system's equilibrium values with some small deviations after some initial fluctuations. This happens regardless of the fact that the initial k values were outside the stable range of (0, 0.1).

The k values selected by the d-Backtest method in all three experiments show significant variations for the second player and less so for the first player. The prevalence of 0.5 values is an artifact of the d-Backtesting method when it has to choose from a range of k values that have the same (and best) outcome (this usually happens for small period backtests) so it chooses the middle value. For the second player there are also many values around 0.15, just outside the stable range for k. The first player chooses k values much lower that the second player in order to achieve stability, which can be explained by the bigger parameters that affect their price changes.

The backtesting periods chosen by the d-Backtest method for both players are small on average, usually 1 or 2 backtesting periods. This happens because the variability metric used by the d-Backtest method has more chances of being small in small periods.

Although the d-Backtest method selects different k values in the duration of the experiments, many of which are not in the stable range of k, it still manages to reach its goal of small price variability and drive the system to its equilibrium point.

5 Conclusions

In this paper the dynamics of a differentiated Bertrand duopoly with homogeneous expectations, linear demand and asymmetric cost functions (regression analysis) are analyzed. By assuming that at each time period each firm maximizes its expected profit function Π under bounded rationality expectation, a discrete dynamic system was obtained. Existence and stability of equilibrium of this system are studied. It is numerically shown that the model gives chaotic and unpredictable trajectories. The main result is that higher

values of the speed of adjustment may destabilize the Bertrand–Nash equilibrium. Finally, in cases where the players choose these values of the parameter k for which, as algebraically and graphically proved, the discrete dynamical system of Bertrand-type model behaves chaotically, the d-Backtest method was applied, giving dynamic values for the k parameter to each player for each time period, through which the system returns in locally asymptotically stable Nash Equilibrium.

References

1. Agiza HN., On the stability, bifurcations, chaos and chaos control of Kopel map. Chaos Solitons Fract. 11: 1909-16, 2004.
2. Agiza HN, Elsadany AA, Chaotic dynamics in nonlinear duopoly game with heterogeneous players. Appl. Math. Comput. 149: 843–860, 2004.
3. Agiza HN, Elsadany AA., Nonlinear dynamics in the Cournot duopoly game with heterogeneous players. Physica A 320: 512–24, 2003.
4. Agiza HN, Hegazi AS, Elsadany AA.m., Complex dynamics and synchronization of duopoly game with bounded rationality. Math. Comput. Simulat. 58: 133–46, 2002.
5. Agliari, A., Gardini, L., & Puu, T., Some global bifurcations related to the appearance of closed invariant curves. Mathematics and Computers in Simulation, 68, 201–219, 2005.
6. Agliari, A., Gardini, L., & Puu, T., Global bifurcations in duopoly when the Cournot point is destabilized via a subcritical Neimark bifurcation. International Game Theory Review, 8, 1–20, 2006.
7. Askar, S.S., On complex dynamics of monopoly market, Economic Modelling, 31: 586-589, 2013.
8. Askar, S. S., Complex dynamic properties of Cournot duopoly games with convex and log-concave demand function, Operations Research Letters 42, 85–90, 2014.
9. Baumol, W.J., Quandt, R.E., Rules of thumb and optimally imperfect decisions, American Economic Review 54 (2): 23–46, 1964.
10. Bischi GI, Kopel M., Equilibrium selection in a nonlinear duopoly game with adaptive expectations. J. Econom Behav. Org. 46: 73–100, 2001.
11. Den Haan WJ., The importance of the number of different agents in a heterogeneous asset-pricing model. J. Econom. Dynam. Control, 25:721–46, 2001.
12. Elsadany A.A., Dynamics of a Cournot duopoly game with bounded rationality based on relative profit maximization. Applied Mathematics and Computation 294, 253–263, 2017.
13. Elaydi, S., An Introduction to Difference Equations, third ed., Springer-Verlag, New York, 2005.
14. Fanti, L., & Gori, L., The dynamics of a differentiated duopoly with quantity competition. Economic Modelling, 29, 421–427, 2012.
15. Hommes, C.H., Heterogeneous agent models in economics and finance, in: L. Tesfatsion, K.L. Judd (Eds.), Handbook of Computational Economics, Agent-Based Computational Economics, vol. 2, Elsevier Science B.V: 1109–1186, 2006.
16. Gandolfo G., Economic dynamics. Berlin: Springer, 1997.
17. Gao Y., Complex dynamics in a two dimensional noninvertible map. Chaos Solitons Fract. 39: 1798–810, 2009.
18. Kopel M., Simple and complex adjustment dynamics in Cournot duopoly models. Chaos Solitons Fract. 12: 2031–48, 1996.

19. Kulenonic, M., Merino, O., Discrete Dynamical Systems and Difference Equations with Mathematica, Chapman & Hall/Crc., 2002.
20. Naimzada, A.K., Ricchiuti G., Complex dynamics in a monopoly with a rule of thumb, Applied Mathematics and Computation 203: 921–925, 2008.
21. Naimzada, A., Sbragia, L., Oligopoly games with nonlinear demand and cost functions: two boundedly rational adjustment processes, Chaos Solitons Fractals 29 (3), 707–722, 2006.
22. Puu, T., The chaotic monopolist, Chaos, Solitons & Fractals 5 (1): 35–44, 1995.
23. Puu T., The chaotic duopolists revisited. J Econom. Behav. Org. 37: 385–94, 1998.
24. Puu T., Chaos in duopoly pricing. Chaos Solitons Fract.1:573–81, 1991.
25. Puu T., Complex oligopoly dynamics. In: Lines M, editor. Nonlinear dynamical systems in economics. Springer Wien NewYork: CISM; p. 165–86, 2005.
26. Sarafopoulos G., On the dynamics of a duopoly game with differentiated goods, Procedia Economics and Finance, 19, 146 – 153, 2015.
27. Sarafopoulos G., Complexity in a duopoly game with homogeneous players, convex, log linear demand and quadratic cost functions, Procedia Economics and Finance, 33, 358 – 366, 2015.
28. Sarafopoulos G., Papadopoulos K., On a Cournot duopoly game with differentiated goods, heterogeneous expectations and a cost function including emission costs, Scientific Bulletin - Economic Sciences , vol. 16 (1), 11-22, 2017.
29. Sarafopoulos G., Papadopoulos K., Complexity in a Bertrand duopoly game with heterogeneous players and differentiated goods, Springer Proceedings in Business and Economic, Article: 2, pages: 15 – 26, Springer Nature Switzerland AG, (ISBN: 978-3-030-12169-3), 2019.
30. Sarafopoulos G., Papadopoulos K., On a Bertrand dynamic game with differentiated goods, heterogeneous expectations and asymmetric cost functions, Springer Proceedings in Business and Economic Article: 14, pages: 223 – 241, Springer Nature Switzerland AG, (ISBN: 978-3-030-39927-6), 2020.
31. Singh, N., Vives, X., Price and quantity competition in a differentiated duopoly. The RAND Journal of Economics 15, 546–554, 1984.
32. Tramontana, F., Heterogeneous duopoly with isoelastic demand function. Economic Modelling 27, 350–357, 2010.
33. Vezeris D., Kyrgos Th., Karkanis I., Bizergianidou V., Automated trading systems' evaluation using d-Backtest PS method and WM ranking in financial markets, Investment Management and Financial Innovations, 17(2), p.198-215, 2020.
34. Vezeris D., Schinas C., Kyrgos Th., Bizergianidou V., Karkanis I., Optimization of Backtesting Techniques in Automated High Frequency Trading Systems Using the d-Backtest PS Method, Computational Economics, 56(4), p. 975–1054, 2019.
35. Vezeris, D., Schinas, C., Papaschinopoulos, G., Profitability Edge by Dynamic Back Testing Optimal Period Selection for Technical Parameters Optimization, in Trading Systems with Forecasting, Computational Economics, 51(4), p.761 – 807, 2018.
36. Westerhoff, F., Nonlinear expectation formation, endogenous business cycles and stylized facts, Studies in Nonlinear Dynamics and Econometrics 10 (4) (Article 4), 2006.
37. Wu, W., Chen, Z., Ip, W.H., Complex nonlinear dynamics and controlling chaos in a Cournot duopoly economic model. Nonlinear Analysis: Real World Applications 11, 4363–4377, 2010.
38. Zhang, J., Da, Q.,Wang, Y., Analysis of nonlinear duopoly game with heterogeneous players. Economic Modelling 24, 138–148, 2007.
39. Zhang J., Da Q., Wang Y., The dynamics of Bertrand model with bounded rationality, Chaos, Solitons and Fractals 39, 2048-2055, 2009.

Multifractal analysis of bioenergy transport in a protein nanomotor

Narmin Sefidkar, Samira Fathizadeh*, and Fatemeh Nemati

Department of Physics, Urmia University of Technology, Urmia, Iran
(*E-mail: s.fathizadeh@sci.uut.ac.ir)

Abstract. The potential application of biological molecules as functional devices has been heralded as the dawn of a new field in biotechnology and medicine. In this regard, molecular motors have attracted the most attention for decades. In the current study, we have studied the bioenergy transfer in a protein chain as a self-powered nanomotor. The effect of different factors on the energy transfer in protein is studied to obtain the best functional condition for the protein machine. The temperature plays the critical role in the control of energy transfer in the system. On the other hand, the external mechanical tension as a vibrator can increase the energy flowing in our system. The chaos theory tools can verify and estimate the results. Generally, one can engineer a self-powered nanomotor based on protein chains and control bioenergy transfer.
Keywords: Nanomotor, Protein, Biological energy, Energy transfer, Multifractal analysis.

1 Introduction

Biological molecules, an exciting field with continuous and robust growth for about half a century of existence, encompass the medical, biological, chemical, and material sciences [1]. In the current study, we have studied a protein chain as a biological molecule and its energy transfer. Protein, as the largest macromolecule in the body, is one of the most important components of the life systems that plays vital role in the body. Proteins are composed of amino acid chain sequences that the number of the amino acids can reach several thousand depending on the type of protein [2].

In the current study, we investigate the bioenergy transfer in protein molecules as an automated nanomotor. Automated nanomotor uses the bioenergy in the protein as self-burning energy and converts it into autonomous motion [3]. These nanomotors, which derive their kinetic energy from the biological energy contained in proteins, are called protein nanomotors. Protein motors have potential medical applications and can collect, transport, and release drug carriers of various sizes. Internal order in eukaryotic cells is created by protein motors that transport organs and molecules along the cytoskeletal pathways of self-assembled proteins such as tubulin and shuttle actin. Three known families of cytoskeletal protein motors include kinesin, dynein, and myosin [4]. kinesins and dyneins, which are the first and second types of protein motors, respectively, move in tubules or microtubules [5]. But Myosins, the third family of protein motors, move on actin filaments and are responsible for muscle contraction in the heart and skeletal muscles [6].

2 Model and Methods

In the current work, the Hamiltonian model used to study the energy transfer in protein molecules is based on the Peng model as follows:

$$H=H_1+H_2+H_3 \tag{1}$$

where H_1 indicates that a boson-type Frankit exciton is excited in protein molecules using the energy released in ATP hydrolysis written as follows:

$$H_1=\sum_n[\varepsilon_0 a_n^{\dagger}a_n-J\left(a_n^{\dagger}a_{n+1}+a_n a_{n+1}^{\dagger}\right)] \tag{2}$$

H_2 defines the harmonic properties of the remaining amino acids:

$$H_2=\sum_n[\frac{P_n^2}{2m}+\frac{1}{2}W(u_n-u_{n-1})^2] \tag{3}$$

H_3 introduces the interaction between the two modes of motion [7]:

$$H_3=\sum_n[\chi_1(u_{n+1}-u_{n-1})a_n^{\dagger}a_n+\chi_2(u_{n+1}-u_n)\,(a_{n+1}^{\dagger}a_n + a_n^{\dagger}a_{n+1})] \tag{4}$$

The parameters used in the calculations are shown in Table 1 [8]:

Table 1: Parameters used

Parameter	Unit	Value
ε_0	eV	0.2035
χ_1	N	6.2×10^{-11}
χ_2	N	$(10\text{-}18)\times10^{-12}$
m	Amu	115
W	$\frac{N}{m}$	13
J	eV	9.68×10^{-4}

Here, a_n and $a_n^{\dagger}$ are the creation and annihilation operators for exciton. u_n and p_n are the displacement and momentum operators for the amino acid residue at site n, respectively. ε_0 is the energy of the exciton. χ_1 and χ_2 are nonlinear coupling constants. m is the mass of amino acid recidue. W is the elasticity constant of the proteins, and J is the dipole-dipole interaction energy between neighboring amino acids [9].

In this work, we have used the classical chaos theory. In this case, the evolution equations for the classical part are derived using the Hamiltonian equation ($\dot{p}_n=-\frac{\partial H}{\partial q_n}$). Also, the evolution equations for the quantum part are analyzed using the Heisenberg equation ($\dot{a}_n=-\frac{i}{\hbar}[a_n,H]$) as follows:

$$\ddot{u}_n = \sum_n [\frac{W}{m}(u_{n+1} - 2u_n + u_{n-1}) + \frac{\chi_1}{m}(a_{n+1}^{\dagger}a_{n+1} - a_{n-1}^{\dagger}a_{n-1}) + \frac{\chi_2}{m}(a_{n+1}^{\dagger}a_n + a_n^{\dagger}a_{n+1} - a_n^{\dagger}a_{n-1} - a_{n-1}^{\dagger}a_n)] \quad (5)$$

$$\dot{a}_n = -\frac{i}{\hbar}\sum_n \{-J(a_{n-1} + a_{n+1}) + \varepsilon_0 a_n + \chi_1(u_{n+1} - u_{n-1})a_n + \chi_2[(u_n - u_{n-1})a_{n-1} + (u_{n+1} - u_n)a_{n+1}]\} \quad (6)$$

To study the energy transfer in protein molecules, we have extracted the energy flux. The energy flux obtains using the continuity equation (I= -$\frac{i}{\hbar}[a_n^{\dagger}a_n, H]$) as follows:

$$I = -\frac{i}{\hbar}\sum_n [-J(a_n^{\dagger} - a_{n-1} - a_{n-1}^{\dagger}a_n + a_n^{\dagger}a_{n+1} - a_{n+1}^{\dagger}a_n) - \chi_2(u_n - u_{n-1})a_{n-1}^{\dagger}a_n + \chi_2(u_{n+1} - u_n)(a_n^{\dagger}a_{n+1} - a_{n+1}^{\dagger}a_n)] \quad (7)$$

3 Results and Discussion

Different factors effect on energy transfer in biological systems. One of the vital parameters on energy transfer in the protein system is the effect of temperature. We have used the Nosé Hoover thermostat to apply the temperature to the system. The evolution equation of thermostat is written as follows [10]:

$$\dot{\xi} = \frac{1}{M}(\sum_n m\dot{u}_n^2 - NK_BT_0) \quad (8)$$

where ξ describes a thermodynamic coefficient of friction. T_0 is the temperature of the system. K_B is the constant of Boltzmann, and M is the thermostat constant. A biological system can be affected by mechanical shocks. Therefore, we have investigated the effect of mechanical stress on energy transfer in protein molecules. The Hamiltonian of mechanical stress is written as follows [11]:

$$H_{str} = -\delta_{1,n}(u_{n+1} - u_n)F_0 sin\omega t \quad (9)$$

where F_0 and ω are the amplitude and frequency of the external mechanical stress. We can also examine the best range of parameters affecting energy transfer in protein molecules using multifractal system analysis. Multifractal analysis of the system can confirm the obtained results. In addition, it can classify system parameters to determine the desired results.

In this regard, we use the Rényi dimension spectrum, analogous of the free energy and analogous of the thermodynamic specific heat.

3.1 Simultaneous effect of ambient temperature and the range of force exerting mechanical stress

Temperature and external stress as the very influential factors in the performance of biological systems can be considered as the control parameters in the energy transfer in the protein system. We have considered the simultaneous effect of ambient temperature and the range of force exerting mechanical stress on the energy flux in the protein system (Fig. 1). The variation of the ambient temperature from 300 to 330 K and at the same time changing the amplitude of the force from 0 to 2 pN has negligible effect on the amount of energy flux transmitted in the system. In this region, the energy flux fluctuates at a minimum of about 10 to 30 μeV. But, when the temperature rises above 330 K, in the force range of about 1.2 pN, we can see a considerable peak in the energy flux, so that the energy flux reaches about 100 μeV. Similar to this phenomenon is also observed at a temperature of about 345 K and a force range of about 0.8 pN. Therefore, it can be said that temperatures above 330 and the applied stress are two critical parameters in the transfer of bioenergy in our protein system.

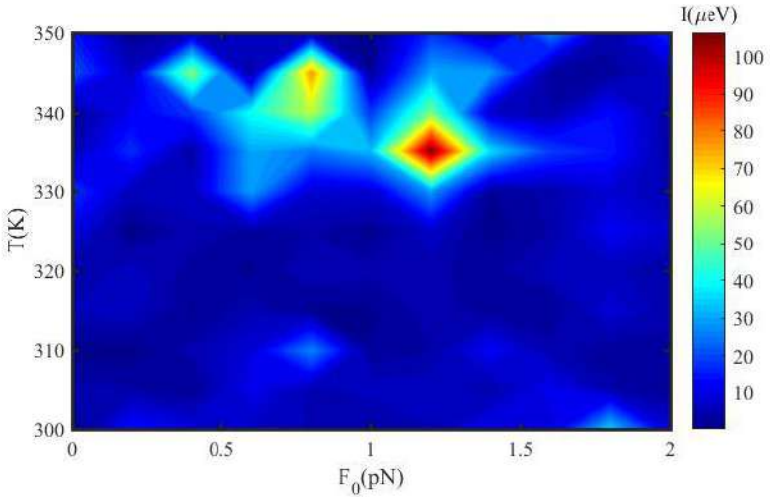

Fig. 1. The energy flux through the system concerning the simultaneous variation of the amplitude of applied stress and the ambient temperature

3.2 Simultaneous effect of temperature and applied stress frequency

The frequency of applied stress simultaneously with the ambient temperature can be another compelling factor in regulating the energy flux through the system. As shown in Figure 2, at 300 to 350 K, the energy flux is more than 50 μV. But there are characteristic frequencies that can significantly increase the energy flux

through the system. A frequency of about 0.09 THz at 310 K causes the energy flux of the system to reach about over 200 μeV, and this shows that energy transport in the protein system is highly sensitive to several frequencies that can be used to optimize the performance of the biological system.

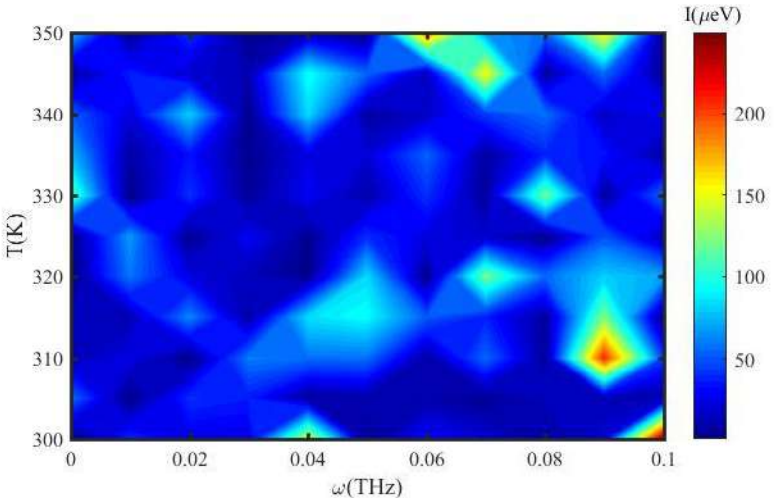

Fig. 2. Energy flux relative to a simultaneous variation of applied stress frequency and temperature (N=150, F_0=3pN)

3.3 Multifractal analysis

We have studied the multifractal spectrum of the energy flux through the protein system by using R*é*nyi dimension. In this regard, we consider the d dimensiontional phase space of system and divide it into cubes of size l and calculate the R*é*nyi dimension (Dq) as follows [12]:

$$D_q = \frac{1}{q-1}\lim_{l\to 0}\frac{\sum_i^M P_i^q}{\ln l} \qquad (10)$$

Figure 3 shows the R*é*nyi dimension spectrum for four different frequencies of applied stress. D_q shows the descending behavior by increasing q which indicates that the system is multifractal. If we go back to the previous results, we observe that the temperature of 300 K for a force amplitude of 3 pN, the frequencies ω = 0.01 THz, ω = 0.03 THz, ω = 0.05 THz are in the blue region where the energy flux crossing the system is minimal (Figure 2). Also, the frequency ω= 0.09 THz is in the red region where the energy flux passing through the system is maximum. As shown in Figure 3, for negative q, the R*é*nyi dimensions at 300 K and the force amplitude of 3 pN corresponds to the frequencies ω = 0.01THz, ω = 0.03THz, ω = 0.05THz are coincident with almost the same amount. But the R*é*nyi dimension of the frequency ω = 0.09THz shows

a greater value for negative values of q. The R*é*nyi dimension distinguishes the regions with the highest energy flux from the regions with the lowest energy flux.

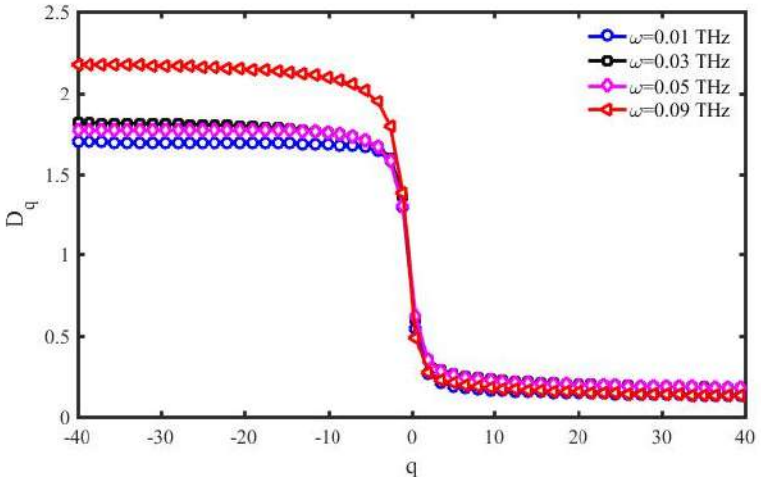

Fig. 3. R*é*nyi dimension spectrum in different values of the stress frequency (T=310K, F_0=3pN, N=150)

To have a similarity between a multifractal system and a thermodynamic state, relations are usually equated with their thermodynamic equivalents. We consider τ(q) as analogous the thermodynamic free energy of the system, and check the multifractality of the system. The analogous of the free energy is written as follows [13]:

$$\tau(q) \equiv (q\text{-}1)D_q \tag{11}$$

The system is a homogenous fractal when $\tau(q)$ have a linear dependence to q. On the other hand, $\tau(q)$ shows a deviation from the linear state when the system is multifractal and the higher deviation from the the linear state shows the more multifractality of the system. According the figure 4, $\tau(q)$ is deviated from the linear state in terms of q for all frequencies at the point q = 0, and this confirms the multifractality of the system. On the other hand, for negative q, $\tau(q)$ is the same for the frequencies in the blue region. But the frequency ω = 0.09 THz, which is in the red area, has the highest deviation from linear behavior. Thus, the analogous of the thermodynamic free energy shows the distinct regions for negative q at 300 K and for the force range of 3 pN.

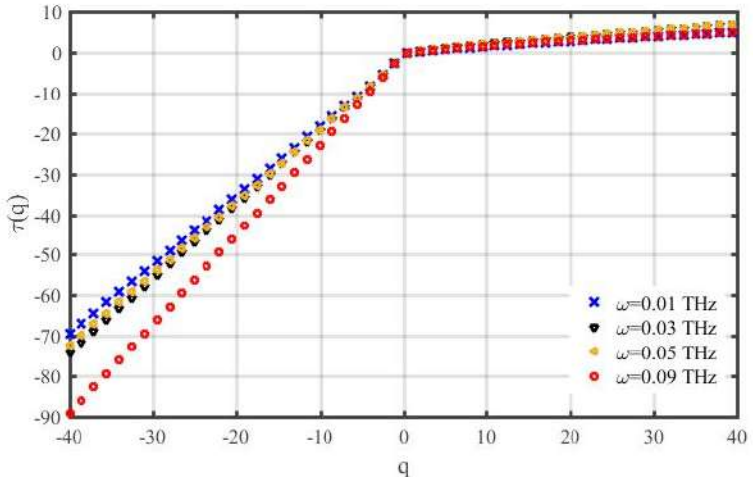

Fig 4. Analogous of the thermodynamic free energy in multifractal systems for different frequencies of the external stress (N=150, F_0=3pN, T=310K)

On the other hand, the analogous of the specific heat *C(q)* which is obtained from a second-order derivative of the analogous of free energy concerning q can be analyze the multifractal behavior of system through the following equation:

$$C(q)=-\frac{\partial^2\tau}{\partial q^2} \approx \tau(q+1)-2\tau(q)+\tau(q-1) \quad (12)$$

Analogous of specific heat is one of the measures to check the multifractality of a system. As shown in figure 5, the frequencies of the blue region overlap in the peak area. The frequency ω = 0.09THz, which is in the red region, shows a higher peak. Therefore, a analogous of thermodynamic specific heat also shows the distinct regions and confirms the previous results.

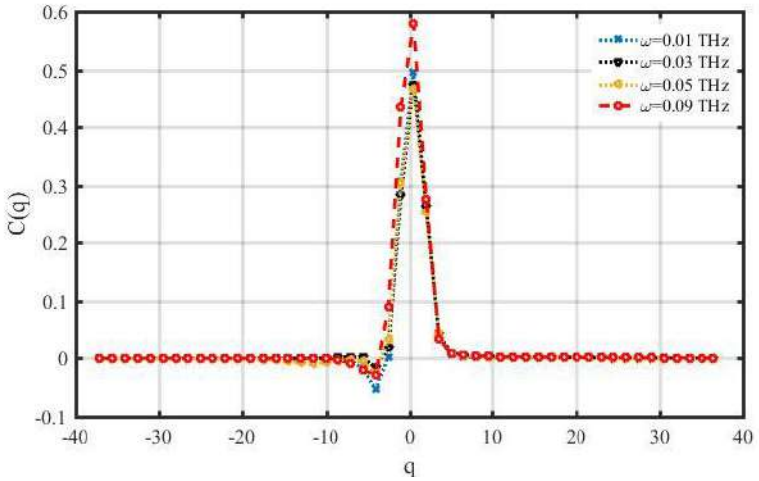

Fig. 5. Analogous of thermodynamic specific heat in multifractal systems for different frequencies (N=150, F_0=3pN, T=310K)

Conclusions

We have studied the bioenergy transfer in a protein system to design a nanomotor. In this regard, we have investigated the effect of various parameters such as temperature and mechanical stress on the energy transfer in protein nanomotors. We have analyzed the multifractal nature of the system using the multifractal analysis methods. Using the multifractal analysis, we are able to confirm the previous results and show the distinct areas.

References

1. Kulinets, I. "Biomaterials and their applications in medicine." In Regulatory affairs for biomaterials and medical devices (2015): (pp. 1-10). Woodhead Publishing.
2. Miller, D. S., & Payne, P. R. "A theory of protein metabolism." Journal of Theoretical Biology 5.3 (1963): 398-411.
3. Zha, F., Wang, T., Luo, M., & Guan, J. "Tubular micro/nanomotors: Propulsion mechanisms, fabrication techniques and applications." Micromachines 9.2 (2018): 78.
4. Vogel, P. D. "Nature's design of nanomotors." European journal of pharmaceutics and biopharmaceutics 60.2 (2005): 267-277.
5. Vale, R. D., Reese, T. S., & Sheetz, M. P. "Identification of a novel force-generating protein, kinesin, involved in microtubule-based motility." Cell 42.1 (1985): 39-50.
6. Brown, M. E., & Bridgman, P. C. (2004). "Myosin function in nervous and sensory systems." Journal of neurobiology 58.1 (2004): 118-130.
7. Pang, X. F., & Liu, M. J. "The Influences of Temperature and Chain–Chain Interaction on Features of Solitons Excited in A-Helix Protein Molecules with Three Channels." International Journal of Modern Physics B 23.10 (2009): 2303-2322.

8. Pang, X. F., & Liu, M. J. "The effects of damping and temperature of medium on the soliton excited in α-helix protein molecules with three channels." Modern Physics Letters B 23.01 (2009): 71-88.

9. Pang, X. F., Zhang, H. W., & Luo, Y. H. "The influence of the heat bath and structural disorder in protein molecules on soliton transported bio-energy in an improved model." Journal of Physics: Condensed Matter 18.2 (2005): 613.

10. Peyrard, M., & Bishop, A. R. "Statistical mechanics of a nonlinear model for DNA denaturation." Physical review letters 62.23 (1989): 2755.

11. Fathizadeh, S., & Behnia, S. "Control of a DNA Based Piezoelectric Biosensor." Journal of the Physical Society of Japan 89.2 (2020): 024004.
12. Behnia, S., Fathizadeh, S., Javanshour, E., & Nemati, F. "Light-driven modulation of electrical current through DNA sequences: Engineering of a molecular optical switch." The Journal of Physical Chemistry B 124.16 (2020): 3261-3270.
13. Fathizadeh, S., & Behnia, "Control of a DNA Based Piezoelectric Biosensor." Journal of the Physical Society of Japan 89.2 (2020): 024004.

Forced van der Pol oscillator – Synchronization from the bifurcation theory point of view

Jan Ševčík[1] and Lenka Přibylová[1]

Department of Mathematics and Statistics, Faculty of Science, Masaryk University, Kotlářská 2, 611 37, Brno, Czech Republic
(E-mail: 460534@mail.muni.cz, pribylova@math.muni.cz)

Abstract. The contribution presents a bifurcation theory point of view to synchronization of a forced van der Pol oscillator, which is coupled to a master oscillator as a system with a stable limit cycle corresponding to harmonic oscillation. We present bifurcation manifolds, 3D sections of the phase space and its Poincaré sections for parameters close to these manifolds providing a clear visualization of the dynamics of the 4D system. Among other things, we present the coexistence of a stable torus and a stable cycle arising from q-fold bifurcation on an Arnold tongue.
Keywords: Synchronization, Van der Pol oscillator, Bifurcations of limit cycles, Neimark–Sacker bifurcation, q-fold bifurcation, Arnold tongues.

1 Introduction

Synchronization of coupled systems of oscillators is an important phenomenon that touches a large class of nonlinear dynamical systems. Synchronization is ubiquitous and methods of applied nonlinear dynamics can thus help to solve problems and create new technologies in neuroscience ([5], [14], [1]), chemistry (Kuramoto[6]), biology (Winfree[12]), superconducting electronics (Welp *et al.*[10], Braginski[3]), spintronics (Sturgis-Jensen *et al.*[9]), computing (Mallick *et al.*[8]), or even particle physics (Beck[2]). Since these nonlinear systems exhibit complex and sometimes even counterintuitive dynamics, the most commonly used methods to study synchronizations are simulations.

Although the theory of bifurcations offers a suitable apparatus for the analysis of the systems mentioned above, it is usually not used. The highly abstract thinking and mathematically generalized view of dynamics needed for such an analysis are not the only obstacles to using bifurcation analysis methods. Another problem occurs because the phase variables present in such models usually enter as harmonic terms. Due to that, the systems are typically stiff, and standard numerical continuation techniques fail.

Our contribution brings a suitable method for analyzing dynamics of forced oscillators concerning synchronization. We present this method on the forced van der Pol oscillator example. In addition, it also allows excellent visualization of the state space in the neighborhood of bifurcation manifolds that belong to the onset of synchronization. All nonlinear phenomena that are closely related to it, as torus birth, resonances, or complex dynamics near double Hopf bifurcation, can be visualized in 3D space which greatly simplifies their explanation. This approach can be used for much more complex systems of coupled oscillators as you can see in Záthurecký and Přibylová[13].

2 Forced van der Pol oscillator representation

Consider the widely known van der Pol oscillator driven by an external harmonic force represented by the equation

$$\ddot{x} - \mu\left(1 - x^2\right)\dot{x} + \omega_0^2 x + A\sin\omega t = 0, \tag{1}$$

where $x \in \mathbb{R}$ is a time-dependent position coordinate, $\mu > 0$ denotes a parameter indicating the nonlinearity (the strength of the damping), and $\omega_0 \in \mathbb{R}$ is the natural frequency. The last term represents the external driving force with amplitude $A > 0$ and frequency $\omega \in \mathbb{R}$.

This second-order differential equation can be expressed in the following form of two-dimensional non-autonomous system

$$\dot{x} = y + \varepsilon\cos\omega t, \tag{2a}$$
$$\dot{y} = \mu\left(1 - x^2\right)y - \omega_0^2 x, \tag{2b}$$

where $\varepsilon = \frac{A}{\omega}$. To obtain an autonomous system, it is usually convenient to rewrite the time-dependent term $\varepsilon\cos\omega t$ in (2a) using a pair of new variables, specifically

$$\dot{x} = y + \varepsilon u, \tag{3a}$$
$$\dot{y} = \mu\left(1 - x^2\right)y - \omega_0^2 x, \tag{3b}$$
$$\dot{u} = -\omega v, \tag{3c}$$
$$\dot{v} = \omega u. \tag{3d}$$

Unfortunately, this system is stiff, and the continuation is impossible since the periodic solution of (3c), (3d) is not asymptotically stable. Therefore, we replace this subsystem with a normal form of supercritical Hopf bifurcation

$$\dot{u} = ru - \omega v - u\left(u^2 + v^2\right),$$
$$\dot{v} = \omega u + rv - v\left(u^2 + v^2\right)$$

with an exponentially stable driving cycle allowing a stable continuation of limit cycles and their bifurcations. Note that the added parameter r provides a possibility to investigate bifurcations connected to the birth of an invariant torus.

Hence, one can examine the forced van der Pol oscillator (1) as two interacting master-slave oscillators in the form

$$\dot{x} = y + \varepsilon u, \tag{4a}$$
$$\dot{y} = \mu\left(1 - x^2\right)y - \omega_0^2 x, \tag{4b}$$
$$\dot{u} = ru - \omega v - u\left(u^2 + v^2\right), \tag{4c}$$
$$\dot{v} = \omega u + rv - v\left(u^2 + v^2\right). \tag{4d}$$

This step also provides an opportunity to clearly visualize synchronization phenomena of the famous van der Pol oscillator since variables u and v are complementary, and one of them can be omitted in the state space description.

3 Basic bifurcation analysis

The studied system (4) is evidently uncoupled for zero coupling, i.e. $\varepsilon = 0$. In this case, one can investigate both subsystems separately. Assuming $\mu = 0$, there is no damping in the van der Pol system, and thus the system exhibits simple conservative harmonic oscillations with frequency ω_0. It is known that the unforced van der Pol oscillator undergoes a supercritical Hopf bifurcation that gives rise to a stable limit cycle while crossing $\mu = 0$ as well as the forcing, master system while crossing $r = 0$. It follows that a double Hopf bifurcation manifold (i.e. parameter subspace $\mu = 0$, $r = 0$, $\varepsilon = 0$) can be detected as a transversal intersection of these two Hopf hyperplanes.

4 Torus birth and synchronization

Double Hopf bifurcation leads to complex dynamics that is related to other bifurcations for nearby parameters. Generically, two branches of Neimark–Sacker bifurcation of a cycle, resulting in a torus birth, emanate from the double Hopf point.

The system (4) gives birth to the stable invariant torus for positive μ and r near zero obviously since supercritical bifurcations appear at $\mu = 0$ and $r = 0$, respectively. An example of a quasiperiodic trajectory densely covering the torus is presented in Fig. 1. The trajectories of the system (4) on the invariant torus can become periodic since the torus is described by a pair of frequencies that can be in a mutually rational proportion. In that moment, the synchronization appears in terms of phase- or frequency-locking. For given external harmonic forcing with nonzero amplitude r and natural frequency ω_0, zero damping μ and zero coupling ε, it is exactly for ratios $\frac{\omega_0}{\omega}$ that are rational. These points are resonances (two-parametric cusp bifurcations of cycles or q-fold bifurcation points in the notation of the bifurcation theory) that correspond to cusp Arnold tongues emanating from Neimark–Sacker bifurcation manifold $\varepsilon = 0$. The Arnold tongues' borders are fold bifurcation manifolds of a stable cycle and a saddle cycle that coincide with each other. The stable cycle persists inside the Arnold tongue and corresponds to the synchronization. Notice that Neimark–Sacker bifurcation, the torus, and fold bifurcation of a cycle manifold continue to positive ε. Since the cusp bifurcation has a typical V-shape, more coupling strength makes the synchronization easier.

From now on, we will consider fixed values $\mu = 0.1$, $r = 0.1$ and $\omega_0 = 1$. The following results are independent of the choice in the sense that we can choose any small μ and r to start with quasiperiodic orbit on a torus. The natural frequency ω_0 is taken as normalized, but it can be easily reparametrized. Let us study the effect of parameters ω and ε on the synchronization in system (4). Using numerical continuation methods in MATCONT toolbox by Dhooge *et al.*[4], one can compute bifurcation curves of (4) in the parameter space (ω, ε).

Since the natural frequency of the van der Pol oscillator is chosen as $\omega_0 = 1$, the Arnold tongues emanate from all rational numbers on the ω-axis, i.e. points $(\omega, \varepsilon) = \left(\frac{p}{q}, 0\right)$ for coprime $p, q \in \mathbb{N}$. Fig. 2 shows several Arnold tongues $\mathcal{A}_{p:q}$

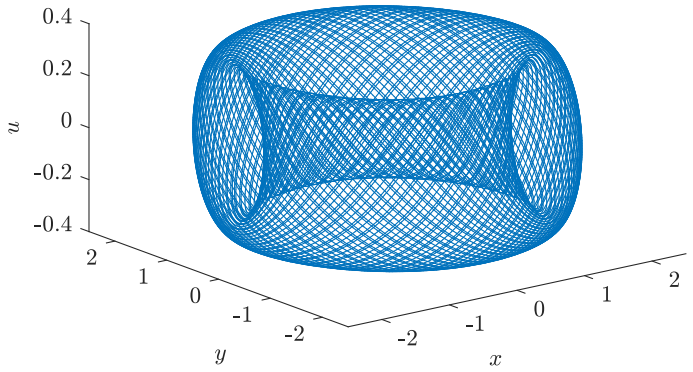

Fig. 1: A segment of a quasiperiodic orbit on a stable invariant torus of system (4) for $\mu = 0.1$, $r = 0.1$, $\varepsilon = 2.5$, $\omega_0 = 1$ and $\omega = \sqrt{5}$.

in space (ω, ε) representing parameter values, for which the synchronization $p : q$ takes place in the studied system (4) ($p : q$ is a ratio between the two frequencies on the torus, $q : p$ is the period ratio). As usual, most of the Arnold tongues are relatively narrow and hence difficult to be manually detected. Notice that we found a non-trivial branch of Neimark–Sacker bifurcation that is different from $\mu = 0$, $r > 0$ or $r = 0$, $\mu > 0$, respectively, in this parameter space. Dynamics near this branch for $1 : 3$ resonance is shortly mentioned in Section 6.

5 Visualizations of the torus birth

In addition to the analysis itself, we focused on visualization of dynamics near bifurcation manifolds. One dimension of the 4D state space of the system (4) can be omitted easily as a complement due to harmonic forcing. The 3D invariant torus that appears in the state space for positive r and μ is projected to a two-dimensional torus. Its natural section in a given phase is a Poincaré 2D plane section of a trajectory on the torus. This situation makes it possible to explicitly show qualitative changes in the neighborhood of bifurcation manifolds in the plane and 3D space.

At first, let's look at the transition between regions 1 and 2 (see Fig. 3). The system possesses a stable limit cycle in the region 1 (see Fig. 4). When crossing the non-trivial Neimark–Sacker curve into region 2, the corresponding Neimark–Sacker bifurcation of a cycle causes a loss of the cycle's stability. It gives rise to a stable invariant torus in its neighborhood (see Fig. 5 and 6). As these figures show, using Poincaré section determined by zero u-coordinate, for example, one can visualize bifurcations of limit cycles via specific orbit topological change of the discrete dynamical system (see Neimark–Sacker bifurcation of maps in Kuznetsov[7]) on the corresponding Poincaré section.

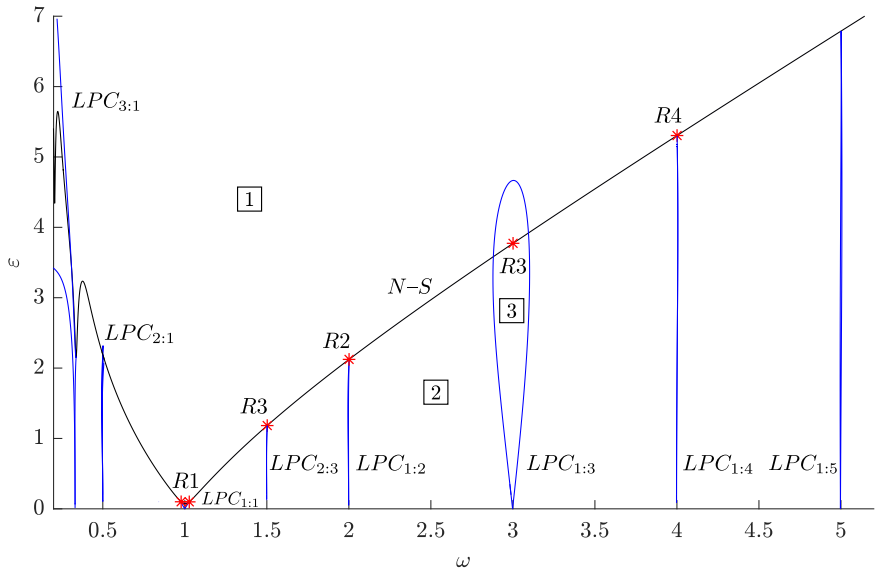

Fig. 2: Bifurcation diagram of system (4) in the parameter space (ω, ε) for $\mu = 0.1$, $r = 1$ and $\omega_0 = 1$.

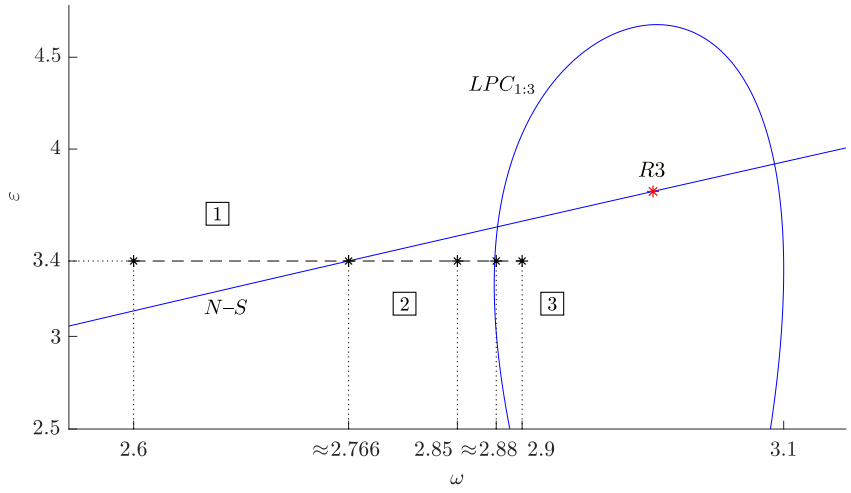

Fig. 3: Considered transitions between regions 1, 2 and 3 in the parameter space (ω, ε) for $\mu = 0.1$, $r = 1$ and $\omega_0 = 1$.

6 Bistability of the forced van der Pol oscillator

Finally, let's look closely to qualitative changes of dynamics near $1:3$ resonance point R3 on the non-trivial Neimark–Sacker branch depicted in Fig. 2 or 3 (for the positive r, μ, ε and ω). Fig. 7 shows a typical symmetric dynamic structure

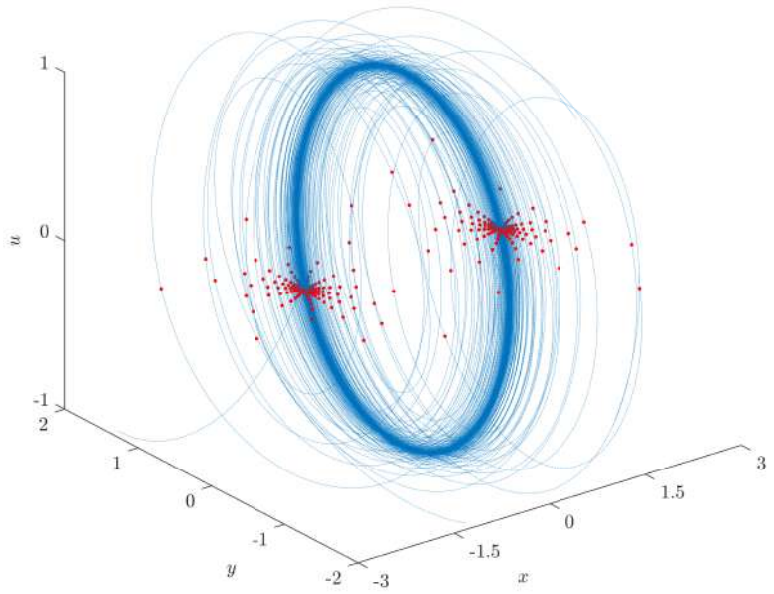

Fig. 4: Poincaré section $\{u = 0\}$ of system (4) for $(\omega, \varepsilon) = (2.6, 3.4)$, region 1.

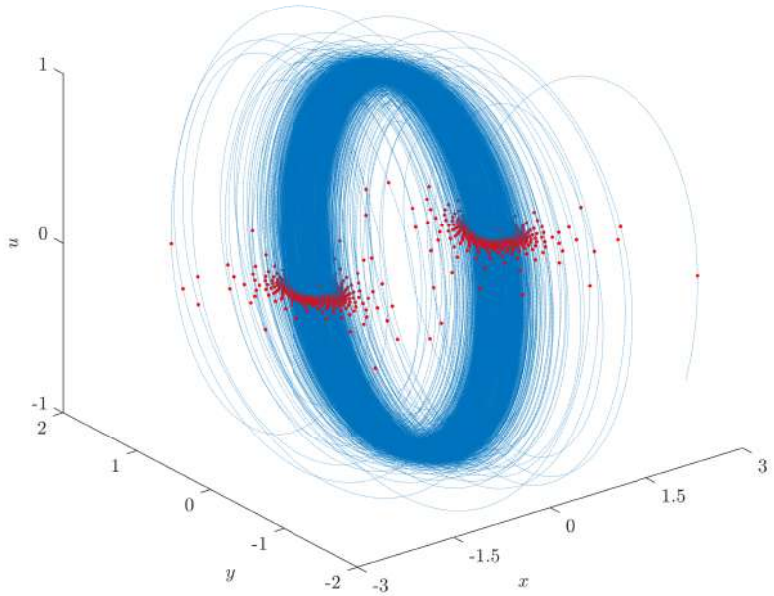

Fig. 5: Poincaré section $\{u = 0\}$ of system (4) $(\omega, \varepsilon) = (2.766, 3.4)$, near N–S manifold.

near 1 : 3 resonance (see Kuznetsov[7]). It visualizes the transition between regions 2 and 3. As we have just seen, in the region 2 (outside the Arnold

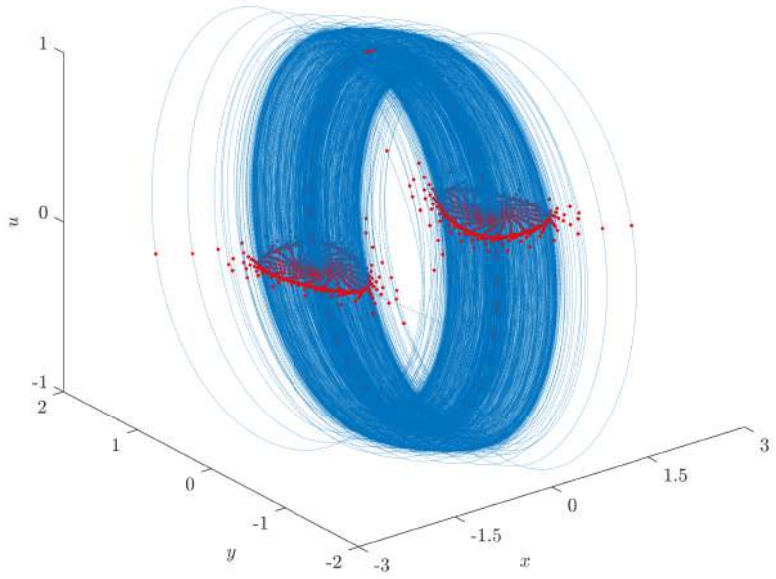

Fig. 6: Poincaré section $\{u = 0\}$ of system (4) for $(\omega, \varepsilon) = (2.85, 3.4)$, region 2.

tongue), the system possesses a stable quasiperiodic invariant torus. When crossing the *LPC* curve (entering the Arnold tongue, 3), the fold bifurcation gives rise to a pair of limit cycles – stable and saddle, respectively. The forced van der Pol oscillator evince bistable behavior for these parameters inside and close to the Arnold tongue border since there are two stable attractors – an outside stable limit cycle and a stable invariant torus. The torus may be destructed via a heteroclinic bifurcation. In the Poincaré section depicted red in Fig. 7 (b)–(c), you can see a symmetric triplet of saddles approaching the invariant loop that belongs to the inside torus. The coincidence of the saddle cycle with the loop destroys the stable torus.

7 Discussion and conclusions

To summarize and outline the possible research connected to synchronizations of forced oscillators, we mention the topics we would like to focus on.

There is much more to study since Arnold tongues interfere with each other, and symmetries near resonances give birth to various types of synchronizations. Also, there is usually a period-doubling cascade inside the Arnold tongues, and this route to a chaotic attractor is possible and likely. Study of all these phenomena is allowed only using a suitable representation (4) of forced van der Pol oscillator (1). The proper transformation of the original system and using Poincaré sections give possibility to use continuation methods of bifurcation theory, and also visualize in 3D the hidden phenomena behind synchronizations of limit cycles.

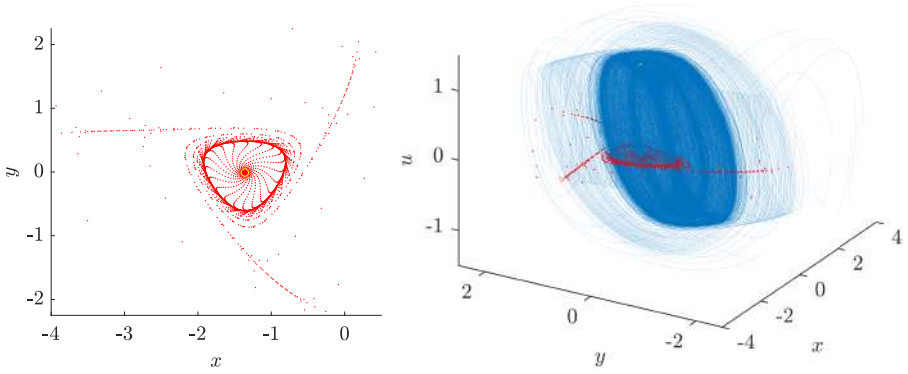

(a) Region 2: $(\omega, \varepsilon) = (2.85, 3.4)$, before crossing $LPC_{1:3}$

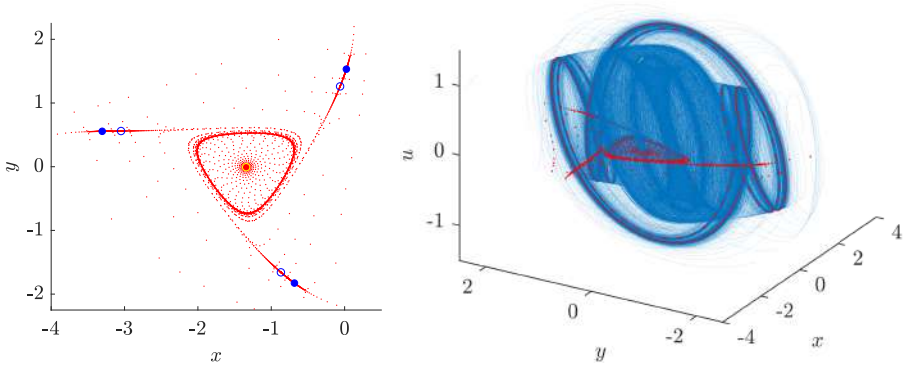

(b) Region 3: $(\omega, \varepsilon) = (2.88, 3.4)$, right after crossing $LPC_{1:3}$

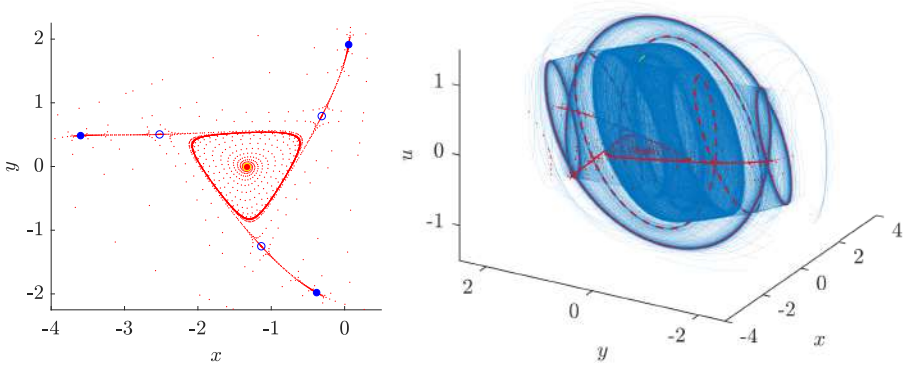

(c) Region 3: $(\omega, \varepsilon) = (2.90, 3.4)$, after crossing $LPC_{1:3}$

Fig. 7: The onset of synchronization $1 : 3$ in system (4) visualized using Poincaré section $\{u = 0, v = -1\}$ in the state space for parameters (ω, ε) from regions 2 and 3, i.e. for the crossing of the $LPC_{1:3}$ curve corresponding to fold bifurcation of limit cycles (see Fig. 3).

We plan to continue with an analysis of bifurcation manifolds near the mentioned double Hopf bifurcation, as well as near resonances. Very interesting dynamics could be found near the torus break on the heteroclinic orbit for parameters inside the Arnold tongues. We would like to focus also on bistability in the case of coupled oscillators. We are convinced that this phenomenon is closely related to chimera-like dynamics, as well as to routes to complexity and chaos.

Acknowledgements

The work has received financial support from Mathematical and Statistical modelling project MUNI/A/1615/2020.

References

1. H. Alinejad, D. Yang, P. A. Robinson, Mode-locking dynamics of corti-cothalamic system response to periodic external stimuli, *Physica D*, 402, 2020.
2. Ch. Beck. Possible resonance effect of axionic dark matter in Josephson junctions. *Physical review letters*, 111, 23, 2013.
3. A. I. Braginski, Superconductor Electronics: Status and Outlook, *Journal of superconductivity and novel magnetism*, 32, 23–44, 2019.
4. A. Dhooge, W. Govaerts and Y. A. Kuznetsov. MATCONT: a MATLAB package for numerical bifurcation analysis of ODEs. *ACM Transactions on Mathematical Software (TOMS)*, 29, 2, 141–164, 2003.
5. H. Ju, A. B. Neiman and A. L. Shilnikov, Bottom-up approach to torus bifurcation in neuron models, *Chaos*, 28, 10, 2018.
6. Y. Kuramoto. *Chemical Oscillations, Waves, and Turbulence.* Chemistry Series. Dover. New York. 1984.
7. Y. A. Kuznetsov. *Elements of applied bifurcation theory.* Vol. 112. Springer Science & Business Media, 2013.
8. A. Mallick, M. Bashar, D. Truesdell, B. Calhoun, S. Joshi and N. Shukla, Using synchronized oscillators to compute the maximum independent set, *Nature communications*, 11, 1–7, 2020.
9. B. Sturgis-Jensen, P.-L. Buono, A. Palacios, J. Turtle, V. In, P. Longhini. On the synchronization phenomenon of a parallel array of spin torquenano-oscillators. *Physica D* 396 (2019) 71–81.
10. U. Welp, K. Kadowaki, R. Kleiner, Superconducting emitters of THz radiation, *Nature Photonics*, 7, 702–710, 2013.
11. S. Wiggins. *Introduction to applied nonlinear dynamical systems and chaos.* Vol.2. New York: Springer-Verlag, 1990.
12. A. T. Winfree. *The Geometry of Biological Time.* Springer. New York. 2001.
13. J. Záthurecký and L. Přibylová. Coupled FitzHugh-Nagumo Type Neurons Driven by External Voltage Stimulation. *14th Chaotic Modeling and Simulation International Conference*, 2021.
14. W. Zhen, and S. A. Campbell. Phase models and clustering in networks of oscillators with delayed, all-to-all coupling. *IFAC-PapersOnLine*, 48, 12, 105–110, 2015.

Fractal nanoparticles of phase-separating solid solutions: nanoscale effects on phase equilibria, thermal conductivity, thermoelectric performance

Alexander V. Shishulin.
G.A. Razuvaev institute of organometallic chemistry, Russian Academy of sciences, Nizhny Novgorod, Russia
Mailing address: 603137, Russia, Nizhny Novgorod, Tropinin str., 49.
E-mail: chichouline_alex@live.ru

Alexander A. Potapov.
V. A. Kotelnikov institute of radio engineering and electronics, Russian Academy of sciences, Moscow, Russia
JNU-IREE RAS Joint lab. of information technology and fractal processing of signals, JiNan University, Guangzhou, 510632, China
Mailing address: 125009, Russia, Moscow, Mokhovaya str., 11-7.
E-mail: potapov@cplire.ru

Anna V. Shishulina.
R.E. Alekseev Nizhny Novgorod State technical University, Nizhny Novgorod, Russia
N.I. Lobachevsky Nizhny Novgorod State University, Nizhny Novgorod, Russia
Mailing address: 603950, Russia, Nizhnij Novgorod, Minin str., 24.

Headings content

Abstract

In recent years, thermoelectric materials and energy converters have attracted considerable attention, especially as a part of advanced "green" energy and space technologies. One of the most promising ways of obtaining high values of the thermoelectric figure of merit is the formation of nanostructured 3D materials with nanoparticles of phase-separating alloys. In this chapter, using the example of low-temperature thermoelectric Bi_{1-x}-Sb_x alloys for the application in space engineering, we have shown how nanoscale effects on phase equilibria in nanoparticles influence on their thermoelectric properties. Such effects consist in nonlinear changes in mutual solubilities of components at a given temperature, phase transition temperatures and even the total suppression of the phase separation depending on the morphology of a nanoparticle as well as on some other factors. The combination of thermodynamic and ab initio approaches has been used while the nanoparticle shape has been determined using the methods of fractal geometry. A method has been suggested in order to calculate the optimal morphology of nanoparticles, at which their equilibrium phase composition leads to a dramatic reduction of the phonon thermal conductivity, favoring the growth of the thermoelectric figure of merit. A decrease in the phonon thermal conductivity in nanoparticles of a pure substance depending on their morphology as well as an approach of calculating the equilibrium size and shape distribution within a nanoparticle ensemble have also been discussed.

2.1 Introduction

Thermoelectric materials and energy converters on their basis have been an object of considerable interest among researchers in recent years [1]. The expanding field of their application includes energy generators which operate in extreme conditions (e.g. radioisotope thermoelectric generators for Voyager-2 and other space modules [1]), thermoelectric converters for utilizing the waste heat dispersed into environment [2], cooling and temperature-control facilities based on the Peltier effect etc [3]. Despite the intensive development of multiple approaches to obtain thermoelectric materials with promising properties based on low-dimension structures (nanofilms [4,5], quantum wires [6] etc), highly-effective and low-cost thermoelectrics can be produced on the basis of 3D nanocrystalline structures [7,8].

The key characteristic parameter determining the materials thermoelectric efficiency is the dimensionless figure of merit, *ZT*, which can be expressed as a function of thermal conductivity κ, electrical conductivity σ and Seebeck coefficient α: $ZT = \alpha^2 \sigma \overline{T} / \kappa$ where $\overline{T}$ is the average temperature between the "hot" and "cold" sides of a thermoelectric converter and $\kappa \approx \kappa_{car} + \kappa_{ph}$ [1,2,7]. Here, κ_{car} and κ_{ph} are the contributions of charge carriers (electrons, holes) and phonons to the thermal conductivity, respectively (several other contributions, e.g. the ones of excitons or spin-orbit coupling, are neglected, being much lower). In every single material, as a rule, electrical conductivity σ and the contribution of carriers to the total thermal conductivity, κ_{car}, cannot be varied separately, and optimal thermoelectric properties can be obtained primarily through the reduction of the phonon contribution κ_{ph}. In nanostructured polycrystalline materials, κ_{ph} is generally decreased through formation of multiple interfaces (grain boundaries) which scatter thermal phonons [9], add to this, the energy filtration of charge carriers at grain boundaries, which reduces the contribution of low-energy carriers to transport properties, results in an additional increase in the Seebeck coefficient [2]. Nanostructured polycrystalline thermoelectric materials can be produced using various technologies of up-to-date powder metallurgy, e.g. spark plasma sintering, selective laser sintering, selective laser melting etc [7,8].

It is necessary to take into account that several specific properties of nanoscale particles provide an additional "knob" which can be used to tune the functional properties of a nanostructured material. On the one hand, promising thermoelectric properties are associated with nanoparticles of bi- and polycomponent solutions (e.g., Si-Ge, Bi-Sb, Bi-Sb-Te, Bi-Te-Se etc) while *ab-initio* calculations demonstrate in many cases a dramatic decrease in phonon thermal conductivity κ_{ph} with an increase in the concentration of a dopant [10]. In several systems including the Bi_{1-x}-Sb_x alloy (which is considered to be one of the most efficient low-temperature thermoelectric materials [10] with multiple possible applications, for example, in space engineering), however, the solid solutions with high dopant

concentrations are thermodynamically unstable at the operation temperatures, according to the available reference data for macroscopic phases, and undergo the phase separation. On the other hand, all characteristics of phase equilibria including the thermodynamical stability of solid solutions with high dopant concentrations as well as phase transition temperatures become morphology-dependent at the nanoscale [11-18]. In the case of stratifying solid solutions, such effects manifest themselves in dramatic changes solubility limits, temperature ranges of the thermodynamical stability of various heterogeneous and homogeneous states including the value of the upper critical dissolution temperature (UCDT) depending of the geometric characteristics of a nanoparticle under consideration, its external environment [19] and some other factors [20-22]. These effects are interpreted as the realization of several mechanisms reducing the free energy of a nanoscale system, which can also be competing in several cases leading to specific non-monotonous dependences of phase equilibria characteristics [15,23]. Being observed experimentally [24], at the particle sizes appropriate for the additive technologies, the mentioned effects can be simulated using the thermodynamical approach (the size limits for the thermodynamics applicability have been discussed in [25]). For much smaller particles, the molecular dynamics approach can be applied which demonstrate a perfect accordance with the thermodynamically obtained results [26].

In this chapter, we present and summarize the brand-new findings on the realization of nanoscale phase equilibria effects in nanostructured thermoelectric materials and their possible influence on the thermoelectric characteristics. The materials morphology has been determined using the methods of fractal geometry which allows to express the materials geometric characteristics in the most general form while the fractal characteristics of nanoparticles can be measured experimentally [27].

2.2 How to simulate phase equilibria at the nanoscale: mathematical formulations

As the object of modeling below, we consider differently shaped nanoparticles of the Bi_{1-x}-Sb_x system with various atomic fractions of Sb (x). The volume of such a particle is set by its effective diameter d_{eff} - diameter of the sphere whose volume is equal to the volume of the particle. We assume that, at the phase equilibrium in the temperature range below the upper critical dissolution temperature (UCDT), such a particle contains a spherical inclusion of a solid solution (*core*-phase) surrounded by a layer of a solid solution with a different composition (*shell*-phase). In a closed binary system with a *core-shell* configuration, the volume of a particle, total amount n of the matter in the system, numbers n_i of moles of each component (subscripts i=1, 2 refer to Sb and Bi, respectively), and concentrations x_{ij} of components i in phases j (subscripts j=c, s correspond to *core*- and *shell*-phases, respectively) are interrelated through the conservation conditions of matter:

$$\pi d_{\text{eff}}^3 \Big/ 6 = \sum_j V_j,\ n_1 = xn,\ n_2 + n_1 = n,\ n_i = \sum_j n_{ij},\ V_j = \sum_i n_{ij} V_i,\ x_{ij} = n_{ij} \Big/ \sum_i n_{ij}.$$

Here, V_j is the volume of phase *j* while V_i stands for the molar volume of component *i*. The molar volumes are V_1=18.4 cm^3/mol and V_2=21.3 cm^3/mol [28,29].

In order to describe the irregular morphology of real nanoparticles, it is convenient to use the methods of fractal geometry. In the terms of the given approach, the phase of a nanoparticle is characterized by fractal dimension *D* which correlates its volume *V* and surface area A_s: $A_s = CV^{2/D}$, where *C* is the numerical coefficient which also matches units. For the sake of convenience, we assume $C = 4\pi$ below (this assumption is not accompanied by any losses of generality). For simple geometric structures, $D \equiv 3.00$ while for structures with a complicated and irregular morphology, $D < 3.00$ and can be non-integer. The examples of nanoparticles with various fractal dimensions can be found in [30,31]. Fractal dimension *D* can also be related to so-called *shape coefficient k* which has been used as a calculation parameter in some previous papers of us [23, 28-30] and other authors [32]: $k\ V, D\ = V^{2/D} \Big/ \left(3V \big/ 4\pi\right)^{2/3}$. The shape coefficient is equal to the ratio between the surface areas of the particle under consideration and the sphere of the same volume, for example, for nanoparticles with the effective diameter of 40 nm and fractal dimensions of 2.60, 2.75 and 2.90, the shape coefficients are equal to 2.51, 1.72 and 1.23, respectively.

Thus, the geometrical parameters of the *core-shell* structure can be described as follows: $A_c = 4\pi \left(3V_c \big/ 4\pi\right)^{2/3}$, $A_s = C \left(\pi d_{\text{eff}}^3 \big/ 6\right)^{2/D}$.

The criterion for an equilibrium state of the system is the minimum of Gibbs function *g* including the energy contribution of all interfaces:

$$\begin{aligned} g &= \sum_j \left(n_{1j} + n_{2j}\right) G_j\left(x_{1j}, T\right) + \sigma_s A_s + \sigma_{cs} A_s, \\ G_j\left(x_{1j}, T\right) &= A_{\text{I}}(T)\, x_{1j}\left(1 - x_{1j}\right) + A_{\text{II}}(T)\, x_{1j} + A_{\text{III}}(T)\left(1 - x_{1j}\right) + \\ &+ RT\left[x_{1j} \ln x_{1j} + \left(1 - x_{1j}\right) \ln\left(1 - x_{1j}\right)\right] \end{aligned} \qquad (1)$$

where *R* is the universal gas constant, σ_s and σ_{cs} are the surface energies on the outer (*shell*-) and inner (*core-shell*) interfaces. $A_{\text{I}}(T) = 6500 - 2.6T$, $A_{\text{II}}(T) = -2.645R\,(903.7 - T)$, $A_{\text{III}}(T) = -2.458R\,(544.6 - T)$. Without any losses of generality, the following approximation has been used to calculate the values of σ_s and σ_{cs} (see also [33]): $\sigma_{cs} = 0.5\sum_j \sigma\left(x_{1j}\right)$,

$\sigma\ x_{1j}\ = \sigma_1 x_{1j} + \sigma_2\ 1 - x_{1j}\ ,\ \ \sigma_s = \sigma_1 x_{1s} + \sigma_2\ 1 - x_{1s}$ where σ_1 =0.300 J/m^2, σ_2 =0.521 J/m^2 [19,28,29].

2.3 Nanoscale phase equilibria and lattice thermal conductivity: specific phenomena

For a *core-shell* structure, Gibbs function (1) has two minima which correspond to heterogeneous states with different mutual arrangements of co-existing solid solutions. The state where the *shell*-phase is formed with a Bi-based solid solution is hereinafter called *state 1*. In *state 2*, in turn, Sb prevails in the *shell*-phase. In the case of a two-component system, simulation results and the main regularities can be illustrated with the θ-diagrams for the Gibbs function. The example of such diagrams is given in Fig. 1 where Gibbs function (1) is plotted using dimensionless variables $\theta_i = n_{ic} \big/ n_1$, corresponding to the atomic fraction of component *i* in the *core*-phase relative to the total amount of component *i* in the system ($\theta_i \in\ 0,1\ $). The minima are indicated with a darker color.

In the heterogeneous state of a macroscopic system (Fig. 1a), the minima of the Gibbs function are symmetric, have equal energies and correspond to the equal compositions of co-existing phases which match the reference data (the mutual arrangement of phases morphology of the system and its total composition (x) have no influence on the phase composition at each temperature as well as on the upper critical dissolution temperature i.e. the temperature value at which the phase separation terminates and all the compositions of a particle become thermodynamically stable). At the nanoscale, at the same time, a notable energy contribution of all the interfaces leads to shifts of the minima in comparison with a macroscopic system while the energy of state 1 becomes somewhat higher than the energy of another one and a high-energy metastable homogeneous state can also emerge in the system (see Fig. 1b). As a result, the equilibrium compositions and relative volumes of co-existing phases are different in states 1 and 2, differ from the "macroscopic" values and depend on the system morphology.

In both states 1 and 2, a decrease in the particle size and/or a decrease in its fractal dimension lead to a considerable reduction of the UCDT. However, the UCDT values differ in different states, the upper critical dissolution temperature in state 1 being always lower than the one in state 2. At the temperatures above the UCDT for state 1, the heterogeneous state with a Bi-based *shell*-phase is replaced with a homogeneous state which co-exists with the heterogeneous one with a Sb-based shell (see Fig. 1c). Above the UCDT for state 2, the homogeneous state becomes the only one in the system. An example of the dependence of the UCDT on the particle morphology is plotted in Fig. 2b for an equiatomic particle of d_{eff}=40 nm in state 1. At D<2.74 the UCTD of such a particle is reduced below 100 K while for a particle of the same volume in state 2 this takes place at D<2.57.

The dependences of the phonon contribution to the thermal conductivity coefficient exhibit its dramatic jumpwise reduction at high concentrations of do-

pants (an example of those dependences is plotted in Fig. 2b for two crystallographic directions in the Bi-Sb crystal lattice at T=100 K. At other temperatures, the characteristic view of such dependences is expected to remain the same). A decrease in the UCDT down to the low operating temperatures leads to the thermodynamical stabilization of phases with equiatomic or near-equiatomic compositions with significantly (by more than 50%) reduced phonon thermal conductivities (for example, in equiatomic nanoparticles of d_{eff}=40 nm in state 1, decreasing the fractal dimension below 2.74 at T=100 K leads to a decrease in the phonon thermal conductivity by 71% as compared to the value of the *shell*-phase of a spherical 40-nm-diameter particle in the same thermodynamical conditions or even by 88% as compared to the one of its *core*-phase).

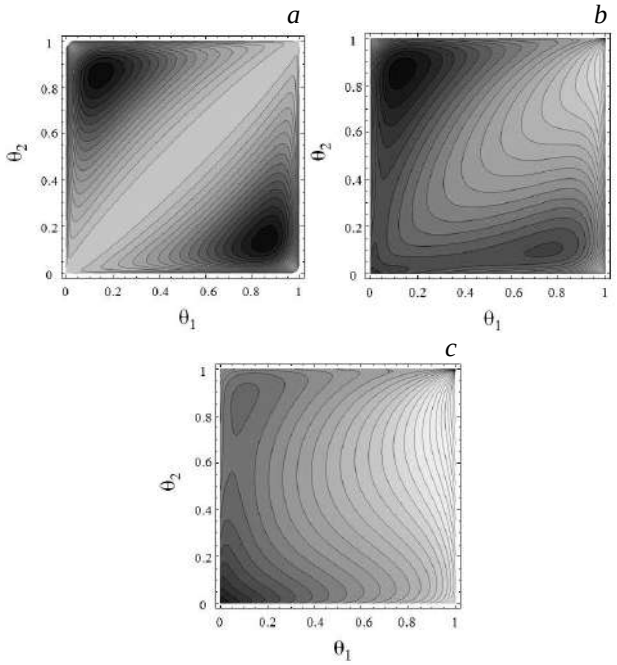

Fig. 1. Examples of θ-diagrams: for a macroscopic structure (*a*), for a nanoscale particle at "low" temperatures with both heterogeneous states and a highly metastable homogeneous one (*b*). for a nanoscale particle upper the UCDT for state 1 (*c*). The minima in the lower right corner and in the upper left one correspond to states 1 and 2, respectively. The homogeneous state corresponds to the minimum located in the lower left corner at $\theta_1 = \theta_2 = 0$.

Morphology-dependent changes in the mutual solubilities below the UCTD can lead to smooth variations of phonon thermal conductivity. The temperature dependences of the solubilities in nanoparticles of the Bi-Sb alloy of different volumes and shapes have been obtained in [19,28,29]. Such dependences result from the implementation of two mechanisms of lowering the free energy of a nanoscale system. In the most general case, these mechanisms have been described in [15,23] along with a specific case when the mechanisms (so-called

"molar-volume-controlled segregation" and "surface-energy-controlled segregation") are competitive. These results should be accompanied by the consideration of one of the most interesting and non-trivial effects in small-volume structures – the effect of the chemical composition. In macroscopic structures, a variation of the chemical composition of the system leads to changes in the volume fraction of co-existing phases (according to the lever rule) but does not affect the mutual solubility of components, in small-volume systems the chemical composition of the system determines not only the volume fractions of the phases, but also their equilibrium composition (previously such effect has been considered in the case of systems with the liquid-liquid phase separation [20] and nanoparticles above the solidus temperature [21,22] and explained according to the abovementioned mechanisms of lowering the free energy). In a spherical 70-nm-diameter nanoparticle containing 50 at. % Sb (x=0.5), for example, the solubility limits are ~1.01 at. % for Bi in Sb, ~8.00 at. % for Sb in Bi (state 1), ~1.49 at. % for Bi in Sb, ~1.56 at. % for Sb in Bi (state 2). But for x=0.3, we have: ~0.96 at. % for Bi in Sb, ~6.98 at. % for Sb in Bi (state 1), ~1.13 at. % for Bi in Sb, ~1.59 at. % for Sb in Bi (state 2). For x=0.6, it turn, the solubilities are: ~0.99 at. % for Bi in Sb, ~10.47 at. % for Sb in Bi (state 1), ~1.82 at. % for Bi in Sb, ~1.53 at. % for Sb in Bi (state 2). Note that despite the fact the term "nanoscale effects" is widely used, there is a broad class of systems, especially polymeric ones with great molecular volumes and masses, in which such effects manifest themselves at characteristic sizes even several thousand times higher [16,20] (and such effects should probably be called "small-amounts-of-matter effects").

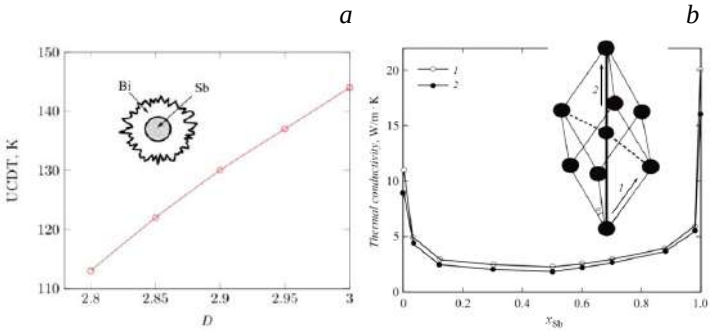

Fig. 2. The dependence of the upper critical dissolution temperature (UCDT) on the fractal dimension for a nanoparticle (d_{eff}=40 nm) in state 1 (*a*) and the influence of the Sb content on the phonon thermal conductivity of Bi-Sb solid solutions for binary (*1*) and trigonal (*2*) crystallographic directions (*b*). In the box, the crystalline structure of Bi and Sb. Angle α is $57^0 30'$ for Bi and $75^0 84'$ for Sb.

All the demonstrated regularities for individual nanoparticles are expected to be realized in nanoparticle-fabricated alloys where the role of interfaces is played by grain boundaries. In such cases, however, some other geometrical configurations of co-existing phases may be preferable (e.g. the nucleation and growth of a new phase in a grain boundary) while the values of grain boundary energies can be estimated using different approaches (see [34], for example)

which may require minor changes in the presented mathematical formulations. In polycrystalline structures, the further optimization of the materials thermoelectric performance can be expected due to additional scattering of phonons at grain boundaries, tunneling of carriers between nanograins and energy filtering of carriers (see [29] and Refs. within). One of the models which describe the phenomenon of grain boundary scattering can be found in [9].

2.4 Conclusions and additional remarks

The obtained results can be accompanied by the estimates which allow predicting an additional decrease in the phonon thermal conductivity coefficients in nanoparticles of a pure substance corresponding to the changes in phonon dynamics in nanoscale particles. In order to establish the morphology-based model to calculate the corresponding changes in the lattice thermal conductivity parameters, one of the possible approaches consists in using one of the models for the morphology-dependent melting temperature as well as the Debye theory and the Lindemann criterion of melting which correlates the melting and Debye temperatures of the crystal, estimating the changes in the average phonon velocity and phonon mean-free path on the basis of the size-dependent Debye temperature, and in applying one of the models which describes phonon scattering effects. An attempt of such calculations is presented in [35] where the expression of G. Guisbiers for the melting temperature of nanoscale structures has been used, and the obtained results demonstrate a good agreement with the experimental data for pure Si and GaAs nanostructures (especially, nanorods and nanofilms). For nanoparticles, however, we suggest using the more convenient model of W.H. Qi and M.P. Wang (experimentally justified, for example, for pure Bi nanoscale structures [32]) for the nanoparticle melting behavior combined with the fractal geometry approach. The Qi-Wang model is based on the correlation between the melting temperature and the cohesive energy of the crystal (note that the cohesive energy is also related to the temperatures of several other types of first-order and second-order phase transitions including the magnetic ones [36]) and leads to the following equation: $T_{\mathrm{m}}^{\mathrm{nano}} = T_{\mathrm{m}}^{\mathrm{bulk}} \left(1 - 6kr_{\mathrm{at}} / d_{\mathrm{eff}}\right)$ where $T_{\mathrm{m}}^{\mathrm{nano}}$ and $T_{\mathrm{m}}^{\mathrm{bulk}}$ are the melting temperatures of a nanoparticle and the bulk material, respectively, r_{at} is the atomic radius and k and d_{eff} are the shape coefficient and the effective diameter of a nanoparticle as they have been introduced above. All these considerations allow expressing the morphology-dependent phonon contribution to the thermal conductivity as follows:

$$\kappa_{\mathrm{ph}}^{\mathrm{nano}} = \eta \exp\left(1 - l_0 / d_{\mathrm{eff}}\right) \left(1 - C\left(\pi/6\right)^{2/D-1} d_{\mathrm{eff}}^{3\left(2/D - 2/3\right)} r_{\mathrm{at}} / d_{\mathrm{eff}}\right) \kappa_{\mathrm{ph}}^{\mathrm{bulk}}$$

where pre-term $\eta \exp\left(1 - l_0 / d_{\mathrm{eff}}\right)$ is included as a quite simplified approach to take into account the phonon scattering which increases with a decrease in the volume of a particle, an increase in the surface-to-volume ratio and surface roughness [35]. $\eta \in (0,1]$ represents the surface roughness parameter while l_0 / d_{eff} is

the Knudsen number, l_0 is the bulk phonon mean-free path value [35]. Coefficient C which matches the units has been introduced above. The larger the value of η is, the smoother the surface of the particle is. Note that the correlation between the surface roughness and fractal dimension of the nanoparticle is not unique (the fractal dimension value is associated with the surface-to-volume ratio while the surface roughness corresponds primarily to the number of edges). Several notes on the dependence of fractal dimension on the surface roughness are given in [37] (see also their graphical representation in Fig. 2 of [37]).

In the case of nanoparticle ensembles, the average phase composition and functional properties depend on the size and shape distributions in an ensemble. In [31], we have suggested a method for calculating such distributions based on the combined usage of number theory, fractal geometry and statistical thermodynamics. For example, the equilibrium size distributions for nanoparticles with fractal dimension D in a free-dispersed system can be expressed as follows:

$$f_D\ \phi_p, D, N\ \square \exp\left(-\frac{\sigma A_{sp}\ D\ + RT \ln f_p}{RT}\right),\ f_p = \frac{N}{N-\phi_p}\exp\left\{\pi\left(\sqrt{\frac{2}{3}}\ N-\phi_p\ -\sqrt{\frac{2}{3}N}\right)\right\}.$$

Here, $\phi_p = \omega\ d_{eff}/d_{at}\ ^3$ is the number of atoms in a nanoparticle, ω is the lattice packing density, N is the total number of atoms in the system, $A_{sp}\ D$ is the specific surface area of the ensemble. The presented estimates are in perfect accordance with the experimental data (see [31] and Refs. within) and make it possible to model the thermodynamical conditions for the realization of optimal average characteristics of nanoparticles (equilibrium compositions, phase transition temperatures, thermoelectric properties etc) as well to predict the degree at which such characteristic are "blurred" in an ensemble.

References

1. Rowe D.M. (ed.) Thermoelectric handbook: macro to nano. – Boca Raton: CRC Press, 2006. 1008 p.
2. Tambasov I.A., Voronin A.S., Evsevskaya N.P. Volochaev M.N., Fadeev Y.V., Simunin M.M., Aleksandrovsky A.S., Smolyarova T.E., Abelian S.R., Tambasova E.V., Gornakov M.O., Eremina V.A., Kuznetsov Yu. M., Dorokhin M.V., and Obraztsova E.D. Thermoelectric properties of low-cost transparent single wall carbon nanotube thin films obtained by vacuum filtration // Phys. E. 2019. Vol. 114, no. 113619. https://doi.org/10.1016/j.physe.2019.113619.
3. Hu J.-Z., Liu B., Zhou J., Li B., and Wang Y. Enhanced thermoelectric cooling performance with graded thermoelectric materials // Jpn. j. appl. phys. 2018. Vol. 57, pp. 71801-71806. www.doi.org/10.7567/JJAP.57.071801.
4. Li Z., Miao N., Zhou J. Sun Z., Liu Z., and Xu H. High thermoelectric performance of few-quintuple Sb_2Te_3 nanofilms // Nano energy. 2018. Vol. 43, pp. 285-290. www.doi.org/10.1016/j.nanoen.2017.11.043.

5. Erofeeva I.V., Dorokhin M.V., Lesnikov V.P., Kuznetsov Y.M., Zdoroveyshchev A.V., and Pitirimova E.A. Thermoelectric effects in nanoscale layers of manganese silicide // Semiconductors. 2017. Vol. 51, no. 11, pp. 1403-1408. www.doi.org/10.1134/S1063782617110112.
6. Caballero-Calero O., Martín-González M. Thermoelectric nanowires: A brief prospective // Scripta materialia. 2016. Vol. 111, pp. 54-57. www.doi.org/10.1016/j.scriptamat.2015.04.020.
7. Dorokhin M.V., Erofeeva I.V., Kuznetsov Yu.M., Boldin M.S., Boryakov A.V., Popov A.A., Lantsev E.A., Demina P.B., and Zdoroveyshchev A.V. Investigation of the initial stages of spark-plasma siltering of Si-Ge-based thermoelectric materials // Nanosyst.: phys., chem., math.. 2018. Vol. 9, no. 5, pp. 622–630. www.doi.org/10.17586/2220-8054-2018-9-5-622-630.
8. Kuznetsov Yu.M., Bastrakova M., Dorokhin M.V., Erofeeva I.V., Demina P.B., Uskova E., Popov A.A., and Boryakov A.V. Molecular dynamics studies on spark-plasma sintering of Si-Ge-based thermoelectric materials // AIP adv. 2020. Vol. 10, no. 6, 065219. https://doi.org/10.1063/5.0011740.
9. Bulat L.P., Drabkin I.A., Karatayev V.V., Osvenskii V.B., and Pshenay-Severin D.A. Effect of boundary scattering on the thermal conductivity of a nanosctructured semiconductor material based on the $Bi_xSb_{2-x}Te_3$ solid solution // Phys. solid state. 2010. Vol. 52, no. 9, pp. 1836-1841. https://doi.org/10.1134/S1063783410090088.
10. Lee S., Esfarjani K., Mendoza J., Dresselhaus M.S., and Chen G. Lattice thermal conductivity of Bi, Sb, and Bi-Sb alloy from first principles // Phys. rev. B. 2014. Vol. 89, pp. 85206-85215. www.doi.org/10.1103/PhysRevB.89.085206.
11. Bajaj S., Haverty M.G., Arróyave R., Goddard W.A., and Shankar S. Phase stability in nanoscale material systems: extension from bulk phase diagrams // Nanoscale. 2015. Vol. 7, no. 9868. www.doi.org/10.1039/C5NR01535A.
12. Guisbiers G., Khanal S., Ruiz-Zapeda F., Roque de la Puente J., and Yakamán M.J. Cu-Ni nano-alloy: mixed, *core-shell* or *janus* nano-particle? // Nanoscale. 2014. Vol. 6, pp. 14630-14635. www.doi.org/10.1039/C4NR05739B.
13. Mndoza-Pérez R., Muhl S. Phase diagrams of refractory bimetallic nanoalloys // J. nanopart. res. 2020. Vol. 22,
no. 36. www.doi.org/10.1007/s11051-020-05035-x.
14. Geoffrion L.-D., Guisbiers G. Chemical ordering in $Bi_{1-x}Sb_x$ nanostructures: alloy, *janus* or *core-shell* // J. phys. chem. C. 2020. Vol. 124, no. 25, pp. 14061. www.doi.org/10.1021/acs.jpcc.0c04356.
15. Shishulin A.V., Fedoseev V.B. On some peculiarities of stratification of liquid solutions within pores of fractal shape // J. mol. liq. 2019. Vol. 278, pp. 363-367. www.doi.org/10.1016/j.molliq.2019.01.050.
16. Shishulin A.V., Fedoseev V.B. Thermal stability and phase composition of stratifying polymer solutions in small-volume droplets // J. eng. phys. thermophys. 2020. Vol. 93, no. 4, pp. 802-809]. www.doi.org/10.1007/s10891-020-02182-9.
17. Fedoseev V.B., Shishulin A.V., Titaeva E.K., and Fedoseeva E.N. On the possibility of the formation of a NaCl-KCl solid-solution crystal from an aqueous solution at room temperature in small-volume systems // Phys. solid state. 2016. Vol. 58, no. 10, pp. 2095-2100. www.doi.org/10.1134/S1063783416100152.

18. Shishulin A.V., Fedoseev V.B. Size effect in the phase separation of Cr-W solid solutions // Inorg. mater. 2018. Vol. 54, no. 6, pp. 546-549. www.doi.org/10.1134/S0020168518050114.
19. Shishulin A.V., Fedoseev V.B., Shishulina A.V. Environment-dependent phase equilibria in a small-volume system in the case of decomposition of Bi-Sb solid solutions // Butlerov commun. 2017. Vol. 51, no. 7, pp. 31-37 [in Russian].
20. Shishulin A.V., Fedoseev V.B. Features of the influence of the initial composition of organic stratifying mixtures in microsized pores on the mutual solubility of components // Tech. phys. lett. 2020. Vol. 46, no. 9, pp. 938-941. www.doi.org/10.1134/S1063785020090291.
21. Shishulin A.V., Fedoseev V.B. Effect of initial composition on the liquid-solid phase transition in Cr-W alloy nanoparticles // Inorg. mater. 2019. Vol. 55, no. 1, pp. 14-18. www.doi.org/10.1134/S0020168519010138.
22. Shishulin A.V., Shishulina A.V. Several peculiarities of high-temperature phase equilibria in nanoparticles of the Si_x-Ge_{1-x} system. In: Physical and chemical aspects of the study of clusters, nanostructures and nanomaterials. 2019. Vol. 11, pp. 380-388. www.doi.org/10.26456/pcascnn/2019.11.268 [in Russian].
23. Shishulin A.V., Fedoseev V.B. Stratifying polymer solutions in microsized pores: phase transitions induced by deformation of a porous material // Tech. phys. 2020. Vol. 65, no. 3, pp. 340-346. www.doi.org/10.1134/S1063784220030238.
24. Straumal B., Baretzky B., Mazilkin A., Protasova S., Myatiev A., and Straumal P. Increase of Mn solubility with decreasing grain size in ZnO. J. Eur. ceram. soc. 2009. Vol. 29, pp. 1963–1970. www.doi.org/10.1016/j.jeurceramsoc.2009.01.005.
25. Samsonov V.M., Demenkov D.E., Karacharov V.I., and Bembel A.G. Fluctuation approach to the problem of thermodynamics' applicability to nanoparticles // Bull. Russ. Acad. sci.: phys. 2011. Vol. 75, no. 8, 1073. www.doi.org/10.3103/S106287381108034X.
26. Magnin Y., Zappelli A., Amara H., Ducastelle F., and Bichara C. Size-dependent phase diagrams of nickel-carbon nanoparticles // Phys. rev. lett. 2015. Vol. 115, no. 205502. www.doi.org/10.1103/PhysRevLett.115.205502.
27. Li J., Du Q., and Sun C. An improved box-counting method for image fractal dimension estimation // Pattern recognit. 2009. Vol. 42, pp. 2460-2469. www.doi.org/10.1016/j.patcog.2009.03.001.
28. Fedoseev V.B., Shishulin A.V. Shape effect in layering of solid solutions in small volume: bismuth-antimony alloy // Phys. solid state. 2018. Vol. 60, no. 7, pp. 1398-1404. www.doi.org/10.1134/S1063783418070120.
29. Shishulin A.V., Fedoseev V.B., and Shishulina A.V. Phonon thermal conductivity and phase equilibria of fractal Bi-Sb nanoparticles // Tech. phys. 2019. Vol. 64, no. 4, pp. 512-517. www.doi.org/10.1134/S1063784219040200.
30. Shishulin A.V., Potapov A.A., and Fedoseev V.B. Phase equilibria in fractal *core-shell* nanoparticles of $Pb_5(VO_4)_3Cl$ - $Pb_5(PO_4)_3Cl$ system: the influence of size and shape . In: Advances in artificial systems for medicine and education II – Cham, Springer, 2019. Pp. 405–413. www.doi.org/10.1007/978-3-030-12082-5_37.

31. Fedoseev V.B., Shishulin A.V. On the size distribution of dispersed fractal particles // Tech. phys. 2021. Vol. 66, no. 1, pp. 34-40. www.doi.org/10.1134/S1063784221010072.
32. Qi W.H., Wang M.P. Size and shape-dependent melting temperature of metallic nanoparticles // Mater. chem. phys. 2004. Vol. 88, pp. 280-284. www.doi.org/10.1016/j.matche,phys.2004.04.026.
33. Hourlier D., Perrot P. Au-Si and Au-Ge phases diagrams for nanosystems // Mater. sci. forum. 2010. Vol. 653, pp. 77-85. www.doi.org/10.4028/www.scientific.net/MSF.653.77.
34. Tyson W., Miller W. Surface free energies of solid metals. Estimation from liquid surface tension measurements // Surf. sci. 1977. Vol. 62. no. 267, pp. 267-276. www.doi.org/10.1016/0039-6028(77)90442-3.
35. Goyal M. Shape, size and phonon scattering effect on the thermal conductivity of nanostructures // Pramana: j. phys. 281. Vol. 91, no. 87. www.doi.org/10.1007/s12043-018-1660-8.
36. Shishulin A.V., Fedoseev V.B., Shishulina A.V. Variation of the Curie temperature in porous materials // Tech. phys. lett. 2020. Vol. 46, no. 7, pp. 680-682. www.doi.org/10.1134/S106378502007024X.
37. Fedoseev V.B. The use of fractal geometry for the thermodynamic description of the free-dimensional crystal structure elements // Lett. mater. 2012. Vol. 2, pp. 78-83.

Maximal Attractors in Nonideal Hydrodynamic Systems

Aleksandr Shvets[1] and Serhii Donetskyi[2]

[1] National Technical University of Ukraine "Igor Sikorsky Kyiv Polytechnic Institue", Kyiv, Ukraine
(E-mail: aleksandrshvetskpi@gmail.com)
[2] National Technical University of Ukraine "Igor Sikorsky Kyiv Polytechnic Institue", Kyiv, Ukraine
(E-mail: dsvshka@gmail.com)

Abstract. Some nonideal hydrodynamic systems of the type "tank with fluid - source of excitation of oscillation" are considered. New types of limit sets of such systems, so called maximal attractors, have been discovered and described. It was found that the maximal attractors can be both regular and chaotic. Main characteristics of the described maximal attractors are analyzed in details. Transitions to deterministic chaos in such systems are considered. Despite the fact that maximal attractors are not attractors in the traditional sense of this term, it is shown that the transition from regular maximal attractors to chaotic maximal attractors can occur by known before scenarios transition to chaos for "usual" attractors.
Keywords: nonideal hydrodynamic systems, maximal attractors, scenarios of transition to chaos..

1 Introduction

Many modern machines, mechanisms and technical devices as structural elements contain cylindrical tanks partially filled with fluid. Therefore, the study of oscillations free surface of fluid in cylindrical tanks over the past decades has been attracting close attention (Narimanov et al.[1], Ibrahim[2], Lukovsky[3], Raynovskyy and Timokha[4]).

Since the end of 70's years of the last century, there have been the so-called "low-dimensional" mathematical models describing such oscillations (Miles[5],[6], Meron and Procaccia[7], Miles and Henderson[8]). These models allow us to describe oscillations of the free surface of the liquid in the tank using nonlinear systems of ordinary differential equations instead of partial differential equations that arise when describing the problem in the general setting. "Low-dimensional" models allow you to get a fairly adequate description of the problem in cases where the power produced by of the source of excitation of oscillations significantly exceeds the power consumed by the oscillating load (cylindrical tank with fluid). These cases are called ideal by Sommerfeld–Kononenko. However, in practice, most often there are cases in which the power source of excitation of oscillations is comparable to the power consumed by the oscillatory load. Such cases are called nonideal. In these cases, it is imperative to take into account the interaction between the source of excitation of oscillations and the oscillatory load, which leads to essential refinement of the mathematical models used in ideal cases. The neglect of the interaction between the

excitation source and the oscillatory load leads to gross errors in the description of the dynamics of the studied systems (Sommerfeld[9], Kononenko[10], Frolov and Krasnopolskaya[11], Krasnopolskaya[12],[13], Krasnopolskaya and Shvets[14]–[17]).

2 Evolution equation

Consider dynamic system, the layout of which is shown in Fig. 1. The electric motor shaft is connected to the platform through the crank mechanism, on which a rigid cylindrical tank of radius R is fixed, partially filled with liquid. When the crank a rotates through an angle Ψ, the platform makes a vertical

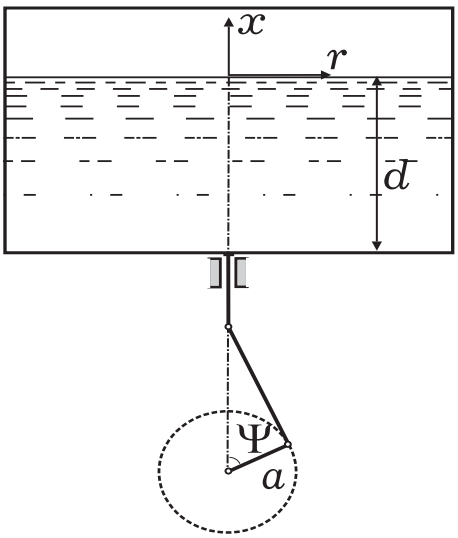

Fig. 1. Scheme of system.

movement of the form $v(t) = a\cos\Psi(t)$. To describe the vibrations of the free surface of a liquid, we introduce a cylindrical coordinate system $Oxr\theta$ with origin in the tank axis, on the undisturbed fluid surface. The relief equation of free surface of the fluid we write down in the form $x = \eta(r, \theta, t)$. Suppose liquid inviscid and incompressible with density ρ and fills a cylindrical tank of cross-section S section to the depth $x = -d$.

We will find function of the relief of surface of liquid in the form of an eigenmode expansion:

$$\eta(r,\theta,t) = \sum_{i,j}[q^c_{ij}(t)k_{ij}(r)\cos i\theta + q^s_{ij}(t)k_{ij}(r)\sin i\theta]. \tag{1}$$

Then we write the kinetic energy of the total system in the form (Krasnopolskaya and Shvets[15,16]):

$$T = \frac{1}{2}I\dot{\Psi}^2 + \frac{1}{2}m_0\dot{v}^2 + \frac{1}{2}\rho S\sum_{i,j,m,n} a_{ijmn}\dot{q}^{c,s}_{ij}\dot{q}^{c,s}_{mn}. \tag{2}$$

Here I is the moment of inertia of the motor shaft; m_0 – mass of the liquid tank; a_{ijmn} – nonlinear functions of $q_{ij}^{c,s}(t), q_{mn}^{c,s}(t)$.

In turn, the potential energy of movements of the free surface of the liquid is (Krasnopolskaya and Shvets[15,16])

$$V = \rho \int\limits_S \int dS \int\limits_0^\eta (g + \ddot{v}) x dx = \frac{1}{2}\rho S(g + \ddot{v}) \sum_{i,j} q_{ij}^{c,s} q_{ij}^{c,s}, \tag{3}$$

where g is the acceleration of gravity.

Therefore, the Lagrangian of the system takes the form

$$\begin{aligned} L = \frac{1}{2} I\dot{\Psi}^2 + \frac{1}{2} m_0 a^2 \dot{\Psi}^2 \sin^2 \Psi + \frac{1}{2}\rho S \sum_{i,j,m,n} a_{ijmn} \dot{q}_{ij}^{c,s} \dot{q}_{mn}^{c,s} + \\ + \frac{1}{2}\rho S a(\dot{\Psi}^2 \cos\Psi + \ddot{\Psi}\sin\Psi) \sum_{i,j} q_{ij}^{c,s} q_{ij}^{c,s} - \frac{1}{2}\rho S g \sum_{i,j} q_{ij}^{c,s} q_{ij}^{c,s}. \end{aligned} \tag{4}$$

As a result, for $\Psi(t)$ we obtain the following evolution equation

$$\begin{aligned} I\ddot{\Psi} = -2m_0 a^2 \dot{\Psi}^2 \sin\Psi\cos\Psi - m_0 a^2 \ddot{\Psi}\sin^2\Psi + a\rho S(\dot{\Psi}^2 \sin\Psi - \\ - \ddot{\Psi}\cos\Psi) \sum_{i,j} q_{ij}^{c,s} q_{ij}^{c,s} - 2a\rho S\dot{\Psi}\cos\Psi \sum_{i,j} q_{ij}^{c,s} \dot{q}_{ij}^{c,s} + \Phi(\Psi) - H(\Psi). \end{aligned} \tag{5}$$

The last two terms on the right side of the equation (5) are the driving moment and the moment internal forces of resistance of the electric motor.

Suppose that the speed of rotation of the shaft $\dot{\Psi}(t)$ in steady state conditions of the engine is close to $2\omega_1$, where ω_1 is natural frequency of main tone of oscillations of the free surface, which corresponds to the modes $q_{11}^c(t)k_{11}(r)\cos\theta$ and $q_{11}^s(t)k_{11}(r)\sin\theta$.

Let us introduce into consideration a small positive parameter

$$\varepsilon = \omega_1 \sqrt{\frac{a}{g}}. \tag{6}$$

Also assume that

$$\dot{\Psi} - 2\omega_1 = \varepsilon^2 \omega_1 \beta. \tag{7}$$

The oscillations of the free surface of the liquid are approximated by oscillations in the main and secondary modes, whose amplitudes are defined as (Krasnopolskaya and Shvets[15,16])

$$\begin{aligned} q_{11}^c(t) &= \varepsilon v \left[p_1(\tau)\cos\frac{\Psi}{2} + q_1(\tau)\sin\frac{\Psi}{2} \right]; \\ q_{11}^s(t) &= \varepsilon v \left[p_2(\tau)\cos\frac{\Psi}{2} + q_2(\tau)\sin\frac{\Psi}{2} \right]; \\ q_{01}(t) &= \varepsilon^2 v \left[A_{01}(\tau)\cos\Psi + B_{01}(\tau)\sin\Psi + C_{01}(\tau) \right]; \\ q_{21}^{c,s}(t) &= \varepsilon^2 v \left[A_{21}^{c,s}(\tau)\cos\Psi + B_{21}^{c,s}(\tau)\sin\Psi + C_{21}^{c,s}(\tau) \right]. \end{aligned} \tag{8}$$

Here τ is slow time, $\tau = \frac{1}{4}\varepsilon^2\Psi$, $\upsilon = \frac{R}{1.8412}\tanh\left(\frac{1.8412}{R}d\right)$. Having determined the dimensionless amplitudes $A_{ij}^{c,s}(\tau), B_{ij}^{c,s}(\tau), C_{ij}^{c,s}(\tau)$ secondary modes by Miles method (Miles[5], [6], Miles and Henderson[8]) through the amplitudes $p_1(\tau), q_1(\tau), p_2(\tau), q_2(\tau)$ and applying the procedure of averaging the Lagrangian over the explicitly entering fast time $\Psi(t)$, for the amplitudes of dominant modes, we obtain the following system of equations (Krasnopolskaya and Shvets[15,16]):

$$\begin{aligned}
\frac{dp_1}{d\tau} &= \alpha p_1 - \left[\beta + \frac{A}{2}(p_1^2+q_1^2+p_2^2+q_2^2)\right]q_1 + B(p_1q_2 - p_2q_1)p_2 + 2q_1;\\
\frac{dq_1}{d\tau} &= \alpha q_1 + \left[\beta + \frac{A}{2}(p_1^2+q_1^2+p_2^2+q_2^2)\right]p_1 + B(p_1q_2 - p_2q_1)q_2 + 2p_1;\\
\frac{d\beta}{d\tau} &= N_3 + N_1\beta + \mu_1(p_1q_1 + p_2q_2);\\
\frac{dp_2}{d\tau} &= \alpha p_2 - \left[\beta + \frac{A}{2}(p_1^2+q_1^2+p_2^2+q_2^2)\right]q_2 - B(p_1q_2 - p_2q_1)p_1 + 2q_2;\\
\frac{dq_2}{d\tau} &= \alpha q_2 + \left[\beta + \frac{A}{2}(p_1^2+q_1^2+p_2^2+q_2^2)\right]p_2 - B(p_1q_2 - p_2q_1)q_1 + 2p_2.
\end{aligned} \tag{9}$$

In the system of equations (9), we have the following designations: $\alpha = -\frac{\delta}{\omega_1}$ – reduced factor of damping, N_0, N_1 – constants of linear static characteristic of the electric motor, $N_3 = \frac{1}{\omega_1}\left(N_0 + 2N_1\omega_1\right); \mu_1 = \frac{\rho S \upsilon R^2}{(1.8412)^2(2I + m_0a^2)\omega_1^2}$; A and B – constants ranging from the diameter of the tank and filling it with liquid. The system of evolutionary equations (9) is used as the main mathematical model for study the dynamics of oscillations of a tank with a liquid, excited by an electric motor of limited power.

The main aim of the research is to study the possible types of limit sets of the system (9). Since this system is a rather complex nonlinear system of equations of the fifth order, then for constructing its limit sets, a whole complex of numerical methods and algorithms were used. The technique for carrying out such numerical calculations for system with limited excitation is described in detail in Shvets[18] and Krasnopolskaya and Shvets[16].

3 Numerical studies of steady-state regimes of oscillations

Initially, we define the conditions under which the system is dissipative. Let us denote by $\boldsymbol{F}$ the vector field generated by the system of equations (9). Accordingly, by F_1, F_2, F_3, F_4, F_5 we denote the components of this vector field, that is, the right-hand sides of the system of equations (9). Then the divergence

of this vector field can be found by the formula

$$div\boldsymbol{F} = \frac{\partial F_1}{\partial p_1} + \frac{\partial F_2}{\partial q_1} + \frac{\partial F_3}{\partial \beta} + \frac{\partial F_4}{\partial p_2} + \frac{\partial F_5}{\partial q_2} = \alpha - Ap_1q_1 + Bp_2q_2 + \alpha +$$
$$+Ap_1q_1 - Bp_2q_2 + N_1 + \alpha - Ap_2q_2 + Bp_1q_1 + \alpha + Ap_2q_2 - Bp_1q_1 = \quad (10)$$
$$= 4\alpha + N_1.$$

So the divergence of the vector field $\boldsymbol{F}$ is constant. The dissipativity condition for the system of equations has the form,

$$4\alpha + N_1 < 0. \quad (11)$$

The quantities included formula (11), α (coefficient of damping) and N_1 (angle of inclination of the static characteristic of electricmotor) are always negative. Therefore, the divergence of the vector field generated by the system of equations (9) will always be negative. Thus, this system will always be dissipative.

We will begin the study of the dynamics of the system (9) by finding its equilibrium positions. Obviously, that

$$p_1 = 0, q_1 = 0, \beta = -\frac{N_3}{N_1}, p_2 = 0, q_2 = 0 \quad (12)$$

is one of those equilibrium position. This equilibrium position is isolated one. The conditions of the asymptotic stability of this equilibrium position may be obtained by using Liénard-Chipart theorem (Liénard and Chipart[19]).

In addition to the isolated equilibrium position (12), there is an infinite number of non-isolated equilibrium positions. These equilibrium positions form a family of non-isolated equilibrium positions, which exists in a form of some closed line. These equilibrium positions can be found only using numerical methods, for example, Newton's method. In Fig. 2, an example of such family of equilibrium positions for one concrete values of parameters of the system (9) is shown. Conditions for the stability of such family can be obtained using the Liénard-Chipart theorem. True, these conditions are extremely cumbersome. Their analysis can be carried out in reality only by using computers. Note that all equilibrium positions shown in Fig. 2 may be stable, but can not be asymptotically stable. In the case of stability of these non-isolated equilibrium positions, each of them belongs to the limit set of system (9), but is not an attractor in the traditional sense of this term. We will give a description of the attractive properties of this family below.

There are sufficiently large regions in space of parameters of the system (9), in which all equilibrium positions are unstable. In these areas, extremely interesting limit sets of this system arise, which can be as regular, and as chaotic.

Limit sets of the first type may be periodic. In this case they form family of an infinite number of closed trajectories (cycles), all of which exists simultaneously. Any cycle neighbourhood contains other cycles of the family, that is, they are not isolated. However, such cycles do not have tangency or intersection points. Each such closed trajectory is itself a limit set. This is due to

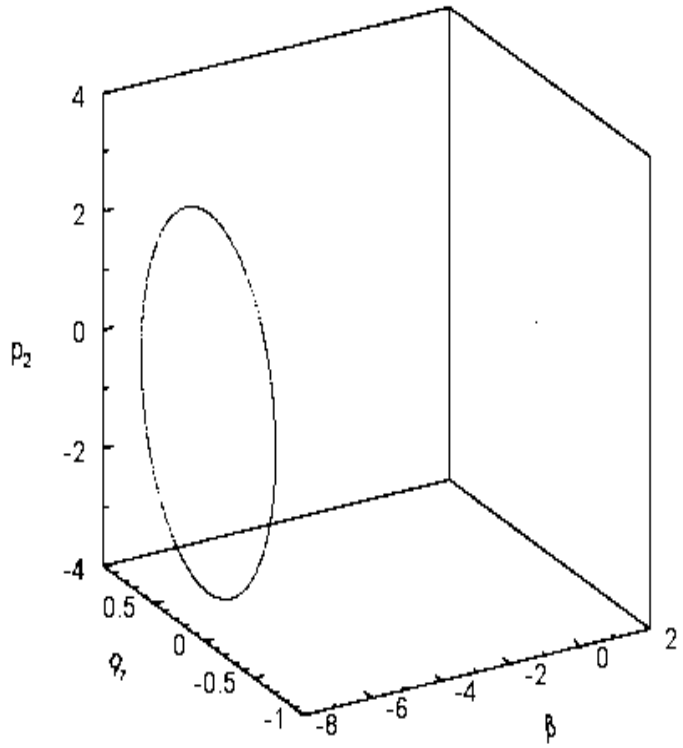

Fig. 2. Family of equilibrium positions .

fact that almost any trajectory that starts in some large area of phase space tends to one of the cycles of the family. But none of cycles is an attractor in the traditional sense of this term. So, each of these cycles is not limit cycle. Moreover, every single cycle has same period, same Lyapunov's characteristic exponents and similar Poincare sections. It is worth noting that the cardinality of this family is equal to continuum.

In Fig. 3 regular periodic limit sets of system (9) are constructed at $\alpha = -0.8, A = 1.12, B = -1.531, N_1 = -1.25, N_3 = 2, \mu_1 = -5.15$. Each cycle is plotted in different color. There are four cycles in total, each of which is a representative of the infinite family of cycles. We emphasize once again that each of the cycles forming the family is not an attractor in the traditional sense of this concept. In our opinion, the most suitable term for describing such family is the concept of maximal attractor.

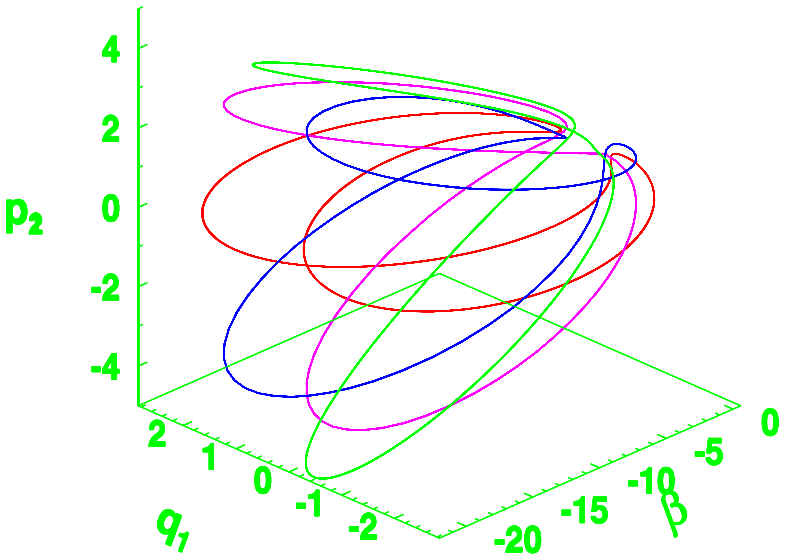

Fig. 3. Four representatives of maximal regular attractor.

A clear definition of the concept of maximal attractor is given by Milnor[20], by Anischenko and Vadivasova[21], as well as by Sharkovsky[22]. Thus, two different families that are shown in Fig. 2 and Fig. 3, are essentially two different types of regular maximal attractors.

With an increase in the value of the parameter μ_1, family of chaotic trajectories arises in the system. The arising family includes an infinite number of chaotic trajectories. It is known that the "traditional" chaotic attractor consists of an infinite number of unstable trajectories. The resulting family, at first glance, is a union of an infinite number of chaotic attractors. However, each member of this family is not an attractor in the "traditional" sense. Here, as before, to define such union, the concept of maximal attractor can be pro-

posed. All trajectories of the chaotic maximal attractor have same spectrum of Lyapunov's characteristic exponents, including positive one. The Poincare sections of each of the trajectories of the family are structurally similar chaotic sets consisted of an infinite number of points.

In Fig. 4 for the values $\alpha = -0.8, A = 1.12, B = -1.531, N_1 = -1.25, N_3 = 2, \mu_1 = -4.6463$ limit sets of second type of the system (9) is constructed. Each represenative of the chaotic maximal attractor is plotted in its own color. In total, there are three chaotic trajectories of the family are presented in the Fig. 4.

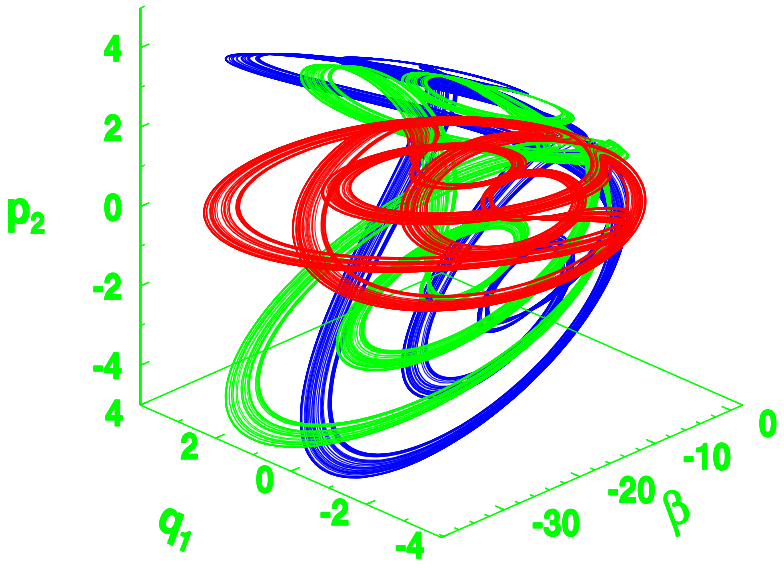

Fig. 4. Three representatives of maximal chaotic attractor of first kind.

In Fig. 5 three representatives of another kind of chaotic maximal attractor, constructed at $\mu_1 = -4.6462$, are shown. On the whole, the chaotic maximal attractor of the second kind are characterized by a much denser filling of the localization region with trajectories. This two kinds of chaotic maximal attractor are typical for system (9).

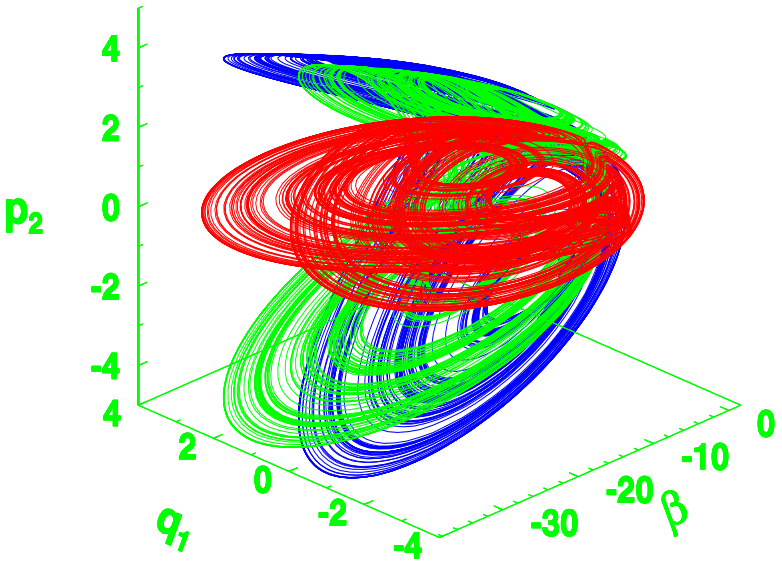

Fig. 5. Three representatives of maximal chaotic attractor of second kind.

We note one more feature of the constructed maximal attractors, both regular and chaotic. Some trajectories of those families are localized in the three-dimensional subspace of the five-dimensional phase space of system (9). So the trajectories shown in red in Fig. 3, 4 and 5 are localized in three-dimensional

space. This means that the coordinates p_2 and q_2 of the "red" trajectories are equal to zero. That is, there are no oscillations in the second dominant mode.

Shortly we underscore one more interesting feature of the maximal attractors of the system (9). Although these attractors are not attractors in the traditional sense, the transition from regular to chaotic regimes and the "chaos-chaos" transitions follow the scenarios inherent in such transitions for traditional attractors. Thus transitions according to the Feigenbaum scenario (Feigenbaum[23,24]), Manneville−Pomeau scenario were found (Manneville and Pomeau [25,26]) along with various scenarios of generalized intermittency (Krasnopolskaya and Shvets[16,17], Shvets and Sirenko[27,28]).

Let us briefly consider the features of the transition to chaos according to the Feigenbaum and Manneville-Pomeau scenarios for maximal attractors. One of the possible scenarios is the transition from regular regime to a chaotic one is a cascade of bifurcations of period doubling of the cycles. At the same value of the bifurcation parameter the period of all cycles, that form the maximal attractor, is doubled. Then, at the next bifurcation point, the period of all cycles of the maximal attractor is again doubled, and so on. This endless process of period doubling bifurcations ends with the emergence of a chaotic maximal attractor. That is, the transition from a periodic limit set to a chaotic limit set is realized according to the classical Feigenbaum's scenario.

The transition to chaos through intermittency (the Manneville-Pomeau scenario) for the maximal attractors occurs as follows. The system has a maximal attractor consisting of an infinite set of simultaneously existing cycles. Moreover, all the trajectories of the family have the same period. When passing through the bifurcation point, all cycles of the family disappear and a chaotic maximal attractor arises in the system. The movement along the trajectories of all representatives of this maximum attractor consists of two phases - laminar and turbulent. That is, for all representatives of the family of cycles, there is a simultaneous transition to chaos, through one rigid bifurcation.

In conclusion, let us illustrate the transition from the maximal chaotic attractor of one type to the maximal chaotic attractor of another type through generalized intermittency. In Fig. 6a the distribution of the invariant measure over the phase portrait projection of the representative of the chaotic maximal attractors of the system (9) constructed at $\alpha = -0.8, A = 1.12, B = -1.531, N_1 = -1.25, N_3 = 2, \mu_1 = -4.6463$ is shown. At $\mu_1 = -4.6462$ (other parameters unchanged) maximal attractor disappears and chaotic maximal attractor of new type is born in the system. The distribution of the invariant measure over the projection of the phase portrait of the representative of the new chaotic maximal attractor is shown in Fig. 6b. The transition from one type of chaotic maximal attractor to the chaotic maximal attractor of another type occurs according to the scenario of generalized intermittency, which was described for attractors in the traditional sense of this term. At such transition, the scenario of generalized intermittency is simultaneously fulfilled for all representatives of chaotic maximal attractor that presented in Fig. 4. For each representative of the new chaotic maximal attractor, the motion along the trajectory consists of two alternating phases, namely rough-laminar phase and turbulent phase. In the rough-laminar phase, the trajectory makes chaotic

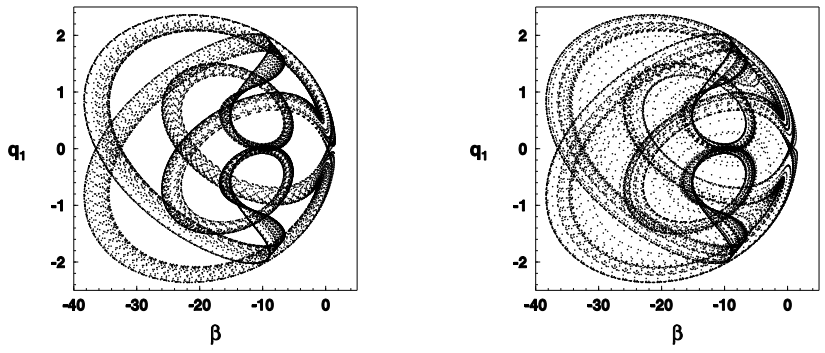

a b

Fig. 6. Distribution of invariant measure over projections of maximal attractors

movements in the neighborhood of the trajectories of the representative of the disappeared chaotic maximal attractor. Then, at an unpredictable moment of time, the trajectory leaves the localization region of the representative of the disappeared maximal attractor and moves to distant regions of the phase space. Rough-laminar phase corresponds to the much blacker areas in fig in Fig. 6. These areas in Fig. 6a are nearly the same as the distribution of the invariant measure from in Fig. 6b. In turn, turbulent phase corresponds to much less darkened areas in Fig. 6b. After some time, the movement of the trajectory returns to the rough-laminar phase again. Then, trajectories switch to turbulent phase again. Such transitions are repeated an infinite number of times. Note that the duration of both rough-laminar and turbulent phases is unpredictable as are the moments of times of transition from one phase to another.

References

1. Narimanov G.S., Dokuchaev L.V., Lukovsky I.A. *Nonlinear dynamics of flying apparatus with liquid*, Mashinostroenie, Moscow, 1977.
2. Ibrahim R.A. *Liquid Sloshing Dynamics: Theory and Applications*, Cambridge University Press, Cambridge, 2005.
3. Lukovsky I. A. *Nonlinear dynamics. Mathematical models for rigid bodies with a liquid*, De Gruyter, 2015.
4. Raynovskyy I., Timokha A. *Sloshing in upright circular containers: theory, analytical solutions and applications*, CRC Press/Taylor & Fransis Group, 2021.
5. Miles J. W. Nonlinear surface waves in closed basins, *J. Fluid Mech.*, 75, 419–448, 1979.
6. Miles J. W. Resonantly forced surface waves in circular cylinder, *J. Fluid Mech.*, 149, 15–31, 1984.
7. Meron E., Procaccia J. Low-dimensional chaos in surface waves: theoretical analysis of an experiment, *Phys. Rev. A*, 34, 3221–3237, 1986.

8. Miles J. W., Henderson D. Parametrically forced surface waves, *Ann. Rev. Fluid Mech.*, 22, 143–165, 1990.
9. Sommerfeld A. Beitrage zum dynamischen Ausbau der Festigkeitslehre, *Physikalische Zeitschrift*, 3, 266–271, 1902.
10. Kononenko V.O. *Vibrating system with a limited power-supply*, Iliffe, London, 1969.
11. K.V. Frolov, T.S. Krasnopol'skaya. *Sommerfeld effect in systems without internal damping*. Sov. Appl. Mech., **23**, 1122–1126, 1987.
12. Krasnopolskaya T.S. *Acoustic chaos caused by the Sommerfeld effect*. J. Fluids Struct., **8**(7), 803–815, 1994.
13. KrasnopolskayaT.S. *Chaos in acoustic subspace raised by the Sommerfeld-Kononenko effect*. Meccanica, **41**(3), 299–310, 2006.
14. Krasnopol'skaya T.S., Shvets A.Yu. Prorerties of chaotic oscillations of the liquid in cylindrical tanks, *Prikladnaya Mekhanika*, **28**(6), 52–61, 1992.
15. Krasnopol'skaya T.S., Shvets A.Yu. Parametric resonance in the system: Liquid in tanks + electric motor *Int. Appl. Mech*, **29**(9), 722–730, 1993.
16. Krasnopolskaya T.S., Shvets A.Yu. Chaotic surface waves in limited power-supply cylindrical tank vibrations, *J. Fluids Struct.*, **8**(1), 1–18, 1994.
17. Krasnopolskaya T.S., Shvets A.Yu. Dynamical chaos for a limited power supply for fluid oscillations in cylindrical tanks, *J. Sound Vibr.*, **322**(3), 532–553 2009.
18. Shvets A.Yu. Deterministic chaos of a spherical pendulum under limited excitation, *Ukr. Math. J.*, **59**, 602–614, 2007.
19. Liénard A., Chipart M. H. Sur le signe de la partie r'eelle des racines d'une quation alg'ebrique, *J. Math. Pures Appl.*, **10**, (4), 291–346, 1914.
20. Milnor J. On the concept of attractor, it Commun. Math. Phys. **99**, 177–195, 1985.
21. Anischenko V.S., Vadivasova T.E. *Lectures on nonlinear dynamics*, R&C Dynamics, Moskow, 2011.
22. Sharkovsky A.N. *Attractors of trajectories and their basins*, Naukova Dumka, Kiev, 2013.
23. Feigenbaum M.J. Quantative universality for a class of nonlinear transformations, *J. Stat. Phys.* **19**(1), 25–52, 1978.
24. Feigenbaum M.J. The universal metric properties of nonlinear transformations, *J. Stat. Phys.* **21**(6), 669–706, 1979.
25. Manneville P., Pomeau Y. Different ways to turbulence in dissipative dynamical systems, *Physica D. Nonlinear Phenom.* **1**(2), 219–226 ,1980.
26. Pomeau Y., Manneville P. Intermittent transition to turbulence in dissipative dynamical systems, *Comm. Math. Phys.* **74**(2), 189–197 ,1980.
27. Shvets A., Sirenko V. Hyperchaos in Oscillating Systems with Limited Excitation, bf In: Skiadas C., Lubashevsky I. (eds) 11th Chaotic Modeling and Simulation International Conference. CHAOS 2018. Springer Proceedings in Complexity. Springer, Cham, 265–273, 2019.
28. Shvets A.Yu., Sirenko V.A., Scenarios of Transitions to hyperchaos in Nonideal Oscillating Systems, *J. Math. Sci.*, **243**(2), 338–346, 2019.

Universality of Boltzmann Statistical Mechanics, Thermodynamics, Quantum Mechanics, and Shannon Information Theory

Siavash H. Sohrab

Northwestern University, Robert R. McCormick School of Engineering and Applied Science, Department of Mechanical Engineering, 2145 Sheridan Road, Evanston, Illinois 60208-3111, U.S.A.
E-mail: s-sohrab@northwestern.edu

Abstract. Universal nature of Boltzmann statistical mechanics, generalized thermodynamics, quantum mechanics, spacetime, black hole mechanics, Shannon information theory, Faraday lines of force, and Banach-Tarski paradox (BTP) are studied. The nature of matter and Dirac anti-matter are described in terms of states of compression and rarefaction of physical space, Aristotle fifth element, or Casimir vacuum identified as a compressible tachyonic fluid. The model is in harmony with perceptions of Plato who believed that the world was formed from a formless primordial medium that was initially in a state of *total chaos* or "*Tohu Vavohu*" [109]. Hierarchies of statistical fields from photonic to cosmic scales lead to universal scale-invariant Schrödinger equation thus allowing for new perspectives regarding connections between classical mechanics, quantum mechanics, and chaos theory. The nature of *external* physical time and its connections to *internal* thermodynamics time and Rovelli *thermal time* are described. Finally, some implications of renormalized Planck distribution function to economic systems are examined.

1 Introduction

The universal nature of turbulence and mathematical similarities amongst transport laws shared by stochastic quantum fields [1-17] and classical hydrodynamic fields [18-30] resulted in introduction of a scale-invariant model of Boltzmann statistical mechanics and its applications to the fields of thermodynamics [31,32], fluid mechanics [33,34], and quantum mechanics [35-37] at intermediate, large, and small scales.

The present study begins with a brief description of invariant model of Boltzmann statistical mechanics and the invariant forms of conservation equations. Next, generalized thermodynamics and Helmholtz decomposition of energy and momentum, and definitions of dark-energy, dark-matter, and dark-momentum are discussed. The concept of internal spacetime versus external independent space and time and their connection to Rovelli *thermal time* are presented. Invariant Schrödinger equation recently derived from invariant Bernoulli equation [37] and some of its implications to a new paradigm for physical foundation of quantum mechanics are described next. In particular, the

14*th* *CHAOS Conference Proceedings, 8 - 11 June 2021, Athens, Greece*
(Converted to virtual conference)

nature of wave function, wave-particle duality, and hierarchies of quantum mechanics wave functions and particles as de Broglie wave-packets [3] are studied. Also, the implication of the model to entropy and the problem of information loss in black hole is addressed. A universal hydrodynamic model of Faraday line of force applicable from very small scale of stochastic chromodynamics to the exceedingly large cosmic scale is presented. Finally, some implications of the model to Banach-Tarski paradox are examined.

2 Scale–Invariant Model of Boltzmann Statistical Mechanics

The scale-invariant model of statistical mechanics for equilibrium galactic-, planetary-, hydro-system-, fluid-element-, eddy-, cluster-, molecular-, atomic-, subatomic-, kromo-, and tachyon-dynamics corresponding to the scale β = g, p, h, f, e, c, m, a, s, k, and t is schematically shown on the left hand side of Fig. 1.

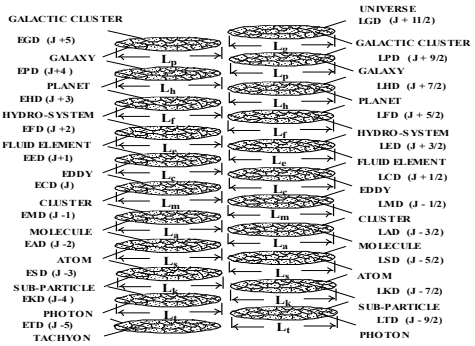

Fig. 1. A scale-invariant model of statistical mechanics. Equilibrium-β-Dynamics on the left-hand-side and non-equilibrium Laminar-β-Dynamics on the right-hand-side for scales β = g, p, h, f, e, c, m, a, s, k, and t as defined in [36]. Characteristic lengths of (system, element, "atom") are $(L_\beta, \lambda_\beta, \ell_\beta)$ and λ_β is the mean-free-path.

For each statistical field, one defines particles that form the background fluid and are viewed as point-mass or "*atom*" of the field. Next, the *elements* of the field are defined as finite-sized composite entities composed of an ensemble of "*atoms*". Finally, ensemble of a large number of "*elements*" is defined as the statistical "*system*" at that particular scale. The most-probable element of scale β defines the "atom" (system) of the next higher β+1 (lower β−1) scale.

Following the classical methods [19, 38-42], the invariant definitions of the density ρ_β, and the velocity of *atom* $\mathbf{u}_\beta$, *element* $\mathbf{v}_\beta$, and *system* $\mathbf{w}_\beta$ at the scale β are given as [36]

$$\rho_\beta = n_\beta m_\beta = m_\beta \int f_\beta du_\beta \quad , \quad \mathbf{u}_\beta = \mathbf{v}_{w\beta-1} \tag{1}$$

$$\mathbf{v}_\beta = \rho_\beta^{-1} m_\beta \int \mathbf{u}_\beta f_\beta du_\beta \quad , \quad \mathbf{w}_\beta = \mathbf{v}_{w\beta+1} \tag{2}$$

Similarly, the invariant definitions of the peculiar and diffusion velocities are introduced as

$$\mathbf{V}'_{\beta} = \mathbf{u}_{\beta} - \mathbf{v}_{\beta} \quad , \quad \mathbf{V}_{\beta} = \mathbf{v}_{\beta} - \mathbf{w}_{\beta} \quad , \quad \mathbf{V}_{\beta} = \mathbf{V}'_{\beta+1} \tag{3}$$

A magnified view of part of hierarchy of statistical fields in Fig. 1 is shown in Fig. 2 where atomic, element, and system velocities of stochastic fields are better revealed.

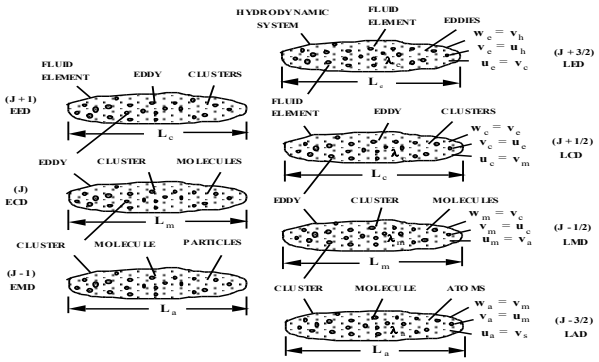

Fig. 2 Hierarchy of embedded statistical fields from LAD to LED scales with atom $\mathbf{u}_{\beta}$, element $\mathbf{v}_{\beta}$, and system $\mathbf{w}_{\beta}$ velocity.

Following the classical methods [19, 38-40], the scale-invariant forms of mass, thermal energy, linear and angular momentum conservation equations at scale β are given as [33, 34]

$$\frac{\partial \rho_{i\beta}}{\partial t_{\beta}} + \nabla.(\rho_{i\beta}\mathbf{v}_{\beta}) = \Re_{i\beta} \tag{4}$$

$$\frac{\partial \varepsilon_{i\beta}}{\partial t_{\beta}} + \nabla.(\varepsilon_{i\beta}\mathbf{v}_{\beta}) = 0 \tag{5}$$

$$\frac{\partial \mathbf{p}_{i\beta}}{\partial t_{\beta}} + \nabla.(\mathbf{p}_{i\beta}\mathbf{v}_{\beta}) = -\nabla.\mathbf{P}_{ij\beta} \tag{6}$$

$$\frac{\partial \boldsymbol{\pi}_{i\beta}}{\partial t_{\beta}} + \nabla.(\boldsymbol{\pi}_{i\beta}\mathbf{v}_{\beta}) = \rho_{i\beta}\boldsymbol{\omega}_{\beta}.\nabla\mathbf{v}_{\beta} \tag{7}$$

involving the *volumetric density* of thermal energy $\varepsilon_{i\beta} = \rho_{i\beta}\tilde{h}_{i\beta}$, linear momentum $\mathbf{p}_{i\beta} = \rho_{i\beta}\mathbf{v}_{i\beta}$, and angular momentum $\boldsymbol{\pi}_{i\beta} = \rho_{i\beta}\boldsymbol{\omega}_{i\beta}$ (since $r_{a\beta-1} = 1$).

Also, $\Re_{i\beta}$ is the chemical reaction rate and $\tilde{h}_{i\beta} = \hat{h}_{i\beta} / m_\beta$ is the absolute enthalpy [36]. It is noted that the time coordinates in Eqs. (4-7) also have a scale subscript β.

3 Generalized Thermodynamics, Helmholtz Decomposition of Thermal Energy and Momentum

To arrive at scale-invariant model of Boltzmann statistical mechanics with (atom, element, system) velocities $(\mathbf{u}_{i\beta}, \mathbf{v}_{i\beta}, \mathbf{w}_{i\beta})$, one requires a stable "atom" stabilized by an external pressure acting as *Poincaré stress* [35,36]. Next, atoms with different energy $\varepsilon_j = h\nu_j$ are grouped in atomic-clusters or elements (energy levels) of various sizes. Atoms of various energy are under constant motion and allowed to make transition between elements by emitting/absorbing sub-particles. The question is, given the total number of atoms *N* of an ideal gas and the total energy *H*, with mean atomic enthalpy $\hat{h}_w = 4kT$ hence $H = 4NkT$ [32], what distribution of element sizes corresponding to various atomic energy, speed, and momenta leads to *stochastically stationary field*. Such state of thermodynamic equilibrium corresponds to energy, speed, and velocity of particles being governed by invariant Planck, Maxwell-Boltzmann, and Gauss (Maxwell) distribution functions [36].

$$\frac{\varepsilon_\beta dN_\beta}{V} = \frac{8\pi h}{u_\beta^3} \frac{\nu_\beta^3}{e^{h\nu_\beta / kT} - 1} d\nu_\beta \tag{8}$$

$$\frac{dN_{u\beta}}{N} = 4\pi \left(\frac{m_\beta}{2\pi kT_\beta}\right)^{3/2} u_\beta^2 \, e^{-m_\beta u_\beta^2 / 2kT_\beta} du_\beta \tag{9}$$

$$f_\beta(v_\beta) = \left(\frac{m_\beta}{2\pi kT_\beta}\right)^{3/2} e^{-m_\beta u_\beta^2 / 2kT_\beta} \tag{10}$$

Also, due to the closure of the gap between photon gas in Planck equilibrium radiation theory and ideal gas in Boltzmann kinetic theory, just like photon gas, the potential and internal energy of ideal gas are related as [37]

$$p_\beta V_\beta = \frac{U_\beta}{3} = \frac{3NkT_\beta}{3} = NkT_\beta \tag{11}$$

Hence, Sommerfeld [44] "total thermal energy" or *enthalpy* H_β for an ideal gas is the sum of internal energy and potential energy [32]

$$H_\beta = U_\beta + p_\beta V_\beta = U_\beta + U_\beta / 3 = \frac{4}{3} U_\beta = 4 N_\beta \mathrm{k} T_\beta \qquad (12)$$

By equations (11)-(12), enthalpy could also be expressed as

$$H_\beta = U_\beta + \frac{U_\beta}{3} = U_\beta + \frac{H_\beta}{4} = U_\beta + \frac{1}{4}(U_\beta + \frac{U_\beta}{3}) = \ldots$$
$$= U_\beta \, (1 + \frac{1}{4} + \frac{1}{4^2} + \frac{1}{4^3} + \ldots) = \frac{4}{3} U_\beta \qquad (13)$$

involving Archimedes [45] theorem on the area under a parabolic segment

$$1 + \frac{1}{4} + \frac{1}{4^2} + \frac{1}{4^3} + \ldots = \sum_{n=0}^{\infty} \frac{1}{4^n} = \frac{4}{3} \qquad (14)$$

With frequency made dimensionless through division by the most probable or Wien frequency ν_w, re-normalized Planck [46] distributions at two adjacent scales appear as shown in Fig. 3

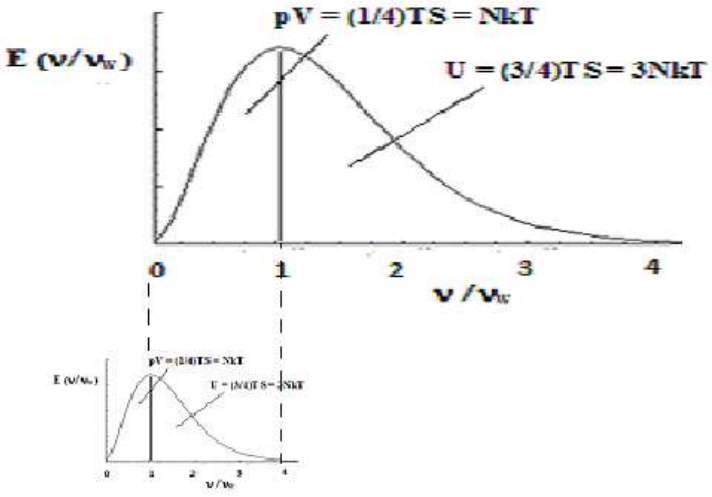

Fig. 3 Re-normalized Planck energy distributions as a function of ν / ν_w.

It is known that precisely 3/4 and 1/4 of the total thermal energy under Planck distribution curve in Fig. 3 fall on $\nu > \nu_w$ and $\nu < \nu_w$ sides of Wien frequency ν_w [32]. In his pioneering study, Helmholtz [43] decomposed the

total thermal energy or enthalpy *H* into what he called *free-heat* and *latent-heat* that were recently identified as *internal energy U* and *potential energy pV* [32]

$$H_\beta = U_\beta + p_\beta V_\beta \tag{15}$$

Hence, the result in Eq. (14) is in exact agreement with the pioneering prediction by Hasenöhrl [47,48] of the relation between total energy and *electromagnetic energy* or *dark-energy* expressed as

$$H_\beta = \mathrm{M_t c^2} = \frac{4}{3}\mathrm{M_{EM} c^2} \tag{16}$$

such that total mass relates to electro-magnetic mass by [37]

$$\mathrm{M_t} = \frac{4}{3}\mathrm{M_{EM}} \tag{17}$$

Since in equilibrium radiation within enclosures photons are at "stationary state", their speed is Wien speed

$$\mathrm{v_{kw}^2} = \mathrm{v_{kw^+}^2} + \mathrm{v_{kw^-}^2} = 2\mathrm{v_{kw+}^2} \tag{18}$$

that is related to the root-mean square speed by [32]

$$\mathrm{c^2} = \mathrm{c_{rk}^2} = 3\mathrm{v_{kw+}^2} \tag{19}$$

Therefore, Lorentz [49] relativistic mass also leads to prediction of Hasenöhrl [47,48]

$$\mathrm{M_t} = \frac{\mathrm{M_{EM}}}{(1-\mathrm{v_{kw}^2}/\mathrm{c^2})^{1/2}} \simeq \mathrm{M_{EM}}(1+\frac{\mathrm{v_{kw}^2}}{2\mathrm{c^2}}) = \mathrm{M_{EM}}(1+\frac{1}{3}) = \frac{4}{3}\mathrm{M_{EM}} \tag{20}$$

As discussed in [31], if *potential energy* is identified as *dark-matter* or *gravitational mass*

$$p_\beta V_\beta = \mathrm{M_{DM\beta}\ c^2} = \frac{1}{3}\mathrm{M_{EM\beta} c^2} = \frac{1}{4}\mathrm{M_{t_\beta} c^2} = \mathrm{N_\beta k T_\beta} \tag{21}$$

total mass becomes the sum of *dark energy* or *electromagnetic mass* $\mathrm{M_{EM}}$, and *dark matter* or *gravitational mass* $\mathrm{M_{GM}}$ [31,50-53]

$$\mathrm{M_{t\beta}} = \mathrm{M_{EM\beta}} + \mathrm{M_{DM\beta}} = \frac{3}{4}\mathrm{M_{t\beta}} + \frac{1}{4}\mathrm{M_{t\beta}} \tag{22}$$

It is most interesting to note that, as discussed in [31], Helmholtz [43] decomposition of system thermal energy at thermodynamic equilibrium in Eq. (19) also extends to cosmological scale (Fig. 1) and is in accordance with predictions of general theory of relativity [54,55] as described by Pauli [55]

> ***The energy of a spatially finite universe is three- quarters electromagnetic and one-quarter gravitational in origin*"**

In addition, predicted fractions 3/4 and 1/4 for *dark energy* and *dark matter* in Eq. 19 are in good agreement with recent cosmological observations [56-59].

On the other hand, according to Planck [46] energy distribution (Fig. 3) and Eq. (18), dark matter of scale β is the total energy or enthalpy of the next lower scale β−1.

$$(Dark\ Matter)_{\beta} = (Total\ Energy)_{\beta-1}$$

Also, it is known that when particles form "cooper pairs" and behave as composite bosons [60, 61], one can derive Schrödinger equation from invariant Bernoulli equation for potential incompressible flow [37]. Hence, following classical methods [62, 63], quantum mechanics wave function may be expressed as products of translational, rotational, vibrational, and potential (internal) wave functions as [61]

$$\Psi_{\beta} = \Psi_{t\beta}\Psi_{r\beta}\Psi_{v\beta}\Psi_{p\beta} = \Psi_{t\beta}\Psi_{r\beta}\Psi_{v\beta}\Psi_{\beta-1} = \ldots \tag{23}$$

At cosmological scale Ψ_g, the wave-particle duality of galaxies is evidenced by their observed quantized red-shifts [64]. Therefore, the scale-invariance of the model (Fig. 1) and Eq. (23) lead to hierarchy of embedded statistical fields with translational TKE, rotational RKE, vibrational VKE kinetic energy (dark energy) and potential energy PE (dark matter) resulting in energy cascade from cosmic to photonic scales shown in Fig. 4.

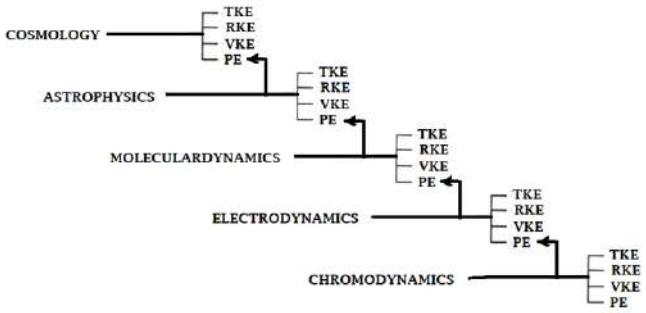

Fig. 4. Cascades of kinetic energy TKE, RKE, VKE (dark energy), and potential energy PE (dark matter) from cosmic to photonic scales.

Following Helmholtz [43], one can consider *decomposition of momentum* in Normalized Maxwell-Boltzmann (NMB) distribution as a function of dimensionless speed with respect to the most-probable or Wien speed $v / v_w = \lambda_w / \lambda$ shown in Fig. 5.

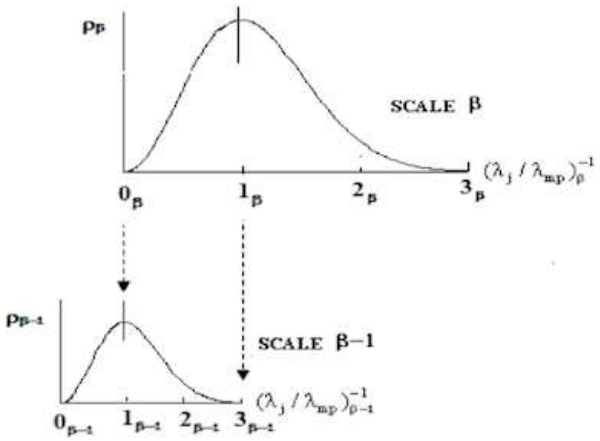

Fig. 5 Normalized Maxwell-Boltzmann distribution as a function of dimensionless speed $v / v_w = \lambda_w / \lambda$ [36].

As compared with (3/4, 1/4) division of energy in Planck curve in Fig. 3, the division of momentum on either side of Wien speed in Fig. 5 is (2/3, 1/3). In view of the equality of translation kinetic and potential energy due to Boltzmann equipartition principle, $m_\beta v^2_{wx+\beta-1} = m_\beta V'^2_{x\beta}$ [37], three components of momentum are equal due to what is called *principle of equipartition of translational momenta*

$$\bar{p}_{x^+} = mv_{x^+} = \bar{p}_{x^-} = mv_{x-} = \bar{p}'_x = mV'_x \tag{24a}$$

Therefore, for an ideal gas, of the total dimensionless translational momentum $\bar{P}_x = (\bar{p}_{x^+} + \bar{p}_{x^-} + \bar{p}'_x) / \bar{p}_{xw} = 3$ under NMB curve in Fig. 5, 2/3 is on $v > v_w$ side of the Wien speed and is associated with root-mean-square momenta due to atomic translational velocity in (x_+, x_-) directions, and 1/3 is on $v < v_w$ side of the Wien speed and is associated with peculiar translational momentum hence,

$$\bar{p}_x = \bar{p}_{x^+} + \bar{p}_{x^-} + \bar{p}'_x = \frac{2}{3}\bar{P}_x + \frac{1}{3}\bar{P}_x \tag{24b}$$

Parallel to the concept of *dark-matter* in Helmholtz energy decomposition, for decomposition of momentum the second part of Eq. (24b) may be referred to as *dark-momentum*.

As discussed in a recent study [65], once physical variables are made dimensionless, *particular* problems of physics become *universal* problems of mathematics and the nature of the specific physical entities being studied no longer matters. As an example, the distribution of annual personal income in economic systems is considered. In a recent study by Roper [66], it is suggested that the *log-Verhulst* distribution function fits the data better than does the *lognormal* distribution function. In view of random nature of economic systems, in some economic literature Gauss normal distribution is considered as "ideal" or optimal income distribution. However, typical data of annual personal income distribution [67] shown in Fig. 6 clearly indicate the non-Gaussian character of actual income distribution.

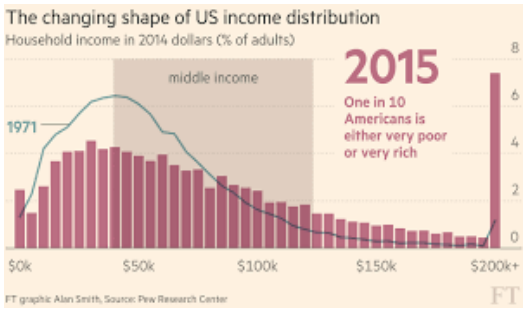

Fig. 6 Comparison between annual income distributions in 1971 and 2015 [67].

If the income in Fig. 6 is made dimensionless by division with the most probable income I_{mp}, the distribution will become similar to Planck energy distribution since I/I_{mp} is in the range (1-4) in Fig. 3 rather than the range (1-3) in Fig. 5. Hence, with dimensionless personal annual income (I/I_{mp}) viewed as dimensionless frequency (ν/ν_w), renormalized Planck distribution could be considered as the optimum or "*ideal"* income distribution because it corresponds to an equilibrium i.e., *maximum entropy* state as discussed below. It is reasonable to anticipate that Gauss normal distribution will govern the vector field corresponding to "velocity" of money flow between various income levels (energy levels), in analogy to kinetic theory of ideal gas [36]. Rather than individuals, at larger scales of companies (corporations), one expects similar normalized Planck distribution of income (like Fig. 3) with thousands (millions) of dollars instead of dollars as "atomic" units exchanging between various income-levels of companies (corporations).

As discussed in [31,32,36,37], in accordance with Boltzmann kinetic theory of ideal gas and Planck theory of photon gas [46], one asks the question: given a total amount of money *M* and total number of income earners *N*, what is the distribution of number of income earners N_j with income I_j that results in

stochastically stationary i.e., equilibrium economic system. On the other hand, entropy of an ideal gas was recently identified [31,32] as the maximum number of Heisenberg-Kramers [68] *virtual oscillators* $S = 4N\mathrm{k}$, given the total system energy or Hamiltonian i.e., enthalpy $TS = H = 4N\mathrm{k}T$. Therefore, maximization of entropy in Planck [46] distribution ensures that the total energy (total monitory wealth) is distributed amongst *maximum number of oscillators* (income levels). In such *quantum mechanical economic model*, the transfer of energy (money) between different energy levels (income levels) will be governed by Schrödinger equation such that at equilibrium all income levels will be in "*stationary states*".

In Fig. 6, one notes the shifting of income from middle-class to upper-class from 1971 to 2015 that constitutes a departure from equilibrium thus having a destabilizing effect on the socio-economic system. The unfortunate *delta function* at the maximum income level in Fig. 6 is even more embarrassing departure from Planck optimal distribution thus further enhancing economic instabilities that may lead to future revolutionary (*quantum*) change in the socio-economic system.

4 Thermodynamic Definition of Spacetime and the Nature of Rovelli Thermal Time

Since Aristotle [69] and St Augustine [70], the nature of physical time has remained a mysterious problem of physics. The central insight of Aristotle namely "*the concept of time without change is meaningless*", although correct remained puzzling and circular since the concept of *change* itself involves the notion of time. The hierarchy of time durations encountered from cosmic to photonic scales (Fig. 1) is described in an excellent recent book by 't Hooft and Vandoren [71]. Although the pioneering insights of Poincaré [72-75], Lorentz [49], Einstein [76], and Minkowski [77] resulted in introduction of the concept of spacetime as a 4-dimentional manifold, the exact physical nature of such mathematical concept remained obscure. Also, even though Einstein [78] general theory of relativity (GTR) attributed a dynamic character to spacetime, the very notion of existence of time was questioned in what is known as the "*time problem*" of GTR [79-90].

In a recent study [91], the nature of physical space and time was investigated and the concepts of *internal spacetime* versus *external space and time* were introduced. Assuming that a statistical field at scale β is in thermodynamic equilibrium with the physical space at scale $(\beta - 1)$ within which it resides, both fields will have a homogenous constant temperature $T_\beta = T_{\beta-1}$ defined in terms of Wien wavelength of particle thermal oscillations as [32]

$$\mathrm{m}_\beta \mathrm{u}_\beta^2 = \mathrm{m}_{\beta-1}\mathrm{v}_{\mathrm{w}\beta-1}^2 = \mathrm{kT}_{\beta-1} = \mathrm{k}\lambda_{\mathrm{w}\beta-1} \tag{25}$$

Hence, by definition of most-probable or Wien speed $\mathrm{v}_{\mathrm{ws}} = \lambda_{\mathrm{ws}} \nu_{\mathrm{ws}} = \lambda_{\mathrm{ws}} / \tau_{\mathrm{ws}}$, one can define constant internal measures of (extension, duration)

$$\begin{cases} \lambda_{\mathrm{ws}} & \text{Internal measure of extension} \\ \tau_{\mathrm{ws}} & \text{Internal measure of duration} \end{cases} \tag{26}$$

to every "point" or "atom" of space in a universe at constant temperature $T_{\beta} = T_{\beta-1}$. Next, external space and time that are independent of each other are defined in terms of the internal spacetime in Eq. (26). For example, at cosmic scale $\beta = \mathrm{g}$, one employs internal (ruler, clock) of the lower scale of astrophysics $\beta = \mathrm{s}$ to define *external space and time* coordinates defined as [91]

$$(\mathrm{x}_{\beta}, \mathrm{y}_{\beta}, \mathrm{z}_{\beta}) = (N_{\mathrm{x}\beta}, N_{\mathrm{y}\beta}, N_{\mathrm{z}\beta}) \lambda_{\mathrm{wx}\beta-1} \qquad , \qquad t_{\beta} = N_{\mathrm{t}\beta} \tau_{\mathrm{w}\beta-1} \tag{27}$$

with the four numbers $(N_{\mathrm{x}\beta}, N_{\mathrm{y}\beta}, N_{\mathrm{z}\beta}, N_{\mathrm{t}\beta})$ being independent numbers. Whereas internal spacetime in Eq. (26) provides *local* structure of spacetime, the external space and time in Eq. (27) describe *global* dynamics of the system and are irreversible. Also, according to Eqs. (26-27) both internal and external space and time are quantized. The four dimensions $(\mathrm{x}_{\beta}, \mathrm{y}_{\beta}, \mathrm{z}_{\beta}, t_{\beta})$ with three real space and one imaginary time coordinates represent Poincaré [74] and Minkowski [77] four-dimensional spacetime manifold.

Recently, the author became aware of a number of wonderful books and articles by Rovelli [92-96] and consequently learned about his much earlier pioneering contributions to the understanding of the nature of time in general and what he called *thermal time* in particular. Clearly, the definition of spacetime in Eq. (26) is in accordance with the perceptions of Rovelli [95]

> **"The theory seems to indicate that there is no explanation for the peculiar properties of the time variable at the mechanical level. We suggest that such an explanation should be searched at the thermodynamical level. We propose the idea that the very concept of time is meaningful only in the thermodynamic context"**

It is emphasized that the definition of internal spacetime in Eq. (26) is based on *thermodynamic equilibrium* corresponding to *stochastically stationary* thus *time-reversible* state. The objective is to define what the variable called physical time represents as noted by Rovelli [95]

> **"It may seem strange that time is determined by an equilibrium state, since in an equilibrium state the system loses track of the**

direction (the versus, the arrow) of time. However, we are not concern here with versus of the time flow: we are concerned with definition of a variable that represents time, which is a very different problem."

Therefore, the external or *physical time* quantitatively defined in Eq. (27) is called *Rovelli thermal time*. Of course, because entropy generation due to various dissipations in all real systems lead to change in temperature, the internal measures of spacetime in Eq. (26) will also change. For example, in cosmology, the internal measure of spacetime change extremely slowly (eons) due to dissipations and the expansion of universe.

In another recent investigation by Rovelli [96] concerning general relativistic statistical mechanics, thermodynamic temperature was related to the ratio between the thermal time τ and physical time t as

$$T = \frac{\tau}{\mathrm{t}} \tag{28}$$

Since dimension of absolute temperature is meters $T = \lambda_w$, Eq. (28) *appears* to be dimensionally non-homogeneous. To reveal the nature of dimensional equality in Eq. (28) we consider the velocity ratio

$$\frac{\mathrm{v}}{\mathrm{v_w}} = \frac{\mathrm{x/t}}{\lambda_w/\tau_w} = \frac{\tau_w}{\mathrm{t}}\frac{\mathrm{x}}{\lambda_w} = \mathrm{N} \tag{29}$$

When the external spatial extension or length is defined as $x = \mathrm{N}\ell_x$ m, Eq. (29) simplifies as

$$\frac{\tau_w}{\mathrm{t}} = \frac{\mathrm{N}\lambda_w}{\mathrm{x}} = \frac{\mathrm{N}\lambda_w}{\mathrm{N}\ell_x} = \frac{\lambda_w}{\ell_x} = \lambda_w = T \tag{30}$$

Equation (30) that is *dimensionally homogeneous* becomes identical to Eq. (28) because of the choice of the metric or *unit of length* $\ell_x = 1$ m. Therefore, Eq. (30) in effect requires that the *unit of length* (say meters) for external spatial coordinate x be *identical* to the internal unit employed to express absolute temperature $T = \lambda_w$ m.

According to Eq (27), external (ruler, clock) = (x_β, t_β) at scale β within the hierarchy (Fig. 1) are always defined in terms of internal (ruler, clock) = ($\lambda_{w\beta-1}$, $\tau_{w\beta-1}$) at the next lower scale $\beta-1$, the definition of (extension, duration) = (space, time) could be relegated to lower scales ad infinitum. This is because infinite divisibility of both extension and duration must follow the philosophy of Anaxagoras [97]

> **"Neither is there a smallest part of what is small, but there is always a smaller, for it is impossible that what is should ever cease to be"**

Therefore, both absolute zero and absolute infinite (extension, duration) are singularities as ideal Aristotle potential limits never actualized as discussed in [65]. The fundamental and quantum nature of both space and time and their role in constitution of matter in quantum field theory and GTR will be further discussed in the following section.

5 Universality of Quantum Mechanics and the Nature of Wave-Particle Duality

The fact that Boltzmann anticipated quantum mechanics by about three decades is evidenced by the following quotation taken from his pioneering and often neglected 1872 paper [98]

> **"We wish to replace the continuous variable x by a series of discrete values ε, 2ε, 3ε … pε. Hence, we must assume that our molecules are not able to take up a continuous series of kinetic energy values, but rather only values that are multiples of a certain quantity ε. Otherwise, we shall treat exactly the same problem as before. We have many gas molecules in a space R. They are able to have only the following kinetic energies:**
>
> **ε, 2ε, 3ε, 4ε, . . . pε**
>
> **No molecule may have an intermediate or greater energy. When two molecules collide, they can change their kinetic energies in many different ways. However, after the collision the kinetic energy of each molecule must always be a multiple of ε. I certainly do not need to remark that for the moment we are not concerned with a real physical problem. It would be difficult to imagine an apparatus that could regulate the collisions of two bodies in such a way that their kinetic energies after a collision are always multiples of ε. That is not a question here. "**

Although more recent theoretical understanding of quantum mechanics based on fundamental contributions of its founders Planck [46,99], Einstein [100], Bohr [101], de Broglie [1-3], Heisenberg [102], Dirac [103], Schrödinger [104], Pauli [101], and Born [105] is fully established, its physical and intuitive understanding encounter difficulties due to abstract nature of its mathematical foundation. As a result, the theory confronts many problems associated with its *physical interpretation* such as

1. The nature of wave function and its probabilistic interpretation.
2. Wave-particle-duality.

3. Particle-particle entanglement.
4. Double-slit experiment.
5. EPR and problem of action-at-a-distance.
6. Quantum-jumps and trajectory problems.
7. Schrödinger cat.

among others.

The problem of lack of intuitive understanding of quantum mechanics mentioned above extends to Newton [106] law of gravitation, Einstein [78] general theory of relativity, and Dirac [107] equation of quantum field theory. This is because, similar to quantum mechanics, such mathematical theories were based on certain desired mathematical properties, such as the inverse square law, the equivalence principle, or relativistic wave equation with positive probability, rather than derivation from the first principles. As a result, in spite of excellent predictive power of the theories, the exact connection between abstract mathematical models and the physical phenomena they aim to reveal remain obscure.

Recent investigations [35, 36] were focused on connections between energy spectrum of photon gas given by Planck [99] distribution and both energy and dissipation spectrum of isotropic stationary turbulence. Thus, the gap between the problems of quantum mechanics and hydrodynamics was closed through connections between Cauchy, Euler, Bernoulli equations of hydrodynamics, Hamilton-Jacobi equation of classical mechanics, and finally Schrödinger equation of quantum mechanics. This resulted in recent derivation of invariant time-independent and time-dependent Schrödinger equations from invariant Bernoulli equation for potential incompressible flow [37]

$$\frac{\hbar^2}{2\mathrm{m}_\beta}\nabla_\xi^2\psi_\beta + (\tilde{H}_\beta - \tilde{V}_\beta)\psi_\beta = 0 \tag{28}$$

$$i\hbar_\beta \frac{\partial \Psi_\beta}{\partial t_\beta} + \frac{\hbar_\beta^2}{2\mathrm{m}_\beta}\nabla_\xi^2\Psi_\beta - \tilde{V}_\beta\Psi_\beta = 0 \tag{29}$$

The quantum mechanics wave function is defined as [37]

$$\Psi_\beta(\xi,t) = \rho^{1/2}\Phi'_\beta(\xi,t) = \rho^{1/2}\,\mathrm{e}^{ik_r\xi}\;\mathrm{e}^{-\mathrm{i}\tilde{H}t_\beta/\hbar} \tag{30}$$

such that $\Psi_\beta\Psi_\beta^* = \rho_\beta$ accounts for *particle localization* in accordance with classical results [108]. The velocity potential Φ'_β of peculiar velocity that is *complex* accounts for normalization and hence the success of Born [105] *probabilistic interpretation* of Ψ_β. In the following, some implications of the

model to the resolution of problems in the list (1-7) above concerning interpretation of quantum mechanics will be briefly examined.

According to the invariant model of Boltzmann statistical mechanics, each equilibrium statistical field (Fig. 1) is composed of a spectrum of cluster or wave-packet sizes containing "atoms" with velocity, speed, and energy respectively following Gauss, Maxwell-Boltzmann, and Planck distribution functions. As discussed in [37], the conventional field of fluid dynamics does not correspond to equilibrium molecular dynamics EMD $\beta = m$ but rather to the next higher scale of equilibrium cluster-dynamics ECD $\beta = c$. Hence, in stationary fluid at ECD scale, Maxwell-Boltzmann distribution function governs the spectrum of cluster sizes that are *stochastically stationary*. Random motion of clusters accounts for the Brownian motion of small suspensions that is known to be a non-dissipative stationary phenomenon [35]. Transition of a cluster from a small fast-oscillating "eddy" (high energy-level-j) to a large slowly-oscillating "eddy" (low energy-level-i) results in emission of a "sub-particle" that is a molecule to carry away the excess energy in harmony with Bohr [101] frequency formula $\Delta\varepsilon_{ji\beta} = h(\nu_{j\beta} - \nu_{i\beta})$ as schematically shown in Fig. 7a.

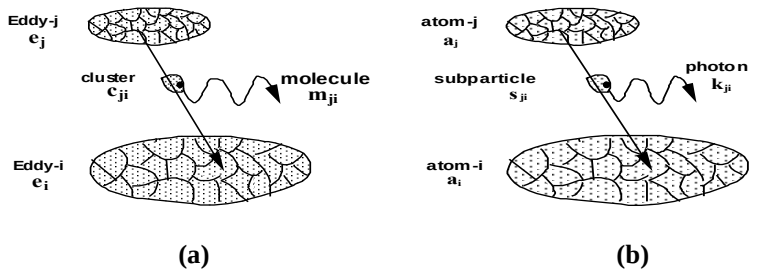

Fig. 7 **(a)** Transition of cluster c_{ij} from eddy-j to eddy-i leading to emission of molecule m_{ij}. **(b)** Electron transitions with emission of photon γ_{ji} [37].

Similarly, but at the much smaller scale of ESD $\beta = s$ or stochastic electrodynamics (SED), transition of an electron from high to low energy atoms lead to emission of a sub-particle namely photon γ_{ji} as shown in Fig. 7b.

As described in [37], derivation of invariant Schrödinger equation from invariant Bernoulli equation results in a new paradigm of physical foundation of quantum mechanics. Considering the case of stationary fluid or equilibrium cluster-dynamics ECD $\beta = c$, the quantum mechanics wave function Ψ_c relates to the velocity potential of particle peculiar velocity. However, particle or "atom" of ECD field namely cluster is the most-probable molecular cluster by definition $\mathbf{u}_c = \mathbf{v}_{wm}$ in Eq. (1). Therefore, particle of scale β is identified as the most probable *wave-packet* of the lower scale β-1. Hence, each statistical field

will have a quantum mechanics wave function Ψ_β and particle P_β that is stationary wave-packet of the lower scale

$$\begin{cases} \Psi_\beta = (\text{Wave Function}) = WF_\beta \\ P_\beta = (\text{Particle})_\beta = (\text{Wave Packet})_{\beta-1} = WP_{\beta-1} \end{cases} \tag{31}$$

In harmony with de Broglie [1-3] picture of quantum mechanics, motion of "particle" P_β as *local* singularity identified as *wave-packet* = $WP_{\beta-1}$ of lower scale is *guided* by a *global* external quantum mechanics wave function Ψ_β as schematically shown in Fig. 8.

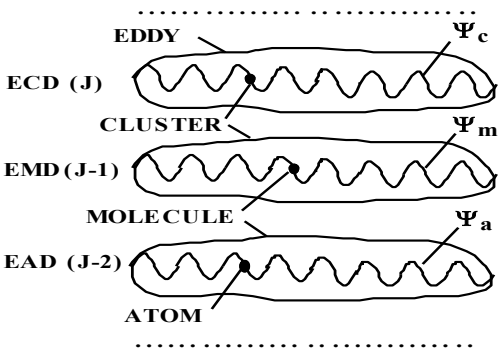

Fig. 8 Macroscopic wave functions Ψ_β or de Broglie guidance waves at (ECD), (EMD), and (EAD) scales that guide particles identified as wave-packets (WP) $_{\beta-1}$ or de Broglie matter-waves [37].

Hence, at any scale within the hierarchy of statistical fields in Fig.1, the solution of Schrödinger equation gives the energy spectrum of "atomic" clusters that represent Bohr [101] *stationary states* or energy levels of the field.

When one moves to the next lower scale of equilibrium molecular dynamics EMD β = m, derivation of Schrödinger equation [37] involves a stationary coordinate moving with velocity $\mathbf{v}_{wa}$ since $\mathbf{v}_m = \mathbf{u}_m - \varepsilon \mathbf{V}'_m = \mathbf{v}_{wa} - \varepsilon \mathbf{V}'_m$ by equations (1-2). Because by Eq. (30) Ψ_m relates to the velocity potential of molecular peculiar velocity $\mathbf{V}'_m$, under thermodynamic equilibrium $\mathbf{v}_{wm} = \mathbf{u}_c$ will also be related to $\mathbf{V}'_m$ thus connecting Ψ_m with P_c. As a result, particle P_β of the upper scale is identified as quantum mechanics wave function of the lower scale $\Psi_{\beta-1}$ and one arrives at a hierarchy of embedded wave functions expressed as

$$\begin{cases} P_{\beta} = \Psi_{\beta-1} = (\text{Wave Function})_{\beta-1} = WF_{\beta-1} \\ P_{\beta-1} = (\text{Wave Packet})_{\beta-2} = WF_{\beta-2} \end{cases} \quad (32)$$

According to Eq. (32) and Figs. 1 and 6, the universe is composed of hierarchies of embedded waves suggesting that the entire universe was formed when the Almighty decided to make some waves!

The results in equations (27-32) and Fig. 8 may help in the understanding of the first and second problems in the list 1-7 above. The wave-particle duality problem is understood in terms of wave function Ψ_{β} that globally guides motion of particles identified as wave-packet of lower scale in accordance with the perceptions of de Broglie [3]. New perspectives provided by the results in Eqs. (27-32) and Fig. 8 concerning problems 1-2 are also expected to facilitate the resolution of the remaining problems 3-7. For example, problem number 6 namely absence of particle trajectories in quantum mechanics becomes understandable because as shown in Fig. 7, any particle from cluster j can make a transition to cluster i through any arbitrary trajectory with exactly the same final results, thus accounting for success of Feynman method of sum-over-paths. Regarding number 7 problem concerning Schrödinger cat, in view of probabilistic aspect of Φ'_{β} hence Ψ_{β} by Eq. (30), it is clear that any interference with the field due to a measuring instrument will disturb the velocity potential thus leading to *collapse of the wave function* Ψ_{β}.

Schrödinger cat problem is more challenging since it involves the phenomenon of *life* and *death* that are not understood. Since as discussed in [109] all living systems are composed of living elements, and living elements are in turn composed of living cells, one may speculate if such infinite regression leads to an "atom of life" or Leibniz "*living Monad*"! Although at present such questions are *metaphysical* and hence outside of jurisdiction of science, some aspects of the problem may be considered within the framework of quantum mechanics.

To introduce the required concepts, we need to consider an example from cosmology. It is well known that sometimes around 380, 000 years after the explosion of Lemaître [110] "atom" of our universe, the Big Bang, there was decoupling of radiation field from the baryonic matter field and the present Penzias-Wilson [111] cosmic background microwave radiation temperature of 2.73 [m] is remnant of the cooling of Casimir **[**112**]** vacuum. It is also reasonable to anticipate that a living system will involve complex dynamics at EMD, EAD, ESD, EKD, END, ETD, … scales (Fig.1) with END denoting *equilibrium-neutrino-dynamics* at scale $\beta = n$ (not shown in Fig. 1). By invariant Schrödinger equation (29) and Eq. (32), hierarchies of wave functions and particles will be associated with such fields. Therefore, due to the well-known decoupling of radiation from matter field in cosmology, one cannot rule out possible *decoupling* of some fields say neutrino-dynamics (END) or lower scale of tachyon-dynamics (ETD) from the baryonic field of molecular-

dynamics of living systems at the moment of death $t = t_f$. In view of the hierarchies of wave functions in Eq. (23), there will be a critical sub-photonic decoupling scale $\beta = \beta_d$ at which the cascade of wave functions in Eq. (23) will be broken

$$\cdots\Psi_{\beta=d+2}\Psi_{\beta=d+1} \Leftarrow \quad \Rightarrow \Psi_{\beta=d}\Psi_{d-1}\Psi_{d-2}\cdots \tag{32.5}$$

Such an event may correspond to what Hegel referred to as the moment in which *the spirit transcends temporality* [94]**.** It is ironic that according to such a model, death or decoupling of Schrödinger cat corresponds to the *collapse of wave function of cat's life*! Of course, strictly speaking, according to the present model (Fig. 1), complete decoupling hence *total isolation* of any part of the universe from the rest should be impossible as noted by Boltzmann [36].

Interestingly, Feynman [113] suggested that Schrödinger equation might in fact explain life

> **"Often people in some unjustified fear of physics say you cannot write an equation for life. Well, perhaps we can. As a matter of fact, we very possibly already have the equation to a sufficient approximation when we write the equation of quantum mechanics:**

$$\mathbf{H}\Psi = -\frac{\hbar}{\mathbf{i}}\frac{\partial\Psi}{\partial\mathbf{t}}$$

Although decoupling of sub-photonic statistical fields from living system at molecular-dynamic scale is plausible, regarding its connection to the mind-body problem of Descartes or Hegel's transcendence of spirit from corporal temporality, I respond by borrowing a quotation from Rovelli [94] about Plato's account of a statement by Socrates: "*I am not sure*".

At the important scale of LKD (Fig. 1) physical space or Casimir vacuum [112] is identified as a compressible fluid, Planck compressible ether [114], as discussed in [115]. A schematic diagram of physical space as states of a compressible fluid from infinite rarefaction (*white hole* WH) to infinite compression (*black hole* BH) is shown in Fig. 9.

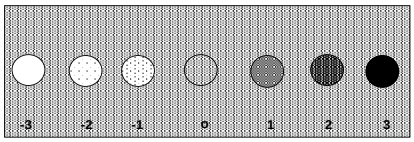

Fig. 9 Different degrees of rarefaction and compression of Casimir vacuum identified as a compressible fluid. **(-3)** White hole $\rho_{WH} = 0$ **(-2, -1)** Anti-matter $\rho_{AM} < \rho_v$ **(0)** Casimir vacuum $\rho = \rho_v$ **(1, 2)** Matter $\rho_{MA} > \rho_v$ **(3)** Black hole $\rho_{BH} = \infty$ [37].

Compressibility of physical space was recently shown [116] to account for relativistic effects when Michelson number *Mi* = v/c approaches unity thus revealing the *causal* [55] nature of Lorentz-FitzGerald contraction in accordance with Poincaré-Lorentz *dynamic theory of relativity* as opposed to Einstein *kinematic theory of relativity* in harmony with ideas of Darrigol [117] and Galison [118].

When physical space or Casimir [112] vacuum is identified as superfluid photon or Bose-Einstein condensate, it is reasonable to anticipate that when heated to a critical vaporization or *boiling temperature* T_b, the vacuum or space will nucleate what could be called photon gas bubbles that following Dirac could be also referred to as holes or anti-matter particles. Similarly, if space or Casimir vacuum cools below certain critical fusion or *melting temperature* T_m liquid photon undergoes phase transition and becomes solidified thus forming *solid-light* that was defined as black hole [119]. Therefore, in such a model, Hawking *evaporation* of BH will instead correspond to Hawking *melting* or *sublimation* of BH. Loss of mass due to melting of black hole could be caused by heating due to absorption of photon gas bubbles, anti-matter particles, that give their excess energy to melt part of BH and convert it to Casimir vacuum, i.e, space. This is in accordance with absorption of negative *curvature energy* in classical model of quantum gravity described by 't Hooft [120]

> **"When a black hole loses energy, it is primarily because it absorbs negative amounts of 'curvature energy'. Clearly, our primordial model must allow for the presence of negative amounts of energy. Actually, this is obviously true for quantum mechanical, because, after diagonalization, the total Hamiltonian has zero eigenvalue. Prior to diagonalization of the total H, the Hamiltonian density $\mathcal{H}$ (x) must have negative eigenstates. We now see that, since the black hole must lose weight, the primordial model must also have local fluctuations with negative 'curvature energy'. Black holes absorb negative amounts of energy, allowing positive energy to scape to infinity.**
>
> **It is due to the postulated thermodynamical stability that the fluctuations surviving at spatial infinity may only have positive energy. Since the total energy balances out, the black hole will therefore receive net amounts of negative energy falling in. Hence it loses weight and decays."**

It is reasonable to expect two surfaces of event-horizon (BHH, WHH) to surround (BH, WH) with the corresponding surface temperatures (T_m, T_b). Under such a paradigm of physical space, Casimir vacuum with constant density $\rho = \rho_v$ will correspond to constant measure (*zero curvature*) Euclidean space, colder and denser $\rho_m > \rho_v$ regions correspond to matter (*positive curvature*)

called Riemannian space, and finally hotter and lighter $\rho_{am} < \rho_{v}$ regions correspond to Dirac anti-matter (*negative curvature*) and called Lobachevskian space [37].

The new perspectives concerning the nature of physical space described in Fig. 9 as well and the identification of dimension of absolute thermodynamic temperature as length [m] associated with Wien wavelength of thermal oscillation will have a major impact on cosmology in general and physical interpretation of Einstein [78] GTR in particular. Compressible nature of physical space (Fig. 9) with "atomic" or quantum volume $\hat{\mathrm{v}} = T^3 = \lambda_{\mathrm{w}}^3$ may facilitate bridging the gap between QM and GTR since it is harmonious with modern paradigms of quantum gravity [120-122]. For example, it is reasonable to anticipate that gravitational forces will be associated with gradient of Casimir [112] vacuum density (scalar curvature) hence pressure of physical space.

In a recent study [32] it was shown that entropy of black hole is $S = 4N\mathrm{k}$ in exact agreement with prediction of Major and Setter [123]. The entropy of black hole according to Rovelli and Vidotto [124] is

$$S = \mathrm{k}\frac{4}{3}\sqrt[4]{\frac{\pi^2\mathrm{L}^3\mathrm{E}^3}{15(\mathrm{c}\hbar)^3}} \tag{33}$$

However, one notes that the power of four in the expression

$$\tilde{N}^4 = \frac{\pi^2\mathrm{L}^3\mathrm{E}^3}{15(\mathrm{c}\hbar)^3} \tag{34}$$

is due to the four degrees of freedom per oscillator associated with its translational, rotational, vibrational, and potential energy such that the actual number of oscillators is

$$\tilde{N} = \frac{\pi^2\mathrm{L}^3\mathrm{E}^3}{15(\mathrm{c}\hbar)^3} \tag{35}$$

From a recent study [36] on closure of the gap between photon gas in Planck equilibrium radiation and Boltzmann kinetic theory of ideal monatomic gas, the number of photons in volume V of Casimir [112] vacuum is

$$N = \frac{8\pi^5 V}{45}\left(\frac{\mathrm{kT}}{\mathrm{hc}}\right)^3 = \frac{\pi^2\mathrm{L}^3}{45}\left(\frac{\mathrm{E}}{\mathrm{c}\hbar}\right)^3 \tag{36}$$

The results in equations (33), (35), and (36) give

$$S = 4N\mathrm{k} \tag{37}$$

in exact agreement with [32, 123].

The result (37) is also in agreement with application of global temperature in general relativistic statistical mechanics of Rovelli [96]

$$S = -\int_{\Gamma} \rho_{\beta} (\beta \ln \rho - \ln Z) = \beta E + \ln Z \tag{38}$$

when mean value of energy

$$h = -\int_{\Gamma} \ln \rho \tag{39}$$

is identified as internal energy U that is related to Hamiltonian (enthalpy) H as

$$E = h = \frac{3}{4} H = U = 3N\mathrm{k}T \tag{40}$$

Substituting for $\beta = 1/\mathrm{k}T = 1/T$, with the assumption k = 1 [96], the translational partition function $Z_{\mathrm{t}} = \mathrm{e}^{N}$, and the mean energy E from Eq. (40) into Eq. (38) gives the black hole entropy in Eq. (37).

Alternatively, the partition function Z in [96]

$$Z(\beta) = \int \mathrm{e}^{-\beta H} = \mathrm{e}^{-\beta F} \tag{41}$$

is the translational partition function $Z_{\mathrm{t}} = \mathrm{e}^{-\beta F}$ and $F = -N\mathrm{k}T$ is Helmholtz free energy of ideal gas [31]. Inclusion of translational, rotational, and vibrational degrees of freedom gives $Z = Z_{\mathrm{t}} Z_{\mathrm{r}} Z_{\mathrm{v}} = \mathrm{e}^{-3\beta F} = \mathrm{e}^{-\beta U}$ such that the mean energy E [124]

$$E = -\frac{1}{\beta} \frac{\mathrm{d} \ln Z}{\mathrm{d}\beta} \tag{42}$$

becomes the internal energy $U = -3F = 3N\mathrm{k}T$ as in Eq. (40). Therefore, result in Eq. (37) is also in exact agreement with entropy given by Rovelli [96] formula

$$S = \beta E - \beta F \tag{43}$$

after substitution for $\beta = 1/T$, $F = -N\mathrm{k}T$, and $E = U = 3N\mathrm{k}T$ from Eq. (42).

An outstanding problem regarding connection between thermodynamics and black hole mechanics [125-131] concerns Shannon information theory [132]

$$I = -\mathrm{K} \sum_{\mathrm{j}} \mathrm{p}_{\mathrm{j}} \ln \mathrm{p}_{\mathrm{j}} \tag{44}$$

and what happens to the information as matter crosses the event horizon into a

black hole. For ideal monatomic gas with four degrees of freedom namely translational, rotational, vibrational, and potential, $Z = Z_r Z_r Z_v Z_p = e^{4N}$ the atomic, element, and system entropy relate to the number of Heisenberg-Kramers [68] virtual oscillators as [32]

$$\hat{s} = -k \ln \hat{p} \quad , \quad \hat{p} = e^{-4} \tag{45a}$$

$$S_j = -k \sum_j \ln \hat{p} = -k \ln p_j \quad , \quad p_j = e^{-4N_j} \tag{45b}$$

$$S = \sum_j S_j = -k \sum_j \ln p_j = -k \ln p \quad , \quad p = e^{-4N} \tag{42c}$$

For a multicomponent mixture, the atomic mixture entropy is [109]

$$\hat{s}_{mix} = \frac{S}{N} = -k \sum p_j \ln p_j \tag{46}$$

Therefore, Shannon formula in Eq. (44) will become identical to Eq. (46) of thermodynamics if one defines Shannon *measure* K in terms of Boltzmann constant as K = *N*k such that Eq. (44) becomes

$$\hat{i} = \frac{I}{N} = -k \sum_j p_j \ln p_j \tag{44}$$

With entropy identified as the number of Heisenberg-Kramers [68] virtual oscillators, the problem of information loss in black hole is resolved since loss of number of oscillators could be attributed to coarse-graining as photons freeze from liquid to solid phase when they cross black hole event-horizon BHH. In other words, as temperature decreases, atoms of space i.e., photons collect in larger and larger clusters, thus decreasing the number of oscillators leading to loss of entropy by Eq. (37) [109]. On the other hand, when anti-matter bubbles enter the black hole, their excess thermal energy leads to melting of part of black hole from solid into liquid photon at BHH increasing entropy and producing more Casimir [112] vacuum that accounts for observed accelerative expansion of the universe [56-59].

In view of the model of physical space in Fig. 9 and entropy of black hole in Eq. (37), it is reasonable to assume that Lemaître [110] primordial "atom" of our universe was in a state of *solid light* extremely close to absolute zero temperature hence having nearly zero entropy as Planck perfect crystal [46,99]. This is in harmony with perceptions of Plato who believed that the world was formed from a formless state of *total chaos* or "*Tohu Vavohu*" [109]. Since according to Fig. 9 matter and anti-matter annihilate each other leaving Casimir [112] vacuum of a flat universe, in harmony with perceptions of Aristotle there is no "void" except the singularity called *white hole* (Fig. 9).

6 Universal Hydrodynamic Model of Faraday Line of Force from Cosmic to Photonic Scales

Because of the scale-invariant nature of the model (Fig. 1) the physical insights available at ordinary scales can help in the understanding of nature at much larger or much smaller scales that are less accessible to ordinary human intuition. For example, it is known that a rotating sphere in an otherwise quiescent fluid causes polar inflow jets (IJ) and equatorial outflowing disk (OD) [133] as shown in Fig. 10.

Fig.10 Direct photograph of swirling equatorial disc outflow (DO) created by a rotating rigid sphere in otherwise stationary silicon oil with aluminum powder illuminated by laser sheet light [133].

However, if the rigid sphere is stationary but instead the surrounding fluid is rotating, Huygens centrifugal forces will reverse direction resulting in accretion by inflowing disk (ID) and polar outflowing jets (OJ). Occurrence of outflow jets (OJ) from black holes is well established in cosmology.

The flow fields in otherwise stationary background fluid induced by rotating spherical particles are shown in Fig. 11

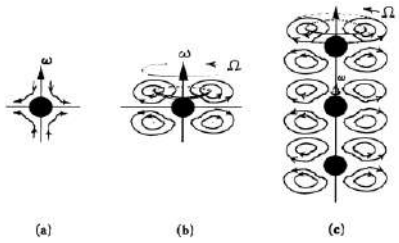

Figure 11. Schematic model (a) flow near a spinning particle (b) locally conserved flow streamlines (c) formation of Faraday line of force from a row of co-spinning particles and the associated vortex field within the subquantum background fluid.

Because of finite available energy and momentum, such flows cannot extend to infinity and instead form a finite spherical volume by outflowing equatorial disk turning around and joining the inflowing polar jets as shown in Fig. 11b resembling magnetic field lines in electrodynamics. When multiple spinning spheres are present, the hydrodynamic forces cause spinning particles to form a chain of alternating particle and “anti-particle” also called “hole” that is

spherical regions of rarefaction, called *hydrodynamic model of Faraday line of force* [115] schematically shown in Fig. 12.

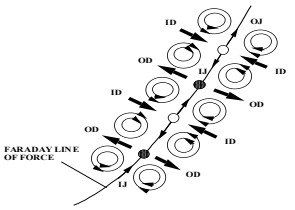

Fig. 12 Faraday line of force as electron (black) and positron (white) string with inflow jet (IJ) of one matching the outflow jet (OJ) of its neighbor. Also shown are alternating outflow (OD) and inflow discs (ID) [115].

In a pioneering study, Dirac [134] introduced the mathematical concept of Faraday line of force as a directional line with an electron at one end and a positron at the other,

> **"This leads us to a picture of discrete Faraday lines of force, each associated with a charge, −e or +e. There is a direction attached to each line, so that the ends of a line that has two ends are not the same, and there is a charge – e at one end and a charge +e at the other. We may have lines of force extending to infinity, of course, and then there is no charge."**

The fluid or Casimir vacuum between two spinning spherical particles is expected to cavitate, because of strong equatorial outflowing disks from spinning particles (Figs. 11, 12), thus forming a spherical region of vapor called "hole" or Dirac "anti-matter" particle. For example, the Faraday line of force in stochastic electro-dynamics at ESD scale (Fig. 1) will be composed of an alternating chain of electron-positron as shown in Fig. 12. The breakage of such stable vortex lines is analogous to the following description of Dirac [134] concerning the breaking of Faraday line of force:

> **"This process −the breaking of the line of force− would be the picture for creation of an electron (e−) and a positron (e+). It would be quite a reasonable picture, and if one could develop it, it would provide a theory in which e appears as a basic quantity. I have not yet found any reasonable system of equations of motion for these lines of force, and so I just put forward the idea as a possible physical picture we might have in the future."**

Similarly, but at much smaller chromodynamics (SU3) or EKD scale, the chromodynamic Faraday line of force will be identified as strings of quark-antiquark as described by 't Hooft [135]

"It took several years before it became clear that these are exactly the expressions obtained if each of these mesons is viewed as being a kind of rope with quark at one end and an antiquark at the other. The ropes can be stretched ad infinitum, because stretching them adds energy to them, which will be turned into more matter: that is, more rope."

At large hydrodynamic scales turbulent eddies are known to form vortex tubes. By Kelvin circulation theorem, it is known that such vortex lines cannot abruptly end within potential flows and instead must be either pinned to a solid boundary or else close on themselves thus forming a closed vortex "loop" in harmony with LQG [121,122] models of quantum gravity. Such behavior is well known in superfluid helium-3 experiments revealing "quantized" vortex lines discussed in [133].

An example at molecular-dynamics scale is combustion of acetylene that results in large amounts of soot or carbon particles that form many centimeters long chains. At the much larger scale of astrophysics, it has recently been observed that our galaxy the Milky Way contains large numbers of very long star streams [136,137]. Finally, at exceedingly large scale of cosmology, it is well known that rotating galaxies form very long streams that could be called *cosmic Faraday lines of force*.

7 Implication to Banach-Tarski Paradox

In this section, application of invariant model of Helmholtz vorticity equation [33, 34] to the interesting mathematical problem of Banach-Tarski [138] paradox (BTP) is examined. To begin, let us consider a spherical flow within a fluid droplet located at the stagnation point of axisymmetric gaseous counterflow jets as shown in Fig. 13. As seen in this figure, induced by the outer flow, two cylindrically closed recirculation flows, or two tori, form in the upper and lower hemispheres of the spherical droplet.

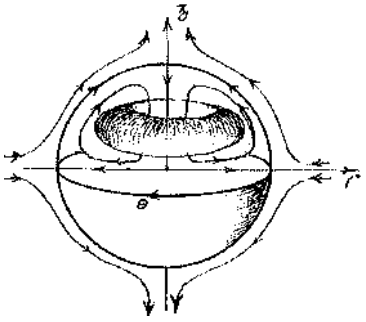

Fig.13 Flow in liquid droplet composed of two semi-spherical Hill vortices at stagnation point of gaseous axisymmetric counterflow [34].

The streamlines for such a flow (Fig. 14a) obtained from solution of modified Helmholtz vorticity equation [34].

$$w_r \frac{\partial \omega_\theta}{\partial \xi} + w_z \frac{\partial \omega_\theta}{\partial \zeta} = \frac{\omega_\theta v_r}{\xi} + \frac{\partial^2 \omega_\theta}{\partial \xi^2} + \frac{1}{\xi}\frac{\partial \omega_\theta}{\partial \xi} - \frac{\omega_\theta}{\xi^2} + \frac{\partial^2 \omega_\theta}{\partial \zeta^2} \tag{45}$$

is given by the stream function

$$\Psi = \zeta\xi^2(1-\xi^2/R^2-\zeta^2/R^2) \tag{46}$$

Because of linearity of Helmholtz vorticity equation (45), one can apply the *superposition principle* and introduce *product solutions* for flow within two immiscible liquid droplets given by the stream function

$$\Psi = \zeta^2\xi^4(1-\xi^2/R^2-\zeta^2/R^2)(3-\xi^2/R^2-\zeta^2/R^2) \tag{47}$$

leading to the flow configurations shown in Figure 14b.

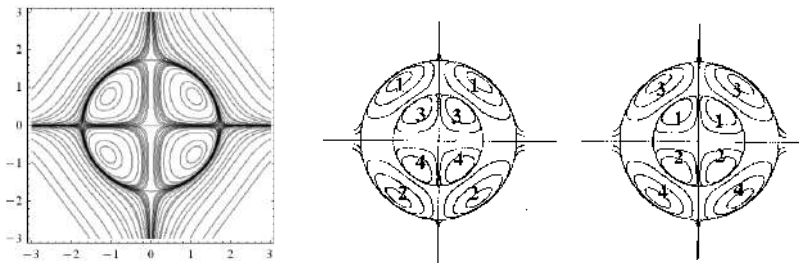

(a) **(b)** **(c)**

Fig.14 **(a)** Streamlines from Eq. (46). Turning a sphere inside out: **(b)** 1-1 and 2-2 as outer tori **(c)** 1-1 and 2-2 as inner tori.

First, the problem of turning a sphere inside-out is considered by looking at flow fields within two concentric spherical flows shown in Fig. 14b. Each hemisphere is composed of two semi-spherical tori, the outer toros 1-1 and the inner toros 3-3 in Fig. 14b. It is easy to imagine that one could compress the inner toros 3-3 towards vertical axis and move it upwards, while the outer toros 1-1 is stretched outwards and pushed down. When one imagines each toros as a cylindrical balloon, the above procedure changes the position of outer 1-1 and inner 3-3 tori thus turning the sphere 14b inside out as shown in Fig. 14c.

A flow configuration that results in fusion of two spheres into one sphere of identical volume is shown in Fig. 15.

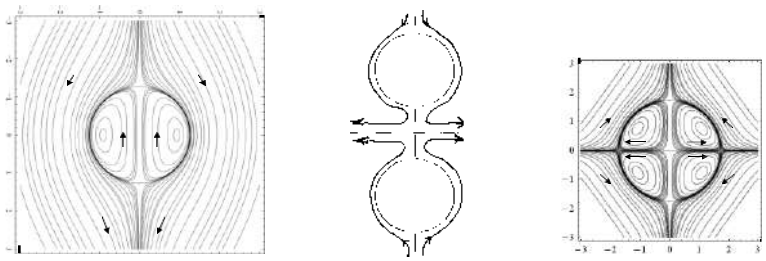

(a) **(b)** **(c)**

Fig.15 **(a)** Hill spherical vortex. **(b)** Fusion of two Hill spherical vortices into **(c)** A spherical flow composed of two semi-spherical Hill vortices [34].

As two spherical Hill vortices (S_1, S_2) in uniform flow (Fig. 15a) in opposing cylindrically-symmetric jets approach each other (Fig. 15b), they form two *semi-spherical Hill vortices* [34] and merge into a single spherical flow S_3 at the stagnation point as shown in Fig. 15c. It is possible to adjust the flow conditions such that spheres (S_1, S_2) containing $N_1 = N_2$ molecules of ideal gas $p_1V_1 = N_1 \mathrm{k} T_1$ and $p_2V_2 = N_2 \mathrm{k} T_2$ form sphere S_3 at temperature T_3

$$T_3 = T_1 / 2 = T_2 / 2 \quad , \quad N_3 = N_1 + N_2 = 2N_1 \tag{48}$$

such that,

$$p_1V_1 = p_2V_2 = p_3V_3 = N_3 \mathrm{k} T_3 = E_1 \tag{49}$$

In the above fusion process, density is doubled, temperature is halved, and energy of S_3 is half that of the original two spheres

$$E_3 = p_3V_3 = E_1 \quad , \quad p_1V_1 + p_2V_2 = E_1 + E_2 = 2E_3 \tag{50}$$

Hence, conservation of energy requires that energy E_1 be removed from the system (*exothermic*). The inverse process of "fission", namely S_3 splitting into two spheres (S_1, S_2) will be *endothermic* and require absorption of energy E_1.

The above transformations of spherical geometry, though related, do not correspond to the mathematical problem of *Banach-Tarski paradox* (BTP) [138] since in BTP problem a sphere is shown to transform to two spheres with identical volume and density as the original. Hence, BTP constitutes a clear violation of rational foundation of mathematics in the spirit emphasized by Nelson [139]. As a result, some mathematicians have raised objection, and justifiably so, against the *assumptions* underlying the set theoretical foundation of BTP. It is important to emphasize that the two spheres generated in BTP are known to be "measureless". In the following, some implications of invariant model of Boltzmann statistical mechanics (Fig. 1) and the associated laws of generalized thermodynamics to BTP is examined.

In the above fusion of spherical objects, whereas the role of number of particles N and volume V as mathematically concepts are clear, that of

temperature is not. According to equations (25) and (26), absolute temperature is the most-probable or *Wien wavelength* of particle thermal oscillation thus constituting a "*measure*" of spatial extension. It is most interesting that in his description of *hyperbolic geometry*, Poincaré [140] anticipated absolute thermodynamic temperature as a "measure" or metric of physical space:

> ***"Suppose, for example, a world enclosed in a large sphere and subject to the following laws: --The temperature is not uniform; it is greatest at the center, and gradually decreases as we move towards the circumference of the sphere, where it is absolute zero. The law of this temperature is as follows: If R be the radius of the sphere, and r the distance of the point considered from the center, the absolute temperature will be proportional to*** $R^2 - r^2$ ***. Further, I shall suppose that in this world all bodies have the same coefficient of dilatation, so that the linear dilatation of any body is proportional to its absolute temperature. Finally, I shall assume that a body transported form one point to another of different temperature is instantaneously in thermal equilibrium with its new environment. There is nothing in these hypotheses either contradictory or unimaginable. A moving object will become smaller and smaller at it approaches the circumference of the sphere. Let us observe, in the first place, that although from the point of view of our ordinary geometry this world is finite, to the inhabitants it will appear infinite. As they approach the surface of the sphere, they become colder and at the same time smaller and smaller. The steps they take are therefore smaller and smaller, so that they can never reach the boundary of the sphere. If to us geometry is only the study of the laws according to which invariable solids move, to these imaginary beings it will be the study of the laws of motion of solids deformed by the differences of temperature alluded to."***

Therefore, $T_\beta = \lambda_{w\beta}$ is called Poincaré *thermal measure*.

To address BTP problem, we begin with the following thought experiment concerning geometry. Let us consider a circle with 360 m circumference and at spacings of 1-meter around the circumference, let straight lines of equal and uniform thickness t = 1 mm be drawn to the origin of the circle as schematically shown in Fig. 16.

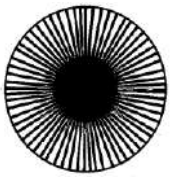

Fig.16 Formation of black-core due to coalescence of radial lines.

Clearly, due to their finite thickness, adjacent lines will coalesce on a circle with approximate circumference of 360 mm beyond which the merged lines form a "*black core*" around the origin as shown in Fig. 16. This thought experiment suggests that there exists a circle with critical minimum radius corresponding to maximum number density even in the limit of infinitesimal thickness of radial lines. Clearly, the diameter of such a "black core" could be used as a measure of maximum resolution of printers.

Therefore, the question is what happens if the above procedure (Fig. 16) is considered in the limits of a circle of infinite radius when infinite number of radial lines of zero thickness are drawn to the origin. For example, at cosmological scale (Fig. 1) the problem corresponds to infinite radial lines from circumference of a spherical universe converging on a galaxy as "atom" at the center like a hologram. As discussed in a recent study on the gap between physics and mathematics [65], the invariant model of statistical mechanics leads to coordinates shown in Fig. 17.

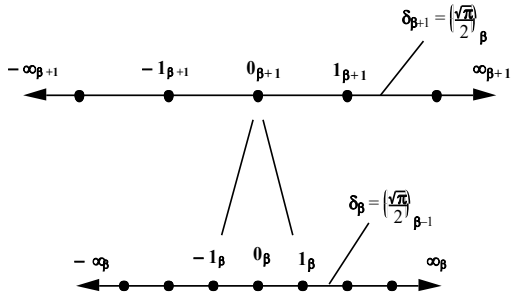

Fig. 17 Hierarchy of normalized coordinates associated with embedded statistical fields [36].

According to this figure, interval $x_{\beta} = (0_{\beta}, 1_{\beta})$ of upper (outer) scale corresponds to interval $x_{\beta-1} = (1_{\beta-1}, \infty_{\beta-1})$ of next lower (inner) scale (Fig. 17). The location of the new origin $x_{\beta-1} = 0_{\beta-1}$ is defined by the new *unit of length* or *measure* at the lower scale.

According to Fig. 5, invariant Maxwell-Boltzmann distribution when *re-normalized* with respect to the *most-probable state* leads to transformation $(x_{mp} \to 1 \ , \ x_{\infty} \to 4/\sqrt{\pi} = 2.567)$. For example, three consecutive scales within the hierarchy of coordinates with $(0_{\beta} = 10^{-120} \ , \ 1_{\beta} = (4/\sqrt{\pi})10^{-100} \ , \ \infty_{\beta} = (4/\sqrt{\pi})^2 10^{-80})$ and the size of zero and infinity relative to unity taken as $(10^{-20}, 1, 10^{20})$ is shown in Fig. 18 from the previous study [65].

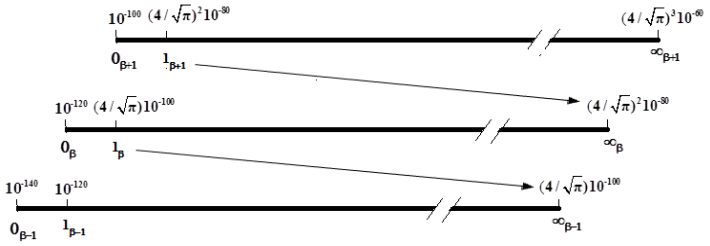

Fig. 18 Hierarchy of coordinates for hierarchy of embedded statistical fields [65].

Applying the hierarchy of normalized coordinates $x_\beta = (0_\beta, 1_\beta, \infty_\beta)$, results in circular geometry corresponding to three generation as shown in Fig. 19.

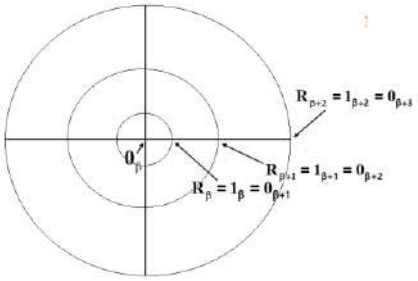

Fig. 19 Formation of hierarchy of embedded black holes due to infinite number of compactified statistical fields at the origin [119].

In Fig. 19, three generations covering the range of radii $(0_\beta, 1_\beta)$, $(0_{\beta+1}, 1_{\beta+1})$, $(0_{\beta+2}, 1_{\beta+2})$ are revealed. Following Aristotle, it is assumed that *potentially infinite* statistical fields are compactified within the *black hole* singularity at the origin. According to equation (25) and Fig. 18, since temperature is Wien wavelength or Poincaré *thermal measure* $T_\beta = \lambda_{w\beta}$, absolute zero of adjacent scales relate as $0_\beta = 1_{\beta-1} = \infty_{\beta-2}$.

As a second thought experiment, let us consider a spherical volume S_1 at scale β composed of two semi-spherical tori as shown in Fig. 14a. The central singularity or *black hole* is at "absolute zero" $r_\beta = 0_\beta$ and located at the origin. Let the sphere S_1 contain total of N_1 atoms of ideal gas ($N_1 / 2$ in each toros) at the average temperature $T_{ave} = \overline{T}$, thus the total energy or enthalpy $E_1 = H_1 = 4N_1 k\overline{T}$ [32]. Let thermal energy E_1 be added to S_1 resulting into N_1 *new atoms* be decompactified from "black hole" singularity, due to phase

transition such as melting, forming a smaller internal spherical volume (tori 3-3 and 4-4 in Fig. 14b) at temperature $T_3 = T_4 = T_L$. It is assumed that half of the added energy E_1 is absorbed by gases in original sphere S_1 (tori 1-1 and 2-2 in Fig. 14b) raising their temperature from $T_{ave} = \overline{T}$ to $T_1 = T_2 = T_H$. Finally, let the two embedded spheres in Fig. 14b undergo fission and split into two spheres S_2 = Tori (1-1)-(3-3) and S_3 = Tori (2-2)-(4-4). It is assumed that during the fission process the heat exchange between tori (1-1) and (3-3) results in their temperatures being respectively lowered and raised to the average temperature $(T_H + T_L)/2 = T_{ave} = \overline{T}$. Exactly similar heat exchange is assumed between (2-2) and (4-4) tori also leading to the same final average temperature $\overline{T}$.

Therefore, the original sphere S_1 has undergone an *endothermic* fission process (absorbed energy E_1) creating two identical spheres S_2 and S_3 with exactly the same number of atoms N_1, volume V_1, pressure p_1, and temperature $\overline{T}$. This process could be repeated ad infinitum, as long as energy E_1 is added to the system each time, due to Aristotle potentially infinite statistical fields that are compactified in the central black hole singularity [119]. Satisfaction of energy conservation principle as well as clarification of "*measureless*" nature of generated spheres in BTP problem, through introduction of what is called Poincaré *thermal measure* $T_\beta = \lambda_{w\beta}$, may help in resolution of the *paradoxical* aspect of Banach-Tarski problem [138].

In connection to BTP problem, it is further noted that due to Poincaré *thermal measure* $T_\beta = \lambda_{w\beta}$, macroscopic (extensive) *system* volume V_β and microscope (intensive) most probable *atomic* volume $\hat{v}_{w\beta}$ are related as

$$V_\beta = N_\beta \hat{v}_{w\beta} = N_\beta \lambda_{w\beta}^3 = N_\beta T_\beta^3 \tag{50}$$

Also, at thermodynamic equilibrium, by NMB distribution in Fig. 5 and in view of speed versus wavelength ratio relation

$$v_j / v_w = \lambda_w / \lambda_j \tag{51}$$

the statistical field is composed of a *spectrum* of cluster or "element" volumes

$$V_{j\beta} = \sum_i \hat{v}_{ij\beta} = \sum_i \lambda_{ij\beta}^3 \tag{52}$$

such that

$$V_\beta = \sum_j V_{j\beta} \tag{53}$$

The quantum nature of physical space with spectrum of "atomic" volumes $\hat{v}_{ij\beta}$ forming a spectrum of cluster volumes $V_{j\beta}$ is in harmony with modern concepts of quantum gravity [120, 121, 122,123, 124].

7 Concluding Remarks

Some implications of a scale-invariant model of Boltzmann statistical mechanics to generalized thermodynamics, Helmholtz decomposition of energy and momentum, and definitions of dark-energy, dark- matter, and dark-momentum were investigated. The model resulted in internal spacetime and external space and time having quantum nature in accordance with thermodynamic *thermal time* of Rovelli [95]. Invariant Schrödinger equation resulted in introduction of hierarchies of quantum mechanics wave functions and particles as de Broglie wave-packets from cosmic to photonic scales.

Physical space, Casimir [112] vacuum, was identified as a compressible fluid with density ρ_v varying from infinite rarefaction $\rho_{WH} = 0$ (white hole) to infinite compression $\rho_{BH} = \infty$ (black hole) as its two singularities. With space curvature viewed as deviation of density from density of Casimir vacuum $\kappa = \rho_\beta - \rho_v$, the states $(\kappa > 0,\ \kappa = 0,\ \kappa < 0)$ of (matter, vacuum, anti-matter) fields were associated with (*Riemannian, Euclidean, Lobachevskian*) geometry. An invariant hydrodynamic model of Faraday line of force was introduced and shown to be in harmony with observations from cosmic to photonic scales. Finally, some implications of the model to black hole entropy and information loss as well as Banach-Tarski paradox were examined. The results were found to be in harmony with quantum gravity considered as dissipative deterministic dynamic system [120].

Acknowledgments: This research was in part supported by NASA grant No. NAG3-1863.

References

1. L. de Broglie, Interference and Corpuscular Light, Nature 118, 441-442, 1926; Sur la Possibilité de Relier les Phénomènes d'Interférence et de Diffraction à la Théorie des Quanta de Lumière, C. R. Acad. Sci. Paris, 183, 447-448, 1927; La Structure Atomique de la Matière et du Rayonnement et la Mécanique Ondulatoire, 184, 273-274, 1927; Sur le Rôle des Ondes Continues en Mécanique Ondulatoire, 185, 380-382, 1927.
2. L. de Broglie, *Non-Linear Wave Mechanics: A Causal Interpretation*, Elsevier, New York, 1960.
3. L. de Broglie, The Reinterpretation of Wave Mechanics, Found. Phys. 1, 5, 5-15, 1970.
4. E. Madelung, Quantentheorie in Hydrodynamischer Form, Z. Physik. 40, 332-326, 1926.

5. E. Schrödinger, Über die Umkehrung der Naturgesetze, Sitzber Preuss Akad Wiss Phys-Math Kl, 193, 144-153, 1931.
6. R. Fürth, Über Einige Beziehungen zwischen klassischer Staristik und Quantenmechanik, Z. Phys. 81, 143-162, 1933.
7. D. Bohm, A Suggested Interpretation of the Quantum Theory in Terms of "Hidden Variables" I, Phys. Rev. 85, 2, 166-179, 1952.
8. T. Takabayasi, On the Foundation of Quantum Mechanics Associated with Classical Pictures, Prog. Theor. Phys. 8, 2, 143-182, 1952.
9. D. Bohm, and J. P. Vigier, Model of the Causal Interpretation of Quantum Theory in Terms of a Fluid with Irregular Fluctuations, Phys. Rev. 96, 1, 208-217, 1954.
10. E. Nelson, Derivation of the Schrödinger Equation from Newtonian Mechanics, Phys. Rev. 150, 4, 1079-1085, 1966.
11. E. Nelson, *Quantum Fluctuations*, Princeton University Press, Princeton, NJ,1 985.
12. L. de la Peña, New Foundation of Stochastic Theory of Quantum Mechanics, J. Math. Phys. 10, 9, 1620-1630, 1969.
13. L. de la Peña, and A. M. Cetto, Does Quantum Mechanics Accept a Stochastic Support? Found. Phys. 12, 10, 1017-1037, 1982.
14. A. O. Barut, Schrödinger's Interpretation of ψ as a Continuous Charge Distribution, Ann. der Phys. 7, 4-5, 31-36, 1988.
15. A. O. Barut, and A. J. Bracken, Zitterbewegung and the Internal Geometry of the Electron, Phys. Rev. D 23, 10, 2454-2463, 1981.
16. J. P. Vigier, De Broglie Waves on Dirac Aether: A Testable Experimental Assumption, Lett. Nuvo Cim. 29, 14, 467-475, 1980; C. Cufaro Petroni, and J. P. Vigier, Dirac's Aether in Relativistic Quantum Mechanics, Found. Phys. 13, 2, 253-286, 1983; J. P. Vigier, Derivation of Inertia Forces from the Einstein-de Broglie-Bohm (E.d.B.B) Causal Stochastic Interpretation of Quantum Mechanics, Found. Phys. 25, 10, 1461-1494, 1995.
17. F. T. Arecchi, and R. G. Harrison, *Instabilities and Chaos in Quantum Optics*, Springer-Verlag, Berlin, 1987.
18. O. Reynolds, On the Dynamical Theory of Incompressible Viscous Fluid and the Determination of the Criterion, Phil. Trans. Roy. Soc. A 186, 1, 123-164, 1895.
19. D. Enskog, Kinetische Theorie der Vorgange in Massig Verdunnten Gasen, Almqvist and Wiksells Boktryckeri-A.B., Uppsala, 1917. English translation: G. S. Brush, *Kinetic Theory*, 125-225, Pergamon press, New York, 1965.
20. G. I. Taylor, Statistical Theory of Turbulence-Parts I-IV, Proc. Roy. Soc. A 151, 873, 421-478, 1935.
21. T. Kármán, and L. Howarth, On the Statistical Theory of Isotropic Turbulence, Proc. Roy. Soc. A 164(917), 192-215, 1938.
22. H. P. Robertson, The Invariant Theory of Isotropic Turbulence, Proc. Camb. Phil. Soc. 36, 209-223, 1940.
23. A. N. Kolmogoroff, Local Structure on Turbulence in Incompressible Fluid, C. R. Acad. Sci. U. R. S. S. 30, 301-305, 1941; A Refinement of Previous Hypothesis Concerning the Local Structure of Turbulence in a Viscous Incompressible Fluid at High Reynolds Number, J. Fluid Mech. 13, 82-85, 1962.
24. A. M. Obukhov, On the Distribution of Energy in the Spectrum of Turbulent Flow, C. R. Acad. Sci. U. R. S. S. 32, 19-22, 1941; Some Specific Features of Atmospheric Turbulence, J. Fluid Mech. 13, 77-81, 1962.
25. S. Chandrasekhar, Stochastic Problems in Physics and Astronomy, Rev. Mod. Phys. 15, 1, 1-89, 1943.

26. S. Chandrasekhar, *Stochastic, Statistical, and Hydrodynamic Problems in Physics and Astronomy*, Selected Papers, vol.3, University of Chicago Press, Chicago, 199-206, 1989.
27. W. Heisenberg, On the Theory of Statistical and Isotropic Turbulence, *Proc. Roy. Soc.* A 195, 402-406, 1948; Zur Statistischen Theorie der Turbulenz, *Z. Phys*. 124, 7-12, 628-657, 1948.
28. G. K. Batchelor, *The Theory of Homogeneous Turbulence*, Cambridge University Press, Cambridge, 1953.
29. L. D. Landau, and E. M. Lifshitz, *Fluid Dynamics*, Pergamon Press, New York, 1959.
30. H. Tennekes, and J. L. Lumley, *A First Course in Turbulence*, MIT Press, 1972.
31. S. H. Sohrab, Some Implications of a Scale Invariant Model of Statistical Mechanics to Classical and Relativistic Thermodynamics, *Int. J. Thermo*. **17**, 4, 233-248, 2014.
32. S. H. Sohrab, On a scale-invariant model of statistical mechanics and the laws of thermodynamics *J. Energy Resources and Technol*. 138, 3, 1-12, 2016.
33. S. H. Sohrab, Invariant Forms of Conservation Equations and Some Examples of Their Exact Solutions, *J. Energy Resources Technol*. 136, 1-9, 2014.
34. S. H. Sohrab, Solutions of modified equation of motion for laminar flow across (within) rigid (liquid) and sphere and cylinder and resolution of Stokes paradox, *AIP Conference Proceedings* 1896, 130004 (2017).
35. S. H. Sohrab, Quantum theory of fields from planck to cosmic scales, *WSEAS Trans. Math.* 9, 734-756, 2010.
36. S. H. Sohrab, On a scale invariant Mmodel of statistical mechanics, kinetic theory of ideal gas, and Riemann hypothesis, *Int. J. Mod. Communication Tech. & Research*. 3, 6, 7-37, 2015.
37. S. H. Sohrab, Connecting Bernoulli and Schrödinger Equations and its Impact on Quantum-Mechanic Wave Function and Entanglement Problems, C.H. Skiadas and Y. Dimotikalis (eds.), *13th Chaotic Modeling and Simulation international Cmiference*, Springer Proceedings in Complexity, 2021.
38. R. S. de Groot, and P. Mazur, *Nonequilibrium Thermodynamics*, North-Holland, 1962.
39. H. Schlichting, *Boundary-Layer Theory*, McGraw Hill, New York, 1968.
40. F. A. Williams, *Combustion Theory*, 2nd Ed., Addison Wesley, New York, 1985.
41. J. O. Hirschfelder, C. F. Curtiss, and R. B. Bird, *Molecular Theory of Gases and Liquids*, Wiley, New York, 1954.
42. S. Chapman, and T. G. Cowling, *The Mathematical Theory of Non-Uniform Gases*, Cambridge University Press, Cambridge, 1953.
43. H. Helmholtz, Uber der Ehaltung der Kraft, Eine Physikalische Abhandlung, G. Reiner, Berlin (English Translation: G. S. Brush, 1965, *Kinetic Theory*, Vol. 1–3, Pergamon Press, New York).
44. A. Sommerfeld, *Thermodynamics and Statistical Mechanics*, Academic Press, New York, 1956.
45. T. Dantzig, *Mathematics in Ancient Greece*, p. 153, Dover, New York, 1954.
46. M. Planck, On the law of the energy distribution in the normal spectrum, *Ann. der Phys.* 4, 1901, pp. 553-558.
47. F. Hasenöhrl, Zur Theorie der Strahlung in bewegten Körpern. *Ann. der Phys*. 16, 589-592, 1905.
48. S. H. Sohrab, Invariant laws of thermodynamics and validity of Hasenöhrl mass-energy equivalence formula m = (4/3) E/c^2 at photonic, electrodynamic, and cosmic scales, *Bull. Amer. Phys. Soc.* 62, 1, 124, 2017.

49. A. Lorentz, Electromagnetic phenomena in a system moving with any velocity less than that of light, *Proc. Acad. Sci. Amst.* 6, 1904, pp. 809-831.
50. M. S. Turner, Dark matter in the universe, *Physica Scripta T36*, 167, 1991.
51. L. M. Krauss, and M. S. Turner, The cosmological constant is back. arXiv:astro-ph/9504003 v1 3, Apr, 1995.
52. M. S. Turner, The case for ΩM = 0.33 ± 0.035. *ApJ.* 576, L101, 2002.
53. Z. G. Dai, E. W. Liang, and D. Xu, Constraining ΩM and dark energy with gamma-ray bursts, *ApJ.* 612, L102, 2004.
54. A. Einstein, Do Gravitational Fields Play an Essential Part in the Structure of the Elementary Particles of Matter, in: *The Principles of Relativity*, Dover, 1952.
55. W. Pauli, *Theory of Relativity*, p. 204, Dover, 1958.
56. A. G. Riess, et al., Observational evidence from supernovae for an accelerating universe and a cosmological constant, *AJ.* 116, 1009, 1998.
57. A. G. Riess, et al., Type Ia supernova discoveries at *z* > 1 from the *Hubble Space Telescope*: Evidence for past deceleration and constraints on dark energy evolution, *ApJ.* 607, 665, 2004.
58. B. G. Schmidt, et al., The high-Z supernovae search: Measuring cosmic deceleration and global curvature using type Ia supernovae, *ApJ.* 507, 46, 1998.
59. S. Perlmutter, et al., Measurements of Ω and Λ from 42 high-redshift supernovae, *ApJ.* 517, 565, 1999.
60. F. Laloe, and J. H. Freed, The effects of spin in gases. *Sci. American* 1988, 258, 94-101.
61. S. H. Sohrab, The physical foundation of a grand unified statistical theory of fields and the invariant Schrödinger equation. *WSEAS Transactions on Circuits and Systems* 2004, 3, 4, 1017-1025.
62. R. E. Sonntag, and G. J. van Wylen, *Fundamentals of Statistical Thermodynamics; John* Wiley, New York, 1966.
63. M. Kardar, *Statistical Physics of Particles;* Cambridge University Press, New York, 2007.
64. M. Dersarkissian, Does wave-particle duality apply to galaxies? *Lett. Nuovo Cim.* 40**,** 390 (1984).
65. S. H. Sohrab, Some Implications of Invariant Model of Boltzmann Statistical Mechanics to the Gap Between Physics and Mathematics, C.H. Skiadas and Y. Dimotikalis (eds.), *12th Chaotic Modeling and Simulation international Cmiference,* Springer Proceedings in Complexity, pp.231-243, 2020.
66. L. D. Roper, Income distribution in the United States; A quantitative study. http://arts.bev.net/RoperLDavid/ 29 November 2007.
67. S. Fleming, and S. Donnan, America's middle-class meltdown: Core shrinks to half of US homes, Financial Times, December 9, 2015. https://www.ft.com/content/98ce14ee-99a6-11e5-95c7-d47aa298f769 .
68. van der Waerden, B. L. Towards Quantum Mechanics, in: *Sources of Quantum Mechanics,* van der Waerden, B. L. Ed.; Dover: New York, 1967, pp. 1-59.
69. Aristotle, In: *Time*, Westphal J. and Levenson, C., (Eds.), Hackett Publishing Company, Indianapolis, Indiana, 1993.
70. St. Augustine, In: *Time*, Westphal J. and Levenson, C., (Eds.), Hackett Publishing Company, Indianapolis, Indiana, 1993.
71. G. 't Hooft, G., and S. Vandoren, *Time in Powers of Ten*, World Scientific, Singapore, 2014.
72. H. Poincaré, La mesure du temps, *Rev. Metaphys. Morale* 6, 1 (1898); English translation; The measure of time, in: Poincaré, H., *The Value of Science*.
73. H. Poincaré, Sur la dynamique de l'électron, *C. R. Acad. Sci.* Paris 140, 1905.

74. H. Poincaré, Sur la dynamique de l'electron, *Rend. Circ. Mat. Palermo* 21, 12, 1906, pp. 9-175.
75. A. A. Logunov, *On the Articles by Henri Poincaré, "On the Dynamics of the Electron"*, Dubna: JINR, 2001.
76. A. Einstein, Zur Elecrodynamik bewegter Körper, *Ann. der Phys.* (Leipzig) 17, p. 891-921 (1905).
77. H. Minkowski, Space and Time, in *Theory of Relativity*, p. 75, Dover, New York, 1952.
78. A. Einstein, The Foundation of General Theory of Relativity, In: *The Principles of Relativity*, Dover, 1952, pp. 111-164.
79. G. Jaroszkiewicz, *Images of Time*, Oxford, 2016.
80. S. Hawking, *A Brief History of Time*, Bantam Book, New York, 1988.
81. H. D. Zeh, *The Physical Basis of the Direction of Time*, Springer-Verlag, 1999.
82. P. Yourgrau, *A World Without Time*, Basic Books, Perseus Books Group, NY, 2005.
83. C. Kiefer, Does time exist in quantum gravity? www.fqxi.org/communitty/forum/topic/265 (2008).
84. C. Rovelli, Forget time, www.fqxi.org/communitty/forum/topic/237 (2008).
85. J. Barbour, The nature of time, www.fqxi.org/communitty/forum/topic/360 (2008).
86. L. Smolin, *The Life of the Cosmos*, Oxford University Press, Oxford, 1997; In: *Conceptual Problems of Quantum Gravity*, Ashtekar, A., and Stachel, J. (eds.), Birkhäuser, Boston, 1991.
87. J. Barbour, The nature of time, www.fqxi.org/communitty/forum/topic/360 (2008).
88. S. B. DeWitt, Quantum mechanics and reality *Physics Today* 23, 9 (1970).
89. S. B. DeWitt, Quantum theory of gravity I. The canonical theory, *Phys. Rev.* 160, 1113 (1967).
90. J. A. Wheeler, Superspace and the Nature of Quantum Geometro-dynamics. *Battelle Rencontres*, C. M. DeWitt, and J. A. Wheeler (Eds)., Benjamin, New York 1968.
91. S. H. Sohrab, An invariant model of Boltzmann statistical mechanics and some of its implications to thermodynamics and quantum nature of space and time, *WSEAS Tran, Appl. Theo. Mech*. 13, 199-212, 2018.
92. C. Rovelli, *The Order of Time*, Riverhead Books, 2018.
93. C. Rovelli, *Reality is Not What it Seems*, Riverhead Books, 2017.
94. C. Rovelli, On the meaning of time, *Financial Times*, April 20, 2018.
95. C. Rovelli, Statistical mechanics of gravity and the thermodynamical origin of time, *Class. Quantum Grav*. 10, (1993).
96. C. Rovelli, General relativistic statistical mechanics. *General Relativity and Quantum Cosmology*, 10.1103/PhysRevD.87.084055 , arXiv:1209.0065v2 (2012).
97. J. L. Bell, *The Continuous and the Infinitesimal in Mathematics and Philosophy*, Polimetrica, Milano, Italy, 2006.
98. L. Boltzmann, Weitere Studien uber das Warmegleichgewicht unter Gasmoleculen, *Sitzungsberichte Akad.Wiss.*, Vienna, Part II, 66, 1872¸ pp. 275-370. English translation: G. S. Brush, *Kinetic Theory*, 88-175, Pergamon press, New York, 1965.
99. M. Planck, *The Theory of Heat Radiation*, Dover, New York, 1991.
100. A. Einstein, Ist die Trägheit eines Körpers vondessen Energieinhalt abhängig? *Ann. der Phys.* 18, 639-643 (1905).
101. van der Waerden, B. L., *Sources of Quantum Mechanics*, B. L. van der Waerden (ed.), Dover, New York, 1967.
102. W. Heisenberg, *The Physical Principles of Quantum Theory*, Dover, New York, 1949.
103. P. Dirac, On the theory of quantum mechanics, *Roy. Soc. Proc.* A, vol. 110, p. 561 (1926).

104. E. Schrödinger, Quantization as a problem of proper values, Part I, *Ann. der Phys.* 79, 4, 1926, pp. 361-376, Quantization as a problem of proper values, Part II, *Ann. der Phys.* 79, 4, 1926, pp. 489-527; Part III, *Ann. der Phys.* 81, 1926, pp. 109-139.
105. M. Born, Zur Quantenmechanik der Stoßvorgänge, *Z. Physik* 37, 863, 1926.
106. I. Newton, *Philosophiae Naturalis Principia Mathematica,* London, 1687.
107. A. M. P. Dirac, *Directions in Physics*, Wiley, New York, 1978.
108. W. Schommers, Evolution of Quantum Mechanics, in *Quantum Theory and Pictures of Reality*, W. Schommers (ed.), Springer, Berlin, 1-48, 1989.
109. S. H. Sohrab, Boltzmann entropy of thermodynamics versus Shannon entropy of information theory, *Int. J. Mechanics* 8, 73-84, 2014.
110. G. H. J. É. Lemaître, A homogeneous universe of constant mass and growing radius accounting for the radial velocity of extragalactic nebulae, *Monthly Notices of the Roy. Astr. Soc.* ***xci***, 483,1931; *PNAS* 20, 12, 1934.
111. A. A. Penzias, and R. W. Wilson, A measurement of excess antenna temperature at 4080 Mc/s. *Astrophysics J.* 142, 419-421 (1965).
112. H. B. G. Casimir, On the attraction between two perfectly conducting plates, Proc. K. Ned. Akad. Wet. 51, 793-795, 1948.
113. R. Feynman, R. B. Leighton, and M. Sands, *Lectures on Physics*, Vol. II, p.41-11, Addison-Wesley Publishing, New York, 1964.
114. H. A. Lorentz, *Selected Works of L.H. Lorentz,* vol.5, Nersessian, N. J., and Cohen, H. F., (Eds), p.7, Palm Publications, Nieuwerkerk, 1987.
115. S. H. Sohrab, Invariant model of statistical mechanics, quantum mechanics, and physical nature of space and time. In: *Proceedings of the International Conference on 8th CHAOS* (Henri Poincare Institute, Paris, France, 2015), pp. 769-801, 26-29.
116. S. H. Sohrab, Scale invariant model of statistical mechanics and quantum nature of space, time, and dimension, *Chaotic Modeling and Simulation (CMSIM)* 3, 231-245, 2016.
117. O. Darrigol, The mystery of the Einstein Poincare´ connection, *Isis* 95, 614-626 (2004).
118. P. Galison, *Einstein's Clocks, Poincaré's Maps*, W. W. Norton & Company, New York, 2003.
119. S. H. Sohrab, Some implications of a scale-invariant model of statistical mechanics to classical and black hole thermodynamics, *Bull. Amer. Phys. Soc.* 62, 1, 124 (2016).
120. G. 't Hooft, Quantum gravity as a dissipative deterministic system, *Class. Quantum Grav.* 16, 1999, pp. 3263-3279.
121. A. Ashtekar, The winding road to quantum gravity, *Current Science*, 89, 12, 2064 (2005).
122. C. Rovelli, and L. Smolin, Loop space representation of quantum general relativity. *Nucl. Phys.* B331, 80 (1990).
123. S. A. Major, and K. L. Setter, 2001, Gravitational Statistical Mechanics: A Model, *Classical Quantum Gravity*, 18(23), pp. 5125–5142.
124. C. Rovelli, and F. Vidotto, *Covariant Loop Quantum Gravity,* p. 198, Cambridge University Press, 2015.
125. J. M. Bardeen, B. Carter, and S. W. Hawking, The four laws of black hole mechanics, *Commun. Math. Phys*., 31(2), pp. 161–170 (1973).
126. S. W. Hawking, Black hole explosions, *Nature*, 248 (5443), pp. 30–31(1974).
127. S. W. Hawking, Black holes and thermodynamics, *Phys. Rev. D*, 13(2), pp. 191–197 (1976).
128. J. D. Bekenstein, Black holes and entropy, *Phys. Rev. D*, 7(8), pp. 2333–2346, (1973).

129. R. M. Wald, Black Holes and Thermodynamics, *Black Holes and Relativistic Stars*, R. M. Wald, ed., University of Chicago Press, Chicago, IL, pp. 155–176, 1998.
130. G. ‘t Hooft, On the quantum structure of a black hole. *Nucl. Phys. B*, 256, pp. 727–745 (1985).
131. D. Grumiller, R. McNees, and J. Salzer, Black Hole Thermodynamics: The First Half Century, *Quantum Aspects of Black Holes*, X. Calmet, ed., *Fundamentals of Theoretical Physics* 178, Springer, Switzerland, 2015.
132. C. E. Shannon, The mathematical theory of communication, *Bell System Tech. J.* 27, pp. 379-423 and 623-656 (1948).
133. S. H. Sohrab, Some implications of a scale invariant model of statistical mechanics to transport phenomena, ICS'09: Proceedings of the 13th WSEAS international conference on systems, July 2009, pp. 557-568.
134. A. M. P. Dirac, The evolution of the physicist's picture of nature, *Sci. American* 208, 45, (1963).
135. G. ‘t Hooft, *In Search of the Ultimate Building Blocks*, p. 161, Cambridge University press, 1998.
136. A. Bonaca, and D. W. Hogg, The information content in cold stellar streams arXiv:1804.06854v1 [astro-ph.GA] 18 Apr (2018).
137. A. H. W. Küpper et al, Globular cluster streams as galactic high-precision scales--The poster child Palomar 5, *The Astrophysical J*., 803:80 (26pp), April 20 (2015).
138. S. Banach, and A. Tarski, Sur la d´ecomposition des ensembles de points en parties respectivement congruentes. *Fund. Math.* 6, 244-277 (1924).
139. E. Nelson, Warning Signs of a Possible Collapse of Contemporary Mathematics, in: *Infinity, New Research Frontiers*, M. Heller and W. Hugh Woodin (eds.), Cambridge University Press, 76-85, 2011.
140. H. Poincaré, *Science and Hypothesis*, Dover, New York, 1952, p. 65.

D-entropy in classical mechanics

V.M. Somsikov

Al-Farabi Kazakh National University, Almaty, 050040, Kazakhstan.
(E-mail: vmsoms@rambler.ru)

Abstract. The work is devoted to a new concept in physics - D entropy, defined as the relative increment of the internal energy of a body due to its energy of motion. D-entropy arises due to taking into account the role of the body structure in its dynamics. It follows from the body's motion equation, which is derived based on the principle of dualism of symmetry (PDS). According to the PDS, the evolution of bodies is determined by both the symmetry of space and the symmetry of the body. According to the PDS, the motion equation is derived from the expression of energy, which is the sum of the body's internal energy and the energy of its motion. Such a representation of energy is carried out in micro- and macro-variables that determine the movements of the elements of the body and the body itself, as a whole, respectively. This made it possible to take into account bilinear terms in the body's motion equation, which depend on micro- and macro-variables, arising when the body moves in an inhomogeneous field of forces, and determining the transformation of its energy of motion into internal energy. The D-entropy for large equilibrium systems, like the Clausius entropy, only increases. For small systems, the D-entropy can decrease. The main advantage of D-entropy is that it is determined through the dynamic parameters of the body. This makes it possible to use it to study the processes of evolution of matter within the framework of the fundamental laws of physics, as well as to substantiate the empirical laws of thermodynamics, statistical physics and kinetics.
Keywords: entropy, symmetry, nonequilibrium, evolution, mechanics.

---

1. Introduction

Entropy is a key concept for all natural sciences. Historically, the concept of entropy arose phenomenologically in thermodynamics because when performing work with a body, part of it, one way or another, from the point of view of useful work, is lost [1, 2, 11]. In statistical physics, there is the following modern definition of entropy [11]: "Entropy is a quantity that characterizes the average properties of a body over a certain nonzero period of time". Today the existing concepts of entropy face common difficulties. Perhaps the main one is that its connection with the fundamental laws of physics has not been fully disclosed. Therefore, it is difficult to answer the following questions: how does the entropy of a body change when it moves in an inhomogeneous external force field; how entropy is related to the symmetry of the body and space; how, while remaining within the framework of the laws of classical mechanics, to explain the concept of entropy. These difficulties create problems in using the concept of entropy in physics, for example, when constructing an evolutionary picture of the world. Some of these difficulties can be removed with the help of the definition of D-entropy, recently proposed within the framework of the laws and principles of classical mechanics. D-entropy was defined as the ratio of the increment in the internal energy of a body, due to its movement in an external nonhomogeneous force field, to its total value. The definition of D-entropy emerged from the search for a solution of the irreversibility problem within the framework of the laws of classical mechanics [3, 4].

The purpose of this work is to consider the physical essence of the concept of D-entropy. To do this, the following questions will be considered here: how the solution to the problem of describing dissipative processes was obtained within the framework of the laws of classical mechanics; how D-entropy follows from the motion equation of structured particles; how D-entropy is related to the second law of thermodynamics; how the recurrent form of D-entropy in hierarchy of open nonequilibrium dynamical systems was obtained.

2. Dissipative equation of the system's motion

The definition of D-entropy follows from the system's motion equation of potentially interacting material points, which takes into account the role of the internal dynamics of the system's elements in its motion [3]. Therefore, in order to explain the essence of D-entropy, let us briefly explain how this motion equation was obtained.

According to classical mechanics, built based on the Newton's motion equation, the dynamics of matter must be reversible. However, all processes in nature are dissipative and therefore irreversible. This contradiction leads to an important problem for physics: how to explain the irreversibility of the dynamics of bodies, if Newton's equation of motion is reversible [5, 6]. At the beginning of solving this problem, a probabilistic mechanism of irreversibility was discovered [5]. A necessary condition for the occurrence of this irreversibility is the presence of arbitrarily small random external influences on the system. Therefore, let us call this mechanism probabilistic. However, this mechanism did not allow answers many questions. For example, how the second law of thermodynamics relates to the fundamental laws of physics; how "order" arises from "disorder", etc. Therefore, further searches for a solution to the problem of irreversibility, but strictly within the framework of the basic laws of physics, were continued.

Our search for a solution to this problem began with the derivation of the motion equation of a structural particle in the framework of the laws of classical mechanics without any restrictions, which were used to obtain the Lagrange and Hamilton equations [3]. The main idea of such a solution to the problem of irreversibility was to try to take into account the role of the body structure in its dynamics. Obtaining this equation was carried out based on fundamental laws and principles that apply both to the system and to its elements. These laws and principles include the laws of conservation of energy and momentum, Galileo's principle. But since we considered the motion of a structured body, instead of a material point, in addition to these principles, ***the principle of symmetry dualism*** was used. This principle claims that *the motion of the structured bodies is defined not only by the space symmetry, as in case of a material point, but also by the body's internal symmetry*. This approach to obtaining the system's motion equation has fully justified itself. As a result, the system's motion equation were found and the explanation of the mechanism of irreversibility that followed from this equation were submitted [3]. Below we will briefly explain how the motion equation for a system from material points was obtained. It will help explain how the concept of entropy emerges within the strict laws of classical mechanics.

In accordance with statistical laws, the motion of a body, taking into account friction, is described by an equation in which the friction forces are proportional to the velocity [11]:

$$M\dot{V}_0 = -F_0 - \mu V_0, \tag{1}$$

where M -is the body's mass, V_0 - is the velocity of the center of mass, - F_0 - is the force acting on the center of mass, μ - is the effective coefficient of friction.

In accordance with this equation, the energy of the body's motion is converted into

the internal energy of the relative motion of its elements. This result is achieved within the framework of the laws of statistics that govern the molecular kinetic theory [11]. Let us show how one can explain the mechanism of transformation of the motion energy into the internal energy of the body, taking into account the role of the structure of the body in its movement [8, 9].

Consider the motion of a body along an inclined rough surface under the action of gravity. For this purpose, we take a body model as an equilibrium system consisting from a sufficiently large number of potentially interacting material points.

At the initial moment of time, the equilibrium system has potential energies. During the sliding of the body, part of potential energy is converted into its kinetic energy. Another part goes to increase the internal energy because of the work of the friction force. This means that each material point of the body participates in two types of motion: in motion together with the center of mass of the system and in motion relative to its center of mass. Therefore, *the invariant of motion is the sum of the motion energies and the internal energy of material points*. *Dissipation is associated with a part of the system's motion energy, which is converted into its internal energy*. Thus, if we want the system's motion equation to describe dissipative processes, it is necessary that it take into account the transformation of the motion energy into internal energy. Below we will show how to do this.

The total energy of the system can be represented as the sum of the energy of motion and internal energy using two groups of variables [3]. The group of variables that determine the internal energy are called micro-variables. The group of variables that determine the system's motion energy are called macro variables. The key point for the possibility of representing the system's energy in the form of this sum is that the following equality holds for the scalar sum of quadratic functions of vectors [3]:

$$N\sum_{i=1}^{N} v_i^2 = NM_N V_N^2 + \sum_{i=1}^{N-1}\sum_{j=i+1}^{N} v_{ij}^2 \qquad (2)$$

The vector v_i determines the velocity of the material point in the laboratory coordinate system; $i, j = 1,2,3...N$ - numbers of material points where the values i, j run from 1 to N and $i \neq j$; $v_{ij} = v_i - v_j$; vector $V_N = (\sum_{i=1}^{N} v_i)/N$ is the velocity of the system's center of mass; $M_N = Nm$; $m = 1$, and therefore $M_N = N$; $U_N^{ins}(r_{ij}) = \sum_{i=1}^{N-1}\sum_{j=i+1}^{N} U_{ij}(r_{ij})$ - is a potential energy of interaction of the material points, where $r_{ij} = r_i - r_j$.

The existence of this equality proves the independence of micro- and macro variables [3]. The total energy in these variables is decomposed into the system's internal energy and the motion energy. That is, micro- and macro-variables belong to two symmetry groups.

The coordinate system in which the total energy is presented according to eq. (2), we will call the *dual coordinate system*. In these variables, the system's energy has the form:

$$E_N = E_N^{tr} + E_N^{ins} = const \qquad (3)$$

Here $E_N^{ins} = T_N^{ins} + U_N^{ins}$ - is the system's internal energy, where $T_N^{ins} = \sum_{i=1}^{N} m\tilde{v}_i^2/2$ is the kinetic component of internal energy; $E_N^{tr} = T_N^{tr} + U_N^{tr}$ - is the motion energy,

T_N^{tr} - is the system's kinetic energy, depending on the macro-variables, U_N^{tr} - is the system's potential energy in the field of external forces.

In a dual coordinate system, the internal energy is determined by micro-variables. This is because the sum of the energies of the relative motions of material points and the energy, determined by the sum of the kinetic energies of their motion relative to the center of mass, coincides. The body's motion energy is associated with a group of macro-variables. The energy of motion of a system is characterized by the fact that the sum of the impulses of its elements is equal to the total impulse of the system, but the internal energy of the system is characterized by the fact that the sum of the impulses of all elements is equal to zero. *The law of conservation of energy of a system is that the sum of the energy of motion of the system and the internal energy is invariant along its trajectory, but each of these types of energy is not an invariant of motion.*

The system's motion equation follows from the eq. (3) by differentiating in relation to time, and then by summing scalar values of energy changes for each material point. It has the form [8, 9]:

$$M_N \dot{V}_N = -F_N^0 - \mu V_N, \tag{4}$$

where $F_N^0 = -\sum_{i=1}^{N} F_i^0$; F_i^0 - is external force acting on the $\dot{i}$ -th material point; $\mu = \dot{E}_N^{\text{int}} / (V_N^{max})^2$; F_{ij} - is the strength of interaction $\dot{i}$ and j material points; $F_{ij}^0 = F_i^0 - F_j^0$; $\dot{E}_N^{\text{int}} = \sum_{i=1}^{N-1} \sum_{j=i+1}^{N} \tilde{v}_{ij} (m\tilde{\dot{v}}_{ij} + F_{ij}^0 + NF_{ij})$; $V_N^{max} + \dot{E}_N^{\text{int}} / F_N^0 = 0$.

The eq. (4) already takes into account the relationship between the body's motion energy and it internal energy during the motion of the system.

In the right hand side of eq. (4), the first term determines the external forces, which applied to the center of mass. These potential forces change the system's velocity.

The second term is nonlinear and bisymmetric, because it depends simultaneously from micro- and macro-variables. This term defines the role of the structure of a system in its dynamics. The coefficient "μ" determines the fraction of the system's motion energy, which is transformed into internal energy. The work of external forces spent on increasing internal energy is nonzero only when we have: $F_{ij}^0 = F_i^0 - F_j^0 \neq 0$, or when the field of external forces is non-homogeneous.

The second term was call as the *evolutionary nonlinearity*, because this term links two symmetry groups, which depended from of micro – and macro-variables and leads to a violation of the time's symmetry and evolution [10].

The nature of the evolutionary nonlinearity can be explained by that that due to the non-homogeneity of the external field of forces, the linking of the vectors from the different symmetry groups is appeared. For the structured bodies these groups of body's symmetry and space symmetry. The linking is determined by bilinear evolutionary nonlinearity terms. These terms is determine the conversion of the body's motion energy into its internal energy. It is lead to a violation of the conservation of motion energy, when total energy is preserved. Thus, *the bilinear terms arise when a body moves in an external non-uniform force field*. An example of inhomogeneous external forces is an inhomogeneous external gravitational field in which the objects of the Universe move. It leads to the transformation of the energy of motion of these objects into their internal energy as a result of the work of forces proportional to the gradients of external fields. This effect can be called "gravitational friction". "Electromagnetic friction" can be defined in a similar way.

In the cases of homogeneity field of the external forces or in approximation of a solid body, this term is equal to zero and eq. (4) becomes the Newton's motion equation.

The dynamics of an equilibrium system in a weak inhomogeneous field of external forces is irreversible [3, 8]. Indeed, in accordance with eq. (4), the magnitude of the change in the internal energy is of the second order of smallness. Therefore, the disturbance of equilibrium of the system can be neglected. However, according to Galileo's principle, the motion energy of an equilibrium system cannot increase due to internal energy. Consequently, we have a decrease in the motion energy of an equilibrium system along its trajectory in an inhomogeneous space.

The existence of dissipation is a necessary condition for formation of attractors [20]. However, the dissipation is possibly only for the structured bodies. The conclusion about the infinite divisibility of matter is following from here [9]. This means that according to the laws of classical mechanics, the matter should be an infinite hierarchy of systems. That is, any arbitrarily small selected part of the body is a system of elements.

According to eq. (4) the efficiency of increasing the internal energy of the system is determined by the ratio of its increment to the value of the internal energy itself. That is, we have [4]:

$$\Delta S_N^d = \Delta E_N^{\text{int}} / E_N^{\text{int}} \tag{5}$$

Here S_N^d - is a D-entropy for system from N elements. This expression was called D-entropy [4]. The symbol "D" was introduced because this entropy determines the measure of the transformation of the ordered energy of motion of the system into the chaotic motion energy of its elements relative to the center of mass of the system.

Below it will be briefly explained how the D-entropy is determined for an open nonequilibrium dynamical system, what are the properties of D-entropy and what is the relationship between D-entropy and existing definitions of entropy.

D-entropy for nonequilibrium systems

A description of the evolutionary processes of matter is impossible without taking into account the fact that all bodies in nature to one degree or another are open nonequilibrium dynamic systems. The nature of such processes is determined by D-entropy, which determines the relationship of external influences on the system with its internal structure in according with the eq. (4).

It turned out that when a sufficiently small system moves in inhomogeneous fields of external forces; its internal energy could either increase or decrease. For example, calculations showed that for an oscillator with N=2 which in motion in an inhomogeneous field of external forces, internal energy can transformed into the motion energy depending on the initial phase of its oscillation and D- entropy can be negative [13]. However, with an increase of the number of particles in the system, the part of the internal energy that can be transformed into the system's motion energy is decreasing. When $N_1 > 100$, the internal energy could only increase and we have: $\Delta S_N^d > 0$. For $N_2 > 10^3$ the increment of internal energy growth do not increase [14]. Thus, $N_2 \sim 10^3$ determines the range of applicability of the thermodynamic description for the system. In the general case, these critical numbers depend on the parameters of the task. This is in consistent with [2] where stated, that the irreversibility is qualitative: the more particles in the system, the more irreversibly it behaves (that is, the more unlikely reversibility). Thus, D-entropy allows us to determine the area of applicability of thermodynamics based on the laws of classical mechanics.

In the approximation of local thermodynamic equilibrium, with a sufficient degree of generality, a nonequilibrium system can be submitted by a set of equilibrium subsystems moving relative to each other [11]. The motion of each subsystem is equivalent to its motion in an inhomogeneous field of forces, created by all other subsystems. When a system is in equilibrium, the relative velocities of its subsystems and the resulting forces acting from other subsystems are zero [15]. If to take the system closed, prepared in a nonequilibrium way, then its total energy is invariant value. In this case, the change of the D-entropy for system is determined by the sum of the increments of the entropies of each subsystem. Therefore, we have [17]:

$$\Delta S_N^d = \Delta E_N^{\text{int}} / E_N^{\text{int}} = \sum_{L=1}^{a} \left\{ N_L \sum_{k=1}^{N_L} [\int \sum_s F_{ks}^L v_k dt] / E_L \right\} \tag{6}$$

E_L - is internal energy of *L*- subsystem; F_{ks}^L -is a force, acting on the k-th particles of the subsystem from the side of the particles of the other subsystems; S - is external particles with respect to L - subsystem, interacting with its k-i particles; v_k -is a speed of the *i*-th particles; N_L – is a number of particles in L - subsystems; L =1,2,3…; a – is a number of subsystems in nonequilibrium system.

The calculations showed that the magnitude of the fluctuations of the system's internal energy due to changes of number of particles, obeys the law [14]:

$$\delta E^{tr} \sim 1/\sqrt{N} . \tag{7}$$

Since statistical laws follow from calculations of the dynamics of systems based on deterministic equations, it can be argued that they follow from the deterministic laws of physics. A similar conclusion was made in [16]. This is also confirmed by the fact that the principle of maximum entropy corresponds to the principle of least action [17]. It follows that the fundamental laws of physics determine the field of application of statistical laws, and these laws can be considered as possible simplifications of the analysis of the dynamics of systems [18].

The proof of equilibrating closed non-equilibrium dynamical systems can be reduced to the proof that the energy of the relative motions of subsystems is irreversibly transformed into their internal energy. Let us show that in accordance with eq. (4) such a transformation takes place. This can be done by assessing the energy flows between subsystems [3].

Obviously, for a non-equilibrium system consisting from equilibrium subsystems, the mechanism for the formation of direct and reverse energy flows for subsystems is associated with the mutual transformation of the energies of the relative motions of the subsystems and their internal energies. Consequently, the proof of the irreversibility of a nonequilibrium system is reduced to the proof that the inflow of internal energy of the subsystems is greater than the outflow.

Let us ΔE^{tr} is the energy of the relative motion of the subsystems, which is transformed into its internal energy. According to eq. (4), ΔE^{tr} is determined by a bilinear term whose value is equal to the second order of smallness. Let us notice that the value ΔE^{tr} is also a second order of smallness in according with the statistical estimations of an increment of entropy [11]. Therefore we can write: $\Delta E^{tr} \sim \chi^2$, where χ is a small parameter, for example, the ratio of the internal forces between material

points and value of external forces. If it so, then $\Delta E^{tr} / E^{\text{int}} << 1$ and the violation of the equilibrium of the subsystems can be neglected. In this case, irreversibility takes place, since the transformation of the internal energy of the subsystem into the energy of its motion is impossible due to the law of conservation of momentum.

Let us consider the second case. If the equilibrium subsystems' interaction forces or their gradients are the great enough, the equilibrium of the subsystems can be disturbed. Then the subsystems can be represented as a set of equilibrium systems moving relative to each other. In this case, to increase the internal energy of the subsystems, one can write: $\Delta E^{tr} = \Delta E^{tr}_{ins} + \Delta E^{h}$, where ΔE^{tr}_{ins} is the increment of the energy of the relative motions and ΔE^{h} is the increment of the internal energies of the subsystems.

That is, $\Delta E^{tr}_{ins} < \Delta E^{tr}$. The energy of the equilibrium subsystems cannot be transformed into their motion energy. Therefore, we will proceed from the fact that only the energy of the relative motions of sub-subsystems can be transformed back into the motion energy of the subsystems. Let us denote such a reverse flow of the subsystems internal energy, as: ΔE^{tr}_{ret}.

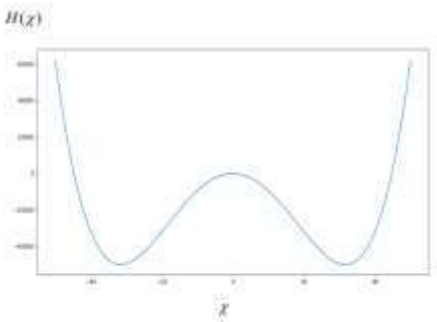

According to eq. (4), the value ΔE^{tr}_{ret} is determined by the bilinear function of the sub-subsystems variables, which determined its motion energies and the internal energies.

Figure. 1. The graph of the formula 8.

These are terms of the second order of smallness of their micro - and macro variables. But because: $\Delta E^{tr} \sim \chi^2$, we will have that $\Delta E^{tr}_{ret} \sim \chi^4$. Thus, the return flow of the internal energy of subsystems into the energy of its motion cannot be more than the fourth order of smallness. The decrease in the energy of motion of the subsystems can be determined by the following equation:

$$\Delta E^{tr}_{dec} = \alpha\chi^2 - \beta\chi^4 \tag{8}$$

and we have:

$$\Delta S^{d} \sim \Delta E^{tr}_{dec} / E_{\text{int}} \tag{9}$$

Here the α, β constants can be determined using of the eq. (4), S^{d} -D-entropy.

Fig. 1 shows a graph of ΔE^{tr}_{dec}. For values: $|\chi| \prec \chi_0$, where $\pm\chi_0$ are the roots of eq. (10), the irreversibility takes place. In general, for $N >> 1$, we have $\Delta E^{tr}_{dec} > 0$. This corresponds to the second law of thermodynamics. For the stationarity of the system it is necessary to fulfill the equality: $\Delta E^{tr}_{dec} = 0$. However, this state is unstable and determined by micro variables [17].

Thus, the concept of D-entropy arose in the mechanics of structured particles, which operates with the total energy of the system, including the system's motion energy. In this mechanics, internal energy is defined, as the energy of motion of the system's elements relative to the center of mass. Thus, the work of external forces, acting on the system, is

divided into mechanical work to move it and work to change its internal energy. The energy of the relative motion of interacting subsystems due to the presence of gradients of external forces can pass into their internal energy, but the reverse process is forbidden by the Galilean principle, since the momentum of the system cannot change due to its internal energy.

D-entropy is valid for any equilibrium and nonequilibrium systems from any number of elements. At its determination, the absent of the interaction between subsystems was not required, as it is required in the case of statistical physics [11]. However, the interaction energy of subsystems, which is not taken into account in statistical physics, determines the processes of evolution of systems.

In thermodynamics, in contrast to the mechanics of structured particles, the concept of internal energy is defined as the total energy of a system minus its motion energy. Therefore, Clausius entropy are a special case of D-entropy.

D-entropy in quantum mechanics is defined in the same way as in classical mechanics in the form of the ratio of the change in the internal energy of quantum systems to its value. D-entropy follows from the expanded Schrödinger equation obtained from the principle of dualism of energy [21].

The entropy for open non-equilibrium systems can be obtained also with a help of distribution function. This function, $f_a = f_a(r, p, t)$, is found using the extended Liouville equation, which has the form [19]:

$$\frac{df}{dt} = \frac{\partial f}{\partial t} + \sum_{i=1}^{N} (\dot{R}_i \frac{\partial f}{\partial R_i} + P_i \frac{\partial f}{\partial P_i}) = -f\sigma \tag{10}$$

Here $i = 1,2,3 \ldots N$ - is a number of subsystem, $\sigma = \sum_{i=1}^{N} \frac{\partial}{\partial P_i} F_i$, F_i - is a forces acted on the i-th subsystems, P_i - is a momentum of the subsystem.

Extended Liouville eq. (10), which can be used to describe open nonequilibrium dynamical systems, was obtained using eq. (4). This equation, given on the phase plane of coordinates and momenta of a system of structured particles, differs from the canonical prototype in that the phase volume of the system is not conserved due to the openness of the system.

From eq. (10), it follows that only non-potential forces contribute to the change in the distribution function of particles of the system. In accordance with eq. (4), the magnitude of the change in the distribution function is proportional to the gradients of potential internal and external forces. For a closed non-equilibrium system, the value of "σ" decreases with a decrease in the energy of the relative motions of the subsystems due to its transformation into the internal energy of the subsystems [9].

Formal solution of the eq. (10) can be written like this:

$$f = f^o \exp \int (-\sigma) dt \,. \tag{11}$$

The generality of the distribution function (11) lies in the fact that it was obtained taking into account the work of dissipative forces. That is, this distribution function directly follows from the motion equation of structured particles. Therefore, it can be used to analyze dissipative systems.

It is known that for entropy can be wright [11]: $S^B = -\int f \ln f dpdq$. From here and eq. (10), we can obtain:

$$dS^B / dt + \sigma S^B = f\sigma \tag{12}$$

Thus, if $\sigma = 0$, then we have: $dS^B / dt = 0$. Thus, "S^B" has a maximum when the subsystems do not have relative speeds. This corresponds to the equilibrium system' state of the.

D-entropy "S^d" is more general than "S^B". This is due to the fact that "S^d" is acceptable for describing the evolution of open nonequilibrium dynamical systems moving in inhomogeneous fields of external forces, without using averaging any statistical hypothesize.

D-entropy for open nonequilibrium dynamical systems

The emergence and existence of all objects in nature is possible only due to dissipative processes as a result of the interaction of bodies, the exchange of energy, momentum and matter [20, 22]. Therefore, to describe evolutionary processes, it is necessary to take into account the openness of bodies. In addition, it must be borne in mind that dissipative processes arise only if the bodies, as well as their elements, have a structure. Hence it follows that matter must be infinitely divisible [9]. The infinite divisibility of matter or the impossibility of the existence of bodies with zero internal energy follows from the mechanics of structural particles. That is, if all bodies possess all these properties and have arisen as a result of evolution, then they must be open nonequilibrium dynamical systems. The idea that the main element of matter is open nonequilibrium dynamical systems was also expressed in [17, 22]. Then *matter is a hierarchy of open nonequilibrium dynamical systems*. One way or another, the model of the body, as an open nonequilibrium dynamical system, should be used to study the processes of self-organization of systems, the emergence of "order" from "chaos" and evolution [9]. To cover general qualitative properties of the structure and dynamics of matter, the chain of the structure of matter can be written as [9]:

Material point's $\Rightarrow$ *structural particles* $\Rightarrow$ *open nonequilibrium dynamical systems*.

Therefore, according to the principle of symmetry dualism, to describe the dynamics at all hierarchical levels of the structure of matter its energy should be represented as the sum of the motion energy and internal energy.

The change in D-entropy at an each hierarchical level consists of the increments of the energies of motion and internal energies for the constituent parts of this level. These increments are carried out due to the energy of the external hierarchical level.

Let us assume that the system is near a stationary state. In this case, dissipative processes within the hierarchical levels can be neglected. Let outside forces begin to work on the system. According to the principle of dualism of energy, this will lead to a change in the energy of motion and internal energies of the elements of the first hierarchical level. Their change, in turn, will lead to a change in the energy of the second hierarchical level, and so on. It can be written like this [9]:

$$\Delta E_0 = \Delta E_1^m + \Delta E_1^{in};\ \Delta E_1^m = \Delta E_2^m + \Delta E_2^{in};\ldots \qquad \Delta E_{N-1}^m = \Delta E_N^m + \Delta E_N^{in}. \tag{13}$$

$$\Delta S_i^d = \Delta E_i^{in} / E_i^{in} \tag{14}$$

Here ΔE_0 -the work of the external energy; the energies of the corresponding hierarchical levels of matter consist of the sum of the energies of motion of elements and their internal energies, denoted by the symbols "m" and "in", respectively.

The eqs. (13, 14) are chains of energy and D-entropy increments for all hierarchical levels of matter due to the work of external forces. These equations can be called the

principle of relativity of energy and D-entropy for the steps of the hierarchical ladder of matter. The motion equation for open nonequilibrium dynamical systems can be obtained from its energy [9].

However, due to nonequilibrium of the internal dissipative processes also determine the state of the system. These processes lead to a decrease in the motion energy of elements of a given level due to its transformation into their internal energy. As a result, the change in the motion energy at each hierarchical levels can be determined by the condition:

$$\delta E_i^m = \Delta E_i^m - \Delta E_i^{dis} \tag{15}$$

The quantity $\Delta W_i^{ND} = \delta E_i^m / E_i^{in}$ we will call *D- negentropy*. Thanks to "ΔW_i^{ND}" , an open nonequilibrium dynamic system can be in a stationary non-equilibrium state. This state takes place when for each hierarchical level of the system the next equality have a place:

$$\delta E_i^m = 0 \tag{16}$$

Of course, not all the factors that determine the stationary state of the system are taken into account here. For example, an external influence on a system can directly affect several hierarchical levels of matter. For example, in the case of a flow of solar radiation to the earth. The spectrum of this flow is wide enough change to directly the state of terrestrial matter at many of its hierarchical levels [24]. However, the nature of such an impact always obeys the principle of symmetry dualism. Moreover, the positive flux of entropy can be compensated by the Planck radiation [12]. However, a complete description of the energy balance goes beyond the scope of classical mechanics.

3.Conclusions

The concepts of **entropy** and **energy** play a key role in all areas of natural science. Their complementarity, unity and opposition becomes clear if we start from the **principle of dualism of symmetry**. Energy determines the measure of possible useful work, the measure of the organization of the system. Therefore, it is logical to associate it with the concept of "**Order**". Entropy defines internal energy. It is logical to associate this with the measure of "**Chaos**". Through "Chaos», nature has found a way to combine two opposite concepts - movement and rest. "Chaos" ensures the existence of bodies at rest, if their elements are constantly in motion. This is possible because the total impulse of the elements can be equal to zero. Consequently, "Chaos" personifies the disappearance of motion or "Order" as a result of the disappearance of the energy of "Order", turning into the energy of "Chaos". Entropy is at its maximum when the system is in equilibrium.

The concept of D-entropy in classical mechanics follows from the motion equation of structured bodies. The physical meaning of D-entropy is that it determines the efficiency of dissipative transformation of the motion energy into the internal energy. The body's motion equation is derived from the energy of the body based on the principle of dualism of symmetry. According to this principle, the evolution of bodies is determined by both the symmetry of space and the symmetry of the body. In accordance with this principle, the body's energy is represented as the sum of the internal energy of the body and the motion energy in the space of micro-variables and macro-variables, respectively.

The derivation of the body's motion equation based on the principle of dualism of symmetry made it possible to take into account the dissipative processes of transformation the body's motion energy into internal energy. This transformation is determined by the bilinear terms of the motion equation of the body. Dissipation occurs when a body moves in an inhomogeneous field of forces.

Mathematically, D-entropy is due to the nonlinear interaction of micro- and macro-variables. The description of the dynamics of the body based on micro- and macro-variables is called “complete description”. It is called complete, because it takes into account the role of the internal dynamics of the elements of the body on its dynamics as a whole. "Complete description" connects the violation of time-symmetry with a change in the internal states of systems due to their motion energy.

D-entropy reveals the physical essence of entropy for open nonequilibrium dynamical systems. The need for such a representation of the body’s model is because only it allows one to take into account and describe the processes of their evolution.

D-entropy is applicable for bodies with a large and small number of elements. For large equilibrium systems, it goes over into the Clausius entropy. For small systems, D-entropy, unlike all other concepts of entropy, can decrease.

Since the D-entropy is obtained from the fundamental equations of physics, it can be used to analyze the nature of evolution of systems and to substantiate empirical branches of physics based on a "complete description" of the dynamics of systems within the framework of the laws of classical mechanics. In addition, it can be used to define the scope of statistical and empirical concepts of entropy.

In general, the D-entropy is convenient when studying the processes of evolution of matter within the framework of the fundamental laws of physics, presented in the form of a hierarchy of open nonequilibrium dynamical systems.

Acknowledgements

The work was carried out with the financial support of the Committee of Science of the Ministry of Education and Science of the Republic of Kazakhstan grant project AP09259554.

References

1. J. L. Lebowitz. Boltzmann’s entropy and time’s arrow, Phys. Today, 46, 9{32, 1993.
2. R. Penrose. The path to reality or the laws governing the universe. Full guide. Moscow, Izhevsk, 2007.
3. V.M. Somsikov Deterministic mechanism of irreversibility. JAP,**14**,5708{5733,2018.
4. V.M. Somsikov. The Dynamical Entropy. Intern. Journ. of Sci.**, 4**, 30{36, 2015.
5. G.M. Zaslavsky Stochasticity of dynamical systems. Moscow, Nauka, 1984.
6. I. Prigogine. From Being to Becoming, Nauka, Moscow, 1980.
7. L.D. Landau, E.M. Lifshits. Physical kinetics. Moscow, Nauka, 1979.
8. V.M. Somsikov. Transition from the mechanics of material points to the mechanics of structured particles. Modern Physics Letter B. 4, 1{11, 2016.
9. V. M. Somsikov. The Irreversibly Mechanics of the Structured Particles Systems, 2nd Chaotic Modeling and Simulation International Conference, Chania, Greece, 1{6, 2009.
10. V.M. Somsikov. Non-Linearity of Dynamics of the Non-Equilibrium Systems, World Journal of Mechanics, 2, 7, 11{23, 2017.
11. L.D. Landau, E.M. Lifshits. Statistical Physics. Moscow, Nauka, 1976.
12. Y. B. Rumer, M. S. Rivkin. Thermodynamics. Stat. phys. and Kinetics. Moscow, Nauka, 1977.
13. V. M. Somsikov, A. Mokhnatkin. Non-Linear Forces and Irreversibility Problem in Classical Mechanics, Journal of Modern Physics, 5, 1, 17{22, 2014.
14. V.M. Somsikov, A.B. Andreev. On the criteria for the transition to a thermodynamic description of the dynamics of systems. Izv.Vuzov. Phys. series. 7, 30{39, 2015.
15. L.D. Landau, E.M. Lifshits. Statistical Physics, Moscow, Nauka, 1976.

16. F. Baldovin, L.G. Moyano, C.Tsallis Boltzmann-Gibbs thermal equilibrium distribution descends from Newton laws: A computational evidence. arXiv:cond-mat/0402635 v1 25Feb 2004.
17. V.M. Somsikov.To the basics of physics evolution, Almaty, Nauka, 2016.
18. V. Famourzadeh, M.Sefidkhosh. Straddling between determinism and randomness: Chaos theory vis-à-vis Leibniz. arXiv:1909.13635v1 [physics.hist-ph] 30 Aug 2019.
19. V.M.Somsikov.The equilibration of a hard-disks system, IJBC, **14**, 4027{4033,2004.
20. A. Yu Loskutov, A.S. Mikhailov Introduction to Synergetics. Moscow, Nauka, 1990.
21. V.M. Somsikov. Limitation of classical mechanics and ways it's expansion. PoS (Baldin ISHEPP XXII-047). September JINR, Dubna, 1{12, 2014.
22. Yu.L Klimontovich. Introduction to the physics of open systems. Moscow, Janus, 2002.
23. V.M.Somsikov. From the laws of classical mechanics to the laws of thermodynamics. Eurasian Physical Technical Journals, 14, 4{9, 2017.
24. A.B. Andreev, V. M. Somsikov, S.N. Mukasheva et all. Nonequilibrium Effects in Atmospheric Perturbations Caused by Solar Radiation Flux, Geomagnetism & Aeronomy, **58**, 106{112, 2018.

Chaotic Modeling and Simulation (CMSIM) : -

Meta-Theories and Scientific Reformation

Alexander V. Sosnitsky[1], Anatoly I. Shevchenko[2]

[1] Berdyansk State Pedagogical University, Berdyansk, Ukraine
(E-mail: sosnitsky.ukr@yandex.ua)
[2] Institute of AI Problems of the MES and NAS of Ukraine, Kiev, Ukraine
(E-mail: ipai.kiev@gmail.com)

Abstract: Modern science intensively develops various (pseudo-) universal meta-theories, consistently opening fundamentally new perspectives in many areas of knowledge in comparison with the gradually exhausting classical traditional approaches. However, even the simplest review points to their limitations and incomplete effectiveness, due to the systemic shortcomings of the modern general scientific paradigm, which undoubtedly must be replaced by more advanced developmental paradigms. 1) If historically the first ancient categorical-phenomenal paradigm gave birth to science, then 2) the modern classical (axiomatic, dogmatic) paradigm has improved it in certain particular subject areas, and 3) the next expected universal (met-) paradigm will presumably unite all knowledge into a single system 4) by increasing the level of abstraction until the achievement of a single initial Universal Axiom and meta-concepts derived from it, 5) which should be adequate for all phenomena and 6) form the ultimate Universal meta-theory, 7) resolving all the problems of scientific knowledge. 8) The presented work summarizes the authors' many years of research on this topic and 9) systematically sets out the main provisions of the meta-universalization of knowledge, 10) substantiates the theoretical and practical possibility of obtaining a single universal meta-formalism of the Universe and derivatives of meta-formalisms of phenomena, 11) describing all things let very complex, but a single universal formula. 12) The results of the work have been successfully applied to solve many chronic conceptual problems and 13) have a universal perspective in all areas. 14) Despite the initial state of the Universal Theory, 15) any of its applications are already radically changing the traditional ideas about the world around them, 16) especially complex chronically unknowable phenomena. 17) The ultimate meta-level of abstraction of universal concepts today is a necessary condition for the radical development of knowledge, 18) in which, undoubtedly, many teams of leading scientists should participate, like the scientific school of Bourbaki.

Keywords: Meta-theory, Modern science, Universal Theory, Harmony, Universal Cosmology, Multi-phase Universe, “Boiling” Universe hypothesis

1 Introduction

If justification (proof) is understood as 1) the derivation of concepts from other justified concepts, then 2) without additional conditions it is an infinite hierarchically recursive unsolvable process (cognition), 3) doomed to unfounded (hence erroneous) assumptions (hypotheses) and 4) unprovability of any universal concepts.

Received: / Accepted:

ISSN 2241-0503

Obviously, such a definition needs additional rules for the beginning / ending of such recursion, specific to our Universe.
Let us accept the following minimum sufficient for this concept of substantiation of universal concepts:
Definition. Justification (definition, proof) is a (justified) conclusion of a concept from other (justified) concepts.
Consequence. The rationale in this definition is an unsolvable infinite recursion that needs natural (Universal) specific conditions for its beginning / end.
Definition. Reasonable is a consistent conclusion of a concept (allowing connectivity with other internal / external concepts).
Definition. (Direct) inference is the composition (synthesis) of the formula (formalism) of the defined (output) concept from other (input) grounded concepts (Figure 1).

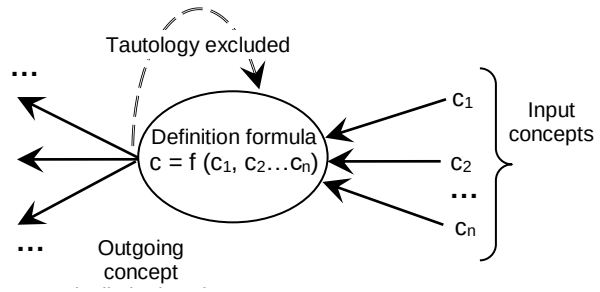

Fig. 1. Schema for the meta-definition of a concept

Consequence. The concept has 3 parts: 1) a set of input concepts, 2) a formula for the composition of a defined concept from input concepts, and 3) one output defined concept, which 4) can participate unrestrictedly in other derived concepts.
Consequence. An unambiguous conclusion of a concept is obtained in the absence of cycles 1) in its definition (the absence of a defined concept among the input concepts) or 2) the part of the concept system associated with it, which 3) is observed in nature and is accepted in this study.
Consequence. An ambiguous conclusion of the concept is obtained in the presence of such cycles that are not observed in nature.
Consequence. The absence of such cycles creates a unidirectional / hierarchy of the concept system.
Consequence. The definition of a concept is a directed relation of a set of input concepts to one definite concept (Figure 1).
Consequence. The use of a concept is a directed relation of one specific concept to a set of using concepts (Figure 1).
Consequence. An increase in the number of combinations with a direct derivation of concepts increases the system of concepts towards its unidirectionality with the predominant formation of its conical (pyramidal) shape with a complete enumeration of justified combinations.

Consequence. Direct direction / hierarchy of a system of concepts presupposes a reverse direction / hierarchy in the same system, which generates their reciprocal dualism.
Consequence. The reverse direction / hierarchy of the system of concepts converges to a certain single initial concept (the original Universal (meta-) Axiom (UA)), which generates all the Universal concepts and is present in each of them.
Consequence. Concepts have two mutually opposite directions of inference: 1) direct complicating (developing) concretization (from higher to lower concepts) and 2) reverse simplifying (reducing) generalization (from lower to higher concepts).
Consequence. The lower limit of (forward) recursion is a network of facts, the upper limit of (reverse) recursion is UA.
Consequence. Concretization is carried out through logical deduction, reasonably combining the concepts achieved in this case.
Consequence. Generalization is performed by logical induction, revealing embedded concepts.
Consequence. With adequate generalizations / concretization, the concepts coincide with the Universal categories and form a grounded formal system of concepts.
Next, we specify the above meta-justifications for our Universe:
Definition. A meta-concept is a concept of a concept.
Consequence. A concept is a meta-concept for all its concretizing concepts and 2) a concretizing concept for all its meta-concepts.
Definition. Definition is a direct (without intermediate meta-concepts) meta-concept of being, from which it begins in the system of universal concepts.
Definition. The axiom is the definition of the class of beings.
Definition. UA is the definition of the system of universal concepts (UAP).
Definition. Category is an active property of the Universe.
Definition. A concept is a copy of a category.
Definition. A link (copy) is a repetition of the components of one entity (object) in another entity (subject).
Definition. Existence is a part of the Universe, separated by some connection as a whole.
Definition. The universe is a complete set of directly or indirectly related entities.
Definition. The Universe is divided into two parts: Real (RW) and Categorical (Abstract) Worlds (AW).
Definition. Phenomenon is existence RW.
Definition. The category is the existent AW.
Hypothesis. Categories have a uniform constant formalization in the Universe.
Consequence. The concepts naturally have an approximate incomplete / inaccurate various formalization by different subjects.
Definition. Truth is the degree to which concepts approach categories.
Consequence. The absolute truth is the universe.
Hypothesis. Categories are the only means of formalizing the universe.

Definition. (Meta-) Theory is a system of grounded (meta) concepts.
Consequence. (Meta-) Theory is an approximate formalism of categories.
The presented meta-concept is the rationale for fundamental problem studies of this work, the purpose of which is to study the state and prospects of meta-theories in modern science on the example of a new universal general scientific paradigm.

2 Meta-theories and general scientific paradigms

New meta-concepts give rise to the corresponding meta-theories that make up the well-known history of world science. The first meta-theories arose in the ancient world at the birth of science through the initial meta-concepts, from where their name came from. From the works of Plato and his school came the first general scientific paradigm of the division of the Universe into RW / AW (Figure 2). Attempts at a scientific description of popular natural and humanitarian phenomena gave rise to the so-called metaphysical theories, naively explaining reality.

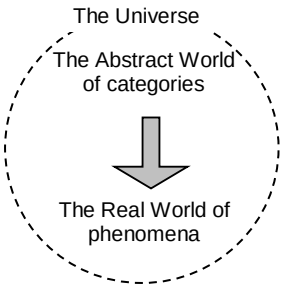

Fig. 2. Schema of the antique paradigm of knowledge

The Renaissance epoch up to the Middle Ages persistently expanded these concepts through empiricism, mathematical formalization and great discoveries plus well-known socio-political events of the 20th century, the conceptual peak of which was the axiomatic (dogmatic) paradigm of Bourbaki, which for the first time, as it seemed, built a single scientific meta-picture the world in the form of a system of highly abstract meta-axioms and multiple consequences from them (Fig. 3).

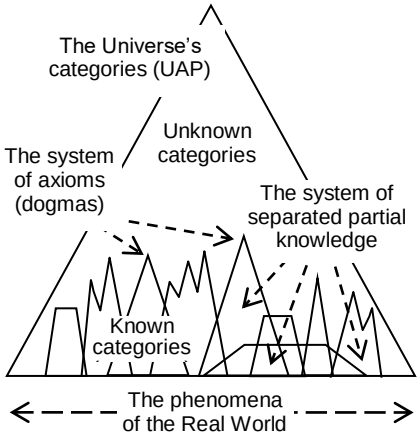

Fig. 3. Schema of the axiomatic (dogmatic) paradigm of knowledge

Axiomatization for the first time formalized knowledge, radically raised the level of abstraction of knowledge and created many high-quality technologies that continue to be improved to this day. But due to the well-known tautology of the invisibility of the unknown and the unknowability of the invisible, unexpectedly for modern science, it was unable to overcome the important chronically unsolvable meta-problems, which are briefly mentioned in the following review.

Based on the above substantiated provisions, one should increase the level of abstraction of problematic phenomena and achieve higher meta-concepts that solve the corresponding problems.

3 Achievements and problems of modern Meta-Theories

First of all, non-formalized important humanitarian, artistic and philosophical concepts that fall out of the strict norms of axiomatic science and thereby delegitize it as a product of exclusively intellectual activity do not reach the required meta-level. The verbal analogies used instead of them fundamentally do not allow formal analysis / synthesis / assessment of the corresponding phenomena.

Modern psychology, as the main subject of its activity, explores the higher physiological and intellectual problems of people, but is forced to use primitive empirical meta-models, which are fundamentally incomplete to explain complex phenomena in living organisms.

Medicine of the 21st century completes the basic questions of the physiology and pathology of living organisms at the biochemical and biological levels, but is unable to fully explain, synthesize, modify and apply the deciphered genetic codes in the corresponding meta-concepts, except for experimenting with ready-made parts of the codes.

Meta-formalization is most developed and applied in the exact sciences by means of the UML language, which contains a large set of particular axiomatic concepts, which, however, do not form a universal language for describing everything, since they are obtained empirically, but not ontologically, from a unifying VA.
Software engineering is developing a generalizing standard for the Meta-Object Facility language, which allows combining heterogeneous computer programs and platforms on the basis of a single type system that increases the degree of abstraction and application of the UML, which also has a private utilitarian focus, like other intensively developed ontological data analysis tools, in in particular, OntoClean, based on formal, domain-independent properties of classes and meta-properties of objects, etc.
Numerous formal semantics and translators of almost all existing natural and artificial languages have a long history, also focused on low-level meta-concepts that cannot be overcome in principle within the framework of the current private axiomatic general scientific paradigm.
All such numerous examples are naturally explained by Gödel's theorem on the emergence and growth of incompleteness of (partial) systems of logical equations (to which many phenomena are usually reduced) with an increase in their complexity, which gives rise to the ambiguity of the formalisms of phenomena and destroys private axiomatic knowledge into weakly interacting areas.
In principle, it is possible to get out of the conditions of this theorem and solve axiomatic problems only in the developing universal general scientific paradigm.

4 Meta-Theories and Cosmology

The original meta-concept justifies the following important directional consequences:
1. The Universe is self-determined and has an exclusively internal existence, which, as will be shown below, naturally develops into self-knowledge and further through living Classes into a grounded Universal Cosmology.
2. The Universe combines strict formalization and, as shown below, free uncertainty, jointly guaranteeing the realization of Universal Cosmology and the achievement of a strictly defined goal of Absolute Harmony / Absolute Nothing.
3. The Universe has a single Universal Meta-Formalism (UMF), which produces all kinds of Universal Formalisms of Private Universe Entities (UMFE) that govern the development of the Universe.
4. All emerging problems of Universal Cosmology are successfully overcome by consistent inner cognition and application of meta-concepts by the Universal phenomena up to VA.
5. Full cognition of VA corresponds to the Universal singularity (hereinafter defined as the Absolute Harmon), presumably completing the Universe.

6. As substantiated below, the Universe has a complex structure of a constructor of Universes, and combines multiple coexisting phases with different joint mechanics, where formalization is one of them.
7. Universal Cosmology and its stages / phases is of great importance in the knowledge of the Universe and, accordingly, in the development of science.
8. This concept justifies the following developmental (Universal) general scientific paradigm.

5 Universal general scientific paradigm

The limiting increase in the level of abstraction from the system of intermediate axioms to VA substantiates the universal system of concepts and the derivative formalization of phenomena as the next universal general scientific paradigm (Fig. 4).

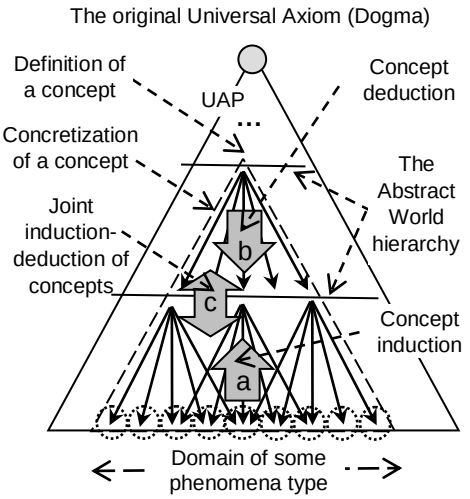

Fig. 4. Schema of the universal paradigm of knowledge

The universal paradigm loses the limitations of Gödel's incompleteness theorem with the transition from particulars to universal formalisms and uses the really established system of categories in the process of the evolution of the Universe instead of artificial concepts.
By definition, a universal paradigm is sufficient for a reasonable formalization of all Universe beings from a single UMF. The modern problem of the Universal Paradigm is the incompleteness of the universal system of concepts and the insufficient degree of formalization of UMF for a fully formal (automatic) derivation of universal formalisms of entities, which should be resolved like the collective work of the Bourbaki school.
If the partial axiomatic paradigm is based on the triad "observation - hypothesis - verification experiment" and is limited to the field of observation of phenomena, then the universal paradigm is based on the notebook "obtaining a

reasonable universal formalism (UV, which should always be a UMF) - identification of a phenomenon in the Universe - identification of a phenomenon in UV - deduction of the formalism of the phenomenon with UV ", which is limited by UV, which can exceed the field of view (Fig. 5).

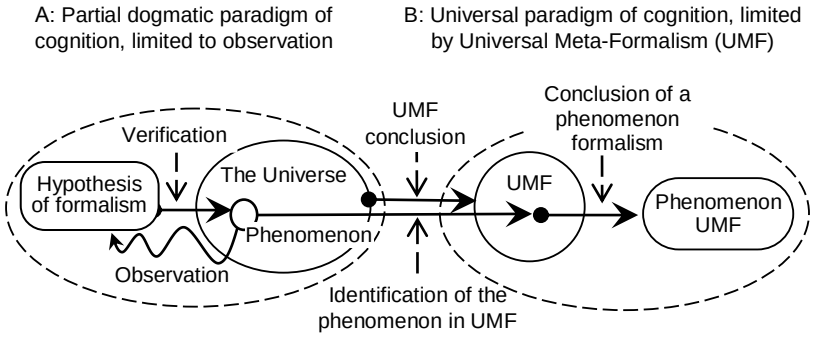

Fig. 5. Execution schemes of axiomatic (A) and universal (B) paradigms of cognition

6 The Universe's dualisms

Universalization reveals many fundamental (meta-) dualisms of the Universe, the most important of which are given below.

Abstract / real dualism. Universal phenomena are divided into a visible real (factual) part and an invisible abstract (categorical) part. The former activate / deactivate the latter, which turn on / off the corresponding properties that control the phenomena, which harmonizes / disharmonizes them, depending on the cognition and use of knowledge.

Continual / discrete dualism. The universe coexists in several fundamentally different joint phases with corresponding mechanics, of which only classical and quantum mechanics are known to modern science. The initial phase is a continual phase, which is sampled (reduced) to the formalization phase, allowing approximate, but successful harmonization to the target phase of Harmon. The sought-after scientific formalisms begin with a sampling phase.

Macro / micro dualism. The Universe is divided into infinitely internally nested hierarchies of the Real and Categorical Worlds, the properties of which differ at different levels of the hierarchy. Science operates exclusively with the Middle World of the Universe and is not available to the extreme macro / micro Worlds.

Border dualism. The universe, by definition, assumes the presence of its opposite part and, accordingly, the border between them. However, universalization substantiates the infinite and limitless in Space-Time-Matter Universe. Consequently, the Universe / non-Universe dualism is observed in another part of it, unknown to modern science and difficult to cognize due to going beyond the Universe. The latter makes it difficult to identify the scope of the Universal laws and undermines scientific knowledge.

Harmony / Chaos dualism. Universalization substantiates the meta-concepts of Harmony / Chaos unknown to traditional science as the presence / absence of connection, respectively, as well as the Meta-law of increasing Harmony, which have the highest irresistible force of action and radically change ideas about the world around them, without which adequate formalization of knowledge is impossible.

Determinism / Freedom dualism. Universalization substantiates the natural emergence of freedom (and the resulting uncertainty) in any (even fully defined and deterministic) unharmonized system, which is understood as any difference from the state of Harmon. The latter, as substantiated below, is on the border of the universe. This stipulates the obligatory combination of Determinism / Freedom within it, which together guarantee the directed achievement of the Harmon state without stopping at the local extrema of the Universal Global Optimization Problem. This justification is a universal analogue of K. Gödel's theorem on the incompleteness of particular formalisms in the axiomatic paradigm.

7 Meta-features of universal knowledge

Universalization 1) continues logical processes from divided dogmatic areas of knowledge to a single Universal system of knowledge (Fig. 6), 2) stabilizes the system of concepts in the process of cognizing phenomena (Fig. 7) and 3) increases the variability of universal formalisms in comparison with private limited low-level dogmatic formalisms by increasing the level of abstraction, starting from the limiting UA (Fig. 8).

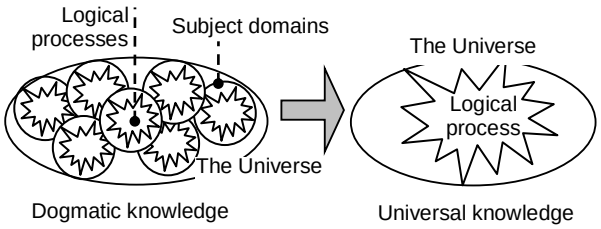

Fig. 6. Scheme of continuation of logical processes in meta-cognition.

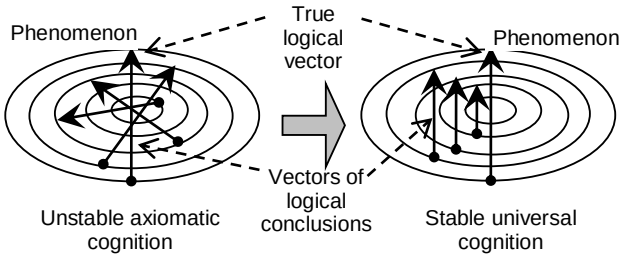

Fig. 7. Scheme of stabilization of meta-cognition of complex phenomena.

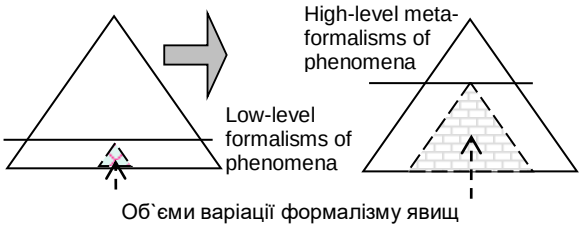

Fig. 8. Схема увеличения вариативности мета-формализмов.

The aforementioned dualisms in the formalization phase combine heterogeneous polar meta-properties of phenomena that specify the diversity of the Universe. For example, at low levels of abstraction with a small number of activated categories, phenomena receive high degrees of determinism / accuracy of axiomatic formalisms, which are mistaken by axiomatizers for justification. But at high levels, even precise meta-formalisms get a long way of causal concretization with random operating factors that turn them into precise but randomly realized asymptotes, mistakenly considered approximate (Fig. 9).

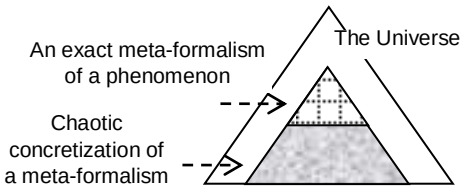

Fig. 9. Scheme of transformation of exact high-level meta-formalisms into chaotic asymptotes.

8 Meta-ontology of the Complexes

Definition. The complex is an entity participating in all Universal entities.
Consequence. The Universe is the original Complex.
Consequence. The Universe has two derivatives of the Complex: AW and RW (Fig. 2).
Consequence. RW has 3 derivatives of real Complexes: Space, Time and Matter (fig.).
Definition. The space is conceptually a regular permanent RW Complex.
Definition. Time is conceptually a regular variable RW Complex.
Definition. Matter conceptually is an irregular RW Complex, containing 2 derivatives of the Complex: Processes - a temporarily variable part of phenomena, and Subjects - a temporarily permanent part of phenomena.
Consequence. Complexes of Space, Time and Matter form a single STM-Complex, which is further divided into phenomena.

Consequence. STM-Complex is conceptually formed by two concepts: Persistence and Regularity and their negations (fig.).
Consequence. AW is a Complex that is divided into UA and an infinite (due to recursive nesting) system of derived categories in the form of a pyramid-like structure (UAP) up to RW.
Hypothesis. AW comes from the inhomogeneity of the meta-existent Prana during the decay of Harmon in the initial coexisting phases of the Universe (see below), the local indistinguishable parts of which condense into the abstract categories of the Universe that are supposedly precise and unchanged in the STM-Complex.

9 Meta-concepts of Harmony / Chaos

Definition. Harmony is a connection between beings (phenomena / categories) (Fig. 10).
Definition. Chaos is a lack of connection between beings.
Consequence. Harmony / Chaos inherits the linkage classification defined by Venn diagrams (Figure 11).
Consequence. Harmony and Chaos are mutually inverse mutually complementary general Universal concepts.
Consequence. Harmony and Chaos together constitute a complete conceptual Universum, describing every state of the Universe and its beings.
Consequence. Universum is realized in the Universe beings as a complete subgraph of realized (existing) and unrealized (resource harmonization of essences) relationships on all components of existence (Fig. 12).
Definition. Harmonization is an increase in the harmony of beings.
Consequence. The limit of harmonization of existent is local Harmon with absent chaos (Fig. 12).
Consequence. The limit of harmonization of the Universe is the Absolute Harmon, which unites all beings in the Universe.
Definition. Existence is a connection between an object and a subject (an object exists for all its subjects).
Consequence. Existence is an asymmetric directional concept relative to an object-subject pair.
Consequence. Harmony harmonizes beings and enhances their existence.
Consequence. Chaos separates and generates a difference between entities with classification up to the emergence of problems of existence and destruction (breaking the defining connection) of entities.
Consequence. Harmonization is the original Meta-Law of the Universe, which generates all other laws of the Universe's existence.
Definition. In incomplete formalization, the Meta-Law is expressed as "all things seeks to increase their harmony."

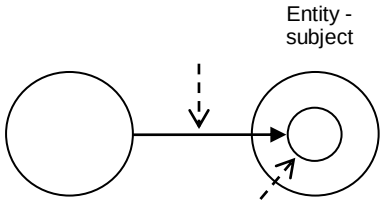

Fig. 10. The scheme of a meta-concept relation

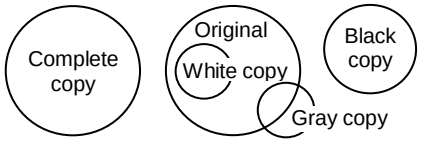

Fig. 11. Schema for the Euler - Venn diagrams

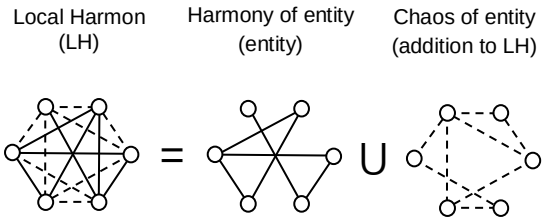

Fig. 12. Scheme of an entity dichotomy for Harmony / Chaos

10 The Harmon/Mandala and the Universe's Perpetuum Mobile

According to the Meta-Law, the limit of harmonization of a reasonably infinite Universe is the state of Absolute Harmon (hereinafter - Harmon) as a Complete Infinite Oriented Graph CIOG (CIOG) = lim COGn (COGn), $n \rightarrow \infty$, whose vertices are the same graphs (Fig. 13).

Absolute Harmon is Absolute Everything, homogeneous continuum and Bose condensate of Harmon, which condenses into Absolute Nothing (Chaos) and disappears due to the impossibility of adding any connections. Absolute Chaos, by analogy with a physical condensate, is presumably capable of decondensing back into the state of Harmon (Fig. 13).

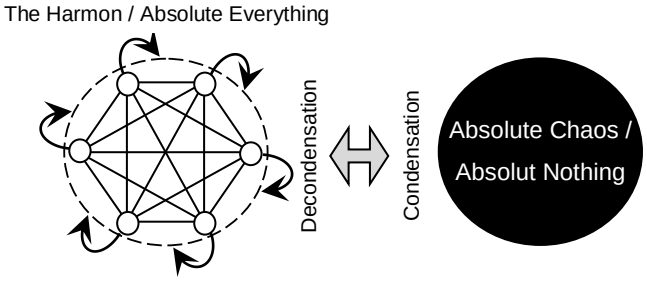

Fig. 13. Scheme of the original Universal Entity – the Harmon and its condensation / decondensation with Absolute Chaos – the Universal Perpetuum

Mobile.

The Absolute Harmon is unstable due to the internal asymmetry of nesting and disintegrates into the Universe known to us. If we assume the infinite resource of Absolute Chaos, then the Absolute Harmon / Absolute Chaos pair forms the inexhaustible Universe's Perpetuum Mobile, which moves our Universe and determines its structure.
Harmon is identical to the well-known religious symbol Mandala / Mangala, which is traditionally worshiped by about 1.5 billion people around the world, which testifies to 1) disappeared civilizations, 2) who knew it well, and 3) the cyclic succession of world civilizations (Fig. 14).

Fig. 14. Typical modern images Mandala / Mangala.

11 Meta-ontology of Intelligence

The meta-ontology of Intelligence begins together with the Universe from UA, associated with the meta-concept of communication (Fig. 10), which is then consistently concretized into the meta-concept of cognition as the cyclical advancement of a copy of an object into a subject in 4 stages: 1) information (on the subject's border) ; 2) knowledge (within the subject); 3) understanding (internal harmonization with other knowledge of the subject) and 4) research (external harmonization with other properties of the object) (Fig. 15).
The meta-scheme of cognition is naturally concretized for 1) multiple objects (Fig. 16), 2) learning through an intermediate subject (teacher) (Fig. 17) and 3) virtualization (exceeding properties) of an object in a virtualizer subject, which enhances harmonization due to active search for harmonious states of the object (Fig. 18).

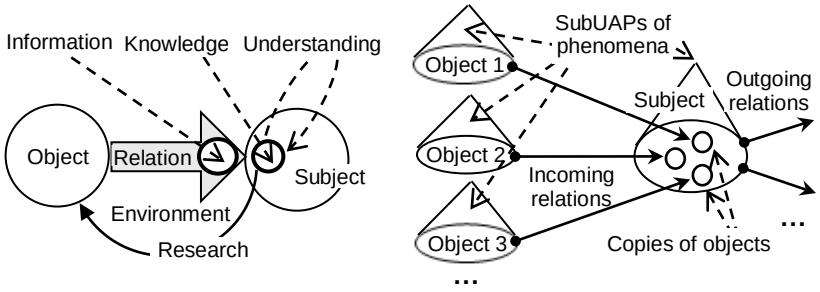

Fig. 15. Schema of a cognition meta-concept

Fig. 16. Schema of a multiple cognition meta-concept

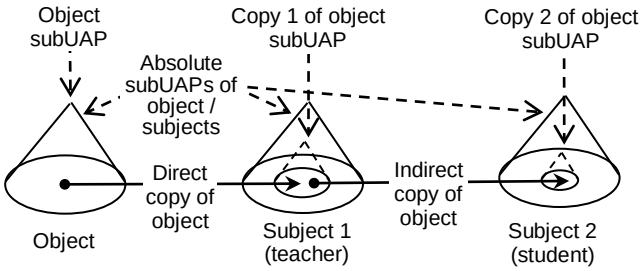

Fig. 17. Schema of a teaching meta-concept.

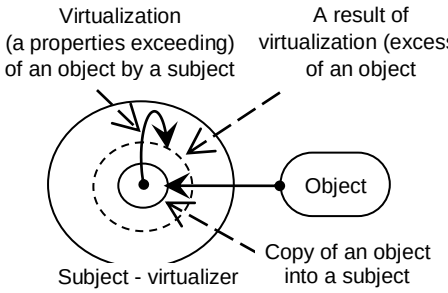

Fig. 18. Schema of a virtualization meta-concept.

12 Meta-methods of cognition

1) Cognition is a special case of harmonization of phenomena with concepts, therefore, 2) Meta-Law is the initial method of cognition, 3) which seeks and implements all possible ways of using categories to establish connections between phenomena, 4) which are further concretized by derivative methods in various situations, 5) specific universal of which RW (STM-Complex) has Conditioned Reflex (CR), 6) developing the ideas of the Nobel laureate I. Pavlov.

The conditioned reflex (CR), according to the original Meta-Law, identifies and copies the invisible categories of the cognized object-phenomenon into the visible concepts of the subject-phenomenon, starting from the subject's zero ability according to the following complementary concept (Fig. 19):

Definition. Knowledge is concepts and facts.

Definition. Cognition is the restoration (copying) of the categories of the phenomenon-object into the concepts of the phenomenon-subject.

Definition. The initial method of cognition in CR is induction, which uses the specifics of the structure of the AW and generalizes the phenomena / lower cognized concepts by highlighting common parts in the corresponding subject area.
Consequence. Induction builds up error quickly and stops prematurely without reaching higher meta-concepts.
Definition. The secondary method of cognition in CR is deduction, which by exhaustive search consistently combines the cognized concepts and reveals additional concepts missed by induction.
Consequence. The joint combination of induction / deduction raises the level of abstraction of concepts, but does not guarantee the achievement of IA.
Consequence. In the subject, two opposite streams of inductive and deductive concepts arise, which, as cognition progresses, should asymptotically converge.
Consequence. Coinciding inductive and deductive concepts in flows form, accumulate and improve a hypothetical system of concepts (knowledge).
Consequence. Inconsistent inductive and deductive concepts in streams are sent for inquiry to eliminate all external (with a cognizable phenomenon) / internal (among themselves) contradictions.
Consequence. As it is inquired, the system of knowledge should asymptotically approach the available Universal categories.
Consequence. The harmonized structure of the CR corresponds to a typical dichotomy of a biological brain into two specialized hemispheres with the expected internal functional similarity (Fig. 20).
Consequence. Higher meta-concepts are learned exclusively by the Method of Sequential Concretization of Hypotheses (CCGM) between the agreed conflicting concepts with a hypothetically surmountable distance between them in order to eliminate the current contradictions / incompleteness of the acquired knowledge system (Fig. 21).
Definition. A hypothesis is a statement that has not been proven false.
Hypothesis. Induction, deduction, and CCGM provide complete knowledge of beings.
Consequence. Any knowledge (concepts and facts) is subjective, hypothetical and has a measurement of truth exclusively by the volume of an externally / internally consistent system of concepts.
Consequence. The universe is the only criterion for truth.

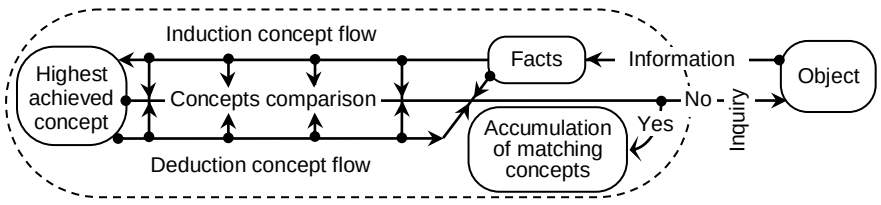

Рис. 19. The scheme of a conditioned reflex

Рис. 20. Typical brain dichotomy.

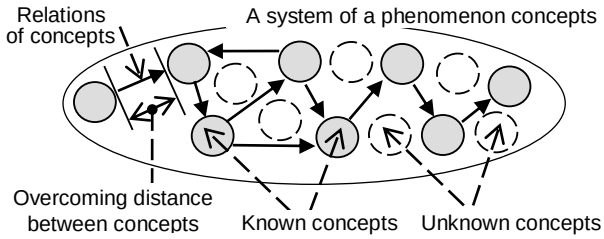

Fig. 21. The scheme of a concepts sequential concretization method with overcoming distance between them

13 Phenomena Universal harmonic meta-classification

Phenomena are harmoniously structured by 3 groups of connections: internal, external and connections between them (Fig. 22).

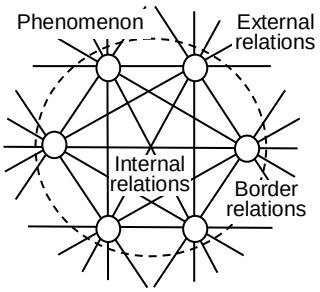

Fig. 22. The scheme of a phenomena harmonic structure

Таблица 1. Универсальная гармоничная классификация явлений (мета-фаза формализации Вселенной)

Continuous harmonization of phenomena sequentially complicates all groups of connections between phenomena and enhances their harmonious properties with the following principal states (Classes), which generate a universal harmonious classification (Table 1).

Table 1. Universal harmonious classification of phenomena (meta-phase of the formalization of the Universe)

Class	*Name*	*Internal structure*	*Harmonious Resource*	*Harmony type*	*Characteristic quantity*
0	Absolute Chaos	No	No	No	No
1	Thermodynamics	No	Real relations in the Present	Starting	Entropy
2	Mechanics	Present	+ virtual relations during the Past interval	Passive	Energy
3	Intelligence	Copy of STM-Complex	+ virtual relations during the Future interval	Active	Harmony
4	The Highest Reason	Real STM-Complex	+ real Present during Time axis	Highest	Harmony
5	The Harmon	Absolute	Absolute connectedness	Absolute	Harmony
6	Absolute Chaos	No	No	No	No

The internal structure of phenomena is sequentially complicated with the formation and increase of the Virtual Channel in Time (VTC) in the interval from the Past to the Future around the current real Present (Fig. 23), which enhances the additional harmonizing ability of the phenomena from degradation (Class 1) through preservation (Class 2) until active harmonization in Class 3, which becomes prevalent in Class 4 due to full access to the entire axis of Time and becomes sufficient for the destruction of STM-Complex into the state of Absolute Harmon. The Upper Classes partially inherit the properties of the lower Classes.

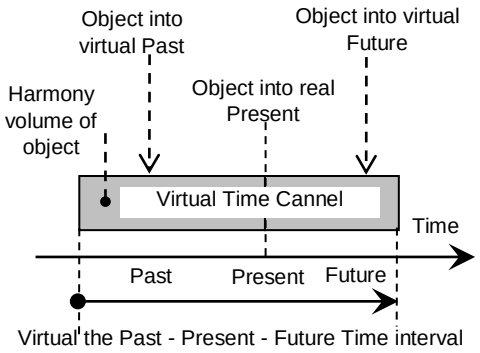

Fig. 23. The scheme of a phenomenon dividing into the Past, Present and

14 Virtual Time Channel and Classes characteristic values

The VTC radically changes the interaction of phenomena (Fig. 24). Thermodynamic phenomena almost do not interact with external relations and pass them with small changes. Mechanical and living phenomena strongly influence external relations with an increase in the VTC and from the passive turn to active and destabilizing ones. The Universe is completely self-determined and depends only on internal relations.

The intellect forms and consistently develops the VTC in time, which is fundamentally different from the Shannon channel in space and provides additional internal temporal switching of phenomena and the harmonious advantage of the higher Classes over the lower Classes (Fig.). VTC is a key attribute of Intelligence as opposed to purely logical non-living phenomena.

The VTC radically changes the interaction of phenomena (Fig. 24). Thermodynamic phenomena almost do not interact with external relations and pass them with small changes. Mechanical and living phenomena strongly influence external relations with an increase in the VTC and from the passive turn to active and destabilizing ones. The Universe is completely self-determined and depends only on internal relations.

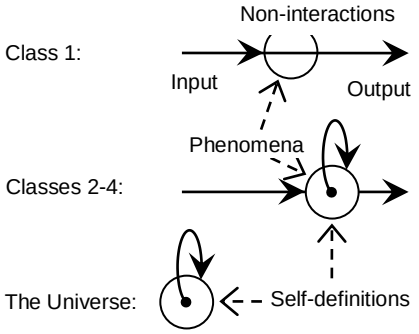

Fig. 24. Classification of the phenomena Classes interaction.

The VTC radically changes the characteristic quantities of phenomena from passive entropy (that tends from complex to the simplest states) and conservative energy (that preserves phenomena) to active harmony that gathers itself back from the simplest to the highest states and thereby creates complex phenomena (Fig. 25).

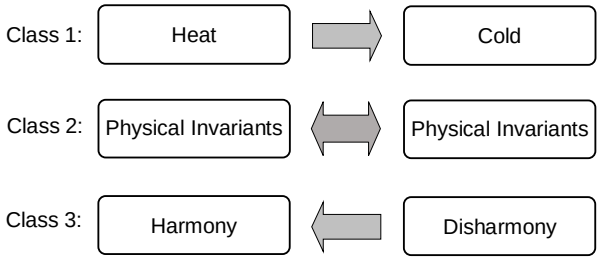

Fig. 25. The scheme of characteristic quantities action on phenomena Classes.

Accordingly, Class 1 destroys, Class 2 saves, and Class 3 develops phenomena (Table 2).
The VTC and additional Time harmony correspond to the desired negative entropy of E. Schrödinger [].

Table 2. Characteristic Quantities of Harmonic Phenomena Classes

Class	*Class name*	*Characteristic quantity*	*Degree of phenomena harmony*
1	Quasi-chaos (Thermodynamics)	Entropy	Degradation
2	Natural selection (Mechanics)	Energy	Conservation
3	Life (Intelligence)	Harmony	Development

15 Meta-definition of Intelligence

The Universe has 3 main conceptually strongly interconnected initial meta-divisions: 1) Abstract AW / RW division, 2) Time Past / Present / Future division, and 3) division into categories that are initial candidates for Meta-Law harmonization.
Consequence. Abstract, Temporal and Categorical meta-divisions of the Universe change only jointly.
Definition. Intellect is the (active) harmonizer of the joint Abstract, Temporal and Categorical meta-divisions of the Universe.
Consequence. Each category generates a corresponding division of the Universe, which is eliminated by deactivation of the category.
Consequence. In the existing unchanged AW, the categories are unchangeable / non-removable and it is only possible to reduce / avoid the conditions of their action on the phenomena that are identified and fulfilled by the corresponding concepts of Intelligence.
Consequence. The Meta-Law seeks and applies all kinds of ways of intellectual harmonization of any divisions through their cognition (copying) and virtualization by a harmonizing subject.

Consequence. Intelligence is divided into 1) the UMF of the Intelligence (UMFI), the same for the entire Universe, and 2) its various harmonization (concretization) with specific ecological niches of existence (ENE) (Fig. 26).

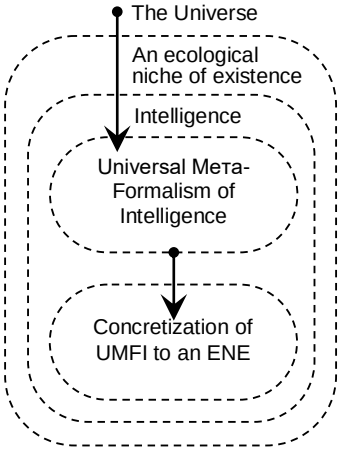

Fig. 26. Intelligence concretization scheme.

16 Meta-definition of ecological niches of existence

Definition. ENE is a part of the Universe harmonized with UMFI.
Hypothesis. UMFI can flesh out with any part of the Universe.
Consequence. RW is the first ENE of the Universe, the concretization of UMFI with which has properties common to the entire RW.
The UMFI cyclically harmonizes an object by the following stages: 1) observing the object over a certain time interval, 2) building a model of an object's process, 3) predicting the development of the model over the next time interval, 4) predicting the required harmonic state of the object taking into account the target of a subject, 5) calculating the control action on the object, 6) returning from the subjective into real time, 7) implementing the control action on the object, 8) comparing the predicted and actual state of the object and 9) correction of the process model (Fig. 27).

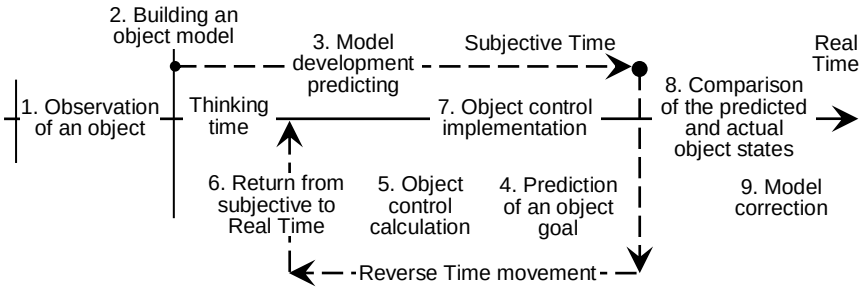

Fig. 27. The scheme of thinking act in RW

17 Meta-ontology of Highest Reason

The Meta-Law harmonizes the Universe from the decondensation of the Harmon by sequential passage of all Classes with the emergence and sequential development of VTC in Classes 4-5 until complete disappearance in Class 6 Absolute Chaos.

Class 4 Highest Reason transforms virtual access to a segment of the Time axis around the current Present into real access to the entire axis, necessary for its destruction by the ultimate harmonization and condensation of Time Complex, like all other Complexes. This is achieved by the ultimate increase in all VTC of the Universal phenomena to the state of Harmon, embedded in their unifying Harmon.

For this, Highest Reason achieves full knowledge / access to all Complexes and activates their condensation by the harmonious resources of the emerging Harmon. These properties bring Highest Reason closer to the historically traditional concept of God as a necessary component of Universal Cosmology / Universe, which for the first time becomes an important object of fundamental scientific research.

18 The living Universe

As biological organisms rationally combine non-living / living Classes, so the Universe does the same, forming a single living organism with 6 Classes of phenomena to effectively achieve the target state of Absolute Chaos.

Due to the high degrees of infinity of the Universe, all admissible possibilities are realized when moving to the limiting state of Harmon as the Absolute Everything, which proves the truth of any consistent formalisms, including those substantiated in this study.

19 Universal Cosmology

Universal Cosmology (UC) следует из следующей непротиворечивой мета-концепции (Fig. 28):

Universal Cosmology (UC) follows from the following consistent meta-concept (Fig. 28):

1. The Absolute Nothing decondenses into the Harmon,
2. The Harmon is unstable due to enclosure asymmetry and
3. Disintegrates into the Universe (in the state of disharmonized inhomogeneous Prana),
4. Where the STM-Complex arises and the Meta-Law joins in,
5. Which brings the Universe back into the state of the Harmon,
6. That condenses back into the Absolute Chaos,
7. And this cycle repeats endlessly.

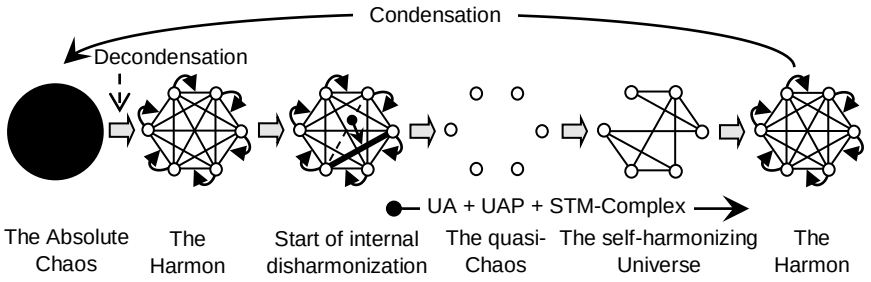

Fig. 28. The scheme of Universal Cosmology

All Classes of the Universe in pure / mixed (with inheritance of the lower Classes) form fulfill their purposes in the phase of formalization of the Universe (Fig. 29). Class 1 Thermodynamics utilizes unpromising weakly harmonious phenomena, Class 2 Mechanics stabilizes phenomena and includes passive natural selection, Class 3 Life actively develops phenomena into Class 4 Higher Intelligence, which activates the entire Universe and, upon reaching the state of Harmon, "burns" everything (Abstract + STM-) Complexes into Absolute Nothing. There are no other consistently substantiated mechanisms of Cosmology for the present.

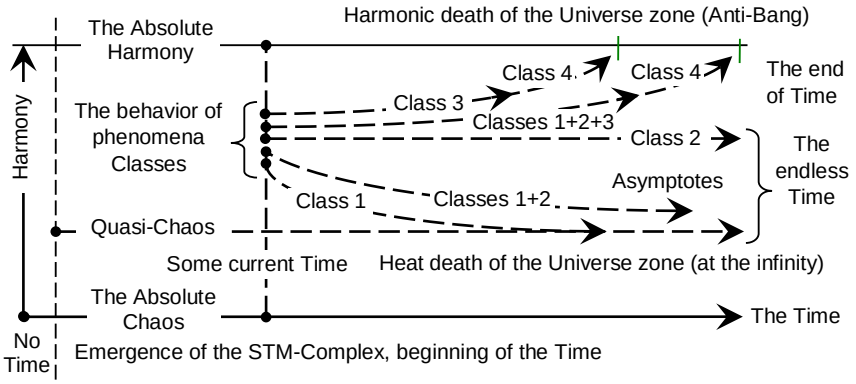

Fig. 29. The scheme of Classes role in the Universal Cosmology

20 Multiphase Universe

Harmon suggests the following meta-concept of its decay, explaining and generalizing the observed properties of our level of existence of the Universe:
1. Harmon is a continuum of limiting complexity $\infty\infty$,
2. Which disintegrates into an inhomogeneous continual Prana
3. With decreasing complexity (reduction),
4. Which further continues through atomization (selection of the most connected inhomogeneous parts) of Prana
5. Before the emergence of relatively weak externally connected with each other (remaining continuous) entities.
6. Weak ties naturally form a nested hierarchy at all levels and between them,
7. Which naturally form the formalisms of beings from phenomena to categories.
8. Categories are supposedly a generalization (condensation) of phenomena to eliminate all kinds of internal contradictions in the existing system of things,
9. Admitting effective combinatorial-logical harmonization of the reduced phenomena
10. Fundamentally similar limited entities
11. According to the reduced, stable categories
12. Until reaching the desired target state of Harmon.

Thus, the Universe exists in several joint successively developing meta-phases with fundamentally different properties / mechanics, presented in the minimum configuration in Table. 3. They are justified exclusively by a complete mutual composition, of which modern science knows only quantum and objective (classical) mechanics.
This work examines only the phases around formalization to obtain a universal meta-paradigm of cognition and the corresponding meta-formalisms.

Table 2. Universal meta-phases of the Universe.

№	*Phase*	*Purpose*	*Properties*
1	Absolute Chaos	Preliminary phase	Unknown origin and resource (limited / unlimited), decondensation into Harmon, mechanics of Nothing.
2	Harmon (Mandala)	Initial homogeneous continuum	Bose-condensate Harmon of extreme complexity ∞^{∞}, nesting asymmetry, explosive instability, decay, Harmon mechanics.

3	Prana	Inhomogeneous continuum	The Universe	Inanimate	Inhomogeneity, stabilization, the emergence of the PVM-Complex, the beginning of the Meta-law, continual mechanics.
4	Discretization	Emergence of entities / relations			Starting harmonization, elementary particles, quantum mechanics.
5	Formalization	Emergence of structures			Simplification of the Universe, the emergence of hierarchies (classifications), decreasing orders of complexity from ∞^{∞}, finite formalisms, partial knowledge, limited knowledge, exhaustive search, subject mechanics.
6	Categorization	Condensation of indistinguishable structures			
7	Cognition	Copying of structures			Complication of phenomena, mechanics of great complexity.
8	Life, Intellect	Partial cognition		Living	Harmonization of phenomena, intellectual mechanics.
9	Higher Reason	Complete cognition			Destruction of the STM-Complex, the mechanic of the Higher Reason
10	The Harmon	Resulting homogeneous continuum			Transformation of phenomena into Harmon, Harmon mechanics.
11	Condensation	Absolute fusion of all structures into Nothing			Exhaustion of the resource of harmonization, the mechanics of condensation.
12	Absolute Chaos	Final phase			Disappearance of all things into Absolute Nothing, mechanics of Nothing.

21 Constructor set of Universes

The hypothetical Universe's Perpetuum Mobile radically changes the classical views of the world order:

1. When a Harmon decays, it obviously creates (“sets fire to”) an infinite number of parent / daughter decaying Harmon, which are involved in its Universe as a source of singularity.

2. Singularities produce Prana (RW), which partially and presumably unambiguously condenses categorically into AW (UAP). In the case of unambiguity, singularities produce the same fully compatible UAP and "merge" Prana into a single Universe. Otherwise different UAPs, they give rise to

separate Universes. Further (our) Universe of 2 concepts and their negations: Constancy / Variability and Regularity / Irregularity forms STM-Complex (Fig. 30).

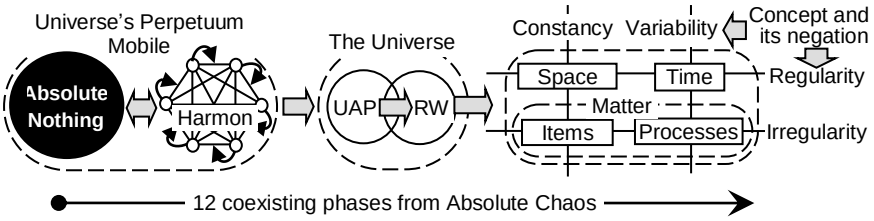

Рис. 30. Схема распада Гармона в его Комплексы.

3. Internal Complexes Space, Time and Matter of the Universe have different formulas and properties that allow to distinguish them as separate entities that can mutually separate and generate internal inhomogeneities with known relativistic effects.
4. Presumably, each part of Harmon -∂H generates proportional parts of Space ∂S, Time ∂T and Matter ∂M:

$$-\partial H = \partial S + \partial T + \partial M;$$

the mutual relationship of which should not change due to the fundamental homogeneity of Harmon. Then the mutual partial derivatives of the Complexes must be constant:

$$\partial S/\partial T = V_{ST}, \qquad \partial M/\partial T = V_{MT},$$
$$\partial T/\partial T = 1, \qquad \partial M/\partial S = V_{MS}$$

which is actually observed for a known constant speed of light VST = c and in principle allows only short-range action and prohibits long-range action inside the STM-Complex.
5. All the Universe meta-phases coexist, starting with the state of Harmon,
all parts of which, by definition, are directly fully interconnected in the absence of a PVM-Complex, and support absolute long-range action, which should slow down as the STM-Complex forms and short-range action arises, but partially acts in the soft transition boundaries between meta-phases.
6. As an inexhaustible source of all that exists from nothing, Universe's Perpetuum Mobile basically allows the preservation of the Past / Future with Time disabled and instantaneous movement throughout the saved Time from the beginning to any previously reached moment, after which the indefinite Future begins (Fig. 31). Time can be switched on at any point of the Past by transferring there any point of singularity, which are formed indefinitely as products of the decay of Harmon.

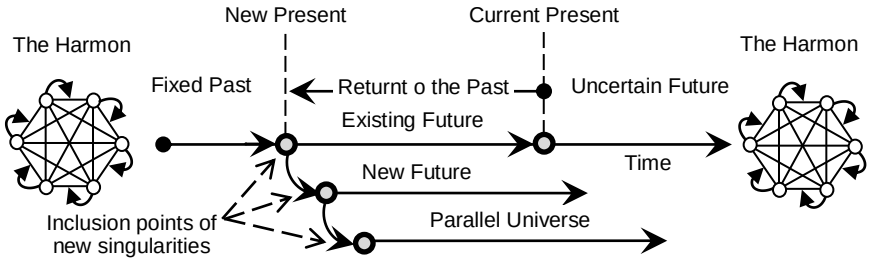

Fig. 31. Control scheme for the structure and long-range action of the Universe.

7. These mechanisms of structuring and long-range action of the Universe allow inanimate / living means to observe / change the entire Universe from beginning to end, cut / insert new trajectories of development, create parallel worlds / Universes, guarantee the achievement of many desired subjective goals by the Higher Intelligence.
8. Thus, the Supreme Intelligence, through direct access to all Complexes, is able to obtain the possibilities of long-range action 1) complete through the meta-phase of Harmon, 2) partial in its vicinity and 3) complete in the saved Universe with Time turned off for effective control of the entire infinite Universe.
9. Due to the infinite number of naturally occurring parameters. The Universe is a constructor set that allows you to create arbitrary universes with the desired characteristics.

22 Structural meta-classifications of relations

An enumeration of elementary structures produces a structural meta-classification of external relations that generate the following important fundamental properties of the Universe. Since universalization refines, simplifies, inherits and brings together concepts, many of them are repeated in their properties and with different names that turn out to be superfluous.
The unary relations, which are the simplest relating to entities themselves (Fig. 32).

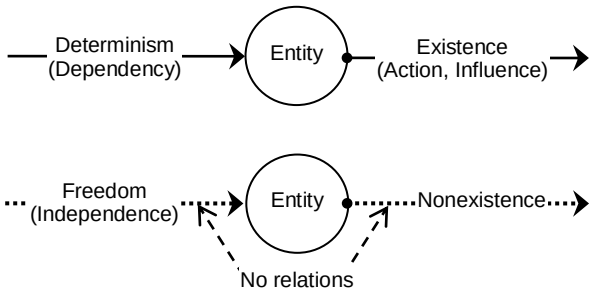

Fig. 32. The schemes of Determinism / Existence and
Freedom / Nonexistence of entities

Definition. Determinism (Dependency) is the presence of incoming relations of entity.
Definition. Freedom (Independence) is the absence of incoming relations of entity.
Definition. Existence (Action, Influence) is the presence of outgoing relations of entity.
Definition. Nonexistence is the absence of outgoing relations of entity.
Consequence. Free non-existent phenomena are deleted from the Universe by its definition.
The combination of these classes generates complex configurations of external relations of an entity with the inheritance of corresponding properties.
The binary relations, which are the next in complexity (Fig. 33).

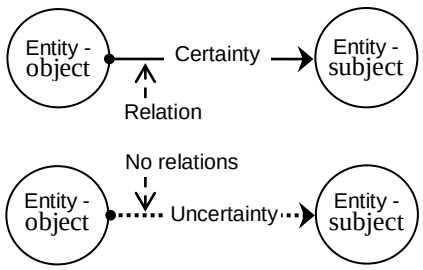

Fig. 33. The schemes of Certainty and Uncertainty of entities.

Definition. Certainty of an entity-object relative to an entity-subject is the existence of relations from the first to the second one.
Definition. Uncertainty of an entity-object relative to an entity-subject is the absence of relations from the first to the second one.
Definition. Relativity is a dependence (structure) of a relation on other relation.
The multiple (indirect) relations of entities through intermediate entities include intermediate entities.They can lose copies of initial entities-objects without the loss of general connectivity (coExistence in the common Universe) with entities-subjects, which generates full indirect Uncertainty of entities.

It is shown in the example how entity 1 loses indirect Existence for entity 4 (inside the common Universe) which results in full Uncertainty of entity 1 for entity 4 and Freedom of entity 4 for entity 1.
The restriction on carrier capacity of entities relations. The relations with limited carrier capacity transfer only part of a copy of entities-objects and generate corresponding partial Uncertainty of entities-objects relative to entities-subjects that has (structural) measurement (Fig. 35).

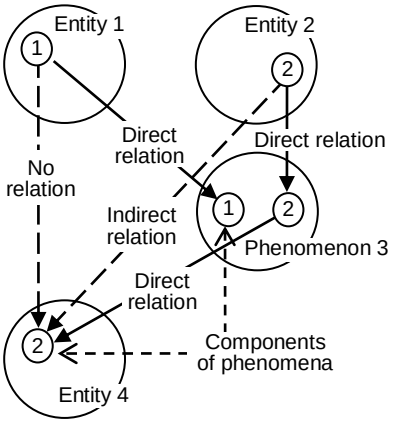

Fig. 34. The scheme of loss of indirect connectivity of entities (on the example of entities 1 and 4)

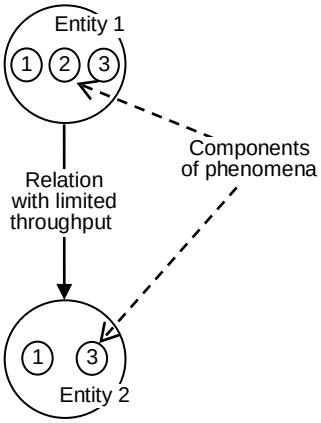

Fig. 35. The scheme of partial Uncertainty of formalization with the restriction on carrier capacity of relations

Division and mixture (distortion) of entities relations. Indirect relations can divide copies of entities-objects into several different copies or mix copies of different entities in one copy. The result is transferred further with the loss of entities-objects membership (Fig. 36). Such copies are perceived as a reduction and distortion (noise) of relations and, therefore, generate Uncertainty of entities.

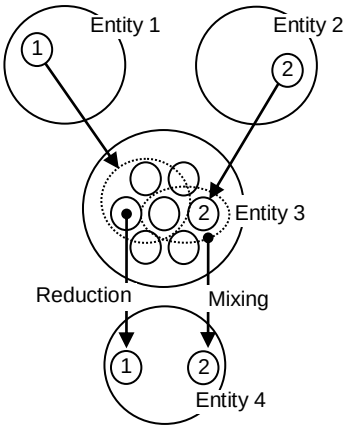

Fig. 36. The scheme of emergence of Uncertainty owing to division and mixture (distortion) of entities relations

23 Stability / instability of phenomena and the "boiling" Universe hypothesis

1) If we use the measure of stability of phenomena ΔH / H, where H is the value of harmony, and ΔH is its change, then 2) phenomena at low degrees of harmonization are less stable than at high ones, which 3) enhances external dependence and 4) facilitates management of them, which 5) is widely observed in nature now and 6) indicates the initial stage of harmonization of the Universe. 7) With an increase in internal harmony, the stability of phenomena increases, 8) as well as external controllability decreases, but 9) the harmonizing ability of phenomena increases, 10) which prevails in combination with pp. 2-4 and 11) explosively (AntiExplosion) forces the environment of the phenomenon into a state of local Harmon 12) with further decondensation into local Absolute Nothing 13) in the final stage of the Universe, 14) where this completely disappearing region returns.

Thus, the hypothesis of the limitless infinitely "boiling" Universe is substantiated, the multiple singularities of the collapsing Harmon of which continuously produce existence from quasi-chaos to the state of local Harmon in some areas, which further "collapse" as they mature under the control of the Higher Mind grown in them. Today it is the only simplest complete way to scientifically consistently explain our Universe (Fig. 37).

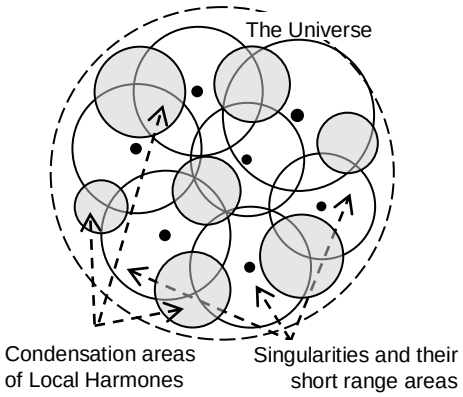

Fig. 37. The scheme of the "boiling" Universe hypothesis

24 Meta-resource of the meta-Universe

Thus, the UC substantiates Absolute All (Harmon) / Nothing by some single persistent (limited) unknown meta-Universal resource Absolute Nothing, which continuously circulates at the meta-Universal level with different forms of existence.

The knowledge of such a resource is very limited due to going beyond the limits of our Universe, on the basis of which we build all kinds of knowledge and assumptions, and, probably, is possible only in Class 4. Perhaps it is a consequence of the Harmon of a higher level of the native Harmon of the Universe, which forces the higher harmonic means return your borrowed part from the low-level collapsing Harmon.

In combination with the possible ambiguity of the structure of the UAP and, therefore, Class 4, one can also assume a diverse society of Class 4 at the meta-Universe level instead of its monoblock identical structure within the Universe.

25 Acknowledgments

The work was carried out according to the research plan of the Institute of Artificial Intelligence Problems of the National Academy of Sciences of Ukraine.

26 Conclusion

1. Any serious system of knowledge begins with the initial meta-concepts, the interest and significance of which has been growing widely and strongly in recent years in many areas of mankind, including fundamental science and high technologies. However, along with high-level technological advances, the well-known chronically unsolvable stagnant problematic of studying complex higher phenomena is growing more and more, indicating the fundamental shortcomings of the existing general scientific paradigm of cognition, up to the formal / actual illegitimacy of the modern scientific system of knowledge.
2. This problem is obviously solved by the transition from an axiomatic private paradigm to a new universal meta-paradigm of knowledge, which for the first time allows to fundamentally achieve UA and unite the system of universal concepts derived from it into a single UMF, which in principle allows formalization of all simple and complex Ecumenical phenomena without exception.
3. In a series of works by the authors, a universal meta-paradigm of knowledge is substantiated and the possibility of creating a likely single exact consistent UMF is shown on the example of the developed Universal system of meta-concepts in a structural representation as the most appropriate to the initial properties of our Universe and allowing in the future a set-theoretic analogy and formal combinatorial -logical transformations.
4. For this, for the first time, it was possible to reasonably limit the fundamentally infinite recursion of the derivation of meta-concepts by the specific properties of the Universe and formally define all the basic concepts used with a supposedly surmountable conceptual distance between them, formulate the initial UA and higher meta-concepts, properties and laws of the Universe, the main of which is reveals the value of Harmony, based on the connectivity of beings, and the meta-Law of its increase, which directs the movement of beings and the Universe as a whole.
5. Universal phenomena are naturally classified according to the degree of internal harmonization into 6 main Classes, of which Life and the Higher Mind play the main role in the existence of the Universe. Universalization allowed for the first time to scientifically define Intellect as an active harmonizer that overcomes the 3 main harmonic Abstract, Temporal and Categorical meta-divisions of the Universe, which has a single initial UMFI for the entire living world and a different concretization for an infinite number of ecological niches

of existence, generating all the living diversity of the Universe. UMFI fundamentally legitimizes both all research / development in this area, and science in general as a product of exclusively intellectual activity.

6. The Universe turns out to be a complex living self-organizing organism, rationally combining all Classes, in which the Supreme Mind for the first time becomes the object of scientific research and the main acting being at the final stage of existence.

7. The limit of any harmonization is the meta-state of Harmon, which turns our ideas about the world around as Absolute Everything, which condenses into Absolute Nothing and decondenses back, overcoming many fundamental contradictions through the meta-concept of the Universal Perpetuum Mobile, impossible within the Universe, but possible on its border.

8. Universal Perpetuum Mobile reasonably deduces UC, which is radically different from the Big Bang hypothesis. The Universe is infinite always / everywhere, has no physical boundaries in Space. Time and Matter, cyclically passes through all Classes of development, has unlimited STM to achieve the state of Harmon / Absolute Nothing (harmonious death of the Universe) and is reborn from the singularities of the disintegrating Harmon, presumably arising from them in separate regions, forming a "boiling" Universe.

9. The Universe has innate parametric properties of a constructor, which may well be used by the Higher Intelligence to create arbitrary Universes with different properties,

10. The Universe has at least 12 coexisting nested phases of the state, sequentially reducing everything that exists to ensure effective harmonization up to the achievement of the final goal - the state of Harmon / Absolute Nothing with the corresponding mechanics, of which axiomatic science knows only two - continuous quantum and discrete formal classical mechanics ... Universalization opens up other previously unknown mechanics to science to reveal new fundamental natural laws.

11. Universalization is fully consistent / does not contradict the known scientific / historical facts and forms the largest system of grounded concepts, including the well-known axiomatic science as a partial derivative case. Continuation of universalization develops UMF and presumably leads to the achievement of a supposedly complete exact state, which deduces the same formalisms of all known / unknown Ecumenical phenomena, as far as possible in the formalization phase, combined with similar reducing means of describing entities in other phases. Despite the initial state of the Universal Theory, any of its applications are already radically changing the traditional ideas about the world around us, especially complex chronically unknowable phenomena.

12. The ultimate meta-level of abstraction of universal concepts today is an urgent prerequisite for the development of knowledge, in which, undoubtedly, many teams of leading scientists should participate, like the scientific school of Bourbaki. The seemingly unusual presentation of many important universal concepts follows exclusively from the incompleteness of modern axiomatic science, as well as ancient knowledge in comparison with the latter.

References

1. A.V Sosnitsky, A.I. Shevchenko. The Chaotic Universe's Cosmogony: The Universe's Perpetuum Mobile, Multivariance of the Universe and the Boiling Universe Hypothesis. Proceedings of the 10th Chaotic Modeling and Simulation International Conference, p. 805-815, 2017.
2. E. Hamilton. H. Cairns. Collected Dialogues of Plato. Princeton University Press, Princeton, 1962.
3. Aristotle. Categoriae. The Works of Aristotle, vol. I, Oxford, Clarendon Press, 1928.
4. T. Jech. Set Theory: The Third Millennium Edition, Revised and Expanded, Springer, 3e éd., 2006.
5. K. Gödel. On Formally Undecidable Propositions of the Principia Mathematica and Related Systems. Davis, Martin (ed.) The Undecidable: Basic Papers On Undecidable Propositions, Unsolvable Problems and Computable Functions, Raven Press, New York, p. 6-8, 1965.
6. V.M. Somsikov. About principles of creating of the structured particles mechanics. Proceedings of the 4th Chaotic Modeling and Simulation International Conference, p. 573-580, 2019.
7. V.M. Somsikov. Deterministic Irreversibility Mechanism and Basic Element of Matter. Springer Proceedings in Complexity, p. 245-256, 2020.
8. S. Legg, M. Hütter. A Collection of Definitions of Intelligence. Proceedings of the 2007 conference on Advances in Artificial General Intelligence: Concepts, Architectures and Algorithms: Proceedings of the AGI Workshop 2006, p. 17-24, 2007.
9. A. Sosnitsky. Beginnings if the Universe Model and Deduction of Initial System of Information Concepts, Information Theories and Applications, 19(1), p. 56-85, 2012.
10. A. Sosnitsky. The Universal Theory as a new general scientific paradigm. Journal of Applied Mathematics and Statistical Applications, 2(1):11-18, 2018.
11. A. Sosnitsky. Harmonious Foundations of Intelligence, Communication of SIWN, 7, p. 66-72, 2009.
12. A. Einstein. Grundgedanken der allgemeinen Relativitätstheorie und Anwendung dieser Theorie in der Astronomie. Preussische Akademie der Wissenschaften, Sitzungsberichte, (Teil 1), 315, 1915.
13. A. Friedman. Über die Krümmung des Raumes. Zeitschrift für Physik, 10 (1), p. 377-386, 1922.
14. E. Hubble. A relation between distance and radial velocity among extra-galactic nebulae. PNAS, 15 (3), p. 168-173, 1929.
15. S. Hawking, R. Penrose. The Singularities of Gravitational Collapse and Cosmology. Proc. R. Soc. A, 314 (1519), p. 529-548, 1970.
16. A. Guth. The Inflationary Universe: The Quest for a New Theory of Cosmic Origins. Perseus, 1997.
17. String theory. Wikipedia, https://en.wikipedia.org/wiki/String_theory#Early_results.
18. J. Earman, J. Mosterín. A Critical Look at Inflationary Cosmology. Philosophy of Science, 66, p. 1-49, 1999.

19. D. Hooper. Is the Big Bang in crisis? Astronomy, 14, 2020, https://astronomy.com/magazine/news/2020/05/is-the-big-bang-in-crisis.
20. A.V. Sosnitsky. The Universal Concept of Chaos. Proceedings of the 8th Chaotic Modeling and Simulation International Conference, p. 831-842, 2015.
21. A. Shevchenko, A. Sosnitsky. Universal Meta-Definition of Intelligence. Proceedings - 2020 IEEE 11th International Conference on Dependable Systems, Services and Technologies, DESSERT 2020, p. 189-195, 2020.
22. A.V. Sosnitsky, A.I. Shevchenko. Application of the Universal Meta-Formalism to Substantiate and Research Intelligence Properties. CEUR Workshop Proceedings, 2608, p. 245-265, 2020.
23. A. Sosnitsky, A. Shevchenko. The Universe Multiphase Meta-Reduction: The Harmon (Mandala), Continuum (Prana), Discretization, Formalization, Knowledge, Cognition, Condensation and Absolute Nothing. Chaotic Modeling and Simulation. В печати.
24. A. Sosnitsky. The Universal Theory of Passionarity. Web Intelligence, vol. 17, issue 1, p. 75-84, 2019.
25. L.N. Gumilev. Les Fluctuations du niveau de la mer Caspienne. Cahiers du Monde Russe et Sovietique, Paris, 6(3), p. 331-366, 1965.
26. L.N. Gumilev. New Data on the History of the Khazars. Acta Archeologica Academiae Scientiarum Hungaricae, 19, p. 61-103, 1967.
27. I.P. Pavlov. Conditioned reflexes. Oxford University Press, London, 1927.
28. K. Saladin. Human anatomy, 3rd ed., McGraw-Hill, New York, 2011.
29. A. Poincaré. Science and Hypothesis. The Walter Scott Publishing Co., New York, 1905.
30. C.E. Shannon. A Mathematical Theory of Communication. Bell System Technical Journal, 27 (3), p. 379-423, 1948.
31. E. Schrödinger. What is Life? The Physical Aspect of the Living Cell. Cambridge, University Press, 1944, 1984, 2019.
32. W. Heisenberg. Über den anschaulichen Inhalt der quantentheoretischen Kinematik und Mechanik, Zeitschrift für Physik, 43 (3-4), p. 172–198, 1927.

POSITIVE SOLUTIONS FOR A FRACTIONAL BOUNDARY VALUE PROBLEM WITH SEQUENTIAL DERIVATIVES

Alexandru Tudorache[1] **and Rodica Luca**[2]

[1] Department of Computer Science and Engineering
Gh. Asachi Technical University, Iasi 700050, Romania
E-mail: alexandru.tudorache93@gmail.com

[2] Department of Mathematics
Gh. Asachi Technical University, Iasi 700506, Romania
E-mail: rluca@math.tuiasi.ro

Abstract. We investigate the existence of positive solutions for a Riemann-Liouville fractional differential equation with sequential derivatives, a positive parameter and a nonnegative singular nonlinearity, subject to nonlocal boundary conditions which contain Riemann-Stieltjes integrals and various fractional derivatives. In the proof of the main result, we use the fixed point index theory.

AMS Subject Classification: 34A08, 34B10, 34B16, 34B18.

Keywords: Riemann-Liouville fractional differential equation, nonlocal boundary conditions, singular functions, positive solutions.

1 Introduction

We consider the nonlinear ordinary fractional differential equation with sequential derivatives

$$D_{0+}^{\alpha}\Big(q(t)D_{0+}^{\beta}v(t)\Big)=\lambda r(t)f(t,v(t)),\ \ t\in(0,1), \tag{1}$$

subject to the nonlocal boundary conditions

$$\begin{cases} v^{(j)}(0)=0,\ \ j=0,\ldots,n-2,\ \ D_{0+}^{\beta}v(0)=0, \\ q(1)D_{0+}^{\beta}v(1)=aq(\xi)D_{0+}^{\beta}v(\xi),\ \ D_{0+}^{\gamma_0}v(1)=\displaystyle\sum_{i=1}^{p}\int_0^1 D_{0+}^{\gamma_i}v(t)\,dH_i(t), \end{cases} \tag{2}$$

where $\alpha\in(1,2]$, $\beta\in(n-1,n]$, $n\in\mathbb{N}$, $n\geq 3$, $p\in\mathbb{N}$, $\gamma_i\in\mathbb{R}$, $i=0,\ldots,p$, $0\leq\gamma_1<\gamma_2<\cdots<\gamma_p\leq\gamma_0<\beta-1$, $\gamma_0\geq 1$, $\lambda>0$, $a\geq 0$, $\xi\in(0,1)$, $q:[0,1]\to(0,\infty)$ is a continuous function, $f:[0,1]\times(0,\infty)\to[0,\infty)$ is a continuous function which may have singularity at the second variable in the point 0, the function $r:(0,1)\to[0,\infty)$ is continuous and may be singular at $t=0$ and/or $t=1$, D_{0+}^{ς} denotes the Riemann-Liouville fractional derivative of order ς, for $\varsigma=\alpha,\beta,\gamma_0,\gamma_1,\ldots,\gamma_p$, and the integrals from the boundary conditions (2) are Riemann-Stieltjes integrals with H_i, $i=1,\ldots,p$ functions of bounded variation.

In this paper, we present some assumptions on the function f and intervals for the parameter λ such that problem (1),(2) has at least one positive solution. By a positive

solution of (1),(2) we mean a function $v \in C[0,1]$ satisfying (1) and (2) with $v(t) > 0$ for all $t \in (0,1]$. In the proof of our main theorem we use some results from the fixed point index theory. In what follows we present some recent results connected with our problem (1),(2). In [9], the authors studied the existence of nonnegative solutions for the fractional integro-differential equation

$$D_{0+}^{\gamma} v(t) + f(t, v(t), \mathcal{T}v(t), \mathcal{S}v(t)) = 0, \;\; t \in (0,1),$$

with the multi-point boundary conditions

$$v(0) = v'(0) = \cdots = v^{(n-2)}(0) = 0, \;\; D_{0+}^{p} v(1) = \sum_{i=1}^{m} a_i D_{0+}^{q} v(\xi_i),$$

where $\gamma \in \mathbb{R}$, $\gamma \in (n-1, n]$, $n \in \mathbb{N}$, $n \geq 3$, a_i, $\xi_i \in \mathbb{R}$ for all $i = 1, \ldots, m$, $(m \in \mathbb{N})$, $0 < \xi_1 < \cdots < \xi_m \leq 1$, p, $q \in \mathbb{R}$, $p \in [1, n-2]$, $q \in [0, p]$, $\mathcal{T}v(t) = \int_0^t \mathcal{K}(t,s)v(s)\,ds$, $\mathcal{S}v(t) = \int_0^1 \mathcal{H}(t,s)v(s)\,ds$ for all $t \in [0,1]$, and f is a nonnegative function which satisfies some assumptions. In the proofs of the main results they used the Banach contraction mapping principle and the Krasnosel'skii fixed point theorem for the sum of two operators. In [13], by using the Guo-Krasnosel'skii fixed point theorem and some height functions defined on special bounded sets, the author proved the existence and multiplicity of positive solutions for the nonlinear fractional differential equation

$$D_{0+}^{\gamma} v(t) + f(t, v(t)) = 0, \;\; t \in (0,1), \tag{3}$$

supplemented with the nonlocal boundary conditions

$$v(0) = v'(0) = \cdots = v^{(n-2)}(0) = 0, \;\; D_{0+}^{p} v(1) = \int_0^1 D_{0+}^{q} v(t)\,d\mathcal{H}(t),$$

where $\gamma \in \mathbb{R}$, $\gamma \in (n-1, n]$, $n \in \mathbb{N}$, $n \geq 3$, p, $q \in \mathbb{R}$, $p \in [1, n-2]$, $q \in [0, p]$, $\mathcal{H}$ is a function with bounded variation, and the nonlinearity f may change sign and may be singular at the points $t = 0$, $t = 1$ and/or $v = 0$. In [1], the authors investigated the existence of multiple positive solutions for the equation (3) with the boundary conditions

$$v(0) = v'(0) = \cdots = v^{(n-2)}(0) = 0, \;\; D_{0+}^{\beta_0} v(1) = \sum_{i=1}^{m} \int_0^1 D_{0+}^{\beta_i} v(t)\,d\mathcal{H}_i(t), \tag{4}$$

where $m \in \mathbb{N}$, $\beta_i \in \mathbb{R}$ for all $i = 0, \ldots, m$, $0 \leq \beta_1 < \beta_2 < \cdots < \beta_m \leq \beta_0 < \gamma - 1$, $\beta_0 \geq 1$, $\mathcal{H}_i$, $i = 1, \ldots, m$ are functions of bounded variation, the nonlinearity f may change sign and may be singular at the points $t = 0$, $t = 1$ and/or in the space variable v. They used in [1] various height functions of the nonlinearity of equation defined on special bounded sets, the Leggett-Williams theorem and the Krasnosel'skii fixed point index theorem. In [19], the authors studied the fractional differential equation

$$D_{0+}^{\gamma} v(t) + \lambda h(t) f(t, v(t)) = 0, \;\; t \in (0,1), \tag{5}$$

subject to nonlocal boundary conditions (4), where λ is a positive parameter, the nonnegative function $f(t,v)$ may have singularity at $v = 0$ and the nonnegative function $h(t)$

may be singular at $t = 0$ and/or $t = 1$. Under some assumptions for the functions h and f, they established intervals for the parameter λ such that problem (5),(4) has positive solutions. These intervals for λ are expressed by using the principal characteristic value of an associated linear operator. In the proof of the main theorems they used the fixed point index theory. A related semipositone problem is also studied in [19] by using the Guo-Krasnosel'skii fixed point theorem. In [14], the author investigated the fractional differential equation (3) with the nonlocal boundary conditions

$$v(0) = v'(0) = \cdots = v^{(n-2)}(0) = 0, \;\; D_{0+}^{\beta_0} v(1) = \sum_{i=1}^{m} \int_0^1 a_i(t) D_{0+}^{\beta_i} v(t)\, d\mathcal{H}_i(t), \tag{6}$$

where $m \in \mathbb{N}$, $\beta_i \in \mathbb{R}$ for all $i = 0, \ldots, m$, $0 \leq \beta_1 < \beta_2 < \cdots < \beta_m < \gamma - 1$, $1 \leq \beta_0 < \gamma - 1$, $\mathcal{H}_i$, $i = 1, \ldots, m$, are functions of bounded variation, the functions $a_i \in C(0,1) \cap L^1(0,1)$, $i = 1, \ldots, m$, and the nonlinearity f is nonnegative and it may be singular at the points $t = 0$, $t = 1$ and/or $v = 0$. She presented conditions for the data of problem connected to the spectral radii of some associated linear operators such that the problem (3),(6) has at least one or two positive solutions. In the proof of the main existence theorems the author used an application of the Krein-Rutman theorem in the space $C[0,1]$ and the fixed point index theory. In [10], the authors studied the system of nonlinear fractional differential equations with sequential derivatives

$$\begin{cases} D_{0+}^{\alpha_1}\left(D_{0+}^{\beta_1} v(t)\right) + \lambda f(t, v(t), w(t)) = 0, \;\; t \in (0,1), \\ D_{0+}^{\alpha_2}\left(D_{0+}^{\beta_2} w(t)\right) + \mu g(t, v(t), w(t)) = 0, \;\; t \in (0,1), \end{cases} \tag{7}$$

supplemented with the nonlocal coupled boundary conditions

$$\begin{cases} v^{(j)}(0) = 0, \; j = 0, \ldots, n-2; \;\; D_{0+}^{\beta_1} v(0) = 0, \;\; D_{0+}^{\gamma_0} v(1) = \sum_{i=1}^{p} \int_0^1 D_{0+}^{\gamma_i} w(t)\, d\mathcal{H}_i(t), \\ w^{(j)}(0) = 0, \; j = 0, \ldots, m-2; \;\; D_{0+}^{\beta_2} w(0) = 0, \;\; D_{0+}^{\delta_0} w(1) = \sum_{i=1}^{q} \int_0^1 D_{0+}^{\delta_i} v(t)\, d\mathcal{K}_i(t), \end{cases} \tag{8}$$

where $\alpha_1, \alpha_2 \in (0,1]$, $\beta_1 \in (n-1, n]$, $\beta_2 \in (m-1, m]$, $n, m \in \mathbb{N}$, $n, m \geq 3$, $p, q \in \mathbb{N}$, $\gamma_i \in \mathbb{R}$ for all $i = 0, 1, \ldots, p$, $0 \leq \gamma_1 < \gamma_2 < \cdots < \gamma_p \leq \delta_0 < \beta_2 - 1$, $\delta_0 \geq 1$, $\delta_i \in \mathbb{R}$ for all $i = 0, 1, \ldots, q$, $0 \leq \delta_1 < \delta_2 < \cdots < \delta_q \leq \gamma_0 < \beta_1 - 1$, $\gamma_0 \geq 1$, $\lambda > 0$, $\mu > 0$, f and g are sign-changing continuous functions that may be singular at $t = 0$ and/or $t = 1$, $\mathcal{H}_i$, $i = 1, \ldots, p$ and $\mathcal{K}_j$, $j = 1, \ldots, q$ are functions of bounded variation. Under some assumptions on the nonsingular/singular functions f and g, they presented intervals for parameters λ and μ such that problem (7),(8) has at least one or two positive solutions. In the main existence results they applied the nonlinear alternative of Leray-Schauder type and the Guo-Krasnosel'skii fixed point theorem. The existence, multiplicity and nonexistence of positive solutions for systems of Riemann-Liouville fractional differential equations with φ-Laplacians and nonnegative nonlinearities, with or without parameters, subject to the coupled boundary conditions (8) or uncoupled boundary conditions which contains various fractional derivatives were investigated in [18] and [4]. We also mention the books [2], [3], [6]-[8], [11], [12], [15]-[17], [20] and their references for other results

obtained in the last years and for the applications of fractional differential equations in various fields.

The paper is organized as follows. In Section 2 we study a linear fractional boundary value problem associated to our problem (1),(2), and we give some properties of the associated Green functions. Section 3 is devoted to the main existence theorem for (1),(2), and in Section 4 we present an example which illustrates our result.

2 Preliminary results

We consider the fractional differential equation

$$D^{\alpha}_{0+}(q(t)D^{\beta}_{0+}v(t)) = x(t), \ \ t \in (0,1), \tag{9}$$

with the boundary conditions (2), where $q \in C([0,1],(0,\infty))$ and $x \in C(0,1) \cap L^1(0,1)$. We denote by

$$\Delta_1 = 1 - a\xi^{\alpha-1}, \ \ \Delta_2 = \frac{\Gamma(\beta)}{\Gamma(\beta-\gamma_0)} - \sum_{i=1}^{p} \frac{\Gamma(\beta)}{\Gamma(\beta-\gamma_i)} \int_0^1 \vartheta^{\beta-\gamma_i-1}\, dH_i(\vartheta). \tag{10}$$

Lemma 2.1 *If $\Delta_1 \neq 0$ and $\Delta_2 \neq 0$, then the unique solution $v \in C[0,1]$ of problem (9),(2) is given by*

$$v(t) = \int_0^1 \mathcal{G}_2(t,\vartheta) \left(\frac{1}{q(\vartheta)} \int_0^1 \mathcal{G}_1(\vartheta,\zeta) h(\zeta)\, d\zeta \right) d\vartheta, \ \ t \in [0,1], \tag{11}$$

where

$$\mathcal{G}_1(t,\vartheta) = g_1(t,\vartheta) + \frac{at^{\alpha-1}}{\Delta_1} g_1(\xi,\vartheta), \ \ (t,\vartheta) \in [0,1]\times[0,1], \tag{12}$$

with

$$g_1(t,\vartheta) = \frac{1}{\Gamma(\alpha)} \begin{cases} t^{\alpha-1}(1-\vartheta)^{\alpha-1} - (t-\vartheta)^{\alpha-1}, & 0 \le \vartheta \le t \le 1, \\ t^{\alpha-1}(1-\vartheta)^{\alpha-1}, & 0 \le t \le \vartheta \le 1, \end{cases} \tag{13}$$

and

$$\mathcal{G}_2(t,\vartheta) = g_2(t,\vartheta) + \frac{t^{\beta-1}}{\Delta_2} \sum_{i=1}^{p} \left(\int_0^1 g_{3i}(\tau,\vartheta)\, dH_i(\tau) \right), \ \ (t,\vartheta) \in [0,1]\times[0,1], \tag{14}$$

with

$$\begin{aligned} g_2(t,\vartheta) &= \frac{1}{\Gamma(\beta)} \begin{cases} t^{\beta-1}(1-\vartheta)^{\beta-\gamma_0-1} - (t-\vartheta)^{\beta-1}, & 0 \le \vartheta \le t \le 1, \\ t^{\beta-1}(1-\vartheta)^{\beta-\gamma_0-1}, & 0 \le t \le \vartheta \le 1, \end{cases} \\ g_{3i}(t,\vartheta) &= \frac{1}{\Gamma(\beta-\gamma_i)} \begin{cases} t^{\beta-\gamma_i-1}(1-\vartheta)^{\beta-\gamma_0-1} - (t-\vartheta)^{\beta-\gamma_i-1}, & 0 \le \vartheta \le t \le 1, \\ t^{\beta-\gamma_i-1}(1-\vartheta)^{\beta-\gamma_0-1}, & 0 \le t \le \vartheta \le 1. \end{cases} \\ & i = 1,\dots,p. \end{aligned} \tag{15}$$

Proof. We denote by $q(t)D^{\beta}_{0+}v(t) = w(t)$. Then problem (9),(2) is equivalent to the following two boundary value problems

$$(I) \qquad \begin{cases} D^{\alpha}_{0+}w(t) = x(t), \ \ t \in (0,1), \\ w(0) = 0, \ \ w(1) = aw(\xi), \end{cases}$$

and

$$(II) \qquad \begin{cases} D^{\beta}_{0+}v(t) = w(t)/q(t), \ \ t \in (0,1), \\ v^{(j)}(0) = 0, \ \ j = 0, \dots, n-2, \ \ D^{\gamma_0}_{0+}v(1) = \sum_{i=1}^{p} \int_0^1 D^{\gamma_i}_{0+}v(t)\, dH_i(t). \end{cases}$$

By Lemma 4.1.5 from [8], the unique solution $w \in C[0,1]$ of problem (I) is

$$w(t) = -\int_0^1 \mathcal{G}_1(t,\vartheta)x(\vartheta)\, d\vartheta, \ \ t \in [0,1], \tag{16}$$

where $\mathcal{G}_1$ is given by (12). By Lemma 2.2 from [1], the unique solution $v \in C[0,1]$ of problem (II) is

$$v(t) = -\int_0^1 \mathcal{G}_2(t,\vartheta)w(\vartheta)/q(\vartheta)\, d\vartheta, \ \ t \in [0,1], \tag{17}$$

where $\mathcal{G}_2$ is given by (14). Now by using (16) and (17) we obtain the solution v of problem (9),(2) which is given by relation (11). □

By applying some properties of functions g_1, g_2, g_{3i}, $i = 1, \dots, p$ given by (13) and (15) (see [8] and [3]), we deduce the following result.

Lemma 2.2 *If H_i, $i = 1, \dots, p$ are nondecreasing functions, $\Delta_1 > 0$, $\Delta_2 > 0$, then the functions $\mathcal{G}_1$ and $\mathcal{G}_2$ given by (12) and (14) have the properties:*

a) $\mathcal{G}_1$, $\mathcal{G}_2 : [0,1] \times [0,1] \to [0,\infty)$ are continuous functions;

b) $\mathcal{G}_1(t,\vartheta) \le \mathcal{J}_1(\vartheta)$, $\forall\, (t,\vartheta) \in [0,1] \times [0,1]$, where

$$\mathcal{J}_1(\vartheta) = h_1(\vartheta) + \frac{a}{\Delta_1} g_1(\xi,\vartheta), \ \forall\, \vartheta \in [0,1],$$

and $h_1(\vartheta) = \frac{1}{\Gamma(\alpha)}(1-\vartheta)^{\alpha-1}$, $\vartheta \in [0,1]$;

c) $\mathcal{G}_2(t,\vartheta) \le \mathcal{J}_2(\vartheta)$, $\forall\, (t,\vartheta) \in [0,1] \times [0,1]$, where

$$\mathcal{J}_2(\vartheta) = h_2(\vartheta) + \frac{1}{\Delta_2} \sum_{i=1}^{p} \int_0^1 g_{3i}(\tau,\vartheta)\, dH_i(\tau), \ \forall\, \vartheta \in [0,1],$$

and $h_2(\vartheta) = \frac{1}{\Gamma(\beta)}(1-\vartheta)^{\beta-\gamma_0-1}(1-(1-\vartheta)^{\gamma_0})$, $\vartheta \in [0,1]$.

d) $\mathcal{G}_2(t,\vartheta) \ge t^{\beta-1}\mathcal{J}_2(\vartheta)$, $\forall\, (t,\vartheta) \in [0,1] \times [0,1]$.

By using Lemma 2.2, we easily obtain the following lemma (see also [8]).

Lemma 2.3 *If H_i, $i = 1, \dots, p$ are nondecreasing functions, $\Delta_1 > 0$, $\Delta_2 > 0$, and $x \in C(0,1) \cap L^1(0,1)$ with $x(t) \ge 0$ for all $t \in (0,1)$, then the solution v of problem (9),(2) given by (11) satisfies the properties $v(t) \ge 0$ for all $t \in [0,1]$ and $v(t) \ge t^{\beta-1}v(\eta)$ for all $t, \eta \in [0,1]$.*

3 Existence of positive solutions

In this section we present some conditions on the function f and intervals for the parameter λ such that problem (1),(2) has at least one positive solution. We consider the Banach space $\mathcal{X} = C[0,1]$ with the supremum norm $\|v\| = \sup_{t\in[0,1]} |v(t)|$, and we define the cones

$$\mathcal{C} = \{v \in \mathcal{X},\ v(t) \geq 0,\ \forall\, t \in [0,1]\},\ \ \mathcal{S} = \{v \in \mathcal{X},\ v(t) \geq t^{\beta-1}\|v\|,\ \forall\, t \in [0,1]\} \subset \mathcal{C}.$$

We also define the operator $\mathcal{E} : \mathcal{C} \to \mathcal{C}$ and the linear operator $\mathcal{F} : \mathcal{X} \to \mathcal{X}$ by

$$\mathcal{E}v(t) = \lambda \int_0^1 \mathcal{G}_2(t,\vartheta)\frac{1}{q(\vartheta)}\left(\int_0^1 \mathcal{G}_1(\vartheta,\tau)r(\tau)f(\tau,v(\tau))\,d\tau\right)d\vartheta,\ \ t \in [0,1],\ v \in \mathcal{C},$$
$$\mathcal{F}v(t) = \int_0^1 \mathcal{G}_2(t,\vartheta)\frac{1}{q(\vartheta)}\left(\int_0^1 \mathcal{G}_1(\vartheta,\tau)r(\tau)v(\tau)\,d\tau\right)d\vartheta,\ \ t \in [0,1],\ v \in \mathcal{X}.$$

We see that v is a solution of problem (1),(2) if and only if v is a fixed point of operator $\mathcal{E}$. For $\theta > 0$ we denote by $\mathcal{S}_\theta = B_\theta \cap \mathcal{S}$ and $\overline{\mathcal{S}}_\theta = \overline{B}_\theta \cap \mathcal{S}$, ($B_\theta = \{v \in \mathcal{X},\ \|v\| < \theta\}$, $\overline{B}_\theta = \{v \in \mathcal{X},\ \|v\| \leq \theta\}$, $\partial B_\theta = \{v \in \mathcal{X},\ \|v\| = \theta\}$).

We present now the assumptions that we will use in this section.

$(H1)$ $\alpha \in (1,2]$, $\beta \in (n-1,n]$, $n \in \mathbb{N}$, $n \geq 3$, $p \in \mathbb{N}$, $\gamma_i \in \mathbb{R}$, $i = 0,\dots,p$, $0 \leq \gamma_1 < \gamma_2 < \cdots < \gamma_p \leq \gamma_0 < \beta - 1$, $\gamma_0 \geq 1$, $\lambda > 0$, $a \geq 0$, $\xi \in (0,1)$, $q : [0,1] \to (0,\infty)$ is a continuous function, $H_i : [0,1] \to \mathbb{R},\ i = 1,\dots,p$ are nondecreasing functions, $\lambda > 0$, and $\Delta_1 > 0,\ \Delta_2 > 0$ ($\Delta_1,\ \Delta_2$ are given by (10)).

$(H2)$ The function $r \in C((0,1),[0,\infty))$ and $0 < \int_0^1 r(\vartheta)\,d\vartheta < \infty$.

$(H3)$ The function $f \in C([0,1]\times(0,\infty),[0,\infty))$ and for any $0 < \theta_1 < \theta_2$ we have

$$\lim_{m\to\infty} \sup_{v\in\overline{\mathcal{S}}_{\theta_2}\setminus\mathcal{S}_{\theta_1}} \int_{I_m} r(\vartheta)f(\vartheta,v(\vartheta))\,d\vartheta = 0,$$

where $I_m = \left[0,\frac{1}{m}\right] \cup \left[\frac{m-1}{m},1\right]$.

Lemma 3.1 *We suppose that assumptions $(H1)-(H3)$ hold. Then for any $0 < \theta_1 < \theta_2$, the operator $\mathcal{E} : \overline{\mathcal{S}}_{\theta_2} \setminus \mathcal{S}_{\theta_1} \to \mathcal{S}$ is completely continuous.*

Proof. By $(H3)$ we obtain that there exists a number $m_1 \geq 3$ such that

$$\sup_{v\in\overline{\mathcal{S}}_{\theta_2}\setminus\mathcal{S}_{\theta_1}} \int_{I_{m_1}} r(\vartheta)f(\vartheta,v(\vartheta))\,d\vartheta < 1. \tag{18}$$

For $v \in \overline{\mathcal{S}}_{\theta_2} \setminus \mathcal{S}_{\theta_1}$, we find that there exists $\omega_0 \in [\theta_1,\theta_2]$ such that $\|v\| = \omega_0$, and then

$$t^{\beta-1}\theta_1 \leq t^{\beta-1}\omega_0 \leq v(t) \leq \omega_0 \leq \theta_2,\ \ \forall\, t \in [0,1].$$

Let $M_1 = \max\left\{f(t,y),\ t \in \left[\frac{1}{m_1}, \frac{m_1-1}{m_1}\right],\ y \in \left[\frac{1}{m_1^{\beta-1}}\theta_1, \theta_2\right]\right\}$. By Lemma 2.2, $(H2)$, $(H3)$ and (18), we deduce

$$\begin{aligned}
&\sup_{v\in\overline{\mathcal{S}}_{\theta_2}\setminus\mathcal{S}_{\theta_1}} \mathcal{E}v(t) = \sup_{v\in\overline{\mathcal{S}}_{\theta_2}\setminus\mathcal{S}_{\theta_1}} \lambda\int_0^1 \mathcal{G}_2(t,\vartheta)\frac{1}{q(\vartheta)}\left(\int_0^1 \mathcal{G}_1(\vartheta,\tau)r(\tau)f(\tau,v(\tau))\,d\tau\right)d\vartheta\\
&\le \sup_{v\in\overline{\mathcal{S}}_{\theta_2}\setminus\mathcal{S}_{\theta_1}} \lambda\int_0^1 \mathcal{J}_2(\vartheta)\frac{1}{q(\vartheta)}\left(\int_0^1 \mathcal{J}_1(\tau)r(\tau)f(\tau,v(\tau))\,d\tau\right)d\vartheta\\
&\le \sup_{v\in\overline{\mathcal{S}}_{\theta_2}\setminus\mathcal{S}_{\theta_1}} \lambda\int_0^1 \mathcal{J}_2(\vartheta)\frac{1}{q(\vartheta)}\left(\int_{I_{m_1}} \mathcal{J}_1(\tau)r(\tau)f(\tau,v(\tau))\,d\tau\right)d\vartheta\\
&\quad+\sup_{v\in\overline{\mathcal{S}}_{\theta_2}\setminus\mathcal{S}_{\theta_1}} \lambda\int_0^1 \mathcal{J}_2(\vartheta)\frac{1}{q(\vartheta)}\left(\int_{\frac{1}{m_1}}^{\frac{m_1-1}{m_1}} \mathcal{J}_1(\tau)r(\tau)f(\tau,v(\tau))\,d\tau\right)d\vartheta\\
&\le \lambda J_{10}\int_0^1 \mathcal{J}_2(\vartheta)\frac{1}{q(\vartheta)}\,d\vartheta + \lambda M_1\left(\int_0^1 \mathcal{J}_2(\vartheta)\frac{1}{q(\vartheta)}\,d\vartheta\right)\left(\int_{\frac{1}{m_1}}^{\frac{m_1-1}{m_1}} \mathcal{J}_1(\tau)r(\tau)\,d\tau\right)\\
&\le \lambda J_{10}\left(\int_0^1 \mathcal{J}_2(\vartheta)\frac{1}{q(\vartheta)}\,d\vartheta\right)\left(1+M_1\int_0^1 r(\tau)\,d\tau\right) < \infty,
\end{aligned}$$

where $J_{10} = \max_{s\in[0,1]}\mathcal{J}_1(s) > 0$. This gives us that the operator $\mathcal{E}$ is well defined.

Next we show that $\mathcal{E}:\overline{\mathcal{S}}_{\theta_2}\setminus\mathcal{S}_{\theta_1}\to\mathcal{S}$. Indeed, for any $v\in\overline{\mathcal{S}}_{\theta_2}\setminus\mathcal{S}_{\theta_1}$ and $t\in[0,1]$, we have

$$\begin{aligned}
\mathcal{E}v(t) &= \lambda\int_0^1 \mathcal{G}_2(t,\vartheta)\frac{1}{q(\vartheta)}\left(\int_0^1 \mathcal{G}_1(\vartheta,\tau)r(\tau)f(\tau,v(\tau))\,d\tau\right)d\vartheta\\
&\le \lambda\int_0^1 \mathcal{J}_2(\vartheta)\frac{1}{q(\vartheta)}\left(\int_0^1 \mathcal{G}_1(\vartheta,\tau)r(\tau)f(\tau,v(\tau))\,d\tau\right)d\vartheta,
\end{aligned}$$

and then

$$\|\mathcal{E}v\| \le \lambda\int_0^1 \mathcal{J}_2(\vartheta)\frac{1}{q(\vartheta)}\left(\int_0^1 \mathcal{G}_1(\vartheta,\tau)r(\tau)f(\tau,v(\tau))\,d\tau\right)d\vartheta.$$

By Lemma 2.2, we also obtain

$$\begin{aligned}
&\mathcal{E}v(t) \ge \lambda t^{\beta-1}\int_0^1 \mathcal{J}_2(\vartheta)\frac{1}{q(\vartheta)}\left(\int_0^1 \mathcal{G}_1(\vartheta,\tau)r(\tau)f(\tau,v(\tau))\,d\tau\right)d\vartheta\\
&\ge t^{\beta-1}\|\mathcal{E}v\|,\ \ \forall\, t\in[0,1],
\end{aligned}$$

hence $\mathcal{E}v\in\mathcal{S}$. Then $\mathcal{E}(\overline{\mathcal{S}}_{\theta_2}\setminus\mathcal{S}_{\theta_1})\subset\mathcal{S}$.

We prove now that $\mathcal{E}:\overline{\mathcal{S}}_{\theta_2}\setminus\mathcal{S}_{\theta_1}\to\mathcal{S}$ is completely continuous. We suppose that $D\subset\overline{\mathcal{S}}_{\theta_2}\setminus\mathcal{S}_{\theta_1}$ is an arbitrary bounded set. By the first part of the proof, we see that $\mathcal{E}(D)$ is uniformly bounded. We show next that $\mathcal{E}(D)$ is equicontinuous. Indeed, for $\epsilon>0$ there exists a natural number $m_2\ge 3$ such that

$$\sup_{v\in\overline{\mathcal{S}}_{\theta_2}\setminus\mathcal{S}_{\theta_1}}\int_{I_{m_2}} r(\vartheta)f(\vartheta,v(\vartheta))\,d\vartheta < \frac{\epsilon}{4\lambda J_{10}}\left(\int_0^1\frac{\mathcal{J}_2(\vartheta)}{q(\vartheta)}d\vartheta\right)^{-1}.$$

Because $\mathcal{G}_2(t,\vartheta)$ is uniformly continuous on $[0,1]\times[0,1]$, for the above $\epsilon>0$ we deduce that there exists $\rho>0$ such that for any $t_1,t_2\in[0,1]$ with $|t_1-t_2|<\rho$ and $\vartheta\in[0,1]$ we have

$$|\mathcal{G}_2(t_1,\vartheta)-\mathcal{G}_2(t_2,\vartheta)| < \frac{\epsilon}{2\lambda r_0 J_{10}M_2}\left(\int_0^1\frac{1}{q(\vartheta)}\,d\vartheta\right)^{-1}.$$

Here $M_2 = \max\left\{1, \max\left\{f(t,y),\ t \in \left[\frac{1}{m_2}, \frac{m_2-1}{m_2}\right],\ y \in \left[\frac{1}{m_2^{\beta-1}}\theta_1, \theta_2\right]\right\}\right\}$ and $r_0 = \max\{1, \max\left\{r(\vartheta),\ \vartheta \in \left[\frac{1}{m_2}, \frac{m_2-1}{m_2}\right]\right\}\}$.

Therefore for any $v \in D$, $t_1, t_2 \in [0,1]$ with $|t_1 - t_2| < \rho$, we find

$$\begin{aligned}
&|(\mathcal{E}v)(t_1) - (\mathcal{E}v)(t_2)| \\
&= \lambda \left| \int_0^1 (\mathcal{G}_2(t_1,\vartheta) - \mathcal{G}_2(t_2,\vartheta)) \frac{1}{q(\vartheta)} \left(\int_0^1 \mathcal{G}_1(\vartheta,\tau) r(\tau) f(\tau, v(\tau))\, d\tau \right) d\vartheta \right| \\
&\le 2\lambda \sup_{v\in D} \int_0^1 \mathcal{J}_2(\vartheta) \frac{1}{q(\vartheta)} \left(\int_{I_{m_2}} \mathcal{J}_1(\tau) r(\tau) f(\tau, v(\tau))\, d\tau \right) d\vartheta \\
&\quad + \lambda \sup_{v\in D} \int_0^1 |\mathcal{G}_2(t_1,\vartheta) - \mathcal{G}_2(t_2,\vartheta)| \frac{1}{q(\vartheta)} \left(\int_{\frac{1}{m_2}}^{\frac{m_2-1}{m_2}} \mathcal{J}_1(\tau) r(\tau) f(\tau, v(\tau))\, d\tau \right) d\vartheta \\
&\le \tfrac{\epsilon}{2} + \tfrac{\epsilon}{2} = \epsilon.
\end{aligned}$$

So we obtain that $\mathcal{E}(D)$ is equicontinuous. By the Arzela-Ascoli, we conclude that $\mathcal{E} : \overline{\mathcal{S}}_{\theta_2} \setminus \mathcal{S}_{\theta_1} \to \mathcal{S}$ is compact.

We prove next that $\mathcal{E} : \overline{\mathcal{S}}_{\theta_2} \setminus \mathcal{S}_{\theta_1} \to \mathcal{S}$ is continuous. We assume that $v_n,\ v_0 \in \overline{\mathcal{S}}_{\theta_2} \setminus \mathcal{S}_{\theta_1}$ for all $n \ge 1$, and $\|v_n - v_0\| \to 0$ as $n \to \infty$. Then $\theta_1 \le \|v_n\| \le \theta_2$ for all $n \ge 0$. By $(H3)$, for $\epsilon > 0$ there exists a natural number $m_3 \ge 3$ such that

$$\sup_{v\in\overline{\mathcal{S}}_{\theta_2}\setminus\mathcal{S}_{\theta_1}} \int_{I_{m_3}} r(\vartheta) f(\vartheta, v(\vartheta))\, d\vartheta < \frac{\epsilon}{4\lambda J_{10}} \left(\int_0^1 \mathcal{J}_2(\vartheta) \frac{1}{q(\vartheta)}\, d\vartheta \right)^{-1}. \tag{19}$$

Because f is uniformly continuous in $\left[\frac{1}{m_3}, \frac{m_3-1}{m_3}\right] \times \left[\frac{1}{m_3^{\beta-1}}\theta_1, \theta_2\right]$, we find

$$\lim_{n\to\infty} |f(\vartheta, v_n(\vartheta)) - f(\vartheta, v_0(\vartheta))| = 0, \ \text{ uniformly for } \ \vartheta \in \left[\frac{1}{m_3}, \frac{m_3-1}{m_3}\right].$$

Then by using the Lebesgue dominated convergence theorem, we deduce

$$\int_{\frac{1}{m_3}}^{\frac{m_3-1}{m_3}} r(\vartheta) |f(\vartheta, v_n(\vartheta)) - f(\vartheta, v_0(\vartheta))|\, d\vartheta \to 0, \ \text{ as } \ n \to \infty.$$

So, for the above $\epsilon > 0$ there exists a natural number m_4 such that for all $n > m_4$ we obtain

$$\int_{\frac{1}{m_3}}^{\frac{m_3-1}{m_3}} r(\vartheta) |f(\vartheta, v_n(\vartheta)) - f(\vartheta, v_0(\vartheta))|\, d\vartheta < \frac{\epsilon}{2\lambda J_{10}} \left(\int_0^1 \mathcal{J}_2(\vartheta) \frac{1}{q(\vartheta)}\, d\vartheta \right)^{-1}. \tag{20}$$

By (19) and (20) we conclude that

$$\begin{aligned}
&\|\mathcal{E}v_n - \mathcal{E}v_0\| \\
&\le \sup_{v\in\overline{\mathcal{S}}_{\theta_2}\setminus\mathcal{S}_{\theta_1}} \lambda \int_0^1 \mathcal{J}_2(\vartheta) \frac{1}{q(\vartheta)} \left(\int_{I_{m_3}} \mathcal{J}_1(\tau) r(\tau) |f(\tau, v_n(\vartheta)) - f(\tau, v_0(\tau))|\, d\tau \right) d\vartheta \\
&\quad + \sup_{v\in\overline{\mathcal{S}}_{\theta_2}\setminus\mathcal{S}_{\theta_1}} \lambda \int_0^1 \mathcal{J}_2(\vartheta) \frac{1}{q(\vartheta)} \left(\int_{\frac{1}{m_3}}^{\frac{m_3-1}{m_3}} \mathcal{J}_1(\tau) r(\tau) |f(\tau, v_n(\tau)) - f(\tau, v_0(\tau))| d\tau \right) d\vartheta \\
&\le \tfrac{\epsilon}{2} + \tfrac{\epsilon}{2} = \epsilon, \quad \forall\, n > m_4.
\end{aligned}$$

So we find that $\mathcal{E} : \overline{\mathcal{S}}_{\theta_2} \setminus \mathcal{S}_{\theta_1} \to \mathcal{S}$ is a continuous operator. Therefore $\mathcal{E}$ is a completely continuous operator. □

Under assumptions $(H1)-(H3)$, by using the extension theorem, the operator $\mathcal{E}$ has a completely continuous extension (also denoted by $\mathcal{E}$) from $\mathcal{S}$ to $\mathcal{S}$.

By using the Krein-Rutman theorem in the space $C[0,1]$ and similar arguments as those used in the proof of Lemma 3.2 from [19], we have the following result.

Lemma 3.2 *We suppose that assumptions $(H1)$ and $(H2)$ hold. Then the spectral radius $r(\mathcal{F}) \neq 0$ and $\mathcal{F}$ has an eigenfunction $\zeta_1 \in \mathcal{C}\setminus\{0\}$ corresponding to the principal eigenvalue $r(\mathcal{F})$, that is $\mathcal{F}\zeta_1 = r(\mathcal{F})\zeta_1$. So $r(\mathcal{F}) > 0$.*

By a similar argument used in the proof of Lemma 3.1 for operator $\mathcal{E}$, we deduce that $\mathcal{F}(\mathcal{S}) \subset \mathcal{S}$.

Theorem 3.1 *We suppose that assumptions $(H1)-(H3)$ hold. If*

$$0 \leq f_\infty^s := \limsup_{y\to\infty} \max_{t\in[0,1]} \frac{f(t,y)}{y} < f_0^i := \liminf_{y\to 0+} \min_{t\in[0,1]} \frac{f(t,y)}{y} \leq \infty,$$

then for any $\lambda \in \left(\frac{1}{f_0^i r(\mathcal{F})}, \frac{1}{f_\infty^s r(\mathcal{F})}\right)$ the problem (1),(2) has at least one positive solution $v(t),\ t \in [0,1]$, (with the conventions $1/(0+) = \infty$ and $1/\infty = 0+$).

Proof. We consider $\lambda \in \left(\frac{1}{f_0^i r(\mathcal{F})}, \frac{1}{f_\infty^s r(\mathcal{F})}\right)$. For f_0^i, there exists $\omega_1 > 0$ such that $f(t,y) \geq \frac{y}{\lambda r(\mathcal{F})}$ for all $t \in [0,1]$ and $y \in [0,\omega_1]$. Then for any $v \in \partial\mathcal{S}_{\omega_1}$ we obtain

$$\begin{aligned}\mathcal{E}v(t) &= \lambda \int_0^1 \mathcal{G}_2(t,\vartheta)\frac{1}{q(\vartheta)}\left(\int_0^1 \mathcal{G}_1(\vartheta,\tau)r(\tau)f(\tau,v(\tau))\,d\tau\right)d\vartheta \\ &\geq \frac{1}{r(\mathcal{F})}\int_0^1 \mathcal{G}_2(t,\vartheta)\frac{1}{q(\vartheta)}\left(\int_0^1 \mathcal{G}_1(\vartheta,\tau)r(\tau)v(\tau)d\tau\right)d\vartheta = \frac{1}{r(\mathcal{F})}\mathcal{F}v(t),\ \ \forall\, t \in [0,1].\end{aligned}$$

We suppose that $\mathcal{E}$ has no fixed point on $\partial\mathcal{S}_{\omega_1}$ (if not, the proof is finished). We will prove that

$$v - \mathcal{E}v \neq \nu\zeta_1,\ \ \forall\, v \in \partial\mathcal{S}_{\omega_1},\ \ \nu \geq 0, \tag{21}$$

where ζ_1 is given in Lemma 3.2. We assume that there exist $v_1 \in \partial\mathcal{S}_{\omega_1}$ and $\nu_1 \geq 0$ such that $v_1 - \mathcal{E}v_1 = \nu_1\zeta_1$. Then $\nu_1 > 0$ and $v_1 = \mathcal{E}v_1 + \nu_1\zeta_1 \geq \nu_1\zeta_1$. We denote by $\nu_0 = \sup\{\nu,\ \ v_1 \geq \nu\zeta_1\}$. Then $\nu_0 \geq \nu_1$, $v_1 \geq \nu_0\zeta_1$ and

$$\mathcal{E}v_1 \geq \frac{1}{r(\mathcal{F})}\mathcal{F}v_1 \geq \frac{1}{r(\mathcal{F})}\nu_0\mathcal{F}\zeta_1 = \nu_0\zeta_1.$$

So $v_1 = \mathcal{E}v_1 + \nu_1\zeta_1 \geq \nu_0\zeta_1 + \nu_1\zeta_1 = (\nu_0+\nu_1)\zeta_1$, which contradicts the definition of ν_0. Then relation (21) holds, and by [5] we conclude that

$$i(\mathcal{E}, \mathcal{S}_{\omega_1}, \mathcal{S}) = 0. \tag{22}$$

For f_∞^s, we deduce that there exist $\eta \in (0,1)$ and $\omega_2 > \omega_1$ such that $f(t,y) \leq \eta \frac{1}{\lambda r(\mathcal{F})} y$ for all $t \in [0,1]$ and $y \in [\omega_2, \infty)$. We define the operator $\mathcal{F}_1 : \mathcal{X} \to \mathcal{X}$ by

$$\mathcal{F}_1 v(t) = \eta \frac{1}{r(\mathcal{F})} \mathcal{F} v(t) = \frac{\eta}{r(\mathcal{F})} \int_0^1 \mathcal{G}_2(t,\vartheta) \frac{1}{q(\vartheta)} \left(\int_0^1 \mathcal{G}_1(\vartheta,\tau) r(\tau) v(\tau)\, d\tau \right) d\vartheta,$$

for all $t \in [0,1]$ and $v \in \mathcal{X}$. The operator $\mathcal{F}_1$ is linear and bounded, and $\mathcal{F}_1(\mathcal{S}) \subset \mathcal{S}$. Because $\eta \in (0,1)$ we find $r(\mathcal{F}_1) = \eta < 1$. We consider the set $\mathcal{U} = \{v \in \mathcal{S} \setminus B_{\omega_1},\ \nu v = \mathcal{E} v \text{ with } \nu \geq 1\}$. For $v \in \mathcal{S}$, we denote by $K(v) = \{t \in [0,1],\ v(t) \geq \omega_2\}$. Then for $v \in \mathcal{S}$, we have $v(t) \geq \omega_2$ for all $t \in K(v)$, and so

$$f(t, v(t)) \leq \eta \frac{1}{\lambda r(\mathcal{F})} v(t), \quad \forall\, t \in K(v). \tag{23}$$

By (23) and the definition of operator $\mathcal{F}$, for any $v \in \mathcal{U}$, $\nu \geq 1$ and $t \in [0,1]$, we obtain

$$\begin{aligned}
v(t) \leq \nu v(t) = (\mathcal{E} v)(t) &= \lambda \int_0^1 \mathcal{G}_2(t,\vartheta) \frac{1}{q(\vartheta)} \left(\int_0^1 \mathcal{G}_1(\vartheta,\tau) r(\tau) f(\tau, v(\tau))\, d\tau \right) d\vartheta \\
&= \lambda \int_0^1 \mathcal{G}_2(t,\vartheta) \frac{1}{q(\vartheta)} \left(\int_{K(v)} \mathcal{G}_1(\vartheta,\tau) r(\tau) f(\tau, v(\tau))\, d\tau \right) d\vartheta \\
&\quad + \lambda \int_0^1 \mathcal{G}_2(t,\vartheta) \frac{1}{q(\vartheta)} \left(\int_{[0,1]\setminus K(v)} \mathcal{G}_1(\vartheta,\tau) r(\tau) f(\tau, v(\tau))\, d\tau \right) d\vartheta \\
&\leq \frac{\eta}{r(\mathcal{F})} \int_0^1 \mathcal{G}_2(t,\vartheta) \frac{1}{q(\vartheta)} \left(\int_{K(v)} \mathcal{G}_1(\vartheta,\tau) r(\tau) v(\tau)\, d\tau \right) d\vartheta \\
&\quad + \lambda \int_0^1 \mathcal{J}_2(\vartheta) \frac{1}{q(\vartheta)} \left(\int_0^1 \mathcal{J}_1(\tau) r(\tau) f(\tau, \widetilde{v}(\tau))\, d\tau \right) d\vartheta \\
&\leq \frac{\eta}{r(\mathcal{F})} \int_0^1 \mathcal{G}_2(t,\vartheta) \frac{1}{q(\vartheta)} \left(\int_0^1 \mathcal{G}_1(\vartheta,\tau) r(\tau) v(\tau)\, d\tau \right) d\vartheta \\
&\quad + \lambda J_{10} \left(\int_0^1 \mathcal{J}_2(\vartheta) \frac{1}{q(\vartheta)}\, d\vartheta \right) M_3 = \mathcal{F}_1 v(t) + \lambda J_{10} \left(\int_0^1 \mathcal{J}_2(\vartheta) \frac{1}{q(\vartheta)}\, d\vartheta \right) M_3,
\end{aligned} \tag{24}$$

where $\widetilde{v}(t) = \min\{v(t), \omega_2\}$ for all $t \in [0,1]$, (which satisfies the inequalities $\omega_1 t^{\beta-1} \leq \widetilde{v}(t) \leq \omega_2$ for all $t \in [0,1]$), $J_{10} = \sup_{s\in[0,1]} \mathcal{J}_1(s)$ and $M_3 = \sup_{v \in \overline{\mathcal{S}}_{\omega_2} \setminus \mathcal{S}_{\omega_1}} \int_0^1 r(\vartheta) f(\vartheta, v(\vartheta))\, d\vartheta$, (as in the proof of Lemma 3.1 we find that $M_3 < \infty$). By the Gelfand formula we know that $(I - \mathcal{F}_1)^{-1}$ exists and $(I - \mathcal{F}_1)^{-1} = \sum_{i=1}^{\infty} \mathcal{F}_1^i$, which gives us $(I - \mathcal{F}_1)^{-1}(\mathcal{S}) \subset \mathcal{S}$. This together with (24) imply

$$v(t) \leq (I - \mathcal{F}_1)^{-1} \left(\lambda J_{10} M_3 \int_0^1 \mathcal{J}_2(\vartheta) \frac{1}{q(\vartheta)}\, d\vartheta \right), \quad \forall\, t \in [0,1],$$

and so

$$v(t) \leq \lambda J_{10} M_3 \left(\int_0^1 \mathcal{J}_2(\vartheta) \frac{1}{q(\vartheta)}\, d\vartheta \right) \|(I - \mathcal{F}_1)^{-1}\|, \quad \forall\, t \in [0,1],$$

which means that $\mathcal{U}$ is bounded. Now we choose $\omega_3 > \max\{\omega_2, \sup\{\|v\|,\ v \in \mathcal{U}\}\}$. We obtain $\nu v \neq \mathcal{E} v$ for all $v \in \partial \mathcal{S}_{\omega_3}$ and $\nu \geq 1$. By [5], we deduce that

$$i(\mathcal{E}, \mathcal{S}_{\omega_3}, \mathcal{S}) = 1. \tag{25}$$

By (22), (25) and the additivity property of the fixed point index , we conclude that

$$i(\mathcal{E}, \mathcal{S}_{\omega_3} \setminus \overline{\mathcal{S}}_{\omega_1}, \mathcal{S}) = i(\mathcal{E}, \mathcal{S}_{\omega_3}, \mathcal{S}) - i(\mathcal{E}, \mathcal{S}_{\omega_1}, \mathcal{S}) = 1.$$

Then operator $\mathcal{E}$ has at least one fixed point on $\mathcal{S}_{\omega_3} \setminus \overline{\mathcal{S}}_{\omega_1}$ which is a positive solution of problem (1),(2). □

4 An example

Let $\alpha = \frac{4}{3}$, $\beta = \frac{7}{2}$ $(n = 4)$, $p = 2$, $a = \frac{11}{10}$, $\xi = \frac{1}{3}$, $\gamma_0 = \frac{9}{4}$, $\gamma_1 = \frac{1}{6}$, $\gamma_2 = \frac{5}{3}$, $q(t) = \frac{1}{t+1}$ for all $t \in [0,1]$, $H_1(t) = \frac{t}{4}$ for all $t \in [0,1]$, $H_2(t) = \left\{\frac{1}{3},\ t \in [0, \frac{1}{2});\ \frac{14}{9},\ t \in [\frac{1}{2}, 1]\right\}$, $r(t) = \frac{1}{\sqrt[4]{t(1-t)^3}}$ for all $t \in (0,1)$, $f(t,x) = \sqrt[3]{x} + t^2 + \frac{1}{\sqrt[7]{x^2}}$ for all $t \in [0,1]$ and $x > 0$.

We consider the fractional differential equation

$$D_{0+}^{4/3}\left(\frac{1}{t+1} D_{0+}^{7/2} v(t)\right) = \frac{\lambda}{\sqrt[4]{t(1-t)^3}}\left(\sqrt[3]{v(t)} + t^2 + \frac{1}{\sqrt[7]{v^2(t)}}\right),\ \ t \in (0,1), \tag{26}$$

with the boundary conditions

$$\begin{cases} v(0) = v'(0) = v''(0) = 0,\ \ D_{0+}^{7/2} v(0) = 0,\ \ D_{0+}^{7/2} v(1) = \frac{33}{20} D_{0+}^{7/2} v\left(\frac{1}{3}\right), \\ D_{0+}^{9/4} v(1) = \frac{1}{4}\int_0^1 D_{0+}^{1/6} v(t)\, dt + \frac{11}{9} D_{0+}^{5/3} v\left(\frac{1}{2}\right). \end{cases} \tag{27}$$

We have $\Delta_1 \approx 0.23730259 > 0$ and $\Delta_2 \approx 1.15334282 > 0$, and so assumption $(H1)$ is satisfied. In addition we find $\int_0^1 r(\vartheta) d\vartheta \approx 4.44288294 \in (0, \infty)$, and then assumption $(H2)$ is also satisfied.

For $0 < \theta_1 < \theta_2$, $v \in \overline{\mathcal{S}}_{\theta_2} \setminus \mathcal{S}_{\theta_1}$ and $I_m = \left[0, \frac{1}{m}\right] \cup \left[\frac{m-1}{m}, 1\right]$, we obtain

$$\begin{aligned} \Lambda_m &= \int_{I_m} r(\vartheta) f(\vartheta, v(\vartheta))\, d\vartheta = \int_{I_m} \frac{1}{\sqrt[4]{\vartheta(1-\vartheta)^3}}\left(\sqrt[3]{v(\vartheta)} + \vartheta^2 + \frac{1}{\sqrt[7]{v^2(\vartheta)}}\right) d\vartheta \\ &\le \int_{I_m} \frac{1}{\sqrt[4]{\vartheta(1-\vartheta)^3}}\left(\sqrt[3]{\theta_2} + 1 + \frac{1}{\sqrt[7]{(\vartheta^{5/2}\theta_1)^2}}\right) d\vartheta \\ &= (\sqrt[3]{\theta_2} + 1) \int_{I_m} \frac{d\vartheta}{\sqrt[4]{\vartheta(1-\vartheta)^3}} + \frac{1}{\sqrt[7]{\theta_1^2}} \int_{I_m} \frac{1}{\vartheta^{27/28}(1-\vartheta)^{3/4}} d\vartheta, \end{aligned}$$

and then $\lim_{m\to\infty} \sup_{v \in \overline{\mathcal{S}}_{\theta_2} \setminus \mathcal{S}_{\theta_1}} \Lambda_m = 0$, because $g_1(\vartheta) = \frac{1}{\vartheta^{1/4}(1-\vartheta)^{3/4}} \in L^1(0,1)$ and $g_2(\vartheta) = \frac{1}{\vartheta^{27/28}(1-\vartheta)^{3/4}} \in L^1(0,1)$. So assumption $(H3)$ is satisfied. We also have $f_\infty^s = 0$ and $f_0^i = \infty$. Then by using Theorem 3.1, we conclude that for any $\lambda \in (0, \infty)$, the problem (26),(27) has at least one positive solution $v(t)$, $t \in [0,1]$, which satisfies the condition $v(t) \ge t^{5/2}\|v\|$ for all $t \in [0,1]$.

References

[1] R.P. Agarwal, R. Luca, Positive solutions for a semipositone singular Riemann-Liouville fractional differential problem, *Intern. J. Nonlinear Sc. Numer. Simul.*, **20** (7-8), (2019), 823-832.

[2] B. Ahmad, A. Alsaedi, S.K. Ntouyas, J. Tariboon, Hadamard-Type Fractional Differential Equations, Inclusions and Inequalities, Springer, Cham, Switzerland, 2017.

[3] B. Ahmad, J. Henderson, R. Luca, Boundary Value Problems for Fractional Differential Equations and Systems, Trends in Abstract and Applied Analysis 9, World Scientific, Hackensack, New Jersey, 2021.

[4] A. Alsaedi, R. Luca, B. Ahmad, Existence of positive solutions for a system of singular fractional boundary value problems with p-Laplacian operators, *Mathematics*, **8** (1890), (2020), 1-18.

[5] H. Amann, Fixed point equations and nonlinear eigenvalue problems in ordered Banach spaces, *SIAM Review*, **18** (1976), 620-709.

[6] D. Baleanu, K. Diethelm, E. Scalas, J.J. Trujillo, Fractional Calculus Models and Numerical Methods. Series on Complexity, Nonlinearity and Chaos, World Scientific, Boston, 2012.

[7] S. Das, Functional Fractional Calculus for System Identification and Controls, Springer, New York, 2008.

[8] J. Henderson, R. Luca, Boundary Value Problems for Systems of Differential, Difference and Fractional Equations. Positive Solutions, Elsevier, Amsterdam, 2016.

[9] J. Henderson, R. Luca, Existence of nonnegative solutions for a fractional integro-differential equation, *Results Math.*, **72**, (2017), 747-763.

[10] J. Henderson, R. Luca, A. Tudorache, Positive solutions for a system of coupled semipositone fractional boundary value problems with sequential fractional derivatives, *Mathematics*, **9** (753), (2021), 1-22.

[11] A.A. Kilbas, H.M. Srivastava, J.J. Trujillo, Theory and Applications of Fractional Differential Equations, North-Holland Mathematics Studies, 204, Elsevier Science B.V., Amsterdam, 2006.

[12] J. Klafter, S.C. Lim, R. Metzler (Eds.), Fractional Dynamics in Physics, Singapore, World Scientific, 2011.

[13] R. Luca, On a class of nonlinear singular Riemann–Liouville fractional differential equations, *Results Math.*, **73** (125), (2018), 1-15.

[14] R. Luca, Existence and multiplicity of positive solutions for a singular Riemann-Liouville fractional differential problem, *Filomat*, **34** (12), (2020), 3931-3942.

[15] I. Podlubny, Fractional Differential Equations, Academic Press, San Diego, 1999.

[16] J. Sabatier, O.P. Agrawal, J.A.T. Machado (Eds.), Advances in Fractional Calculus: Theoretical Developments and Applications in Physics and Engineering, Springer, Dordrecht, 2007.

[17] S.G. Samko, A.A. Kilbas, O.I. Marichev, Fractional Integrals and Derivatives. Theory and Applications, Gordon and Breach, Yverdon, 1993.

[18] A. Tudorache, R. Luca, Positive solutions for a system of Riemann–Liouville fractional boundary value problems with p-Laplacian operators, *Adv. Difference Equ.*, **2020** (292), (2020), 1-30.

[19] A. Tudorache, R. Luca, On a singular Riemann–Liouville fractional boundary value problem with parameters, *Nonlinear Anal. Model. Control*, **26** (1), (2021), 151–168.

[20] Y. Zhou, Basic Theory of Fractional Differential Equations, World Scientific, Singapore, 2014.

Some aspects of rainbows and black hole linked to Mandelbrot set and Farey diagram

Alberto Tufaile[1], Lori-Anne Gardi[2], and Adriana Pedrosa Biscaia Tufaile[3]

[1] Soft Matter Lab, EACH, University of São Paulo, 03828-000, São Paulo, Brazil (E-mail: tufaile@usp.br)
[2] Western University, 1151 Richmond St, London, ON N6A 3K7, Ontario, Canada. (E-mail: lori.anne.gard@gmail.com)
[3] Soft Matter Lab, EACH, University of São Paulo, 03828-000, São Paulo, Brazil (E-mail: atufaile@usp.br)

Abstract. We present in this work some experiments involving the optics of systems where the paraxial optics approximation cannot be applied, as in the case of rainbow formation by raindrops and the case of light deflection by massive objects, such as in the vicinity of black holes. The first experiment is the injection of laser light into a glass cylinder, while the other is a circular billiard formed by a circular mirror and a laser beam. We use the theory of dynamical systems and the Mandelbrot set as an analogy to represent the paths of the light beam, as well as the properties involving the Farey sequence.

Keywords: Farey mediant, Optics, Dynamical Systems, Mandelbrot set.

1 Introduction

This work was developed due to the authors' interest in different aspects of dynamical systems that involve optics [1, 2], gravitation and the aesthetic appeal of fractal forms [3,4]. In this way we will present some connections between concepts of optics and Mandelbrot sets resulting from recursion formulas, feedback processes or systems in which we have the repeated application of some mapping rule.

How to compare trajectories of light rays with a recursive mapping normally used in dynamic systems? In Fig. 1 we have a luminous ray inside a glass plate that undergoes multiple reflections. A change in the path of this ray can be associated with the series of events shown in Fig. 1 (b). This series of events is reproduced topologically with the "circle map" of the graphic diagram in Fig. 1 (c), with the Poincaré section shown in Fig. 1 (d) [1]. We can see the same thing applied to period-3 in Fig. 1(e) for the case of the circle map, and the same dynamical system in a circular billiard in (f) and (g). For the cases found in nature, we know from optics that light rays in a raindrop of Fig. 2, which can behave like particles in a circular billiard, forming multiple rainbows, through recurring internal reflections. In this case, in addition to the rays of light that hit the droplet wall several times, obeying the law of reflection, we have rays that escape the droplet by refraction forming multiple rainbows, which give us some information about the shape of the droplet, as in the case of twin rainbows, in which we see an ellipsoidal rainbow between two circular rainbows, which

appears to be a bifurcation, as it also occurs in other atmospheric optics phenomena, as in the case of the circumscribed halo surrounding the 22-degree solar halo of Fig. 3.

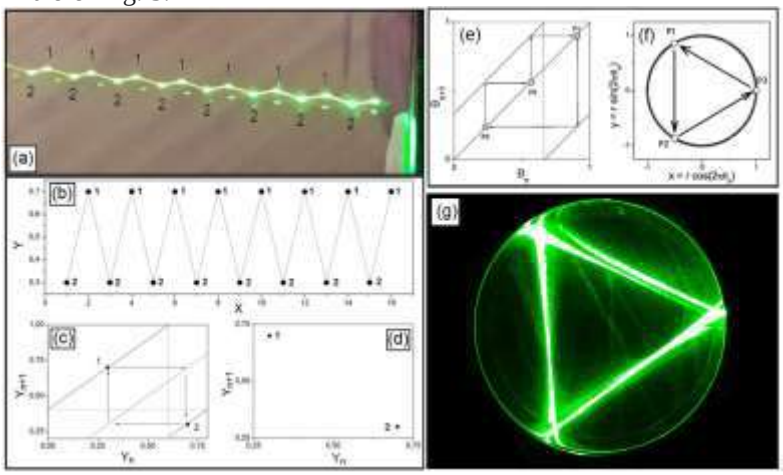

Fig. 1. Multiple reflections of a laser beam in a glass plate in (a). (b) sequence of events (c) Iterations in the circle map for a period-2 (d) Poincaré section of this period-2. Circle map in a period-3 in a circle map and its respective orbits in a circle in (f). Experiment showing multiple reflections in a period-3 in a reflective cylinder in (g).

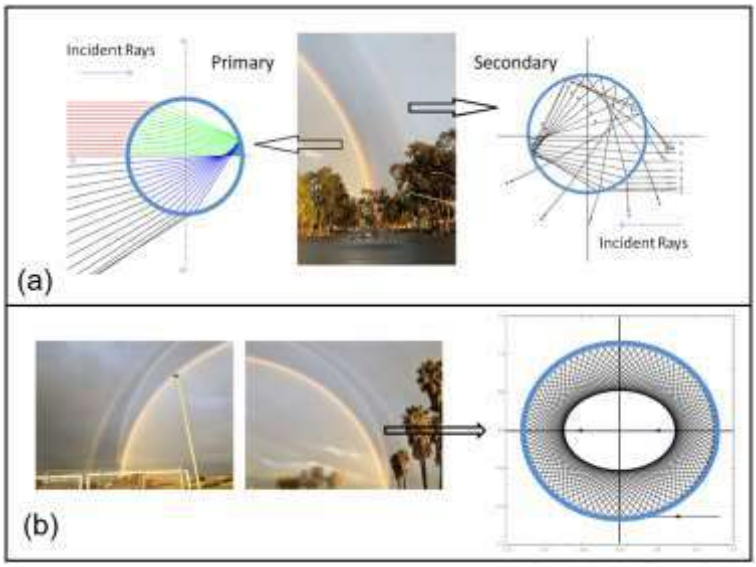

Fig. 2. In (a) reflections in a rain drop and primary rainbow, and reflections in a drop and secondary rainbow. In (b) the curious case of twin rainbows that could be explained considering elliptical drops.

In the context of relativity, massive objects can "bend" light, forming Einstein's rings [1], which behave like lenses, as in the case of the lens in the form of a pseudo-sphere. In the case of a black hole acting as a lens in Fig. 3(b), the properties of Minkowsky's space-time are altered by the presence of the mass, causing it to curve around itself, as if it were an optical lens. We also observed the reverse shape of this lens causing light to be distorted in Fig. 3(c).

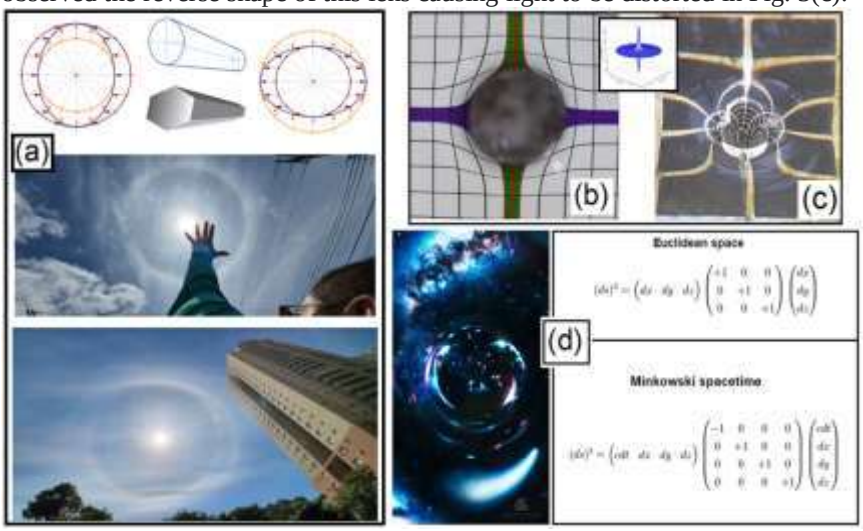

Fig. 3. In (a) cylinders and hexagonal bars can be used as lens with a laser to generate patterns. For the case of cylinder, we can associate elliptical profile with two circles. In 22 degree halo formed by hexagonal column of ice crystals can be measured with a hand flat. The 22 degree halo and the circumscribed halo. A pseudosphere lens in (b) and inverse pseudosphere lens from a pool drain in (c). Comparing the three-dimensional Euclidean space and Minkowski spacetime in (d) with a representation of the optical effects of a massive object such as black hole. In the four-dimensional Minkowski spacetime used in general relativity equations, time and space expand in opposite direction, with one solution of these equations being the black hole depicted in (d).

In our previous work on this subject, we studied rainbows and massive objects in the formation of luminous halos, starting from an optical system composed of a cylinder with the injection of a laser beam of Fig. 4, where we use the circular section of the cylinder and compare it with the circular section of a drop. The modification of the cylinder topology led to the case of the pseudo-sphere.

This optical system formed by the laser hitting obliquely in the glass cylinder of Figs. 4(c)-(d), behaves like an open billiard, with which we can see the formation of curious patterns associated with the star polygons, which due to the fact of restrictions to the total internal reflection, follow some rules related to a Farey mediant of Fig. 4(f). This system is related to the phenomenon known

as period locking (mode-locking), which can be observed in patterns projected on a screen of Fig. 5. This mode-locking is also seen in Mandelbrot set systems.

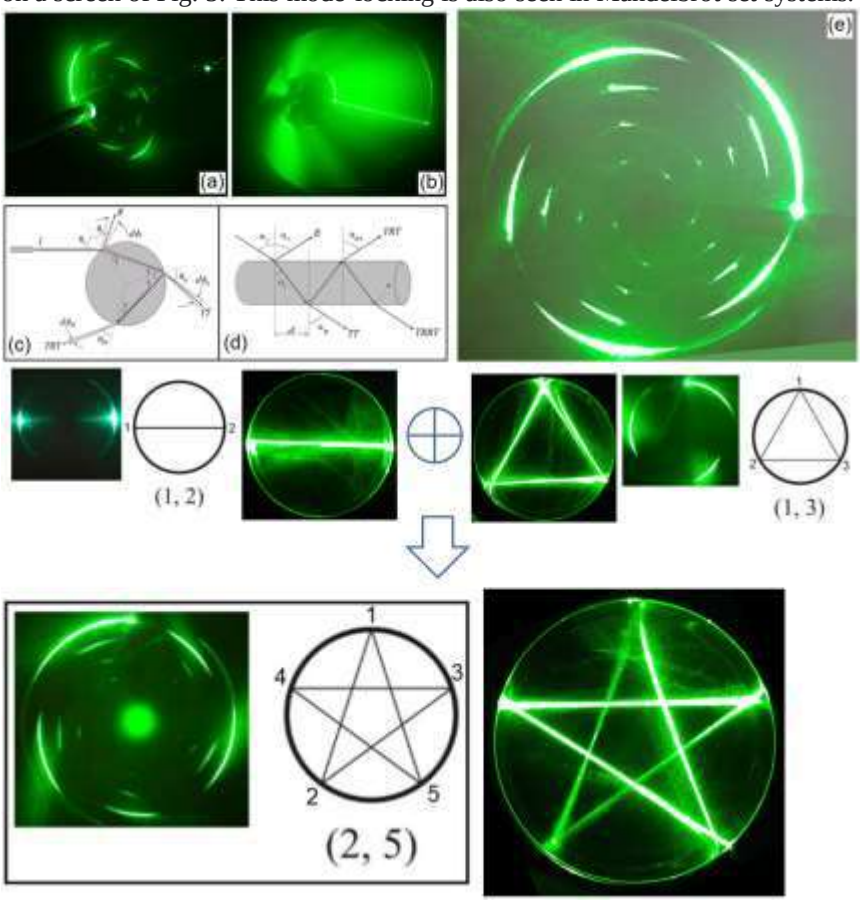

Fig. 4. Images of light scattering in cylinders in (a) and (b). Diagrams of light rays in the glass cylinder in (c) and (d). Light spiral in (e) obtained from this experiment. Comparison between stellar polygons in a billiard and the case of the glass cylinder, in which we can observe the case of Farey's mediant in (f).

Increasing the inclination of the laser beam in the cylinder, we perceive a process of “optical deformation” of the circular section of the cylinder, for an elliptical billiard. With that, we recognize some interesting effects like the formation of caustics in the rainbow angle, which unfolded in separated branches [1]. This suggested to us the possibility that elliptical rainbows may be related to caustics unfolded from the cylinder, as discussed in the literature for ellipsoidal drops of fig. 2(b).

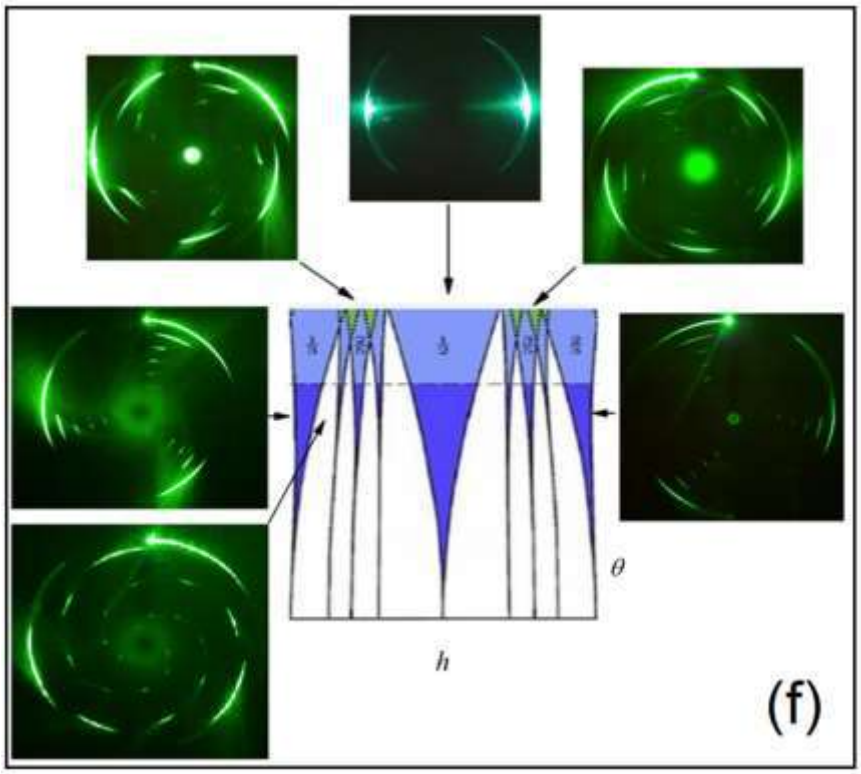

Fig. 5. Circle map and cone of light. In (a) and (b) images of cone laser scattering from a cylinder of the diagrams shown in (c) and (d). Light spiral of this system in (e). (f) Mode-locking and Farey sequence in the Arnold tongues with some light patterns.

2 Mandelbrot set and star polygons.

Motivated by the observation of geometric patterns in the laser / cylinder system, we realized that the formation of caustics in cylinders may be related to the recursive rotations of maps in the complex plane, as in the case of the Mandelbrot Set, with the formation of star polygons for different initial conditions. The evolution of the iterations in Mandelbrot set presents a rich dynamics, with some complete routes to chaos, like Feigenbaum route and mode-locking route to chaos, besides intermittency. The Mandelbrot can be used as a toy model to explore the dynamics of the light in the cylinder, in order to help to explore this system and the pseudo-sphere used to simulate black holes or massive objects bending light.

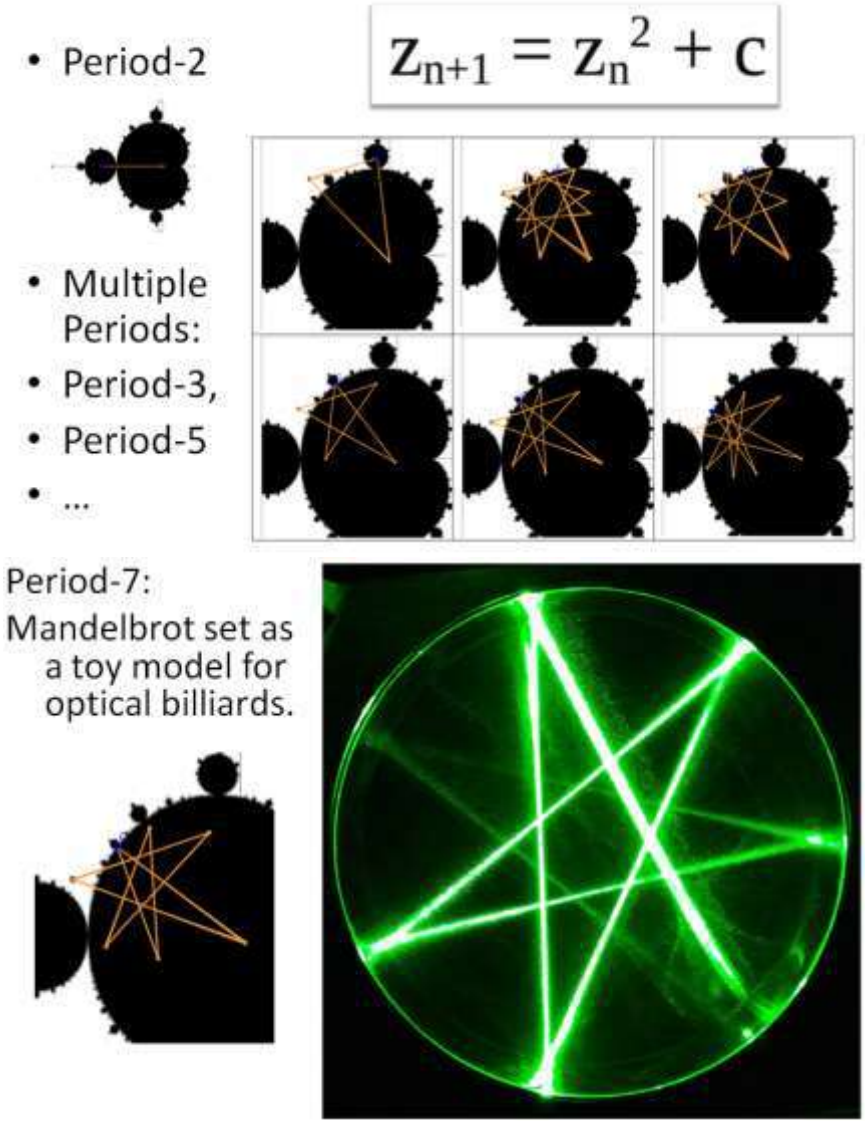

Fig. 6. Some star polygons in the Mandelbrot set. Period-7 in the Mandelbrot set and in the circular billiard.

For example in Fig. 6, we present the existence of star polygons in the Mandelbrot set, with period-2, peripd-3, period-5 and period-7. For this last case we can compare the dynamics of ray in a billiard forming a period-7 with the Mandelbrot set.

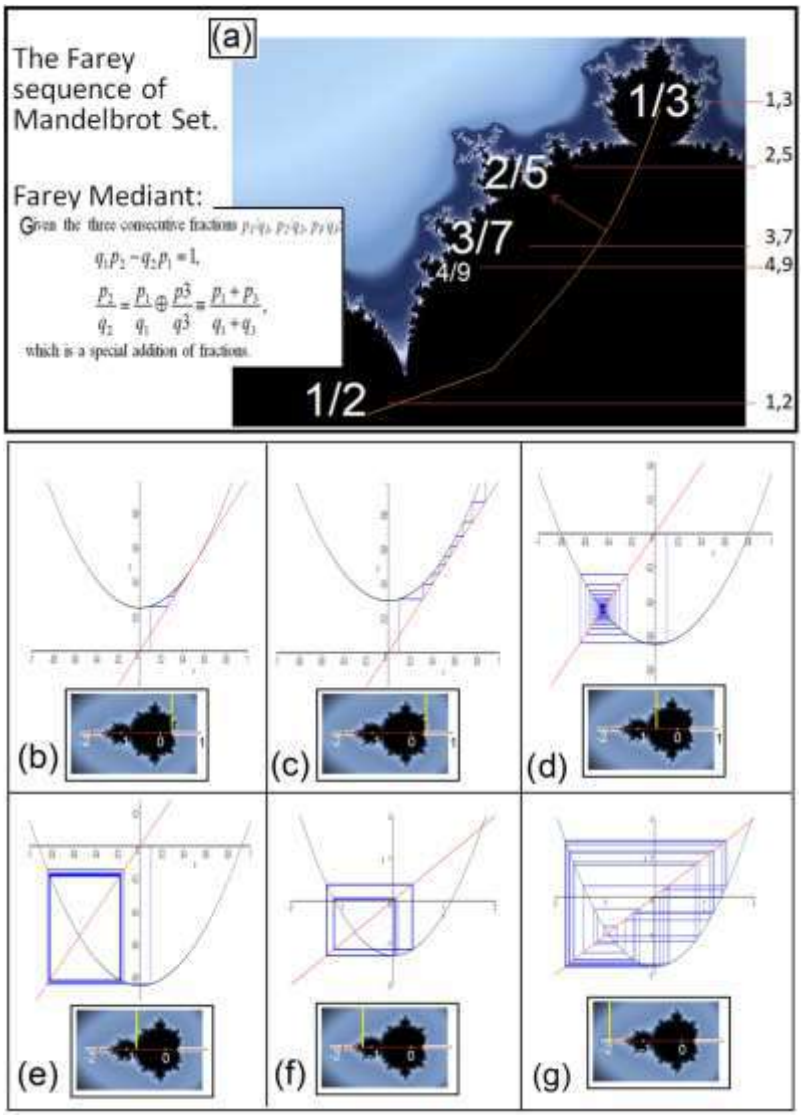

Fig. 7. Example of Farey sequence in the mandelbrot set ans the stability for some initial conditions in the Mandelbrot set.

The orbits of the Mandelbrot system are directly related to the Farey mediant, as shown in the diagram in Fig. 7(a). The stability of the orbits can be observed with the cobweb diagram for values of the Mandelbrot set with real numbers. We can observe the stability of the system converging to a fixed point in Fig. 7(b). When the control parameter is changed in 7(c), we have different behaviors such as intermittency in Fig. 7(b), or this fixed point becoming a saddle point in which a doubling of period occurs in Fig. 7(e). Changing the

control parameter further, we have a period-4 in Fig. 7(f), followed by chaotic behavior in Fig. 7(g).

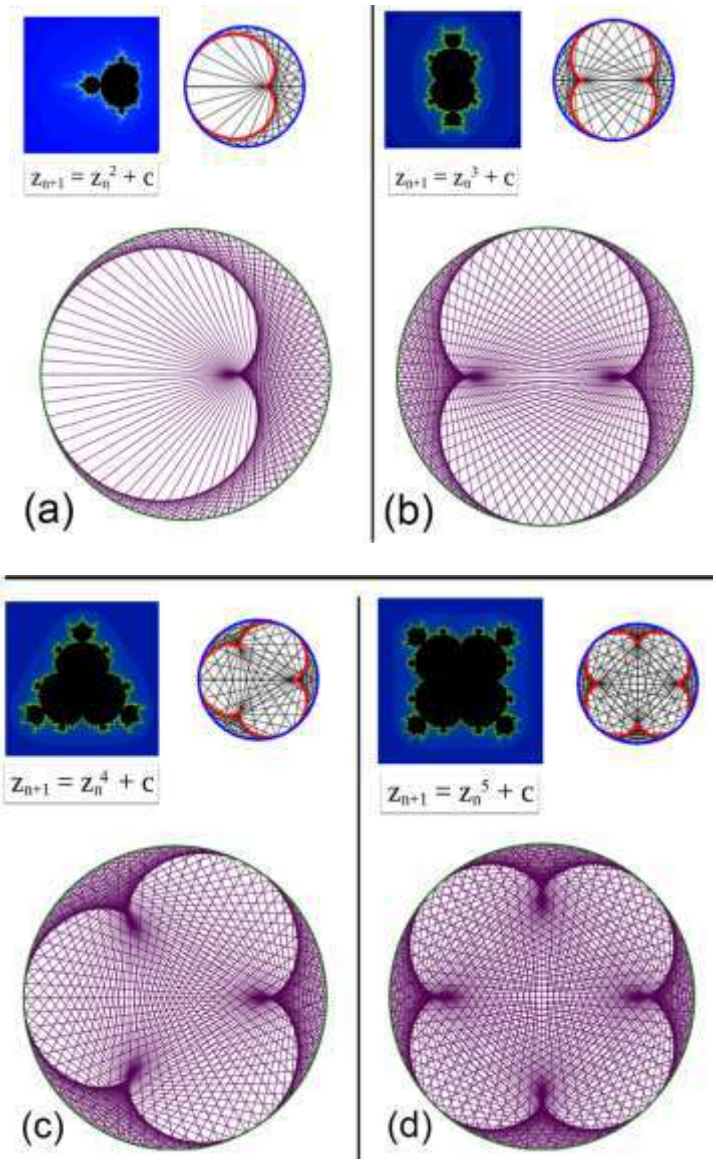

Fig. 8. Mandelbrot set and some caustics obtained with multiplication table applied to ray dynamics in a circle: in (a) the cardioid, in (b) the nephroid, with three lobes in (c) and with four lobes in (d).

Another interesting relationship between the Mandelbrot set and the formation of caustics in a circular billiards is shown in Fig. 8. This relationship can be better understood by watching the video cited in the references [5] along with the papers describing the process of caustic formation [6, 8]. The central idea is that these caustics are related to the fractal pattern profile associated with different polynomials of the Mandelbrot set.

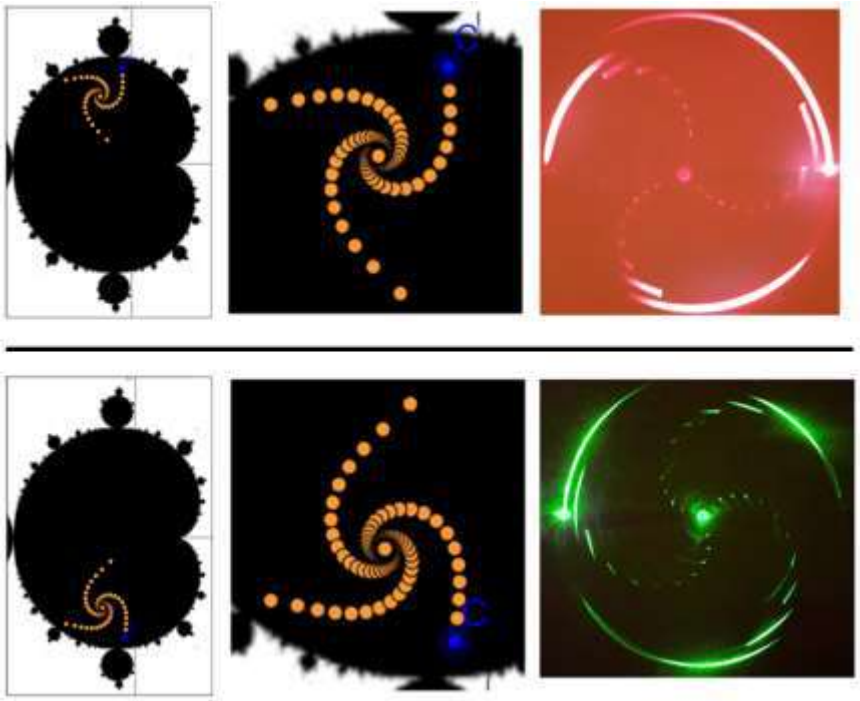

Fig. 9. Dynamics of spiral formation in the Mandelbrot set compared to the laser in the glass cylinder.

Finally, we show in Fig. 9 two examples of initial conditions in the Mandelbrot set for the case of orbits forming spiral patterns and compare them with the case of the experiment with the laser beam in the glass cylinder. We can see that the rotation orientation of the spiral depends on the position of choice of the initial condition, represented by the blue dot, with respect to the horizontal axis, which makes the spiral clockwise or counterclockwise. The same happens with the experimentally observed dynamical system, with the choice of the starting point that the laser beam touches the glass cylinder with respect to the horizontal axis, with the red spiral rotating clockwise and the green spiral rotating counterclockwise. For more information about these experiments, we recommend this video in references [9].

Conclusions

These connections between billiard systems, Optics, Mandelbrot set and caustics were explored due to their interesting aesthetic appeal, which facilitates the investigation of the optical system with the well-known system formed by Mandelbrot set. Multiple reflections of a laser inside a cylinder, which escapes by refraction and can projected in a screen, can be compared to the trajectories of the iterations of Mandelbrot map for certain regions in the Argand plane. In systems like the ones discussed in this paper, we can observe mode-locking and the formation of star polygons. These comparisons allow us to extract the essence of the dynamics existing in experimental optical systems that we cannot use the well-known paraxial optics, as happens in real physical systems such as light in raindrops or in a black hole. In the case of massive object optics, such as the bending of light around black holes, matrix operations involving Minkowski space can generate rotations that cause the doubling of light rays from distant stars, as well as the formation of halos, such as Einstein rings, which were discussed in the case of light patterns in the laser/glass cylinder system.

Nonlinear dynamical systems that involve some kind of rotation as the case of the map of the circle presented in our previous works, or the Mandelbrot set, or matrix operations for the case of general relativity, can lead to certain results that can be observed experimentally with a non-paraxial optic that involves multiple reflections as in the case of the cylinder/laser and circular billiards. In this work, we emphasize how the use of Mandelbrot systems helps us to explore the different behaviors in a practical way, observing the different types of orbits based on the choice of initial conditions, which allows us to analyze the stability behavior of these orbits. Furthermore, we reproduce some interesting results of the formation of caustics in circular billiards through the multiplication rules, which are directly connected with Mandelbrot polynomials and their remarkable fractal representation. Overall, we believe that a lot can still be explored in the context of these analogies.

References

1. A. Tufaile, A. P. B. Tufaile, Halo Dynamics: From Rainbows to Black Holes, Proceedings of 13th Chaotic Modeling and Simulation International Conference, https://www.researchgate.net/publication/344929431_Halo_Dynamics_From_Rainbows_to_Black_Holes
2. Lori Gardi, The Mandelbrot Set as a Quase-Black Hole, Proceedings of CNPS, http://www.theomparticle.com/OMparticle/Paper.pdf
3. A. Tufaile, A. P. B. Tufaile, Parhelic-like circle from light scattering in Plateau Borders, Phys. Let. A, 379, 529-534, 2015.
https://doi.org/10.1016/j.physleta.2014.12.006
4. A. Tufaile, A. P. B. Tufaile, The dynamics of diffracted rays in foams, Phys. Let. A, 379, 3059-3098, 2015. https://doi.org/10.1016/j.physleta.2015.10.011

5. Multiplication Table, Mandelbrot and the Heart of Mathematics (Tabuada de Multiplicação, Mandelbrot e o Coração da Matemática), Mathologer, YouTube, https://youtu.be/qhbuKbxJsk8
6. E. Pegg Jr., Modular multiplication on a circle, Wolfram Demonstration Project. https://demonstrations.wolfram.com/ModularMultiplicationOnACircle/
7. J. Kowszun, Mandelbrot set, https://www.geogebra.org/m/VbRZXqDV
8. S. Plouffe, The reflection of light rays in a cup of coffee or the curves obtained with bˆn mod p,
http://xahlee.info/SpecialPlaneCurves_dir/Cardioid_dir/_p/LightsRaysReflections.pdf
9. Chaos, Rainbows and Black Holes, Alberto Tufaile, YouTube, https://youtu.be/zljw0GxNvc4

Sequences of PRN's from algebraic curves over the ring $\mathbb{Z}_{p^m}$

Sergey Varbanets[1] and Yakov Vorobyov[2]

[1] Department of Computer Algebra and Discrete Mathematics, Odessa I.I. Mechnikov National University, Dvoryanskaya street 2, Odessa, Ukraine (E-mail: varb@sana.od.ua)

[2] Department of Mathematics, Informatics and Information Activities, Izmail State University of Humanities, Repina street 12, Odessa, Ukraine (E-mail: yashavo@mail.ru)

Abstract. In this work there is considered the method of producing the sequences of pseudorandom numbers basing on solutions of congruences of two variables modulo the power of prime number. The estimates of discrepant function of constructed sequences of pseudorandom numbers have been obtained.
Keywords: pseudorandom numbers, elliptic curve, exponential sum, discrepancy.

1 Introduction

Following the revelation of public-key cryptography that arose at the last quarter of XX century, in 1985 Nil Koblitz and Victor Miller have found that the elements over the group of points from elliptic curve over finite field are able to store the secrete information due to of complexity on addition operation. And it would serve as motive to study the cryptography on elliptic curves. The sequences of pseudorandom number at every time was being intrinsic part of cryptography, and therefore for the last 20 years the theory of elliptic curves has application in problem of generating of sequences of pseudorandom numbers. The useful survey in this direction belongs to I. Shparlinskii[4].

In our paper we consider the algorithm of producing the sequences of pseudorandom numbers from algebraic curves over the ring $\mathbb{Z}_{p^m}$ of residue classes of prime power modulus. The according elements of such sequences accept the polynomial representation over $\mathbb{Z}_{p^m}$. We demonstrate this concept to construct the sequences of pseudorandom numbers of algebraic curves

$$y^2 \equiv x^3 + ax + b \pmod{p^m}$$

and

$$ax^3 + y^3 \equiv 1 \pmod{p^m}.$$

The constructed sequences have the fixed period $\tau = p^{m-1}$ that can be grown as for the growth of prime number p or factor m.

Notations. The letter p denotes a prime number, $p \geq 3$. For $n \in \mathbb{N}$ the notations $\mathbb{Z}_{p^m}$(accordingly, $\mathbb{Z}_{p^m}^*$) denote the complete (accordingly, reduced)

system of residues modulo p^m. We write (a, b) for notation a great common divisor of a and b. For $z \in \mathbb{Z}$, $(z, p) = 1$ let z' or z^{-1} be the multiplicative inverse of a modulo p^m. We write $\nu_p(A)$ if $p^{\nu_p(A)} | A$, $p^{\nu_p(A)+1} \nmid A$. Landau symbol "O" is equivalent to Vinogradov symbol "$\ll$". The notation $f(x) \ll g(x)$ means that for $x \to \infty$ the inequality $|f(x)| \leq C \cdot g(x)$ holds with arbitrary constant C. Through $[x]$ we will denote the integral part of real number x.

2 Auxiliary results

Let $E(\mathbb{F}_p)$ be an elliptic curve defined over $\mathbb{F}_p$ given by an affine Weierstraβ equation of the form

$$Y^2 + (a_1X + a_3)Y = X^3 + a_2X^2 + a_4X + a_6,$$

where $a_1, a_2, a_3, a_4, a_6 \in \mathbb{F}_p$ such that the partial derivations $\frac{\partial F}{\partial X}$ and $\frac{\partial F}{\partial Y}$ for the function

$$F(X, Y) = Y^2 + (a_1X + a_3)Y - X^3 - a_2X^2 - a_4X - a_6$$

do not become zero simultaneously at the points of the curve $(x, y) \in E(\overline{\mathbb{F}}_p)$ over the algebraic closure $\overline{\mathbb{F}}_p$ of $\mathbb{F}_p$.

For the case $p > 3$ the previous equation can be deduce to form

$$Y^2 = X^3 + ax + b \tag{1}$$

for some $a, b \in \mathbb{F}_p$ with $4a^3 + 27b^2 \neq 0$.

We recall that the set of points of curve $E(\mathbb{F}_p)$ together with point at infinity $\mathcal{O}$, relatively to a special operation $\oplus$, forms the abelian group E_p of order $\mathcal{N}(E_p)$ which satisfies inequality

$$|\mathcal{N}(E_p) - p - 1| \leq 2p^{\frac{1}{2}}.$$

For a point $Q \in E(\mathbb{F}_p)$ we use $x(Q)$, $y(Q)$ to denote its coordinates, that is, $(x(Q), y(Q))$.

For $m > 1$ we denote $E_p(m)$ as the set of solutions (x, y) satisfying to the congruence

$$y^2 \equiv x^3 + ax + b \pmod{p^m} \tag{2}$$

The set $E_p(m)$ we will call the elliptic curve over the ring $\mathbb{Z}_{p^m}$ and $\mathcal{N}(E_p(m))$ be a number of solutions of (2) with condition $(y, p) = 1$.

Lemma 1. *Let (x_0, y_0) be a solution of (2) with $(y_0, p) = 1$ and $m = 1$. Then for any integer t the congruence*

$$y^2(t) \equiv (x_0 + pt)^3 + a(x_0 + pt) + b \pmod{p^m} \tag{3}$$

has just two incongruent solutions modulo p^m for every positive m.

The assertion of this lemma follows from the fact that any solution (x_0, y_0) of congruence (3) with $m = 1$ we can grow to the solutions $y_1(t) = y(t)$, $y_2(t) = -y(t)$.

Denote by $y_i(t)$, $i = 1, 2$ the solution of congruence (3).

Lemma 2. *Let $p > 2$ be a prime, $m \geq 3$ be an integer, $s = \left[\frac{p-1}{p-2}m\right]$. There exist the polynomial $\varphi(t) \in \mathbb{Z}_{p^m}[t]$ of degree s*

$$\varphi(t) = \phi_0(x_0) + p^{\lambda_1}\phi_1(x_0)t + \cdots + p^{\lambda_s}\phi_s(x_0) \cdot t^s,$$

where $(\phi_i(x_0), p) = 1$, $i = 0, 1, \ldots, s$, and $\lambda_1, \lambda_2, \ldots, \lambda_s \in \mathbb{N}$, moreover

$$\lambda_j \geq j\frac{p-2}{p-1},\ j = 1, \ldots, s.$$

such that

$$y_i(t) = y_i(0)\varphi(t) \pmod{p^m},\ i = 1, 2,$$

and the points $(x_0 + pt, y_i(t))$, $i = 1, 2$, belong to the elliptic curves (2).

Proof. Let (x_0, y_0) is the solution of (2) for $m = 1$, $(y_0, p) = 1$. For every t, $0 \leq t \leq p^{m-1} - 1$, we denote $y_1(t)$, $y_2(t)$ as two different solutions of the congruence

$$y^2(t) \equiv (x_0 + pt)^3 + a(x_0 + pt) + b \pmod{p^m}.$$

Denote by x_0' the multiplicative inverse of $x_0^3 + ax_0 + b$, i.e.

$$x_0'(x_0^3 + ax_0 + b) \equiv 1 \pmod{p^m}.$$

Such solution exists since $(y_0, p) = 1$.
Hence, we find that (3) is equivalent to

$$y^2(t) \equiv (x_0^3 + ax_0 + b)(1 + (3ptx_0^2 + 3p^2t^2x_0 + p^3t^3)x_0').$$

Let $U^2(\omega) = (1 + (3\omega x_0^2 + 3\omega^2 x_0 + \omega^3)x_0')$.
Expanding the function $U(\omega)$ to series in powers of ω

$$U(\omega) = \sum_{i=0}^{\infty} X_i(x_0, x_0')\omega^i$$

and its logarithmic derivation

$$\frac{d\log U(\omega)}{d\omega} = \frac{U'(\omega)}{U(\omega)} = \frac{\sum\limits_{i=1}^{\infty} iX_i(x_0, x_0')\omega^{i-1}}{\sum\limits_{i=0}^{\infty} X_i(x_0, x_0')\omega^i}$$

gives the following recursion formulas for $j = 2, 3, \ldots$:

$$\begin{aligned} X_{j+1} = & -\frac{2j+1}{2(j+1)}(3x_0^2x_0' + ax_0)X_j \\ & -\frac{3(j-2)}{j+1}x_0x_0'X_{j-1} \\ & -\frac{2j-7}{2(j+1)}x_0'X_{j-2}, \end{aligned} \tag{4}$$

$$X_0 = 1,$$

$$X_1 = \frac{1}{2}(3x_0^2x_0' + ax_0),$$

$$X_2 = \frac{1}{2}3x_0x_0' - \frac{1}{8}(3x_0^2x_0' + ax_0')^2.$$

Let show that the formal p-adic series for $U(pt)$ converges in p-adic metric and modulo p^m the congruence

$$U(pt) \equiv \varphi(t) \pmod{p^m},$$

where

$$\varphi(t) = \phi_0(x_0) + p^{\lambda_1}\phi_1(x_0)t + \cdots + p^{\lambda_s}\phi_s(x_0)\cdot t^s, \tag{5}$$

and $\varphi_j(x_0) \in \mathbb{Z}$, $\lambda_j \in \mathbb{N}$ and $\lambda_j \geq m$ for $j > s$. holds.

In our reasoning we will use p-adic analysis by schema of L.P. Postnikova[3].

Let us introduce the variables Y_j, Z_j, $j = 1, 2, \ldots, s$ defined by the conditions

$$Y_1 = 0,\ Y_2 = 1,\ Y_3 = \frac{1}{2}(3x_0^2x_0' + ax_0'),$$
$$Z_1 = 0,\ Z_2 = 0,\ Z_3 = 1$$

and for $j \geq 4$ Y_j, Z_j be determined by recursion formulas of type (4).

Let us consider determinants

$$\Delta_j = \begin{vmatrix} X_{j-2} & X_{j-1} & X_j \\ Y_{j-2} & Y_{j-1} & Y_j \\ Z_{j-2} & Z_{j-1} & Z_j \end{vmatrix},\ j = 3, 4, \ldots, s.$$

In particular, we have modulo p^m

$$\Delta_3 = \frac{1}{2}(3x_0x_0' + ax_0').$$

From this moment on, we suppose that $-3a$ is the non-quadratic residue modulo p. Therefore, we have

$$(x_0', p) = 1,\ (3x_0^2 + a, p) = 1.$$

(since otherwise the congruence $x^2 \equiv -3a \pmod{p}$ has the solution).

But then $\nu_p(\Delta_3) = 0$.

Also for $j \geq 4$ we easily obtain

$$\Delta_j = -\frac{2j-9}{2j} x_0' \Delta_{j-1} =$$
$$\cdots = (-x_0')^{j-s} \frac{(2j-9)(2j-11)\cdots 3 \cdot 1 \cdot (-1)}{2^{j-s} j(j-1)\cdots 4} \Delta_3 =$$
$$= (-x_0')^{j-3} \frac{(2j-9)! \cdot 6}{2^{2j-7} j!(j-4)!} \Delta_3.$$

Let $\nu_p(X_j p^j) = \lambda_j$, $\nu_p(Y_j p^j) = \mu_j$, $\nu_p(Z_j p^j) = \tau_j$.

Now let take out a common factor $p^{\min(\lambda_{j-1}, \lambda_j, \lambda_{j-2})}$ from the first row of determinant Δ_j. From the second and third rows let do the same with $p^{\min(\mu_{j-1}, \mu_j, \mu_{j-2})}$ and $p^{\min(\tau_{j-1}, \tau_j, \tau_{j-2})}$, respectively.

It easy prove that

$$\lambda_j \geq j\frac{p-2}{p-1},\ \mu_j \geq j\frac{p-2}{p-1},\ \tau_j \geq j\frac{p-2}{p-1}.$$

Now, taking into account the relation between Δ_j and Δ_3 we easily find

$$\min(\lambda_j, \lambda_{j-1}, \lambda_{j-2}) \leq 3j - 3 - 2(j-2)\tfrac{p-2}{p-1} +$$
$$+ \sum_{k=1}^{\infty} \left[\tfrac{2j-9}{p^k}\right] - \sum_{k=1}^{\infty} \left[\tfrac{j}{p^k}\right] - \sum_{k=1}^{\infty} \left[\tfrac{j-4}{p^k}\right].$$

Also take into account that $[2x] \leq 2[x] + 1$ for $x \geq 0$, and the quantity of nonzero summand in sum $\sum\limits_{k=1}^{\infty} \left[\tfrac{2j-9}{p^k}\right]$ be at most $\tfrac{2j-9}{p} < \tfrac{2j}{p-1}$.

Then we have

$$\min(\lambda_j, \lambda_{j-1}, \lambda_{j-2}) \leq j + 1 + \frac{4(j-1)}{p-1}.$$

Bringing up the definition for $\varphi(t)$ (5) we at once obtain the proof of Lemma 2. □

Corollary 1. *In the conditions of Lemma 2 we obtain p-adic description of the solutions of the congruence*

$$y^2 \equiv x^3 + ax + b \pmod{p^m}$$

in the form

$$x = x_0 + pt,\ \ y_i(t) = y_i(0)(1 + A_1 pt + A_2 p^2 t^2 + A_3 p^{\lambda_3} t^3 + \cdots)\ (mod p^m),$$

where

$\lambda_1 = 1,\ \lambda_2 = 2,\ \lambda_3 \geq 3,\ j = 3, 4, \ldots;$

$A_0 = 1,\ A_1 = 2^{-1}(3x_0^2 x_0' + a x_0'),\ A_2 = 3 \cdot 2^{-1} x_0 x_0' - 2^{-3}(3x_0^2 x_0' + a x_0')^2;$

$(A_i, p) = 1,\ i = 1, 2, 3, \ldots.$

(here 2^{-1} be the multiplicative inverse for 2 modulo p^m).

Corollary 2. *For the fixed $x_0, y_0 \in E_p$ and $y_i(0)$, $i = 1, 2$ we have*

$$y_i(t_1) \equiv y_i(t_2) \pmod{p^m}$$

if and only if $t_1 \equiv t_2 \pmod{p^{m-1}}$. And hence, the sequences $y_i(t)$, $t = 0, 1, \ldots, p^{m-1} - 1$ have the least period $\tau = p^{m-1}$ (here $i = 1$ or 2, $y_2(t) = -y_1(t)$). Thus we obtain the family of different sequences $\{y(t)\}$, which define by selection of initial point (x_0, y_0) on the curve E_p and by selection of index $i \in \{1, 2\}$.

Bellow we will show that the sequence of real numbers $\{\frac{y(t)}{p^m}\}$, $t = 0, 1, \ldots$, $p^{m-1} - 1$ be the sequence of real numbers from $[0, 1)$ that may be considered as the sequence of pseudorandom numbers passes the serial test on pseudorandomness.

Note that the same point (x_0, y_0) of elliptic curve E_p generate two sequences $y_i(t)$ defined by Lemma 2, the selection of which defines by the values of $y_i(0)$ as the solution of congruence

$$y^2 \equiv x^3 + ax + b \pmod{p^m}.$$

If $0 < y(0) < \frac{p}{2}$ then $y_i(t)$ denotes by $y_1(t)$, otherwise we have $y_2(t)$.

Over constructed set of sequences $\{y(t)\}$ we can define operation "$*$" by the following way:

$$y'(t) * y''(t) = y'''(t),$$

where $y'''(t)$ defines by sum of two points (x'_0, y'_0) and (x''_0, y''_0) of elliptic curve E_p

$$(x'_0, y'_0) \oplus (x''_0, y''_0)$$

and by Lemma 2, where $0 < y'''(0) < \frac{p}{2}$ if $y'(0)$ and $y''(0)$ simultaneously belong to $\left[0, \frac{p}{2}\right]$ or $\left[\frac{p}{2}, p\right]$. Otherwise, $y'''(0)$ is selected from interval $\left[\frac{p}{2}, p\right]$.

Similarly, we can construct the sequence $\{y(t)\}$ same to the sequence from Lemma 2 produced by the congruence

$$y^\ell \equiv f(x) \pmod{p^m},$$

where $f(x)$ be the polynomial with integer coefficients of degree ≥ 3.

In particular, let see the congruence

$$ax^3 + y^3 \equiv 1 \pmod{p^m}. \tag{6}$$

We will assume that p be the prime number of form $6k - 1$.

Define by $y(t)$ the solution of congruence

$$y^3 \equiv 1 - a(x_0 + pt)^3 \pmod{p^m}. \tag{7}$$

where (x_0, y_0) be the anyone solution of congruence

$$y^3 \equiv 1 - ax^3 \pmod{p}.$$

with $1 - ax_0^3 \not\equiv 0 \pmod{p}$. Every of such x_0 uniquely define the respective y_0. So, the solution $y(t)$ of congruence (7) defines uniquely.

Lemma 3. *Let* $s = \left[\frac{p-1}{p-2}m\right]$. *There exists the polynomial of degree* s

$$\varphi(t) = \Phi_0(x_0) + p^{\lambda_1}\Phi_1(x_0)t + \cdots + p^{\lambda_s}\Phi_s(x_0)t^s,$$

where $(\Phi_i(x_0), p) = 1$, $i = 0, 1, \ldots, s$; $\lambda_1, \ldots, \lambda_s$ *are the natural numbers satisfy the inequalities* $\lambda_j \geq j\frac{p-2}{p-1}$, *such that*

$$y(t) \equiv y(0)\varphi(t) \pmod{p^m}.$$

The proof of this lemma passes simultaneously to proof of Lemma 2 and the respective coefficients $\Phi_j(x_0)$ define by recurrent relation

$$\Phi_{j+1} = \frac{3j-1}{j+1}ax_0^2x_0'\Phi_j + \frac{3j-5}{j+1}ax_0x_0'\Phi_{j-1} + \frac{j-3}{j+1}ax_0'\Phi_{j-2},$$

moreover,

$$\Phi_0 = 1,\ \Phi_1 = -ax_0^2x_0',\ \Phi_2 = -ax_0x_0' - a^2x_0^4x_0'^2.$$

Here, x_0' is the multiplicative inverse modulo p^m for $1 - ax_0^3$.

3 Discrepancy

Let $\{x_n\}$ be the sequence of points from $[0, 1)$. As characteristic property of equidistribution of such sequences the following discrepant function D_N is used

$$D_N(x_0, x_2, \ldots, x_{N-1}) = D_N := \sup_{\Delta\subset[0,1)} \left|\frac{A_N(\Delta)}{N} - |\Delta|\right|,$$

where $A_N(\Delta)$ is the number of points among $x_0, x_2, \ldots, x_{N-1}$ falling into Δ, and $|\Delta|$ denotes the length of Δ.

In the same way there is defined the discrepancy for the sequence of s-dimensional points $X_n \subset [0, 1)^s$.

From definition of equidistribution of sequences of s-dimensional points we can conclude that for $D_N^{(s)} \to 0$ with $N \to \infty$ we can obtain better uniformly distributed sequences $\{X_n^{(s)}\}$.

Every sequence $\{x_n\}$, $x_n \in [0, 1)$ defines the sequence of s-dimensional points $X_n^{(s)}$, where $X_n^{(s)} = (x_n, x_{n+1}, \ldots, x_{n+s-1})$.

It is clear that for every equidistributed sequence $\{x_n\}$, which elements are statistically independent (unpredictable) for every integer $s \in \mathbb{N}$, the according sequence $\{X_n^{(s)}\} = \{x_n, x_{n+1}, \ldots, x_{n+s-1}\}$ be the equidistributed sequence.

We say that the sequence $\{x_n\}$, $x_n \in [0, 1)$ passes s-dimensional test on pseudorandomness if every sequence $\{X_n^{(s)}\}$, $s = 1, 2, \ldots, s$ be the equidistributed on s-dimensional unit interval $[0, 1)^s$.

To estimate the s-dimensional discrepant function of sequence $\{X_n^{(s)}\}$ the following lemmas is used.

For integers $s \geq 1$ and $q \geq 2$, let $C_s(q)$ be the set of all nonzero lattice

points $\mathbf{h} = (h_1, \ldots, h_s) \in \mathbb{Z}^s$ with $-\frac{q}{2} < h_j \leq \frac{q}{2}$ for $1 \leq j \leq s$. Define for $\mathbf{h} \in C_s(q)$

$$r(h,q) = \begin{cases} 1 & if\ h = 0, \\ q \sin(\pi \frac{|h|}{q})\ if\ h \neq 0, \end{cases}$$
$$r(\mathbf{h},q) = \prod_{j=1}^{s} r(h_j,q) \tag{8}$$

Lemma 4. *Let $N \geq 1$ and $q \geq 2$ be integers. Suppose that $\mathbf{y_0}, \mathbf{y_1}, \ldots, \mathbf{y_{N-1}} \in \mathbb{Z}_q^s$. Then the discrepancy of the points $\mathbf{t_k} = \frac{\mathbf{y_k}}{q} \in [0,1)^s$, $k = 0, 1, \ldots, N-1$, satisfies*

$$D_N(\mathbf{t_0}, \mathbf{t_1}, \ldots, \mathbf{t_{N-1}}) \leq \frac{s}{q} + \frac{1}{N} \sum_{\mathbf{h} \in C_s(q)} \frac{1}{r(\mathbf{h},q)} \left| \sum_{k=0}^{N-1} e(\mathbf{h} \cdot \mathbf{t_k}) \right| \tag{9}$$

(Proof of this lemma see in [1],[2]).

From the last statement it follows the classical statement of Turan-Erdös-Koksma inequality.

Lemma 5. *Let $T \geq N \geq 1$ and $q \geq 2$ be integers, $\mathbf{y_k} \in \{0, 1, \ldots, q-1\}^s$ for $k = 0, 1, \ldots, N-1$; $\mathbf{t_k} = \frac{\mathbf{y_k}}{q} \in [0,1)^s$. Then*

$$D_N(\mathbf{t_0}, \mathbf{t_1}, \ldots, \mathbf{t_{N-1}}) \leq \frac{s}{q} + \frac{1}{N} \sum_{\mathbf{h} \in C_s(q)} \sum_{h_0 \in \left(-\frac{T}{2}, \frac{T}{2}\right]} \frac{1}{r(\mathbf{h},q) r(h_0,T)} \times$$
$$\times \left| \sum_{k=0}^{T} e(\mathbf{h} \cdot \mathbf{t_k} + \frac{k h_0}{T}) \right| \tag{10}$$

This assertion follows from Lemma 4 and from an estimate of incomplete exponential sum through complete exponential sum.

Lemma 6 (Niederreiter,[1]). *Let $q \geq 2$, $T > 1$ be integers. Then*

$$\sum_{\substack{\mathbf{h} \in C_s(q) \\ \mathbf{h} \equiv 0\,(mod\ v)}} r(\mathbf{h},q) < \frac{1}{v} \left(\frac{2}{\pi} \log q + \frac{7}{5} \right)^s$$

for any divisor v of q with $1 \leq v < q$, and

$$\sum_{h_0 \in \left(-\frac{T}{2}, \frac{T}{2}\right]} \frac{1}{r(h_0,T)} \leq \frac{2}{\pi} \log T + \frac{7}{5} \tag{11}$$

Lemma 7. *The discrepancy of N arbitrary points $\mathbf{t_0}, \mathbf{t_1}, \ldots, \mathbf{t_{N-1}} \in [0,1)^2$ satisfies*

$$D_N(\mathbf{t_0}, \mathbf{t_1}, \ldots, \mathbf{t_{N-1}}) \geq \frac{1}{2(\pi+2)|h_1 h_2|N} \left| \sum_{k=0}^{N-1} e(\mathbf{h} \cdot \mathbf{t_k}) \right| \tag{12}$$

for any lattice point $\boldsymbol{h} = (h_1, h_2) \in \mathbb{Z}^2$ with $h_1 h_2 \neq 0$.

(It is the special version of Niederreiter result in [1]).

From these lemmas we can to see that the character of equidistribution of sequence $\{x_n\}$, $x_n \in [0,1)$ completely defines by estimate of exponential sum

$$S_N := \sum_{n=1}^{N} e^{2\pi i h x_n},\ h \in \mathbb{N}.$$

In section 2 we constructed two sequences $\{x_t\}$, $x_t = \frac{y(t)}{p^m}$ that were being produced by the algebraic curves over the ring $\mathbb{Z}_{p^m}$ defined by the congruences (2) and (6). From lemmas 2 and 3 it is clear to see that $y(t)$ are defining by special polynomials from the ring $\mathbb{Z}_{p^m}[t]$. These polynomials have the form

$$y(t) = A_0 + A_1 pt + A_2 p^2 t^2 + A_3 p^{\lambda_3} t^3 + \cdots,$$

moreover, $\lambda_j \geq 3$, $(A_j, p) = 1$ for $j \geq 3$.

The according sums S_N can be estimated by use of the generalized Gauss sums and the last can be estimated using the following lemma.

Lemma 8 (see, [5], Lemma 3). *Let $p > 2$ be a prime number, $m \geq 2$ be a positive integer, $m_0 = \left[\frac{m}{2}\right]$, $f(x)$, $g(x)$, $h(x)$ be polynomials over $\mathbb{Z}$*

$$f(x) = A_1 x + A_2 x^2 + \cdots,$$
$$g(x) = B_1 x + B_2 x^2 + \cdots,$$
$$h(x) = C_\ell x + C_{\ell+1} x^{\ell+1} + \cdots,\ \ell \geq 1,$$

$$\nu_p(A_j) = \lambda_j, \quad \nu_p(B_j) = \mu_j, \quad \nu_p(C_j) = \nu_j,$$

and, moreover,

$$k = \lambda_2 < \lambda_3 \leq \cdots, \quad 0 = \mu_1 < \mu_2 < \mu_3 \leq \cdots,$$
$$\nu_p(C_\ell) = 0,\ \nu_p(C_j) > 0,\ j \geq \ell + 1.$$

Then the following bounds occur

$$\left| \sum_{x \in \mathbb{Z}_{p^m}} e_m(f(x)) \right| \leq \begin{cases} 2p^{\frac{m+k}{2}} & if\ \nu_p(A_1) \geq k, \\ 0 & if\ \nu_p(A_1) < k; \end{cases}$$

$$\left| \sum_{x \in \mathbb{Z}^*_{p^m}} e_m(f(x) + g(x^{-1})) \right| \leq I(p^{m-m_0}) p^{\frac{m}{2}}$$

$$\left| \sum_{x \in \mathbb{Z}^*_{p^m}} e_m(h(x)) \right| \leq \begin{cases} 1\ if\ \ell = 1, \\ 0\ if\ \ell > 1, \end{cases}$$

where $I(p^{m-m_0})$ is a number of solutions of the congruence

$$y \cdot f'(y) \equiv g'(y^{-1}) \cdot y^{-1} \pmod{p^{m-m_0}},\ y \in \mathbb{Z}^*_{p^{m-m_0}}.$$

This lemma is the estimation of complete generalized Gauss sum. The incomplete generalized Gauss sum

$$\sum_{t=1}^{N} e^{2\pi i \frac{f(t)}{p^m}}, \ \ 1 \le N \le p^m$$

we can estimate by using the inequality

$$\left|\sum_{t=1}^{N} e^{2\pi i \frac{f(t)}{p^m}}\right| \le \sum_{k=1}^{p^m} \frac{1}{\max(k, p^m - k)} \left|\sum_{t=1}^{p^m} e^{2\pi i \frac{f(t)+kt}{p^m}}\right| =$$

$$= \max_{1 \le k \le p^m} \left|\sum_{t=1}^{p^m} e^{2\pi i \frac{f(t)+kt}{p^m}}\right| \log p^m \ll p^{\frac{m}{2}} \log p^m.$$

Now we can obtain the estimate of discrepancy for sequences generated in Lemmas 2 and 3.

Indeed, the function $y(t)$ for the sequence generated by elliptic curve (2) as the function $y(t)$ for the sequence generated by (6) both satisfy for all conditions of Lemma 8 and so the sum $\sum\limits_{t=1}^{p^m} e^{2\pi i \frac{y(t)}{p^m}}$ can be estimated as $O(p^{\frac{m+1}{2}} \log p^m)$. And now using lemmas 4 and 5 we obtain the estimate of discrepancy for the sequence $\{x_t\}$, where $x_t = \frac{y(t)}{p^m}$, $t = 1, 2, \ldots, N$, $N \le p^{m-1}$

$$D_N^{(1)} \le \frac{3p^{\frac{m+1}{2}}}{N} \log N$$

This proves the equidistribution of the sequence $\{x_t\}$. Moreover, $h_1 y(t) + h_2 y(t+1) + \cdots + h_s y(t+s-1)$ be the polynomial which for the nontrivial set of coefficients $h_1, \ldots, h_s$ generates the polynomial $Y(t)$ that satisfies to condition of Lemma 8 and so the discrepancy of s-dimensional sequence $\{X_n^{(s)}\}$ has an estimate

$$\frac{s}{N} + \frac{p^{\frac{m+1}{2}}}{N} (3 \log N)^s.$$

Therefore, the sequences produced by congruences (2) and (6) pass serial test for $s \le p - 2$.

To obtain the lower bounds for discrepancy of sequences generated from elliptic curve we apply Lemma 7.

From Corollary 1 we can write

$$y(t) = y(0)(1 + A_1 pt + A_2 p^2 t^2 + A_3 p^{\lambda_3} t^3 + \cdots) \ (\mathrm{mod} p^m)$$

Therefore, we have

$$\begin{aligned} y(t+k) = y(0)(1 + A_1 p + 2A_2 p^2 + 3A_3 p^{\lambda_3} + \cdots)t + \\ + (A_2 t^2 + 3A_3 p^{\lambda_3} + \cdots)t^2 + \\ + (A_3 p^{\lambda_3} + 2p^{\lambda_4} A_4 + \cdots)t^3 + \cdots \end{aligned}$$

And hence,

$$\begin{aligned} h_1y(t)+h_2y(t+1) =& \textit{free term} + (A_1h_1 + A_1h_2 + 2A_2h_2p)pt + \\ &+ (A_2h_1 + A_2h_2 + 3A_3h_2p)p^2t^2 + \\ &+ p^{\lambda_3}t^3\psi(t) \end{aligned}$$

where $\psi(t)$ is a polynomial with coefficients from $\mathbb{Z}_{p^m}$.

By form of coefficients for A_1 and A_2 it is clear that we can find x_0 such that the coefficient at t in the last equality is divided at least by p^2 but the coefficient at t^2 exactly divided by p^2. Let define this conditions as (*).

Now Lemma 8 gives

$$\left| \sum_{t=0}^{p^{m-1}-1} e^{2\pi i \frac{h_1y(t)+h_2y(t+1)}{p^{m-1}}} \right| = \begin{cases} p^{\frac{m+\nu}{2}} & if \text{ conditions (*) hold,} \\ 0 & otherwise. \end{cases}$$

Theorem 1. *Let $\{x_t\}$ be the sequence of PRN's produced by elliptic curve $y^2 \equiv x^3 + ax + b \pmod{p^m}$. There exists the point (x_0, y_0), $y_0 \neq 0, \infty$ on the curve $y^2 \equiv x^3 + ax + b \pmod{p}$ such that the sequence of two-dimensional points $\{X_t\}$, $X_t = (x_t, x_{t+1})$ has discrepancy $D_\tau^{(2)}$, $\tau = p^{m-1}$ for which the following inequalities*

$$\frac{1}{4(\pi+2)h^*} p^{-\frac{m-1}{2}} \leq D_\tau^{(2)} \leq 3p^{-\frac{m-1}{2}} \log^2 p^m,$$

hold, where $h^* = \min(h_1, h_2)$, (h_1, h_2) is a point from $(\mathbb{Z}^*_{p^{m-1}})^2$ with conditions (*).

This theorem together with Lemma 8 shows that the obtained upper bound is, in general, the best possible up to the logarithmic factor for any inversive congruential sequence $\{(x_t, x_{t+1})\}$, $t \geq 0$ (defined by the congruence (2)).

Hence, on the average, the discrepancy $D_\tau^{(2)}$ has an order of magnitude between $p^{-(\frac{m-1}{2}-\nu)}$ and $p^{-(\frac{m-1}{2}-\nu)} \log^2 p^m$. In the certain sense, inversive congruential pseudorandom numbers model the random numbers very closely.

4 Conclusion

In conclusion let introduce the step by step algorithm of constructing the sequences of PRN's with a period $\tau = p^{m-1}$, associated with elliptic curve over finite ring $\mathbb{Z}_{p^m}$, $p > 3$ be a prime, $m \geq 3 \in \mathbb{N}$, that can be described by the following way.

First of all for $(x_0, y_0) \in E_p$, $(y_0, p) = 1$, i.e. for the point of elliptic curve $y^2 \equiv x^3 + ax + b \pmod{p}$ over $\mathbb{Z}_p$ with non-quadratic residue $-3a$ we construct the points $(x(t), y(t))$, $0 \leq t \leq p^{m-1} - 1$ which belongs to elliptic curve over $\mathbb{Z}_{p^m}$. Then

1) we select (x_0, y_0), where $y_0 \neq 0$ and $y_0 \neq \infty$;
2) calculate $x(t) \equiv x_0 + pt \pmod{p^m}$;

3) calculate $y_i(0)$, $i = 1, 2$ as the solutions of congruence

$$y^2 \equiv x_0^3 + ax_0 + b \pmod{p^m};$$

4) we will use the Taylor series for the function of ω at the point $\omega = 0$ in form

$$\sqrt{1 + (3\omega x_0^2 + 3\omega^2 x_0 + \omega^3)x_0'} = X_0 + X_1\omega + X_2\omega^2 + \cdots . \qquad (13)$$

(here x_0' is the multiplicative inverse modulo p^m for $x_0^3 + ax_0^2 + b$).

5) In (13) we put $\omega = pt$ and then modulo p^m we construct the following polynomial:

$$\begin{aligned}\varphi(t) &\equiv 1 + X_1 pt + X_2 p^2 t^2 + \cdots + X_s p^s t^s \equiv \\ &\equiv \Phi_0(x_0) + p^{\lambda_1}\Phi_1(x_0)t + \cdots + p^{\lambda_s}\Phi_s(x_0)t^s \pmod{p^m},\end{aligned}$$

where $\Phi_j(x_0) \in \mathbb{Z}$, $(\Phi_j(x_0), p) = 1$, $\lambda_j \in \mathbb{N}$, $\lambda_j \geq j\frac{p-2}{p-1}$, $j = 1, 2, \ldots, s$.

6) This polynomials and the solutions $y_i(0)$, $i = 0, 1$ we use to construct the following representations modulo p^m:

$$y_i(t) \equiv y_i(0)(\Phi_0(x_0) + \Phi_1(x_0)p^{\lambda_1 t} + \cdots + \Phi_s(x_0)p^{\lambda_s}t^s) \equiv$$

$$\equiv y_i(0)(1 + A_1 pt + A_2 p^2 t^2 + A_3 p^{\lambda_3} t^3 + \cdots + A_s p^{\lambda_s} t^s)$$

for each $i = 1, 2$, which produce two sequences of PRN's

$$\left\{\frac{y_i(t)}{p^m}\right\},\ t = 0, 1, \ldots$$

with the period $\tau = p^{m-1}$.

Using the results obtained in previous sections we can say that the constructed sequence of PRN's, associated with elliptic curve $y^2 \equiv x^3 + ax + b \pmod{p^m}$, passes the serial test on pseudorandomness, and therefore may be used in cryptographic applications.

References

1. H. Niederreiter. *Random Number Generation and Quasi-Monte Carlo Methods*, SIAM, Philadelphia, 1992.
2. H. Niederreiter. Quasi-monte carlo methods and pseudorandom numbers. *Bull. Amer. Math. Soc.*, 84, 957–1041, 1978.
3. L.P. Postnikova. Distribution of solutions of the congruence $x^2 + y^2 \equiv 1 \pmod{p^n}$. *Matem. sb.*, 65(2), 228–238, 1964 (in Russian).
4. I. Shparlinski. Pseudorandom Number Generators from Elliptic Curves. *Contemporary Mathematics*, 477, 121–141, 2009.
5. Sergey Varbanets. Exponential sums over the sequences of PRN's produced by inversive generators. *Annales Univ. Sci. Budapest., Sect. Comp.*, 48, 225–232, 2018.

Fractional Chaotic system solutions and their impact on chaotic behaviour

Chunxiao Yang[1], Ina Taralova[2], and Jean Jacques Loiseau[3]

Laboratoire des Sciences du Numérique de Nantes LS2N, UMR CNRS 6004 Ecole Centrale de Nantes Nantes, France
(E-mail: chunxiao.yang@ls2n.fr[1], ina.taralova@ls2n.fr[2], jean-jacques.loiseau@ls2n.fr[3])

Abstract. This paper is devoted to the analysis of calculation methods for solving fractional chaotic systems and the impact of these different approaches on the behavior of the fractional chaotic system. Two widely used time domain fractional differential equations solving approaches are discussed, the fractional ABM corrector-predictor method based on Caputo fractional derivative definition, and the long memory calculation approach based on Grunwald fractional derivative. These numerical solutions calculation methods are employed to depict the phase portrait of a class of commensurate fractional chaotic systems. The Lyapunov exponent and bifurcation diagrams of the systems over various fractional orders and parameters are illustrated to detect the impact on the dynamics of the chaotic system applying different calculation approaches.
Keywords: Fractional calculus, Numerical solution, Fractional Chaotic system, Non-linear dynamics.

1 Introduction

Chaos is a random-like behavior exhibited by many nonlinear dynamic systems. The very first proponent on this topic can be dated back to 1880 while the three body problem was studied [1]. Eighty years latter, when Edward Lorenz worked on weather prediction, the so-called 'Lorenz attractor' was found [2]. By giving it a description and a poetic name of 'butterfly effect', the gate of mathematical and scientific world of Chaos was opened. Since then, many researchers have tried to uncover the deterministic laws behind the apparently random states of disorder of different chaotic systems.
One of the characteristics of chaotic system is that it is very sensitive to the initial conditions as described by butterfly effect. This sensitivity can be measured by Lyapunov Exponent(LE) which calculates the rate of exponential divergence of trajectories starting from two close initial conditions. This characteristics also contributes to the application of chaotic systems in many domains of science and engineering, such as biology [3], economics [4], finance [5], cryptography [6][7] and etc.
In the meantime, fractional calculus is considered as the generalization of classical integer-order integration and differentiation operators to real, or complex orders [8]. Many mathematicians have discussed the fractional calculus since 1695 by introducing different mathematical characterisations (definitions) for fractional derivative and integration. In many cases, these characterisations

are equivalent if the initial conditions are ad hoc [9], and the most well known three are Rienmann-Liouville(RL), Grunwald-Letnikov(GL) and Caputo characterisations.
The analysis and discussion of fractional calculus remained purely in the domain of mathematics for centuries. It was not until 1980s that the application of fractional calculus in the domain of science and engineering has started to be studied and explored. Due to the memory effect possessed by fractional calculus, it is considered to be suitable to model many real-life systems. After years of research, the fractional differential equations have now been used in diverse disciplines like physics, biology, and economics, etc. [10][11].
The fractional chaotic system also attracts a lot of attention. The difficulties for this research owes to the intricate geometric interpretation of fractional derivatives [12] and the fact that there exist, as mentioned above, different definitions for fractional derivatives. One basically considers continuous systems, and uses numerical methods to approximate the solution. In the case of a fractional system, the discrete approximating system may inherit the chaotic behaviour of the initial continuous system, but this relationship is somehow complex. What adds to the intricacy is that the chaotic behavior of the approximating can be different for different numerical methods employed to solve the fractional differential equations [13]. Therefore, the understanding of the impact on the chaoticity of the system applying one or another numerical calculation approaches is of great importance, in order to choose the most appropriate one for a given application.
In the following, two numerical calculation methods under GL and Caputo characeterizations for fractional differential equations are recalled. Then, we employ both methods to obtain the states of two fractional chaotic systems extended from classical integer order chaotic system. The impact on the chaoticity of the systems applying the two approaches has been analyzed in terms of LE and from the aspect of bifurcation diagram and time responses.

2 Preliminaries on fractional calculus and fractional systems

In this section, some preliminaries on fractional calculus and fractional systems are introduced to give a rough idea on the topic. The widely-accepted stability criteria for a commensurate fractional system is also illustrated.

2.1 Fractional calculus

As mentioned before, the fractional calculus studies the fractional derivative and integral which can be considered as the extension of classical integer order differentiation and integration to real or complex orders. In the long history of the study of fractional calculus, many mathematicians have contributed and introduced different characterisations(referred as 'definitions' in many paper) towards the topic. Here after, we give two well-known definitions Grünwald-Letnikov (GL) and Caputo definitions [14][15].

The fractional derivatives under GL characterisation can be writen as

$$ {}_aD_t^{\alpha} f(t) = \lim_{h \to 0} \frac{1}{h^{\alpha}} \sum_{j=0}^{[\frac{t-a}{h}]} (-1)^j \binom{\alpha}{j} f(t - jh) \tag{1} $$

The term $[\frac{t-a}{h}]$ in equation (1) stands for the integer part of $\frac{t-a}{h}$; a and t are the bounds of the derivative operation ${}_aD_t^{\alpha}$ for $f(t)$; α represents the fractional derivative order. The $\binom{\alpha}{j}$ in (1) is defined in (2), where $\Gamma(.)$ is the Eular Gamma function in the form of (3).

$$ \binom{\alpha}{j} = \frac{\Gamma(\alpha + 1)}{\Gamma(j + 1)\Gamma(\alpha - j + 1)} \tag{2} $$

$$ \Gamma(\alpha) = \int_0^{\infty} \frac{t^{\alpha - 1}}{e^t} dt \tag{3} $$

The caputo type fractional derivative holds the form as following,

$$ {}_a^cD_t^{\alpha} f(t) = \frac{1}{\Gamma(n - \alpha)} \int_a^t \frac{f^{(n)}(\tau)}{(t - \tau)^{\alpha - n + 1}} d\tau, \text{ for } n - 1 < \alpha < n \tag{4} $$

where α denotes the fractional derivative order; a and t are the bounds for the operation; n is the smallest integer greater than α; $\Gamma(.)$ is the Eular Gamma function in equation (3); and $f^{(n)}(t)$ is the n-th derivative of $f(t)$.
The Caputo type fractional derivative is often used for engineering application since the fractional differential equations with this type of derivative can provide the applied problem with an interpretive initial condition.

2.2 Fractional system

A fractional system is a dynamic system which can be modeled by fractional differential equations [16]. A general form of fractional system is as follows,

$$ \begin{aligned} &{}_aD_t^{\alpha_i} x_i(t) = f_i(x_1(t), x_2(t), ..., x_n(t), t) \\ &x_i(0) = c_i, i = 1, 2, ..., n. \end{aligned} \tag{5} $$

In (5), bound a is equal to 0; $x_i(0)(i = 1, 2, ...n)$ denotes the initial conditions for each component constituting the state vectors; $\alpha_i(i = 1, 2, ...n)$ is the fractional derivative order for i-th differential equations consisting the system, and f_i is a linear or non-linear function.
The equilibrium points of system (5) can be obtained by solving equation $f_i(x) = 0(i = 1, 2, ..., n)$. If a commensurate system with $\alpha_i = \alpha, i = 1, 2, ..., n$ is considered, then, according to the stability theorem defined in [17], the equilibrium points are locally asymptotically stable if the eigenvalue of the Jacobian matrix of system (5) satisfies the following equation evaluated at equilibria.

$$ |\arg(\text{eig}(\text{J}))| = |\arg(\lambda_i)| > \alpha \frac{\pi}{2}, i = 1, 2, ..., n \tag{6} $$

where J denotes the Jacobian matrix of (5), $\lambda_i(i = 1, 2, ...n)$ are its eigenvalues.

3 Numerical calculation methods for fractional differential equations

In this section, two numerical solutions calculation methods for fractional differential equations are introduced. The methods are based on Gr$\ddot{u}$nwald-Letnikov and Caputo fractional derivative characterisations.

3.1 Gr$\ddot{u}$nwald-Letnikov calculation method

The explicit numerical approximation of q-th derivative under GL characterisation at the points $kh, (h = 1, 2, ...)$ is expressed as follows [14]

$$ {}_{(k-L_m)/h}D^{\alpha}_{t_k} f(t) \approx h^{-\alpha} \sum_{j=0}^{k} (-1)^j \binom{\alpha}{j} f(t_{k-j}). \tag{7} $$

In expression (7), L_m is the memory length; $t_k = kh$, where h is the calculation time step; the binomial coefficient $(-1)^j \binom{\alpha}{j}$ can be denoted as $c_j^{(\alpha)} (j = 0, 1, ...)$ which is expressed use the following expression[18],

$$ c_0^{(\alpha)} = 1, c_j^{(\alpha)} = \left(1 - \frac{1+\alpha}{j}\right) c_{j-1}^{(\alpha)}. \tag{8} $$

Thus, the general numerical solution of fractional differential equation described by equation(9) can be expressed as given in (10).

$$ {}_aD^{\alpha}_t y(t) = f(y(t), t) \tag{9} $$

$$ y(t_k) = f(y(t_k), t_k) h^{\alpha} - \sum_{j=\nu}^{k} c_j^{(\alpha)} y(t_{k-j})) \tag{10} $$

The sum in (10) stands for the memory term. If a 'long memory effect' is considered, then the lower index $\nu = 1$ for all k, otherwise $\nu = 1$ for $k < (L_m/h)$ and $\nu = k - L_m$ for $k > (L_m/h)$.

3.2 Fractional ABM corrector-predictor method

The fractional ABM corrector-predictor method is another widely used time domain numerical calculation method in the domain of engineering. It is a generalization of the classical Adams–Bashforth–Moulton integrator which is used for the numerical calculation of classical first order problem.
From the analytical point of view, the fractional differential equations under Caputo characterization with initial conditions $y^k(0) = y_0^k, k = 0, 1, 2...m-1$ where $m := \lceil \alpha \rceil$, is equivalent to Volterra integral equation expressed as follows,

$$ y(x) = \sum_{k=0}^{\lceil \alpha \rceil - 1} y_0^{(k)} \frac{x^k}{k!} + \frac{1}{\Gamma(\alpha)} \int_0^x (x-t)^{\alpha-1} f(t, y(t)) dt \tag{11} $$

The algorithm is developed on a uniform grid $\{t_n = nh : n = 0, 1, ...N\}$. The basic idea of the algorithm is to obtain the approximation of the latter point on the grid from the former point. Detailed formula derivation for the algorithm can be found in [19]. Here, we only give out the derived equations for the next states values in equation (12)-(15).

$$\begin{aligned} y_h(t_{n+1}) = &\sum_{k=0}^{\lceil\alpha\rceil-1} \frac{t_{n+1}^k}{k!} y_0^{(k)} + \frac{h^\alpha}{\Gamma(\alpha+2)} f(t_{n+1}, y_h^P(t_{n+1})) \\ &+ \frac{h^\alpha}{\Gamma(\alpha+2)} \sum_{j=0}^{n} a_{j,n+1} f(t_j, y_h(t_j)), \end{aligned} \tag{12}$$

$$y_h^P(t_{n+1}) = \sum_{k=0}^{\lceil\alpha\rceil-1} \frac{t_{n+1}^k}{k!} y_0^{(k)} + \frac{1}{\Gamma(\alpha)} \sum_{j=0}^{n} b_{j,n+1} f(t_j, y_h(t_j)). \tag{13}$$

$$a_{j,n+1} = \begin{cases} n^{\alpha+1} - (n-\alpha)(n+1)^\alpha, & \text{if } j = 0, \\ (n-j+2)^{\alpha+1} + (n-j)^{\alpha+1} - 2(n-j+1)^{\alpha+1}, & \text{if } 1 \le j \le n, \\ 1, & \text{if } j = n+1. \end{cases} \tag{14}$$

$$b_{j,n+1} = \frac{h^\alpha}{\alpha}((n+1-j)^\alpha - (n-j)^\alpha) \tag{15}$$

In the above equations, $y_h(t_{n+1})$ stands for the next state, $y_h^P(t_{n+1})$ denotes the predictor value for the next state, a and b are coefficients.

4 Fractional chaotic Chen and Lu systems

4.1 Fractional chaotic Chen systems

The system equation for fractional Chen system can be expressed as following[20],

$$f_c(x) = \begin{cases} D^{\alpha_c} x_1(t) = a_c(x_2(t) - x_1(t)) \\ D^{\alpha_c} x_2(t) = (c_c - a_c) x_1(t) - x_1(t) x_3(t) + c_c x_2(t) \\ D^{\alpha_c} x_3(t) = x_1(t) x_2(t) - b_c x_3(t) \end{cases} \tag{16}$$

In the equation, D^{α_c} denotes the fractional derivative with order α_c, (a_c, b_c, c_c) are the parameters of the system. The system is an extension from integer order chaotic Chen system studied in [21].
The equilibria of the system can be obtained through the same way as its original integer order system, by setting the right hand sand system equation equal to zero $f_c(x^*) = 0$ as given below,

$$\begin{cases} a_c(x_2(t) - x_1(t)) = 0 \\ (c_c - a_c) x_1(t) - x_1(t) x_3(t) + c_c x_2(t) = 0 \\ x_1(t) x_2(t) - b_c x_3(t) = 0 \end{cases} \tag{17}$$

The singularity of the equilibrium points can also be acquired through the classical method as given below, by evaluating the eigenvalue of the jacobian matrix of the system at equilibrium points.

$$\det\left(\lambda_c \mathrm{I}-\mathrm{J}_c\right)=\begin{bmatrix} \lambda_c+a_c & -a_c & 0 \\ -c_l+a_l+x_3^* & \lambda_c-c_c & x_1^* \\ -x_2^* & -x_1^* & \lambda_c+b_c \end{bmatrix}=0 \tag{18}$$

$\mathrm{J_c}$ in equation (18) represents the Jacobian matrix of the system equation, I is the identity matrix, λ_c denotes the eigenvalue, and (x_1^*, x_2^*, x_3^*) stands for the equilibrium point.
The singularity of the three equilibrium points of fractional Chen system for system parameters $(a_c, b_c, c_c) = (35, 3, 28)$ can be obtained through above analytical expressions and are given in Table 1.

4.2 Fractional chaotic Lu system

The system equation for fractional chaotic Lu system extended from integer order Lu system can be described as follows [22],

$$f_l\left(x\right)=\begin{cases} D^{\alpha_l} x_1\left(t\right)=a_l\left(x_2\left(t\right)-x_1\left(t\right)\right) \\ D^{\alpha_l} x_2\left(t\right)=-x_1\left(t\right)x_3\left(t\right)+c_l x_2\left(t\right) \\ D^{\alpha_l} x_3\left(t\right)=x_1\left(t\right)x_2\left(t\right)-b_l x_3\left(t\right) \end{cases} \tag{19}$$

where D^{α_l} denotes the fractional derivative with order α_l, a_l, b_l, and c_l are the parameters of the system. The equilibrium points of the system can be acquired calculating the solutions of the following system of equations,

$$\begin{cases} a_l\left(x_2\left(t\right)-x_1\left(t\right)\right)=0 \\ -x_1\left(t\right)x_3\left(t\right)x_1\left(t\right)+c_l x_2\left(t\right)=0 \\ x_1\left(t\right)x_2\left(t\right)-b_l x_3\left(t\right)=0 \end{cases} \tag{20}$$

The singularity of the equilibria can be obtained the same way as discussed previously for the fractional Chen system through the following identities,

$$\det\left(\lambda_l \mathrm{I}-\mathrm{J}_l\right)=\begin{bmatrix} \lambda_l+a_l & -a_l & 0 \\ x_3^* & \lambda_l-c_c & x_1^* \\ -x_2^* & -x_1^* & \lambda_l+b_l \end{bmatrix}=0 \tag{21}$$

where $\mathrm{J_l}$ in equation (21) represents the Jacobian matrix of the fractional Lu system, λ_l denotes the eigenvalue, and (x_1^*, x_2^*, x_3^*) stands for the equilibrium point. When the parameters of the system is set to $(a_c, b_c, c_c) = (36, 3, 20)$, three equilibirum points $E_1^* = (0, 0, 0)$, $E_2^* = (7.460, 7.460, 20)$ and $E_3^* = (-7.460, -7.460, 20)$ can be obtained applying equation (20). The singularity of the equilibria is also given in Table 1.

5 Solutions for the chaotic systems applying different approaches

In this section, the solutions for fractional Chen and Lu solution are obtained applying both GL method and fractional ABM corrector-predictor method dis-

cussed in section 3. The impact of the two approaches on the chaotic behavior of the systems are also discussed.

5.1 Chaotic system applying GL method

With the numerical solution of fractional differential equation calculated under GL method derived as in (10), the calculation for the states of fractional Chen system and fractional Lu system (expression (16) and (19)) can be expressed by the following identities (22) and (23) respectively.

$$\begin{cases} x_1(n) = (a_c(x_2(n) - x_1(n-1)))h^{\alpha_c} - \sum_{j=\nu}^{n} c_j^{(\alpha_c)} x_1(n-j) \\ x_2(n) = ((c_c - a_c)x_1(n) - x_1(n)x_3(n-1) + c_c x_3(n-1))h^{\alpha_c} - \sum_{j=\nu}^{n} c_j^{(\alpha_c)} x_2(n-j) \\ x_3(n) = (x_1(n)x_2(n) - b_c x_3(n-1))h^{\alpha_c} - \sum_{j=\nu}^{n} c_j^{(\alpha_c)} x_3(n-j) \end{cases} \tag{22}$$

$$\begin{cases} x_1(n) = (a_l(x_2(n-1) - x_1(n-1)))h^{\alpha_l} - \sum_{j=\nu}^{n} c_j^{(\alpha_l)} x_1(n-j) \\ x_2(n) = (-x_1(n)x_3(n-1) + c_l x_2(n-1))h^{\alpha_l} - \sum_{j=\nu}^{n} c_j^{(\alpha_l)} x_2(n-j) \\ x_3(n) = (x_1(n)x_2(n) - b_l x_3(n-1))h^{\alpha_l} - \sum_{j=\nu}^{n} c_j^{(\alpha_l)} x_3(n-j) \end{cases} \tag{23}$$

System	**Equilibrium**	**Eigenvalue**		**singularity**
		λ_1	λ_2, λ_3	
Fractional	(0, 0, 0)	-30.8359	23.8359,-3	Saddle
Chen	(-7.9379,-7.9379,21)	-18.4280	4.2140±14.8846i	Saddle Focus
system	(7.9379,7.9379,21)	-18.4280	4.2140±14.8846i	Saddle Focus
Fractional	$(0, 0, 0)$	-36	$20, -3$	Saddle
L$\ddot{u}$	$(-7.460, -7.460, 20)$	-22.6516	$1.8258 \pm 13.6887i$	Saddle Focus
system	$(7.460, 7.460, 20)$	-18.4280	$1.8258 \pm 13.6887i$	Saddle Focus

Table 1: Fractional Chen and Lu systems' equilibria and their singularity

To be mentioned is that in our work, the 'long memory effect' is adopted applying GL method which means that the number ν in equaitons (22) and (23) is equal to 1. The time step h in above equations is set to a fixed value 0.001.
We plotted the phase portraits of the two systems with fractional orders $\alpha_c = 0.9$ and $\alpha_l = 0.95$ in Fig.1a and 1b, respectively. The parameters and initial conditions for Chen system are $(35, 3, 28)$ and $(-9, -5, 14)$. Those of Lu system are chosen to be $(36, 3, 20)$ and $(0.2, 0.5, 0.3)$.

5.2 Chaotic systems applying ABM corrector-predictor approach

Based on the fractional ABM corrector-predictor numerical calculation approach for the solution of fractional differential equations given in equations (12)-(15), the states of fractional Chen system applying ABM predictor corrector approach can be expressed as follows,

$$\begin{aligned} \mathrm{X}_c(n+1) &= \mathrm{X}_c(0) + \frac{h^{\alpha_c}}{\Gamma(\alpha_c+2)} f_c(\mathrm{X}_c^P(n+1)) \\ &\quad + \frac{h^{\alpha_c}}{\Gamma(\alpha_c+2)} \sum_{j=0}^{n} a_{j,n+1} f_c(\mathrm{X}_c(j)) \end{aligned} \tag{24}$$

$$\mathrm{X}_c^P(n+1) = \mathrm{X}_c(0) + \frac{1}{\Gamma(\alpha_c)} \sum_{j=0}^{n} b_{j,n+1}^1 f_c(\mathrm{X}_c(j))$$

$$a_{j,n+1} = \begin{cases} n^{\alpha_c+1} - (n-\alpha_c)(n+1)^{\alpha_c}, & \text{if} j = 0, \\ (n-j+2)^{\alpha_c+1} + (n-j)^{\alpha_c+1} - 2(n-j+1)^{\alpha_c+1}, & \text{if} 1 \le j \le n, \\ 1, & \text{if} j = n+1. \end{cases}$$

$$b_{j,l+1} = \frac{h^{\alpha_c}}{\alpha_c}((n+1-j)^{\alpha_c} - (n-j)^{\alpha_c}) \tag{25}$$

In the above equations, $\mathrm{X}_c(n+1)$, $\mathrm{X}_c(n)$ and $\mathrm{X}_c^P(n+1)$ are state vectors comprised of all the state components x_1m x_2, and x_3; α_c is the fractional order between $(0, 1)$; f_c stands for the Chen system equations.
The formula for the calculation of the states of fractional Lu system can be obtained by substituting the state vectors, fractional order and system equations in equations (24)-(25) with X_l, α_l and f_l where $0 < \alpha_l < 1$. The phase portraits of the two systems acquired employing corrector-predictor approach are given in Fig.1c and 1d, respectively. The fractional orders, parameters and initial conditions are the same as those for the GL method.

5.3 Impact on system chaoticity with chosen methods

For the work in this section, we used the same parameters and initial conditions for the two systems as adopted in the previous section, which are $(a_c, b_c, c_c) = (35, 3, 28)$, $\mathrm{X}_c(0) = (-9, -5, 14)$; $(a_l, b_l, c_l) = (36, 3, 20)$, $\mathrm{X}_l(0) = (0.2, 0.5, 0.3)$, respectively. The time step h is set to 0.005. The MATLAB code[23] for ABM corrector-predictor method and [24] is employed for the following simulation and the calculation of LE.
According to the stability criteria introduced by equation (6), [17] states that for a fractional system $D^\alpha x = f(x)$ to remain chaotic, a necessary condition is keeping the eigenvalue λ in the unstable region, which gives the following equation for the fractional derivative order α.

$$\alpha > \frac{2}{\pi} tan^{-1}\left(\frac{|Im(\lambda)|}{Re(\lambda)}\right) \tag{26}$$

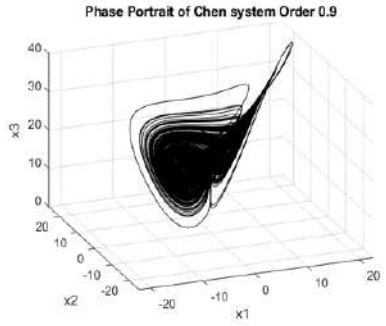

(a) GL method Chen system ($\alpha_c = 0.9$)

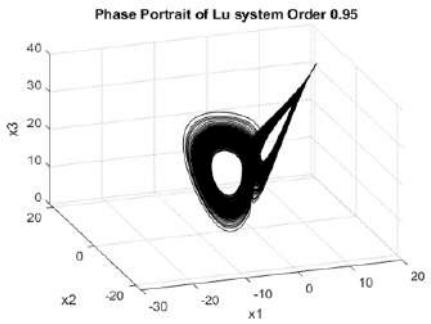

(b) GL method Lu system ($\alpha_l = 0.95$)

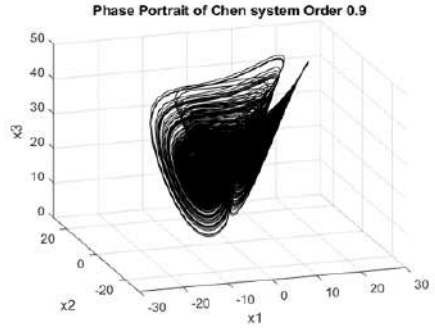

(c) GL method Chen system ($\alpha_c = 0.9$

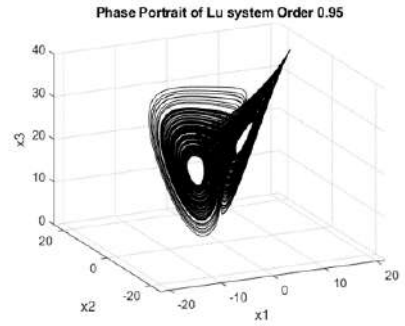

(d) ABM method Lu system ($\alpha_l = 0.95$

Fig. 1: Phase Portrait of fractional Chen and Lu systems characterized by GL and ABM method

where λ is the eigenvalue of the Jacobian matrix of the system, α is the commensurate fractional order. Therefore, for the given parameter values, the fractional chaotic Chen system should have a fractional order α_c greater than or equal to 0.8244.

In Fig. 2, we plot the phase portrait of fractional Chen system at boundary fractional values 0.82 and 0.83 applying both GL and ABM corrector-predictor methods. The time response of the last 2000 states obtained through both methods are also given. The states calculated by GL method is in red and ABM corrector-predictor in blue. It is not difficult to observe from Fig. 2a and 2c that with order 0.82 there are only one red point in the figure, which indicates that the states stays at the same fixed point applying GL method. Whereas for the applied ABM method(blue dots), they appear to have a shape of the attractors. When the system order is equal to 0.83, both methods display the shapes with attractors. This indicates that when applying GL calculation method with long memory effect, the system's dynamic behavior is in accordance with the stability criteria given by equation (26). While the ABM calculation method applied in this paper provides the system with a smaller derivative order for the system to be chaotic.

The time response figures given by Fig. 2b and 2d confirms the founding. The

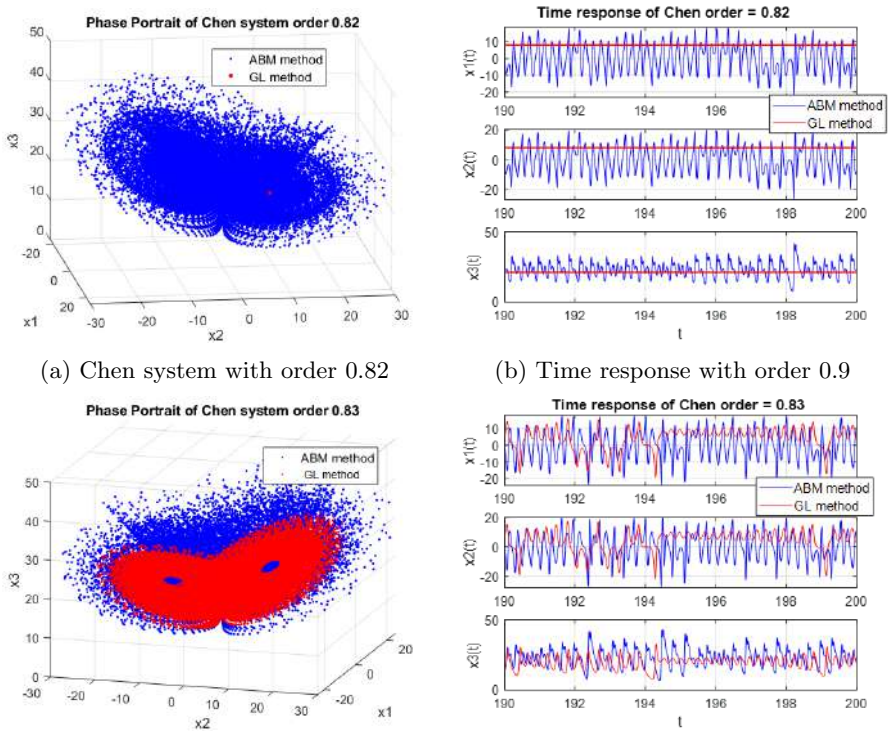

(a) Chen system with order 0.82 (b) Time response with order 0.9

(c) Chen system with order 0.83 (d) Time response with order 0.83

Fig. 2: Phase Portrait and time response of Chen system at boundary fractional order values

blue curve stands for the states obtain through ABM method and red for GL. It is clear that for derivative order 0.82, the red attractors stays at the same value for the three state vector components x_1, x_2 and x_3, while the blue curves appear to be oscillating.

We also give the Lyapunov exponent and bifurcation diagrams over different fractional orders of fractional Chen and Lu systems in Fig.3. For each fractional derivative orders, 10^4 states were generated and the LEs were calculated throughout the iterations. The LE spectrum curves in 3a and 3b are obtained by combining LE values of the last iteration for every evaluated orders. The plots show that only x_1 component possesses LE value greater than 0 applying both methods. It can be observed that applying ABM corrector-predictor approach, for the fractional Chen system, the LE of x_1 greater than 0 appears before order 0.53, whereas for GL method, the LE exceeds 0 after fractional order of 0.8. The LEs for fractional Lu system calculated using both methods show the similar results, with ABM method having a smaller chaotic fractional derivative value. This is in accordance with our previous findings concerning the phase portrait and time response which draws to the conclusion that GL method give a more accurate approximation of original fractional system.

Apart from this, from the y-coordinates of the bifurcation diagram where the system is non-chaotic, it can be observed that the solution obtained using ABM method stays at the equilibrium point as obtained through analytical analysis.

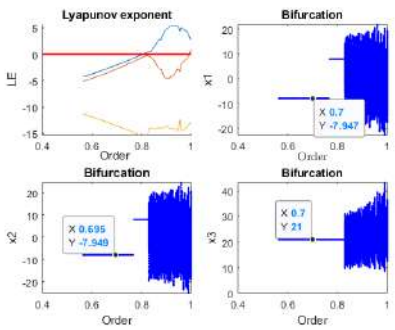

(a) Chen system GL method

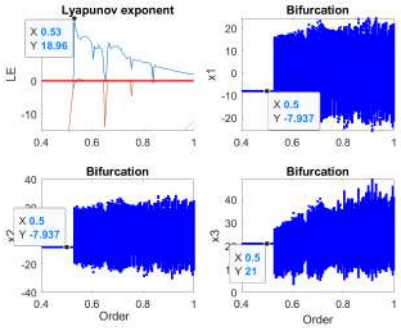

(b) Chen system ABM method

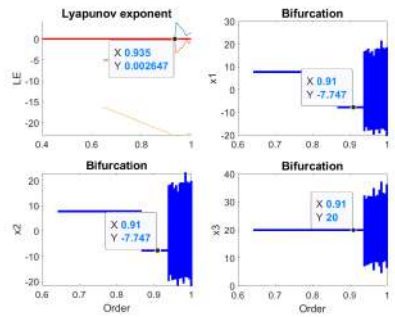

(c) Lu system GL method

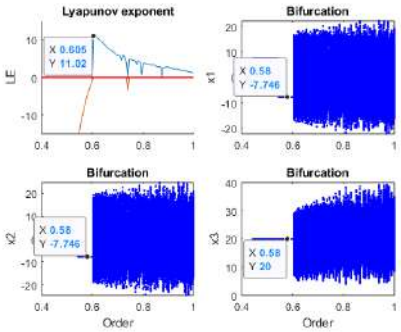

(d) Lu system ABM method

Fig. 3: LE and bifurcation results for Chen and Lu systems over different fractional derivatives employing different methods $((a_c, b_c, c_c) = (35, 3, 28)$,$(a_l, b_l, c_l) = (36, 3, 20)$

The LEs results and bifurcation diagram over different parameters of fractional Lu system are also given in Fig.4 to illustrate the dynamics possesses by the system. We set the system fractional order fixed to 0.9. It can be observed that applying different numerical calculation methods, the system dynamic is quite different. It is worth mentioning that is that the results for different parameters are conducted by changing one parameter at a time and fixing the other two unchanged.

6 Conclusion

In this paper, we recalled two numerical solutions calculation methods for fractional differential equations adopting Grünward-Leinikov and Caputo charac-

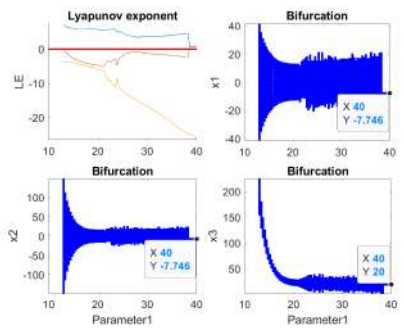

(a) Lu system GL method a_l LE results

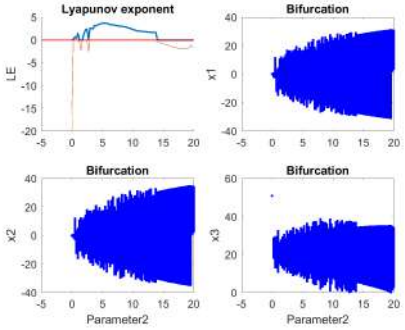

(b) Lu system ABM method a_l LE results

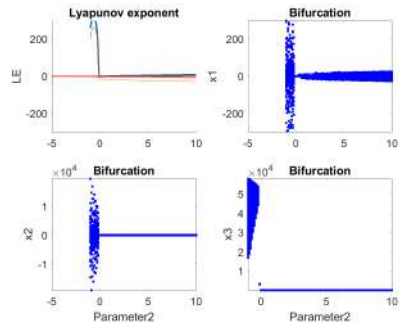

(c) Lu system GL method b_l LE results

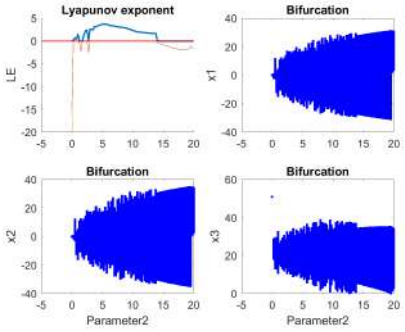

(d) Lu system ABM method b_l LE results

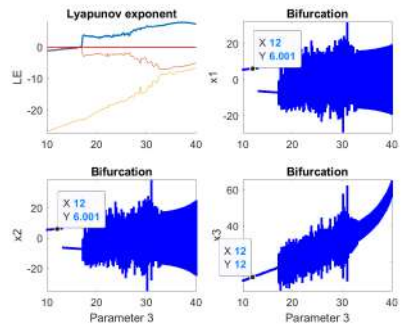

(e) Lu system GL method c_l LE results

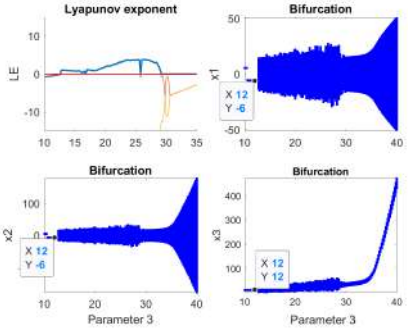

(f) Lu system ABM method C_l LE results

Fig. 4: LE and bifurcation results for Chen and Lu systems over different fractional parameters employing different methods

terization of fractional derivative, respectively. Two fractional chaotic systems, fractional Chen system and fractional Lu system are discussed and their discretized states were calculated employing both methods. The results show that compared to the adopted ABM corrector-predictor method, the GL approach with long memory effect provide the original fractional system with a better approximation in coherence with the analytical studies. At the contrary, employing ABM method, the approximation accuracy appears to be deteriorate. However, in terms of chaoticity, it has a greater chaotic range for fractional derivatives.

References

1. H. Poincaré. Sur le problème des trois corps et les équations de la dynamique. Divergence des séries de M. Lindstedt. *Acta Mathematica*. 13 (1–2): 1–270,1890.
2. E.N. Lorenz. The Predictability of Hydrodynamic Flow. *Transactions of the New York Academy of Sciences*. 25 (4): 409–432, 1963.
3. E. Liz and A. Ruiz-Herrera. Chaos in discrete structured population models.*SIAM Journal on Applied Dynamical Systems*. 11 (4): 1200–1214, 2012.
4. C. Kyrtsou and W. Labys. Evidence for chaotic dependence between US inflation and commodity prices. *Journal of Macroeconomics*. 28 (1): 256–266, 2006.
5. J. Fernando. Applying the theory of chaos and a complex model of health to establish relations among financial indicators.*Procedia Computer Science*. 3: 982–986, 2011.
6. Z. Qiao, I. Taralova, S. El Assad. Efficient Pseudo-chaotic Number Generator for Cryptographic Applications.*International Journal of Intelligent Computing Research*, 11: 1041-1048, 2020.
7. M. Babaei. A novel text and image encryption method based on chaos theory and DNA computing. *Natural Computing*. 12 (1): 101–107, 2013.
8. I. Petráš. *Fractional-order nonlinear systems*, Springer, Berlin, Heidelberg, 2011.
9. K. Diethelm.*The Analysis of Fractional Differential EquationsThe Analysis of Fractional Differential Equations*. Springer, Berlin, Heidelberg, 2010.
10. F. Mainardi.*Fractional Calculus and Waves Linear Viscoelasticity: An Introduction to Mathematical Models*. Imperial College Press, London, UK, 2010.
11. V.E. Tarasov and V.V. Tarasova. Macroeconomic models with long dynamic memory: Fractional calculus approach. *Applied Mathematics and Computation*. 338: 466-486, 2018.
12. T. Li and M. Yang, and al. A Novel Image Encryption Algorithm Based on a Fractional-Order Hyperchaotic System and DNA Computing. *Complexity*. vol. 2017, Special issue, 2017.
13. C.Yang, I. Taralova and al. Design of a Fractional Pseudo-Chaotic Random Number Generator. *International journal of chaotic computing*. 7(1) :166-178, 2021
14. I. Podlubny. *Fractional Differential Equations*. Academic Press, San Diego, 1999.
15. M. Caputo. Linear Models of Dissipation whose Q is almost Frequency Independent—II. *Geophysical Journal International* 13(5): 529–539, 1967.
16. B. J.West, M. Bologna and P. Grigolini. *Physics of fractal operators*. Springer, New York, 235-270, 2003.
17. M.S.Tavazoei and M. Haeri. A necessary condition for double scroll attractor existence in fractional-order systems. *Physics Letters A*. 367: 102–113, 2007b.
18. L.Dorcak. Numerical Models for the Simulation of the Fractional-Order Control Systems. *UEF-04-94, The Academy of Sciences, Inst. of Experimental Phsic*, Kosice, Slovakia,1994.

19. K. Diethelm. N.J.Ford and A. Freed. A predictor-corrector approach for the numerical solution of fractional differential equations. *Nonlinear Dynamics*. 29: 3-22, 2002.
20. J. Lu and G. Chen. A note on the fractional-order Chen system. *Chaos, Solitons and Fractals*. 27: 685–688, 2006.
21. J. Lu and G. Chen. A new chaotic attractor coined. *International Journal of Bifurcation and Chaos* 12:659–661, 2002.
22. W. H. Deng and C. P. Li. Chaos synchronization of the fractional L$\ddot{u}$ system. *Physica A*. 353:61–72, 2005.
23. R.Garrappa. Predictor-corrector PECE method for fractional differential equations. MATLAB Central File Exchange. Retrieved June 29, 2021.
24. M.F Danca and N. Kuznetsov. Matlab Code for Lyapunov Exponents of Fractional-Order Systems, *International Journal of Bifurcation and Chaos*. 28(5),1850067, 2018.

Coupled FitzHugh-Nagumo Type Neurons Driven by External Voltage Stimulation

Jakub Záthurecký[1] and Lenka Přibylová[1]

Department of Mathematics and Statistics, Faculty of Science, Masaryk University, Kotlářská 2, Brno, 61137, Czechia
(E-mail: 437099@mail.muni.cz, pribylova@math.muni.cz)

Abstract. We have extended some results of previous works on coupled FitzHugh-Nagumo type neurons stimulated by an external alternate voltage source. At first a few electronic circuits modeling the influence of brain waves on particular groups of coupled neurons are constructed. Bifurcation analysis of limit cycle dynamics is carried out, and route to chaotic dynamics is described with respect to coupling strength and forcing amplitude. This analysis enables constructing systems of coupled oscillators with specified dynamic behavior. We show that for appropriate values of parameters, a chimera-like state can be observed in a system of four coupled forced oscillators. A similar approach can generally be used, and the chimera state in coupled systems may be explained by means of bifurcation theory.
Keywords: FitzHugh-Nagumo, neuronal cells, brain waves, chaos, chimera state.

1 Introduction

This short text is inspired by the works Kyprianidis *et al.*[7] and Kyprianidis and Makri[8] about coupled FitzHugh-Nagumo oscillators. Nonlinear dynamics, especially chaos theory, is becoming a very important tool in understanding brain activity, as can be seen, for example, in Faure and Korn[2] and Korn and Faure[5]. Here we attempt to demonstrate this fact by using bifurcation theory to explain some kinds of behavior in systems of coupled FHN type neurons. At first, we recall basic results about dynamics of a single oscillator driven by external periodic voltage source. Such a system can model a neuron influenced by brain waves (an externally driven FHN type neuron). We describe an electric circuit that is characterised by the studied equations. Next, we investigate two coupled oscillators driven by the same voltage source as a model of two externally driven FHN type coupled neurons influenced by brain waves. In every case, the coupling is realized by a resistor, hence we model gap junctions between cells.

Finally, we use these results to construct a system of four coupled oscillators exhibiting a stable state similar to a chimera state. As a model of four neurons coupled in a ring topology, we construct a minimum system that exhibits such dynamics with two groups of two mutually synchronized neurons with two different dynamic behaviors. Bifurcation analysis (using continuation program MATCONT, Dhooge *et al.*[1]) explains the choice of parameters for presented synchronizations and chimera-like states.

2 Dynamics of externally driven FHN type neuron

The starting point of the work Kyprianidis *et al.*[7] is an electric circuit depicted in Fig. 1. The component denoted by N_R is a resistor with a cubic

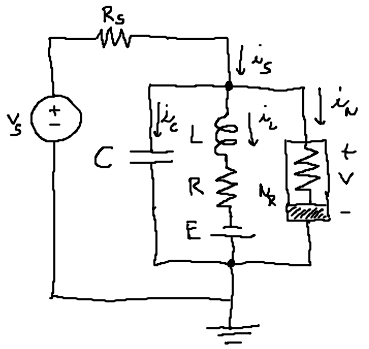

Fig. 1: Electric circuit modelling FitzHugh-Nagumo equations.

$i - v$ characteristic. The dynamics of this system is described by the following equations, that can be derived using Kirchhoff's laws and dimensional analysis:

$$\begin{aligned} x' &= x - \frac{x^3}{3} - y + \varepsilon(u - x), \\ y' &= k(a - by + x), \end{aligned}$$

where x is proportional to the voltage v, y is proportional to the current i_L, ε is proportional to the reciprocal of the resistance R_S and finally u is proportional to the voltage v_S. The alternate voltage u is given by the formula $u(t) = U_0 \cos 2\pi\omega t$. To make the system autonomous, non-stiff, and suitable for bifurcation continuations, we attach two more equations:

$$\begin{aligned} u' &= 2\pi\omega(\mu u - w - u(u^2 + w^2)), \\ w' &= 2\pi\omega(u + \mu w - w(u^2 + w^2)). \end{aligned}$$

Since these equations exhibit a stable solution given by the formula

$$(u, w)(t) = (\sqrt{\mu}\cos(2\pi\omega t), \sqrt{\mu}\sin(2\pi\omega t)),$$

the parameter μ, $\mu \geq 0$, corresponds to the earlier introduced parameter U_0, $\mu = {U_0}^2$. From now we assume the following values of parameters: $a = 0.7$, $b = 0.8$, $k = 0.1$ and $\omega = 0.16$. This is a typical choice that leads to oscillatory dynamics (from regular neuron spiking to more complex firing patterns). The nonlinear phenomenon is generic and another parameter choice in domain of the limit cycle stability can be taken with analogous results. We briefly reconstruct a bifurcation analysis from the original paper. A stable (globally attractive) limit cycle undergoes period-doubling cascade of bifurcations with respect to

parameter μ that corresponds to variation in amplitude of the external forcing. The results are illustrated in figures 2, 3, 4, and 5.

Two-parameter bifurcation curves with respect to parameters μ and ε are depicted at Fig. 6 (numerically computed with MATCONT, Dhooge *et al.*[1]). Evidently, the occurrence of oscillations with different frequencies depends both on the amplitude of the external waves and on the strength of the coupling. The selection of only one of the parameters is not sufficient to create a complete cascade of period-doubling. Various levels of coupling give birth to bifurcation diagrams with bubbles that correspond to bounded parts of the Sharkovski sequence of periods with respect to parameter μ. For a deeper insight into the theory of two-parameter bifurcations of limit cycles, see Kuznetsov[6] or Wiggins[11].

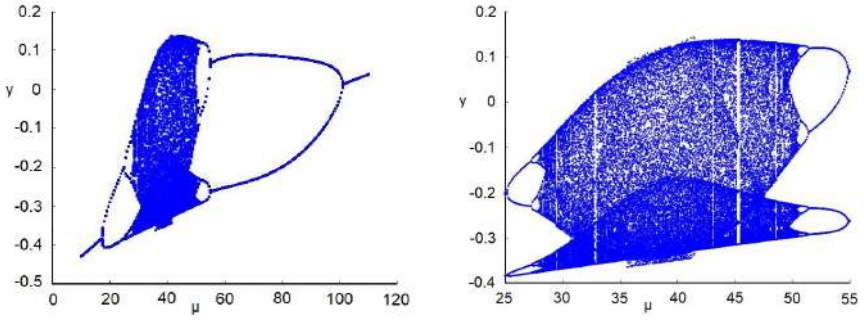

Fig. 2: Poincaré section by the hypersurface $x = -0.75$ for different values of the parameter μ, values of y are plotted. The value of the parameter ε is 0.15.

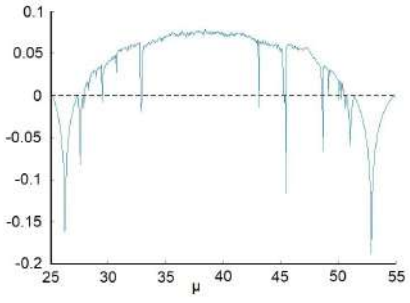

Fig. 3: Maximal Lyapunov exponent for different values of the parameter μ, $\varepsilon = 0.15$.

According to the mentioned figures, a chaotic bubble appears for $\varepsilon = 0.15$. Especially, an increase of the parameter μ from initial values around 10 or a decrease of this parameter from initial values around 110 leads to an infinite cascade of period-doubling bifurcations. Positive values of maximal Lyapunov exponent indicate the presence of a chaotic attractor for appropriate values of the parameter μ. Visible windows corresponding to stable periodic orbits with

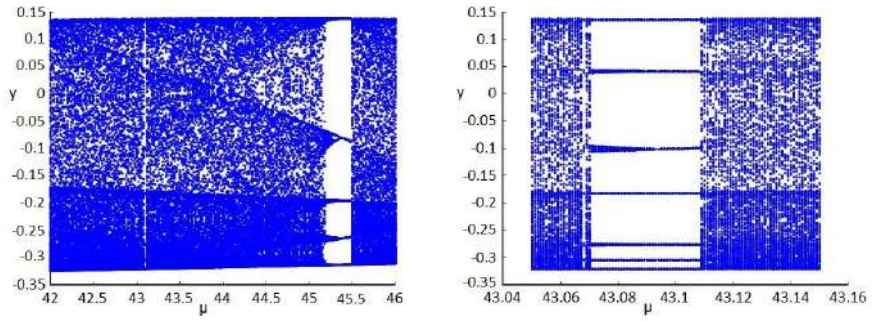

Fig. 4: Zoomed windows of stable cycles of odd period. The value of the parameter ε is 0.15.

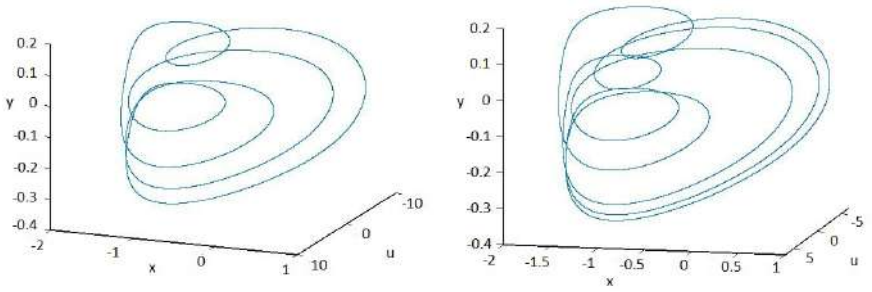

Fig. 5: Left: 5-cycle for $\mu = 45.4$, right: 7-cycle for $\mu = 43.1$. The value of the parameter ε is 0.15.

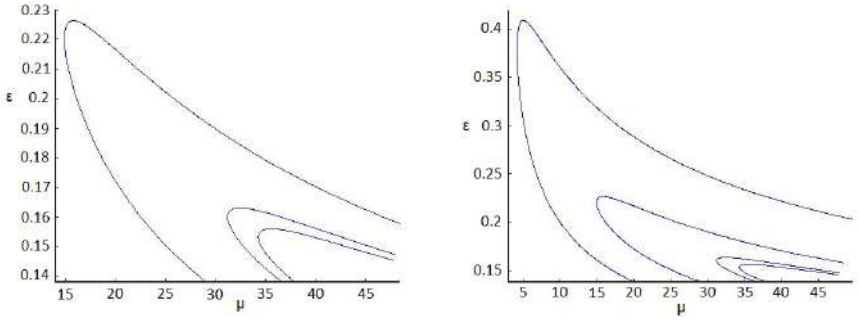

Fig. 6: Right: Bifurcation curves of a stable limit cycle (from the left upper corner to the right lower corner) of period-doubling (2-cycle birth), period-doubling (4-cycle birth), fold bifurcation of 5-cycle, and fold bifurcation of 7-cycle, continued in MATCONT. Left: Magnification of the right picture.

odd period can be observed after magnification (recall Sharkovski ordering).

Particularly, a 5-cycle and a 7-cycle windows are large enough to be detected easily. Curves of fold bifurcations of these cycles can be used for specifying borders of the stable oscillatory dynamics and domains of the chaotic attractor in $\varepsilon - \mu$ plane. Evidently, the cell exhibits chaotic behaviour for example for the values $(\varepsilon, \mu) = (0.15, 38)$ (see also Fig. 4), whereas the choice $(\varepsilon, \mu) = (0.3, 38)$ lead to periodic oscillations. We can possibly use a different pair of parameter values. Bifurcation diagrams in Fig. 6 agree with the results of the original paper Kyprianidis *et al.*[7], which demonstrate an extinction of the chaotic bubble with the increase of the parameter ε.

3 Dynamics of two coupled externally driven FHN type neurons

Further, we study a system of two coupled oscillators, both of which are driven by the same alternate voltage source. This situation can be interpreted as an influence of brain waves on two coupled neurons and is represented by the electric circuit depicted in Fig. 7. Again, Kirchhoff's laws and dimensional

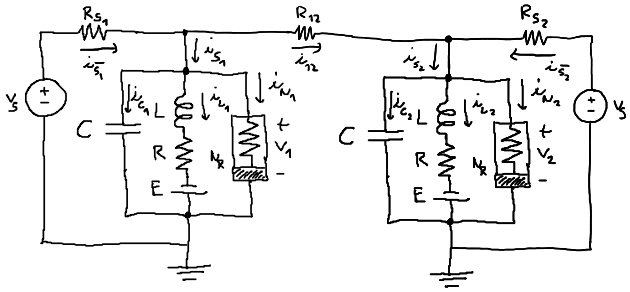

Fig. 7: Electric circuit modelling two coupled FitzHugh-Nagumo oscillators.

analysis give us the following set of equations which describes dynamics of the circuit:

$$\begin{aligned}
x_1' &= x_1 - \frac{x_1^3}{3} - y_1 + \varepsilon_1(u - x_1) + \xi(x_2 - x_1),\\
y_1' &= k(a - by_1 + x_1),\\
x_2' &= x_2 - \frac{x_2^3}{3} - y_2 + \varepsilon_2(u - x_2) + \xi(x_1 - x_2),\\
y_2' &= k(a - by_2 + x_2).
\end{aligned}$$

The new parameter ξ is proportional to the reciprocal of the resistance R_{12}. Now, we investigate an influence of the coupling strength ξ on attenuation of chaos in the first cell, hence we choose $(\varepsilon_1, \varepsilon_2, \mu) = (0.3, 0.15, 38)$. The results can be seen in figures 8, 9 and 10.

For sufficiently large ξ, the first cell makes the second one oscillate periodically, which is a natural state of the first one. The second cell would behave

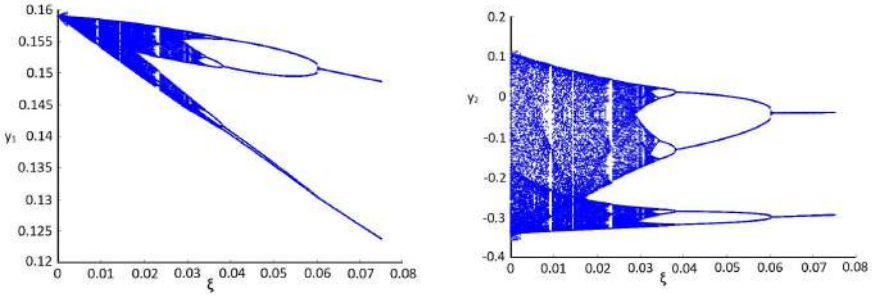

Fig. 8: Left: Poincaré section by the hypersurface $x_1 = -0.75$ for different values of the parameter ξ, the values of y_1 are plotted. Right: Poincaré section by the hypersurface $x_2 = -0.75$ for different values of the parameter ξ, the values of y_2 are plotted. The remaining parameters are $(\varepsilon_1, \varepsilon_2, \mu) = (0.3, 0.15, 38)$.

Fig. 9: Maximal Lyapunov exponent for different values of the parameter ξ.

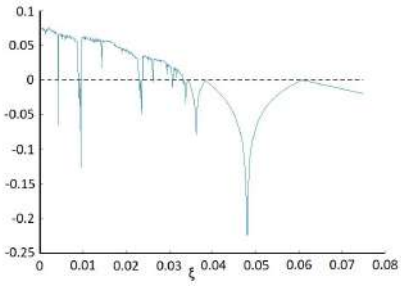

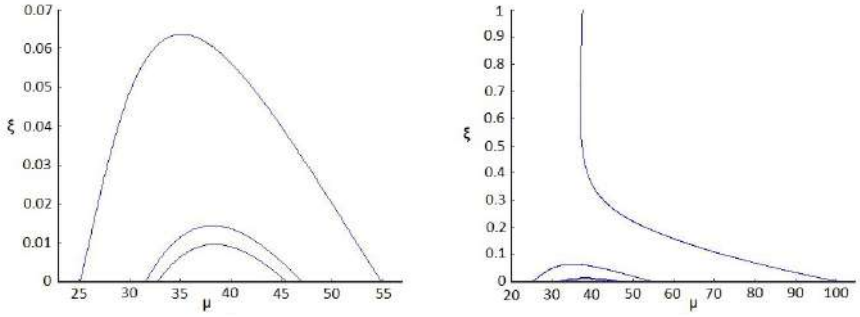

Fig. 10: Right: Bifurcation curves of a stable limit cycle (from the right upper corner to the left lower corner) of period-doubling (2-cycle birth), period-doubling (4-cycle birth), fold bifurcation of 7-cycle and fold bifurcation of 5-cycle. Left: Magnification of the right picture.

chaotically without the coupling. On the other hand, we can say that the strength of coupling is not sufficient for changing the natural behavior, if ξ is small. Poincaré sections indicate a presence of small deviations from periodic oscillation in the case of the first cell. However, they do not change behaviour

qualitatively and can be considered as fluctuations caused by the environment. Bifurcation curves demonstrate an extinction of the chaotic bubble with the increase of the parameter ξ, see Fig. 11.

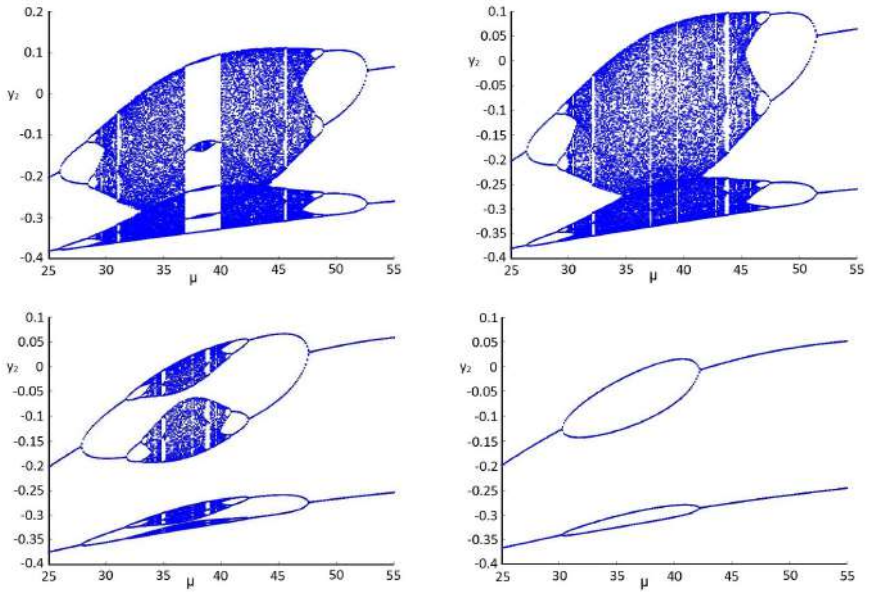

Fig. 11: Poincaré section by the hypersurface $x_2 = -0.75$ for different values of the parameter μ, the values of y_2 are plotted. The values of the parameter ξ are as follows $\xi_1 = 0.009$, $\xi_2 = 0.014$, $\xi_3 = 0.03$ and $\xi_4 = 0.05$. The remaining parameters are chosen to be $(\varepsilon_1, \varepsilon_2) = (0.3, 0.15)$.

Before we proceed to the case of four oscillators, we focus on the influence of the parameter ξ on emerging of synchronization. We deal with two situations in which we couple a chaotic cell together with a periodically oscillating cell and two chaotic cells together, respectively. The dependence of synchronization on the parameter ξ is depicted in Fig. 12. In the first case, we couple two cells driven by different forces, which leads to coupling between different oscillators. It is not surprising that there will always be some difference between phases of these oscillators, no matter how strong the coupling is. On the other hand, we know that two identical chaotic oscillators are able to achieve complete synchronization if the coupling is strong enough. A comprehensive treatment of a concept of synchronization can be found in Pikovsky *et al.*[9].

4 Chimera-like states

The main result of this contribution is the explanation of the chimera-like behavior of a system of coupled oscillators by means of bifurcation theory. We

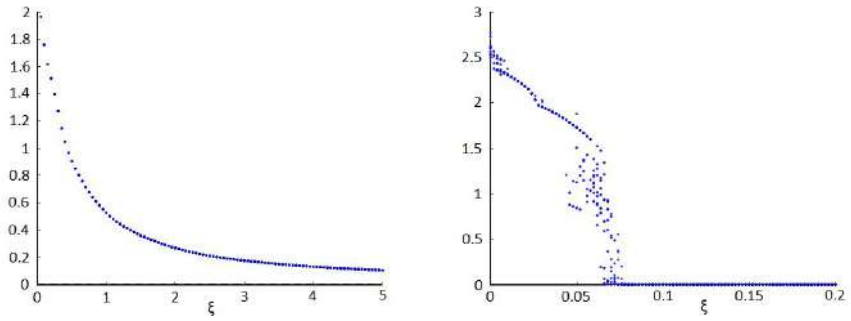

Fig. 12: Dependence of synchronization on the parameter ξ. For the values of the parameter ξ from appropriate intervals ten sets of initial conditions were chosen randomly. Uniform distribution on the interval $[-2, 2]$ has been used. Maxima of deviations $|x_1(t) - x_2(t)|$ for t in the interval $[1000, 2000]$ are plotted. The values of parameters are $(\varepsilon_1, \varepsilon_2, \mu) = (0.3, 0.15, 38)$ for the left diagram and $(\varepsilon_1, \varepsilon_2, \mu) = (0.15, 0.15, 38)$ for the right diagram.

can easily use previous bifurcation analysis results to construct various systems of four coupled cells exhibiting synchronizations/non-synchronizations, chaotic behavior and partial synchronizations, and especially stable chimera state, which means that two groups of oscillators have qualitatively different dynamics. One group of two oscillators behave chaotically (in a synchronized or non-synchronized state), the other group exhibits synchronized oscillations. The same approach can be analogously used for other systems of Hodgkin–Huxley type, Morris-Lecar type, Hindmarsh–Rose type, or others.

We are interested in an electric circuit depicted in Fig. 13 with the following equations governing its dynamics:

$$
\begin{aligned}
x_1' &= x_1 - \frac{x_1^3}{3} - y_1 + \varepsilon_1(u - x_1) + \xi_{12}(x_2 - x_1) + \xi_{13}(x_3 - x_1),\\
y_1' &= k(a - by_1 + x_1),\\
x_2' &= x_2 - \frac{x_2^3}{3} - y_2 + \varepsilon_2(u - x_2) + \xi_{12}(x_1 - x_2) + \xi_{24}(x_4 - x_2),\\
y_2' &= k(a - by_2 + x_2),\\
x_3' &= x_3 - \frac{x_3^3}{3} - y_3 + \varepsilon_3(u - x_3) + \xi_{13}(x_1 - x_3) + \xi_{34}(x_4 - x_3),\\
y_3' &= k(a - by_3 + x_3),\\
x_4' &= x_4 - \frac{x_4^3}{3} - y_4 + \varepsilon_4(u - x_4) + \xi_{24}(x_2 - x_4) + \xi_{34}(x_3 - x_4),\\
y_4' &= k(a - by_4 + x_4).
\end{aligned}
$$

Three different situations are going to be considered all of which are illustrated in figures 14, 15 and 16. The choice of parameters in Fig. 14 represents a situation in which the natural state of the first cell is periodic oscillations, while

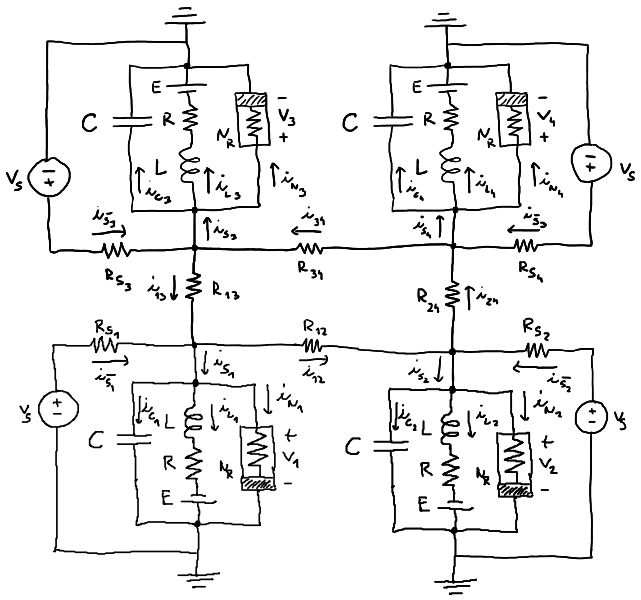

Fig. 13: Electric circuit modelling four coupled FitzHugh-Nagumo oscillators.

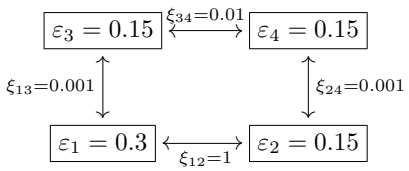

Fig. 14: Bottom: projection of the trajectory on the phase space of the third and of the fourth cell on the left and on the phase space of the first and of the second cell on the right, respectively.

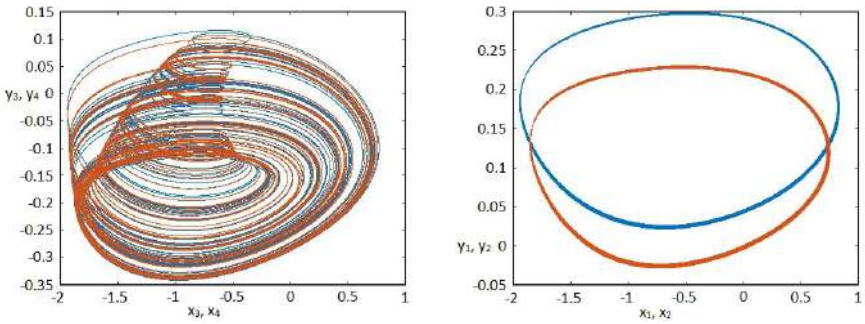

the remaining cells behave chaotically. Moreover, the coupling between the first two cells is strong enough to suppress chaos in the second cell. Finally, chaotic cells are not able to synchronize, and respective groups do not influence each other too much. Since the first two cells are different oscillators, they are not able to achieve complete synchronization. However, frequency locking appears obviously. If the natural state of the second cell is periodic oscillations, then the choice of parameters in Fig. 15 leads to complete synchronization in the

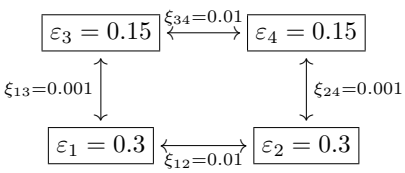

Fig. 15: Bottom: projection of the trajectory on the phase space of the third and of the fourth cell on the left and on the phase space of the first and of the second cell on the right, respectively.

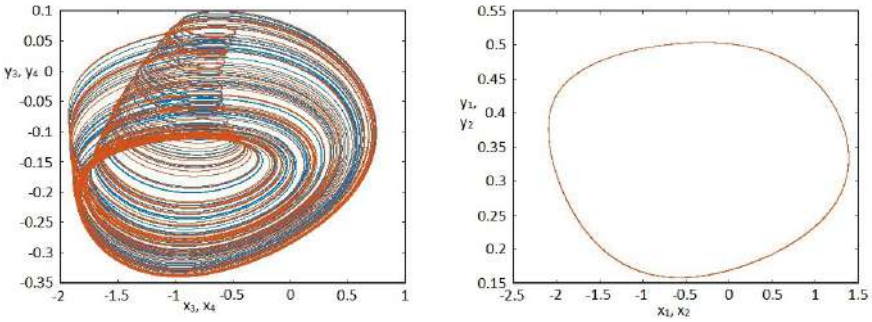

first group. On the other hand, the fluctuations caused by the group of chaotic cells are still present, but they are much weaker. Finally, we can consider a

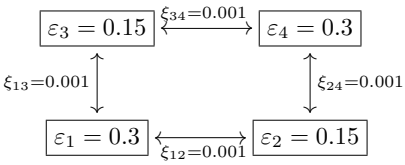

Fig. 16: Bottom: projection of the trajectory on the phase space of the second and of the third cell on the left and on the phase space of the first and of the fourth cell on the right, respectively.

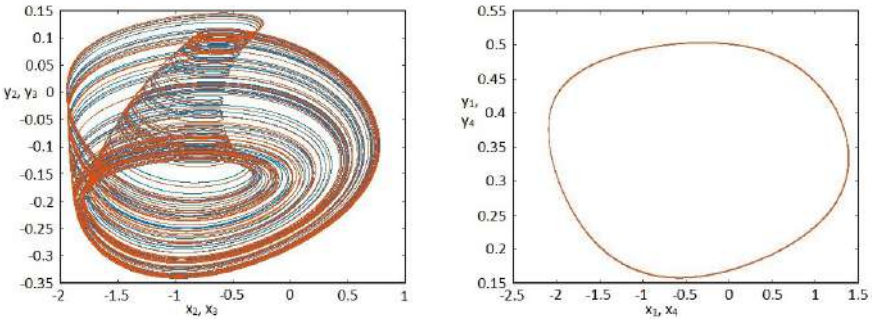

situation in which cells are connected to cells of the other group only, which is illustrated in Fig. 16. Since periodically oscillating cells are driven by the same force, they do not need to be coupled in order to achieve synchronization. The stability of partial synchronization in the second and the third situation is demonstrated in figures 17 and 18.

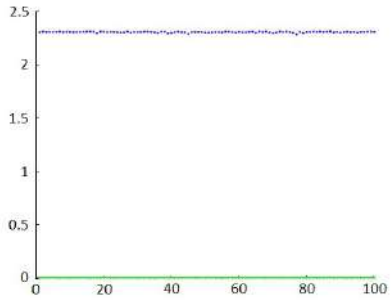

Fig. 17: Deviations between pairs of oscillators for one hundred initial conditions chosen randomly from the interval $[-2, 2]$ with uniform distribution. Maxima of deviations $|x_1(t) - x_2(t)|$ for $t \in [1000, 2000]$ are displayed in green colour and maxima of deviations $|x_3(t) - x_4(t)|$ for $t \in [1000, 2000]$ are displayed in blue colour. Parameters are the same as in Fig. 15.

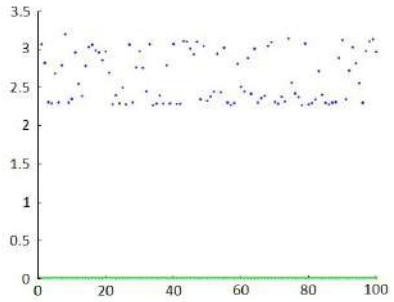

Fig. 18: Deviations between pairs of oscillators for one hundred initial conditions chosen randomly from the interval $[-2, 2]$ with uniform distribution. Maxima of deviations $|x_1(t) - x_4(t)|$ for $t \in [1000, 2000]$ are displayed in green colour and maxima of deviations $|x_2(t) - x_3(t)|$ for $t \in [1000, 2000]$ are displayed in blue colour. Parameters are the same as in Fig. 16.

5 Conclusion

The majority of this work can be considered as a straightforward extension of ideas and analyses published in Kyprianidis *et al.*[7] and Kyprianidis and Makri[8]. On the other hand, the system of coupled oscillators can be seen as a prototype for the description of chimera-like dynamics, which can be explained by bifurcation analysis. It is possible to explain changes in dynamics with respect to the coupling force between the oscillators or the external excitation (brain waves) by crossing bifurcation manifolds. We have observed two main types of cell behavior: a cell can exhibit periodic oscillations that lead to participation in the generation of brain waves, or it can behave chaotically. There could also be various ratios of phase-locking observed as the period-doubling route to chaos takes place. It thus explains the phenomenon when a neuron can contribute both to a synchronized brain wave activity but also have different and even chaotic dynamics (Korn and Faure[5]). Analysis of phase-locking is connected with fold bifurcations on a torus, more precisely birth of torus via Neimark-Sacker bifurcation of a cycle and near Arnold tongues existence. This analysis is not included in this contribution, but a possible analysis approach is explained in Ševčík and Přibylová[10].

All studied systems of differential equations describe dynamics of some electric circuit which is presented in detail. We have seen that the resulting type of behavior strongly depends on the topology of the network, the strength of coupling between cells, and the amplitude of the forcing signal. Our further re-

search will be focused on applications of functional analysis, singularity theory, and group theory to the investigation of the origin of partial synchronization based on ideas from Golubitsky and Schaeffer[3] and Golubitsky *et al.*[4] since in the case of similar coupled neurons, symmetry can be used to study and describe idealized and perfectly same coupled neurons, and breaking symmetry can lead to chimera states that could be explained by means of equivariant bifurcation theory.

Acknowledgements

The work has received financial support from Mathematical and Statistical modelling project MUNI/A/1615/2020.

Conflict of interest

The authors declare that they have no conflict of interest.

References

1. A. Dhooge, W. Govaerts and Y. A. Kuznetsov. MATCONT: a MATLAB package for numerical bifurcation analysis of ODEs. *ACM Transactions on Mathematical Software (TOMS)*, 29, 2, 141–164, 2003.
2. P. Faure, H. Korn. Is there chaos in the brain? I. Concepts of nonlinear dynamics and methods of investigation. *Comptes Rendus de l'Académie des Sciences-Series III-Sciences de la Vie*, 324, 9, 773–793, 2001.
3. M. Golubitsky and D. G. Schaeffer. *Singularities and groups in bifurcation theory*. Vol. I, volume 51 of. Applied Mathematical Sciences, 1985.
4. M. Golubitsky, I. Stewart and D. G. Schaeffer. *Singularities and groups in bifurcation theory*. Vol. II, Vol. 69 of Applied Mathematical Sciences, 1988.
5. H. Korn and P. Faure. Is there chaos in the brain? II. Experimental evidence and related models. *Comptes rendus biologies*, 326, 9, 787–840, 2003.
6. Y. A. Kuznetsov. *Elements of applied bifurcation theory*. Vol. 112. Springer Science & Business Media, 2013.
7. I. M. Kyprianidis, et al. Dynamics of Coupled Chaotic Bonhoeffer–van der Pol Oscillators. *WSEAS Trans. Syst*, 11, 9, 516–526, 2012.
8. I. M. Kyprianidis and A. T. Makri. Complex dynamics of FitzHugh-Nagumo type neurons coupled with gap junction under external voltage stimulation. *Journal of Engineering Science and Technology Review*, 6, 4, 104–114, 2013.
9. A. Pikovsky, M. Rosenblum and J. Kurths. *Synchronization: a universal concept in nonlinear sciences*. No. 12. Cambridge university press, 2003.
10. J. Ševčík and L. Přibylová. Forced van der Pol oscillator – Synchronization from the bifurcation theory point of view. *14th Chaotic Modeling and Simulation International Conference*, 2021.
11. S. Wiggins. *Introduction to applied nonlinear dynamical systems and chaos.*. Vol.2. New York: Springer-Verlag, 1990.

Demographic Dynamics of Inhomogeneous Economic Communities as an Institutional Trap

Zhulego V.G.[1,2], Balyakin A.A.[2]

[1] NPO ANEK, 16 Maksimova, Moscow, Russia
(E-mail: zhulego@mail.ru)
[2] NRC Kurchatov Institute, 1, ac. Kurchatov sq., Moscow, Russia
(E-mail: Balyakin_AA@nrcki.ru)

Abstract. In this article we discuss the demographic dynamics modelling in communities of countries with different levels of economic development. Our approach is based on the stratum model of population growth, proposed by the authors earlier. The observed processes of depopulation of the periphery of such communities were studied within the framework of the model. The phenomenon of institutional trap is considered as an explanatory principle of the functioning of complex socio-economic structures. Its main traits are discussed. Based on the proposed model, the forecasts of population growth in several countries were calculated. Within the proposed model of institutional trap a set of measures to overcome the negative demographic trends were formulated.
Keywords: Simulation, Demographics, Institutional Trap, Stratum Model, Forecast.

1 Introduction

Significant progress has been made in the field of creating mathematical models for complex social systems in recent decades [1]. The results of scientific forecast (foresight) of socio-economic processes of countries and the world as a whole by methods of social, humanitarian and natural sciences are used both in the field of public administration and strategic planning, and in large business when developing a growth strategy [2]. Mathematical modeling of social processes, and, in particular, the population growth forecasts should be recognized as an integral element of foresight that enlightens the trends of economic development of the society [3]. The topic of forecasting the population growth of countries and the whole world continues to be relevant not only because of the limited life resources and the prospect of overpopulation of the planet, but also because countries tend to build management decisions based on reliable long-term forecasts. The study of this problem leads to the conclusion that such forecasts can be made on the basis of adequate mathematical models.

One of the first and most famous experiences of successful modeling in the field of social and economic sciences was the work of Malthus [4], which caused sharp criticism at the time. The main idea of T.R. Malthus was the point that the difference in the growth of the population and the productive forces (the wealth of society) leads to a complication of the social situation, producing wars, crises and diseases. The discussion of the "overpopulation crisis" predicted by Malthus, which was expected by 2004, led to the correction of the

growth model and the creation of several variants of such model. In general, the proposed approaches can be divided into 3 groups:

- models-concepts based on the identification and analysis of general historical patterns and their representation in the form of cognitive schemes describing logical connections between various factors affecting historical processes (ideas of J. Goldstein, I. Wallerstein, L.N. Gumilev, N.S. Rosov, etc.). These models have a high degree of generalization, but they are not mathematical, but purely logical, conceptual in nature;
- pure mathematical models of the simulation type devoted to the description of specific historical events and phenomena (Yu.N. Pavlovsky, L.I. Borodkin, D. Meadows, J. Forrester, etc.). The applicability of such models is usually limited to a fairly narrow space-time interval since they are related to a specific geopolitical situation;
- "intermediate" mathematical models between the two specified types. Their task is to identify the basic patterns that characterize the flow of processes of the type under consideration.

Our work aimed at studying the relationship between socio-economic life and demographic processes, thus relating to the third type of models. This approach involves both conducting mathematical modeling, and taking into account and describing the factors and processes that affect the phenomena under consideration.

One of the first steps in this direction that should be named is the Verhulst logistics model [5] and the concept of "world-systems" [6]. Within the framework of these approaches, the unified system (the world) was divided into subsystems (economic subsystem, and/or social and demographic ones). Later, dynamic models were proposed that go beyond the neoclassical model of economic growth by R. Solow [7], based on equilibrium, when in a stationary state the rate of labor productivity growth is equal to the rate of technological progress, and the rate of economic growth is the sum of the rate of technological progress and the rate of population growth

At the same time, the Solow model could not explain many problems related to economic growth, which was caused by the fact that many parameters of the model were set exogenously. The next step was the Cobb-Douglas model [8], the Ramsey-Kass-Koopmans model [9] and the Mankiw Romer and Vail model [10].

All the models considered assumed a different format of "combining" social, economic and demographic parameters [6,11]. In practice, we should mention the Gushchin-Malkov model of macroeconomic dynamics (which describes the economic cycles of US GDP growth, see [12])) and the Korotaev model of great divergence/convergence [13], as well as the Kapitsa population growth model [11]. The last work proposed an exponential model of world population growth, showing the "limits of growth" beyond which a global catastrophe can await the planet. Based on this model, the trend change point or "transition point" (2005) was also predicted, when exponential growth is replaced by a slowdown in growth. Although this model made it possible to

predict global trends quite well, it was completely unsuitable for calculating population growth forecasts for individual countries, in particular because migration processes play an important role in these processes, which were not taken into account in the model in any way.

Methodologically, our study continues the approach of dividing a single system into a number of subsystems, and in this sense, the approach can be called hierarchical. The subject of our study will be the population growth in the subsystems of a single "economic community", taking into account the socio-economic development of this system. It is assumed that in the system under consideration, it is possible to explicitly allocate the Center and the Periphery (i.e., to allocate subsystems). A similar problem was solved earlier in the course of mathematical modeling of the population size based on the stratum model [14].

Our special attention was attracted by the Korotaev's model [13] of great divergence/convergence, in which an attempt is explicitly made to take into account population growth in the economic model of the development of countries. The authors drew the conclusion about the "inevitable convergence of heterogeneous economic systems of the Periphery-Center type". Meanwhile, this conclusion contradicts the trends observed in some similar situations, in particular in the EU-Baltic states, where not only convergence is not observed, but rather divergence occurs, accompanied by the process of depopulation of the Periphery.

The obvious disadvantage of mentioned model is the lack of migration in it – and, as it seems to us, this process leads to the opposite effect: to the growth of the economic gap between these parts of the system and, ultimately, leads to the depopulation of the Periphery. The most important resource of economic growth is the labor force leaving depressed regions, which leads to a significant decrease in the economic growth potential of these regions.

The way out of this situation, in our opinion, may be the stratum model of population growth proposed by us in 2014 [14], which can be generalized to the case of a heterogeneous economic system/commonwealth of countries with different levels of development. An additional argument in favor of the attempt to combine the convergence model with the stratum model of population growth was our analysis of population growth forecasts for 2014 for several countries in comparison with statistical data for these countries over the past 4 years, which showed a good agreement of these forecasts with statistics.

The essence of the stratum model is that the population of a country is considered not as homogeneous, but as consisting of several strata. We used following denotations: x (t) – the number of urban population, y(t) - the number of rural population. The parameters that determine the dynamics of changes in each stratum are different, in particular, both the birth rate and mortality in the strata can differ significantly, in addition, there is a significant migration of the population (almost always it is the move of the rural population to the city). Taking into account these circumstances, the model of population growth in a particular country can be presented in this form:

$$\begin{aligned}\frac{dx}{dt} &= a_x x(t) - d_x x^2(t) + c_x \frac{x(t)y(t)}{x^2+\alpha^2} \\ \frac{dy}{dt} &= a_y y(t) - d_y y^2(t) - c_y \frac{x(t)y(t)}{x^2+\alpha^2}\end{aligned} \quad (1)$$

The meaning of the parameters a_x and a_y is that they are determined by the balance of instantaneous fertility and mortality in each stratum. Since the economic conditions for the existence of strata and the way of life within strata are different, the characteristic coefficients a_x and a_y can vary greatly. The parameters d_x and d_y conditionally determine the "capacity of the corresponding niche", i.e. they reflect the limited life resources, and the ratio of the parameters (a_x,a_y) and (d_x,d_y) determines the linear "transition point".

The system (1) is written in a symmetric form, the coefficients (a_x, a_y) and (d_x, d_y) determine the internal dynamics of the stratum, and c_x and c_y determine the migration between the strata. The migration flow may depend on many factors, but for each specific country it is a fairly stable parameter, and the last term in the equations should be proportional to the frequency of meetings of residents of the city and village, it is this part of the equation that can significantly accelerate the dynamics of changes in the system.

This is also connected with the possibility of economic growth of the country exceeding the population growth rate, since the migration of the rural population to the city provides additional needs for industrial labor resources. For a particular country, the migration rate is determined by the coefficients $c_{x,y}$ (in the simplest case, these coefficients are equal and opposite in sign, which means that all those who left the "village" ended up in the "city"). If we start from the stratum model of population growth of one country (1), then it is easy to build a model of world population growth based on the principle of hierarchy: for this it is necessary to determine the coefficients (a_x, a_y), (d_x, d_y), (c_x, c_y) for each individual country, moreover, an additional term describing the emigration of the population from one country to other countries should be introduced, this term will be similar to the third in the system (1). The forecast calculated in this order for each country allows us to find the total population of the world.

It should be said that in this approach, the amount of calculations increases significantly, but the accuracy of the forecast also increases. It should be emphasized that it was the forecasts for these countries that led us to the idea of the existence of so-called "institutional traps" that individual countries fall into, i.e. such situations that do not disappear by themselves, but require a purposeful restructuring of the institutional environment. It is for this reason that below we present the results of calculations of forecasts for a group of countries, the choice of which is due to the fact that, using the example of these countries, we will try to construct and test a mathematical model of an "institutional trap", i.e. a situation caused by the institutional characteristics of countries and a way out of which is possible only as a result of serious institutional changes.

In the next section we present the results of numerical simulation for population growth of countries that can be considered as good axample of center-periphery system.

2 The dynamics of population growth as an institutional trap. Former USSR republics case

Let us discuss the demographics dynamics of former soviet republics, precisely – Russia, Belarus, Ukraine and Baltic states. Here we do not take into account the pandemic influence, hoping its negative consequences will be overcome soon, and the population trend will restore.

A characteristic feature of the demographic dynamics of Russia was a change in the trend from neutral (fluctuation in the population near 147 million) to moderately optimistic growth since 2010 year. The trend change was mainly due to the growth of urban population, while the rural population continued to decline. The graph on the right shows statistics for 4 years from 2014 to 2018. Thus, it can be argued that the managerial decision made in Russia on cash payments at the birth of the second and third child has already influenced the dynamics of population growth.

Since the collapse of the USSR, Belarus is the only post-Soviet republic where the population began to grow. Urban growth continued after the collapse of the USSR, the rural population continued to decline at a constant rate, while the total population began to grow only in 2014. These changes however are not stable and can be reversed due to political tensions.

Since 1991, Ukraine has shown a steady population decline dynamics: population was decreasing at a constant rate of 1% per year. Moreover, the decrease in the population is taking place both in the countryside and in the city at almost the same rate. This dynamic indicates the ongoing economic crisis in the country. Data for 4 years (from 2014 to 2018) do not provide any indication of a change in trend.

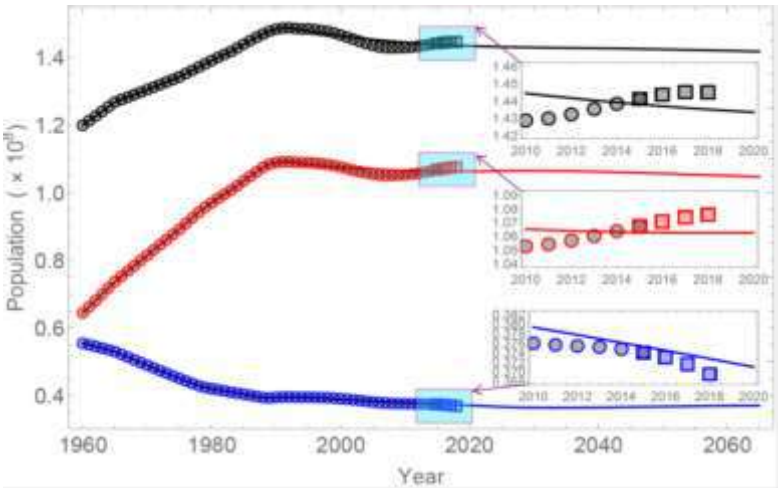

Fig. 1. Russia population forecast and statistical data

After the collapse of the USSR in the period up to 2000, the population decline in Estonia was the fastest among the post-Soviet countries, and then it diminished. The shift of the dynamics in recent years (positive growth) should be considered separately, since there is no obvious explanation for such a change.

After 1991, the most dramatic situation developed in Lithuania - depopulation was stable both in the city and in the countryside, and there is no need to talk about a change in trend. In Latvia the situation is almost completely similar to Lithuania: depopulation is going on at a constant pace, and no change in the trend is expected.

The graphs indicate the presence of two groups of countries: these are the post-Soviet countries that remained outside the economic blocs and the post-Soviet countries that entered the EU (or are associated with the EU). The demographic situation in these groups is radically different.

All this suggests that a mathematical model should be created that would take into account migration between countries and at the same time reveal the reasons for such large-scale population migrations. In our opinion stratum model is the best possible starting point on the way to such a socio-demographic model. As an explanatory principle we rely on institutional reasons. Since the ideas to link demographic variables with economic and social variables have appeared for a long time, we decided to make an attempt to create an economic-socio-demographic model that would allow us to consider the problems of demography in connection with economic and social ones. Moreover, one of these attempts raised the problem of convergence of countries with different levels of economic development.

Our explanation of the differences in dynamics boils down to the following causal chain: joining the EU (or association) opens borders for migration of the population, the existing gap in the standard of living and education leads to the flow of migrants from conditionally “poor countries” towards rich ones. Such migration deprives poor countries of human development resources, and then their economic development slows down.

The problem of heterogeneity or uneven development of countries has already been considered in the above mentioned work [13]. Obviously, without taking into account migration, such a model leads to “great convergence” - a completely fair goal, which was set by the countries that joined the EU. However, in fact, the entry of the Baltic countries into the EU led to depopulation and an increase in the income gap. A similar process is underway in the case of Ukraine (although with some delay). We can expect the same situation with Belarus – Russia case, or Ukraine – Russia (if political tensions declined).

All this allows us to conclude that accounting for migration in the Center-Periphery model is necessary. Otherwise, the model will not adequately describe the dynamics of the system.

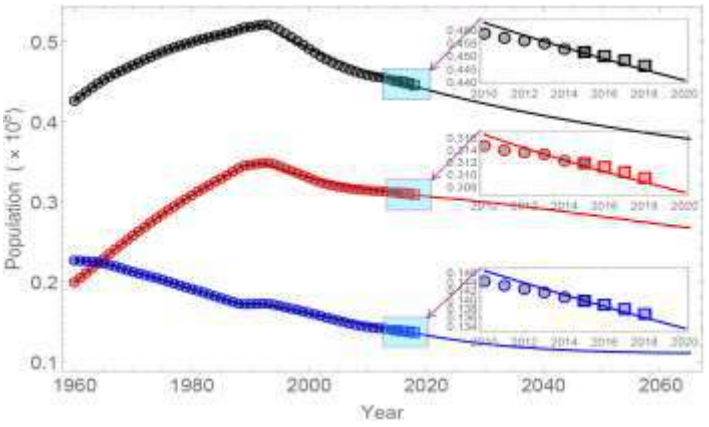

Fig. 2. Ukraine population forecast and statistical data

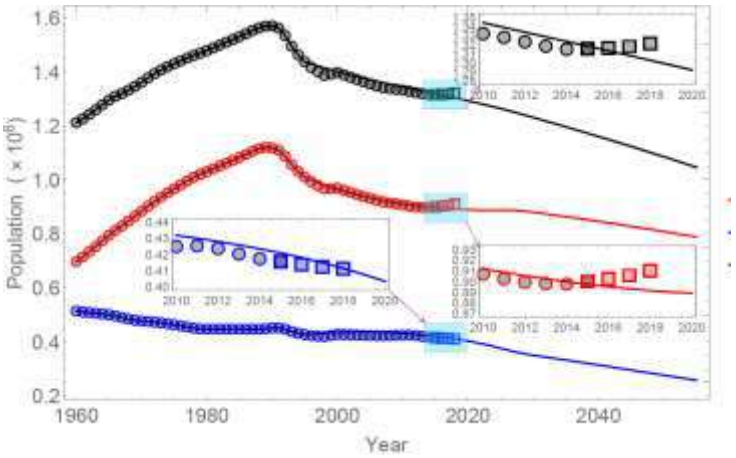

Fig. 3. Estonia population forecast and statistical data

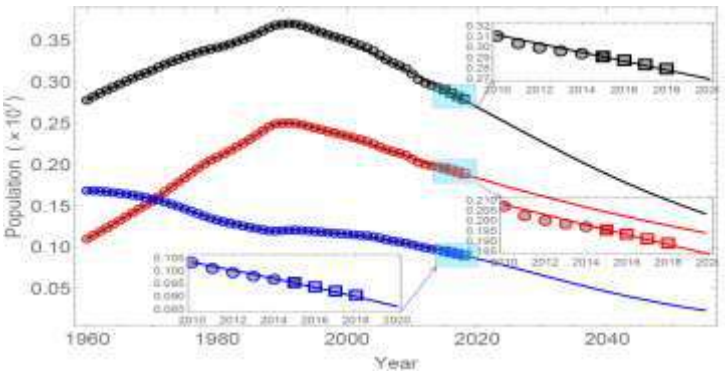

Fig. 4. Lithuania population forecast and statistical data

Of course, we will model a system that is simplified compared to the real one, but we will keep its most important features: the free movement of people (migration) and the heterogeneity of the system. Therefore, we will assume that the system consists of a developed Center and a backward Periphery. From the point of view of the stratum model, the new EU countries represent the same "city" and "rural" in the country, and there is unlimited and practically unregulated migration between these strata. We note that the proposed model should transform into previous model of [14] in the case of low migration process.

3 Model improvement: inclusion of social and economic factors.

For the sake of generality, we will keep the previous designations: x(t) – the population of the Center, y(t) - the population of the Periphery. Let's supplement system (1) by adding equations to take into account the socio-economic development of the regions. By analogy with the work [13], we will introduce the level of "wealth" – $S_{x,y}$ and "education" $E_{x,y}$.

In practice, these factors reflect material wealth and other intangible benefits. The meaning of the parameters a_x and a_y is that they are determined by the balance of instantaneous fertility and mortality in each of the subsystems: in the Center and Periphery. Since the economic conditions of existence in the Center and on the Periphery, as well as the way of life within each subsystem are different, the characteristic coefficients ax and ay can be very different. The parameters d_x and d_y conditionally determine the "capacity of the corresponding niche", i.e. they reflect the limited life resources in the subsystems.

$$
\begin{aligned}
&\frac{dx}{dt} = a_x x(t) - d_x x^2(t) + \left(A\frac{S_x - S_y}{S_x + S_y} + B\frac{E_x - E_y}{E_x + E_y} \right) \frac{x(t)y(t)}{x^2 + \alpha^2} \\
&\frac{dy}{dt} = a_y y(t) - d_y y^2(t) - \left(A\frac{S_x - S_y}{S_x + S_y} + B\frac{E_x - E_y}{E_x + E_y} \right) \frac{x(t)y(t)}{x^2 + \alpha^2} \\
&\frac{dS_x}{dt} = b_x S_x E_x \left(1 - \frac{G}{G_{\lim}} \right) \\
&\frac{dS_y}{dt} = b_y S_y E_y \left(1 - \frac{G}{G_{\lim}} \right) + \varphi \\
&\frac{dE_x}{dt} = f_x E_x (1 - E_x) \\
&\frac{dE_y}{dt} = f_y E_y (1 - E_y) + \psi
\end{aligned}
\qquad (2)
$$

The first two equations of the system (2) is written in a symmetric form, the coefficients (a_x,a_y) and (d_x,d_y) determine the internal dynamics of the subsystem Center and the Periphery, here, instead of the coefficients c_x and c_y, which determine the migration of the population from one part of the subsystem to another, some functions of the variables $S_{x,y}$ and $E_{x,y}$ are selected, which characterize the per capita income and the level of education in each part of the system: S_x is a relatively excess product per capita of the Center population, and

S_y is a relatively excess product per capita of the Periphery population; E_x is the level of education of the population in the Center, and E_y is the level of education of the population in the Periphery. Differences in income level and in the level of education in the Center and on the Periphery will induce migration of the population to the Center. Additionally, the following notation is introduced in system (2): G (t) = x (m + S_x) + y (m + S_y) is the GDP of the Center-Periphery system, m is the minimum necessary product (estimated as $ 440), G_{lim} is a certain fundamental limitation and a normalization term that defines a fundamental constraint in the system. In the model [14] describing the world-system, G_{lim}= $ 400 trillion, in the model we propose, G_{lim} should coincide in order with the EU GDP, i.e. about $ 100 trillion.

Let us pay attention to the choice of signs in these terms in the first two equations of the system (2) that fixes the direction of migration from the Periphery to the Center. Thus, to describe the dynamics of interaction of the heterogeneous Center-Periphery system, a socio-economic demographic mathematical model (2) of the system is proposed, which takes into account both the dynamics of the population of individual parts of the system, and the migration of the population from one part of the system to another, due to the difference in income in different subsystems and the difference in the level of education. Equations (2) contain φ, ψ which we will call “convergence functions”, which show the relationship between the Center and the periphery. Unlike [13], we do not postulate the form of these functions, moreover, in our opinion, their form needs serious refinement.

At the same time, the choice of convergence functions should reflect the main trends in the modern world. Thus, according to the authors [12,13], the gap between highly and medium-developed countries has been decreasing at a particularly rapid pace in recent years, and the gap between highly and underdeveloped countries is decreasing at a noticeably slower pace, at the same time they show an increase in the gap between medium and underdeveloped countries. In practice, it turns out that advanced economies are “going into isolation”, medium-developed countries receive the greatest benefits from globalization, catching up with developed countries, but underdeveloped countries are moving to increasingly worse positions. According to the author [15], we are talking about the reconfiguration of the world-system and the trend towards the concentration of income. There is a discrepancy between the richest and the poorest people in the world, despite the general convergence of average incomes.

These conclusions, in our opinion, are very controversial. The existing practice shows that a country's participation in a successful economic community does not guarantee its automatic convergence, does not automatically raise it to the level of the Center. In our opinion, correct accounting of migration can lead simultaneously to depopulation and economic degradation of the Periphery, and "on average" (or "per capita") there will be an increase in welfare.

In the model we propose, in the simplest case:

$$\varphi = 0$$
$$\psi = -\gamma E_x E_y$$

Note that the function ψ must be non-zero, otherwise the resulting solutions for E_y will tend to 1, i.e. the village becomes fully educated, which will lead to a drop in the birth rate. Practically, in the system (5), the presence of the term ψ ensures, with the simplest choice of the convergence function, the presence of a stable stationary solution of the form

$$(E_x, E_y) = (1, 1 - \frac{\gamma}{c_y})$$

It corresponds to full education in the Center and some non-zero (but not 100%) education in the Periphery.The proposed equations (2) are essentially nonlinear, and may contain complex dynamics, such as periodic oscillations, periodic oscillations with attenuation or increase in amplitude, or, conversely, an asymptotic output to constant values.

Stability analysis for the system (2) reveals that there are always trivial solutions for $E_{x,y} = 0$ or 1 (totally educated or fully uncivilized strata). Assuming two extreme cases Sx >> Sy (the welfare of the Center significantly exceeds the welfare of the Periphery) and Sx = Sy (the convergence occurred) we obtain following results. For Sx >> Sy we get A> $A_{(\text{critical value})} = x^{(0)} a_y = a_y a_y/d_x$

For the case Ex = 1, Ey = 0 (developed center and backward periphery) we get the restriction $(A + B)_{(\text{critical value})} = x(0)$ ay . The system loses stability if the sum of the parameters (A + B) exceeds the critical value. Thus interesting realistic solutions system (2) will be played out around the adiabatic values of variables x(t) and y(t).

A similar approach (adiabatic change of parameters) can be applied in the case of convergence functions, assuming that they are a small perturbation that has the greatest impact on the population of the periphery.

It seems that the next step would be reasonable to choose the convergence functions by analogy with the terms in the first two equations in the form

$$\varphi = \delta\left(A\frac{S_x - S_y}{S_x + S_y} + B\frac{E_x - E_y}{E_x + E_y} \right) S_x S_y$$
$$\psi = -\gamma\left(A\frac{S_x - S_y}{S_x + S_y} + B\frac{E_x - E_y}{E_x + E_y} \right) E_x E_y \qquad (3)$$

The obtained equations (2) are characterized by the following properties. Firstly, there are no exogenous variables in them, taking into account external factors is contained only in the parameters (coefficients) of the equations. Secondly, the meaning of the parameters contained in the model follows from the equations themselves, and the values of these parameters can be determined from the analysis of statistical data for a certain period. Third, the type of convergence functions is not defined a priori.

It seems that this system of equations will allow us to study various modes of behavior of the Center-Periphery system depending on the values of the parameters, as well as to predict the behavior of the Center-Periphery

system, in the case when the parameters are determined. This model is a development of the stratum model, taking into account the ideas about the functioning of the “world-system” [6]. The authors suggest that the developed approach will allow us to consider complex systems where simplified approaches do not work.

Conclusion

The proposed model of the institutional trap is described by a system of equations (2), which is characterized by the following properties:

Firstly, there are no exogenous variables in them, external factors are taken into account only in the parameters (coefficients) of the equations.

Secondly, the meaning of the parameters contained in the model follows from the equations themselves, and the values of these parameters can be determined from the analysis of statistical data for a certain period.

Third, the type of convergence functions is not defined a priori and may vary depending on the task.

It seems that this system of equations will allow us to study various modes of behavior of the Center-Periphery system depending on the values of the parameters, as well as to predict the behavior of the Center-Periphery system, in the case when the parameters are determined.

We emphasize once again that this model is a development of the stratum model [14], taking into account the ideas about the functioning of the "world-system" [6,13]. The authors suggest that the developed approach will allow us to consider complex systems where simplified approaches do not work. The results obtained, however, should be used with caution: their applicability to specific situations is limited by both the initial conditions and the current operating conditions of the system under consideration. In terms of the institutional trap, this is equivalent to the destruction of the trap in the course of institutional restructuring (reform). Note that a similar effect can be achieved by a sharp change in the initial parameters of the system (the population in the Periphery, which has changed dramatically, for example, in the results of uncontrolled migration), which is equivalent to the "transfer" of the system to the pool of attraction of another attractor.

Given the almost unlimited labor migration within the EU, it is assumed that the proposed model will adequately describe the case of an institutional trap that occurs in the Center-Periphery system, in which economic integration does not lead to an equalization of the level of per capita income in the subsystems, but leads to the depopulation of the Periphery. The results of computer modeling should make it possible to estimate the characteristic times of the development of unfavorable dynamics (the "half-life" of the Periphery countries). The authors also hope that the study of this model will allow us to formulate recipes for getting out of emerging institutional traps (by controlling the parameters of the system).

Acknowledgments

The work was supported by the RFBR grant No. 20-010-00576.

References

1. Complex Systems and Society - Modeling and Simulation. Springer, 2013.
2. M. Eberlin Foresight: How the Chemistry of Life Reveals Planning and Purpose. Discovery Institute. 2019
3. Unido Technology Foresight Manual. United Nations Industrial Development Organization. Vienna, 2005. V. 1. P. 8.
4. Clark G. Malthusian Economy // The New Palgrave Dictionary of Economics / Macmillan Publishers Ltd. — L.: Palgrave Macmillan UK, 2018. — P. 8148—8155.
5. Verhulst P.F. Notice sur la loi que la population poursuit dans son accroisment // Correspondence mathematique et physique. 1838. N 10, P. 113-121
6. Forrester J.W. World Dynamics. Wright-Allen Press 1971.
7. Uzawa H. Models of Growth // The New Palgrave Dictionary of Economics / Macmillan Publishers Ltd. — L.: Palgrave Macmillan UK, 2018. — P. 8885—8893. — ISBN 978-1-349-95188-8
8. Renshaw, Geoff. Maths for Economics (англ.). — New York: Oxford University Press, 2005. — P. 516—526. — ISBN 0-19-926746-4.
9. Spear S. E., Young W. Optimum savings and optimal growth: Ramsey — Mavlinvaud — Koopmans nexus // Macroeconomic Dynamics (англ.)русск.. — 2014. — Vol. 18, № 1. — P. 215—243. — doi:10.1017/S1365100513000291.
10. Romer P. M. Human Capital And Growth: Theory and Evidence // NBER Working paper. — 1989. — № 3173. — doi:10.3386/w3173.
11. Kapitsa S.P. Global population blow-up and after. The demographic revolution and information society. Moscow, 2006.
12. Korotayev A., Malkov A., Khaltourina D. 2006. Introduction to Social Macrodynamics: Secular Cycles and Millennial Trends. Moscow: KomKniga/URSS.
13. A. Korotayev, L. Grinin, J. Goldstone Great Divergence and Great Convergence. A Global Perspective. Springer. 2015
14. V.G. Zhulego, A.A. Balyakin. Chaos Modeling and Simulation (CMSIM) 3: “2-Phase Model for Population Growth” p. 193-204, 2015
15. Turchin P. Complex Population Dynamics: a Theoretical/Empirical Synthesis. Princeton, NJ: Princeton University Press. 2003.